FRAGILITY OF A SHEAR WALL BUILDING WITH TORSIONAL IRREGULARITY

THESIS SUBMITTED TO
THE GRADUATE SCHOOL OF NATURAL AND APPLIED SCIENCES
OF
MIDDLE EAST TECHNICAL UNIVERSITY

BY

VESİLE HATUN AKANSEL

IN PARTIAL FULFILLMENT OF THE REQUIREMENTS
FOR
THE DEGREE OF THE MASTER OF SCIENCE
IN
CIVIL ENGINEERING

AUGUST 2011

I hereby declare that all information in this document has been obtained and presented in accordance with academic rules and ethical conduct. I also declare that, as required by these rules and conduct, I have fully cited and referenced all material and results that are not original to this work.

Name, Last name : Vesile Hatun AKANSEL

Signature :

ABSTRACT

FRAGILITY OF A SHEAR WALL BUILDING WITH TORSIONAL IRREGULARITY

AKANSEL, Vesile Hatun

M.Sc., Department of Civil Engineering

Supervisor: Prof. Dr. Polat GÜLKAN

August 2011, 149 pages

Buildings with torsional irregularity represent the main focus of many current investigations. However, despite this volume of research, there is no established framework that describes adequately the seismic vulnerability of reinforced concrete shear wall systems. In this study, the three-dimensional behavior of a particular shear-wall structure under earthquake effects was examined with regard to the nonlinear behavior of the reinforced concrete assembly and the parameters that characterize the structure exposed to seismic motion for damage assessment.

A three story reinforced concrete shear-wall building was analyzed using the finite element method based ANSYS software. The scaled model building was subjected to shaking table tests at Saclay, France. The project was led by the Atomic Energy Agency (CEA Saclay, France) under the “SMART 2008 Project.” The investigation was conducted in two phases. In the first phase, the results of the finite element method and experiments were examined, and were reported in this study. For time history analysis, micro-modeling was preferred due to allowing inclusion the nonlinear effects of concrete and steel for analysis. The guiding parameters (acceleration, displacement, strain) of analytical results are compared with the corresponding values that were measured in the experiments to be able to quantify the validity of models and simulation. For the comparison of

the numerical model results with the experimental results FDE (Frequency Domain Error) method was used.

After comparison of the numerical model results with the experimental results, the second phase of the SMART 2008 Project was undertaken. The second phase consisted of two parts summarized as “Sensitivity Study” and “Vulnerability Analyses”. However, in this report only the sensitivity study and fragility analyses will be reported.

Sensitivity study was done to understand which parameters affect the response of the structure. Twelve parametric cases were investigated under two different ground motions. Different behavior parameters were investigated. The effective damping coefficient was found to affect the structural response at 0.2 g design level as well as at 0.6 g over-design level. At the design level, it was observed that elasticity modulus of concrete and additional masses on the specimen determined as effective on the calculated results.

To derive the failure probabilities of this structure under various earthquake forces for the given limit states, fragility curves were obtained. Different seismic indicators such as PGA (Peak ground acceleration), PGV (Peak ground velocity), PGD (Peak ground displacement) and CAV (Cumulative absolute velocity) were used as seismic indicators and MISD (Maximum inter-story drift) were used as damage indicator for fragility curves. In all 30 time history analyses were done. Regression analyses using least squares method were performed to determine the median capacity and its deviation.

Correlation coefficients of the time history data versus fitted curves obtained from the regression analyses changes between 0.65 and 0.99. The lower cases were for PGD- MISD graphs. The scatter of the fragility curves calculated for each damage limit was slightly wider. HAZUS MH MR1 (2003) damage states were also used for the calculation of the fragility curves and compared with the SMART 2008 damage states.

Keywords: Shear Wall Building, Azalee Shaking Table, Finite Element Method, Fragility Curves, Sensitivity (Parametric study)

ÖZ

BURULMA DÜZENSİZLİĞİNE SAHİP PERDE DUVARLI BİR YAPININ HASAR GÖREBİLİRLİĞİ

AKANSEL, Vesile Hatun

Yüksek Lisans, İnşaat Mühendisliği Bölümü

Tez Yöneticisi: Prof. Dr. Polat GÜLKAN

August 2011, 149 pages

Burulmalı davranışa sahip yapılar günümüzde yapılan birçok araştırmanın ana konusunu teşkil etmektedir. Ancak yapılan araştırmalara rağmen betonarme perde duvarlı sistemlerin davranışını doğrudan tanımlayan ve uygulaması kolay somut metotlar bulunmamaktadır. Bu çalışmada perde duvarlı yapının deprem kuvvetleri altındaki üç boyutlu davranışı, betonun elastik ötesi davranışı ve depreme maruz kalmış yapıların değerlendirmesine yönelik parametrelerin ışığı altında incelenmektedir.

Çalışmada sonlu elemanlar metoduna dayanarak ANSYS programı ile perde duvarlardan teşkil edilmiş üç katlı betonarme bir binanın davranışı incelenmektedir. Modellemesi yapılan bina SMART 2008 Projesi kapsamında Fransa'nın Saclay bölgesinde yer alan Atom Enerji Kurumu'nun (CEA) yürüttüğü proje kapsamında ¼ ölçekli olarak sarsma tablası deneylerine tabi tutulmuştur. Deney sonuçları ile yapının sonlu elemanlar yöntemi ile yapılan modellemesinin ne kadar uyumlu olduğu irdelenmiştir. Zaman tanım alanında hesap için betonun ve çeliğin lineer ötesi davranışını hesaba katacak olan mikro modelleme tercih edilmiştir. Analitik modelleme sonucu elde edilen davranış parametreleri (ivme,yer değiştirme, birim uzama), deneylerde ölçülmüş olan değerler ile karşılaştırılarak model ve simülasyonun geçerliliği ölçülmüştür. Deney sonuçları ile nümerik modelin karşılaştırması için frekans bazında hata ölçme metodu

(FDE) kullanılmıştır. Sonuçların büyük genliğe sahip yer hareketlerinde daha iyi örtüştüğü gözlemlenmiştir.

Nümerik model sonuçları deney sonuçları ile karşılaştırıldıktan sonra SMART 2008 Projesinin ikinci kısmına başlanmıştır. İkinci kısım, iki bölümden oluşmaktadır. Bunlar parametrik çalışma ve hasar görebilirlik analizleridir.

Parametrik çalışmada hangi parametrelerin yapının zaman alanında tanımlı dinamik analiz sonuçlarını daha fazla etkilediği araştırılmıştır. Farklı iki yer hareketi altında 12 farklı durum incelenmiştir. Parametrik çalışma sonucunda farklı davranış parametreleri incelemiş, sönümlenme katsayısının hem 0.2 g, tasarım seviyesinde hem de 0.6 g seviyesinde sonuçları etkilediği görülmüştür. Ayrıca, 0.2 g tasarım seviyesinde betonun elastisite modülünün ve ek yüklerin de sonuçlar üzerinde etkili olduğu gözlemlenmiştir.

Yapının hasar görme ihtimalinin tespiti için hasar görebilirlik eğrileri oluşturulmuştur. Bu hasar görebilirlik eğrileri için PGA (azami yer ivmesi), PGV (azami yer hızı), PGD (azami yer değiştirmesi) ve CAV (birikimli mutlak hız) gibi farklı deprem göstergeler kullanılmıştır. Hasar göstergesi olarak katlar arası maksimum ötelenme değerleri kullanılmıştır. Zaman alanında tanımlı 30 dinamik hesap yapılmıştır. Medyan kapasitelerinin ve standart sapma değerlerinin hesaplanabilmesi için en küçük kareler metodu kullanılarak regresyon analizi yapılmıştır. Projede tanımlanan her nokta için bu eğriler elde edilmiştir.

Regresyon analizi sonucunda elde edilen eğriler ile data arasındaki korelasyon katsayıları 0.65 ile 0.99 arasında değişmektedir. 0.65 civarındaki değerler PGD- MISD (katlar arası maksimum ötelenme) grafikleri içindir. Limit değerler için hesaplanan hasar görebilirlik eğrileri arasındaki mesafeler biraz geniş çıkmıştır. Ayrıca HAZUS MH MR1 (2003) hasar limitleri için de hasar görebilirlik eğrileri oluşturulmuş ve SMART 2008 hasar limitlerinden elde edilen eğriler ile karşılaştırılmıştır.

Anahtar Kelimeler: Perde Duvarlı Binalar, Azalee Sarsma Tablası, Sonlu Elemanlar Metodu, Hasar Görebilirlik Eğrileri, Parametrik Çalışma

To My Family for Their Love and Support

ACKNOWLEDGMENTS

The author is grateful to her advisor, Prof. Dr. Polat Gülkan and her co-advisor Prof. Dr. Ahmet Yakut for their invaluable guidance, assistance, support and insight throughout the research and is grateful for the opportunity to work with them.

Scientific and Technological Research Council of Turkey (TÜBİTAK – 109M707), which is the supporter of this study, is gratefully acknowledged.

The author also thanks to all of her friends, especially; Tuba Eroğlu, Abdullah Dilsiz, Saiedeh Nazirzadeh, Aida Azeri for their support and kind friendship and special thanks to Dr. İlker Kazaz and Inst. Dr. Engin Karaesmen for their guidance and suggestions throughout this study.

Finally, the author wishes to express her gratitude to her family for their love and encouragement.

TABLE OF CONTENTS

LIST OF TABLES

TABLES

LIST OF FIGURES

FIGURES

CHAPTER 1

INTRODUCTION

1.1. The Statement of Problem

Calculation of three dimensional seismic effects on buildings involving torsion is a challenge for structural engineering, especially for non – linear behavior under earthquake effects. Modeling these types of buildings needs much more care to generate acceptable results. In spite of the developing computer technology and existence of many numerical models, there are still deficiencies in modeling because of the assumptions made in the numerical models for material and seismic excitation estimation. One way to test the versatility of a model is to do parametric studies which may be helpful for identifying the importance of the variables in the models.

The other crucial concept is the fragility curves for different structural categories. These statistically-evaluated or empirically-derived curves provide a basis for the assessment of the performance of buildings under different ground motion intensities so that loss estimates can be made.

Most of the numerical models must be confirmed through comparisons with experimental results. There are several experimental techniques that can be used to test the response of structures to verify their seismic performance. One of these is the shaking table test which is the most reliable experiment type developed in the last four decades. A shaking table is a platform for shaking structural models or building components with a wide range of simulated ground motions, including reproductions of recorded earthquakes time-histories. Even though shaking table tests give good results for earthquake simulations, it is hard to test the structures in full scale because of the technological challenge and expense that it represents. Thus, the model buildings are mostly scaled mock-ups, although facilities such as the E-Defense in Kobe, Japan, permit full-size structures to be tested realistically (Nakashima et al., 2008; Chung et al., 2010).

In this study, SMART[1] - 2008 project model structure is studied for sensitivity and fragility analysis. This structure was a highly idealized ¼ scaled mock – up of a French shear wall nuclear power plant structure component. It was subjected to the AZALEE shaking table tests in which different seismic excitation simulations were carried out in Saclay, Paris, in France under the leadership of Commissariat Energie Atomique (CEA). The details of project will be provided in the following chapters.

1.2.Literature Survey

The buildings in which most of the earthquake effects are absorbed by the shear walls need advanced structural analyses techniques for not only design but also the assessment of performance. For structural analyses representative mathematical models for real systems should be created.

Evaluation of analytical methods for static and dynamic calculations with basic solution approaches for the design of shear wall buildings goes back to the 1960s. Computers were not extensively available in those years owing to their accessibility and lack of capacity. Due to this fact, early analytical methods based on basic hand calculations were developed in design offices (Khan and Sbarounis, 1964; Rosman, 1968). In these methods, buildings consisting of shear walls and frames, were modeled by simulating the shear walls under flexure and shear. These methods were used by many researchers and designers because they yield the structural forces, moments and lateral displacements in a somewhat more practical and less time consuming manner. However, after the 1960s, increasing capacity and speed of computers owing to the developments in technology caused

[1] SMART = Seismic design and best – estimate Methods Assessment for Reinforced concrete buildings subjected to Torsion and non – linear effects

the hand calculations to be replaced with the commercial software based on finite element methods in design offices.

Developments in computer technology also affected the reliability of experimental studies. Gülkan and Sözen (1974) performed the dynamic tests on one– storey reinforced concrete frames. They concluded that the maximum inelastic earthquake response of a single degree of freedom system can be estimated by analyzing its linear model with reduced stiffness and a substitute damping ratio. Wallace and Moehle (1992) estimated the displacement capacity and demands in walls according to past earthquakes such as the Chile Earthquake, 1986. They made use of ideas presented by Sözen (1989) to be able to get the fundamental period of a building and then used the single degree of freedom oscillator method developed by Newmark and Hall (1982) and Shimazaki and Sözen, (1984) to determine the maximum inelastic and elastic response. Kabeyasawa et al (1983) tested a full – scale seven storey reinforced concrete structure for its pseudo – dynamic earthquake response. Then, analytical models were developed for estimating the response under earthquakes by comparing and calibrating with the experimental results and past earthquakes. Vulcano et al. (1988) used three–vertical-line-element model to be able to estimate a reinforced concrete wall flexural response, with hysteretic material models and predicted accurately the measured flexural response. However, under high shear stresses, further improvements of the wall model were needed to accurately predict the hysteretic shear response as well as the flexural and shear displacement components. The scope of earthquake engineering turned into displacement based design from force based design through the time. Moehle (1996) gives the development of displacement based seismic design in detail.

The calculation of the effects of earthquakes on buildings in terms of inter – storey drift and floor acceleration demands, method in which the loads are applied uniformly are developed for dynamic elastic and inelastic behavior by many researchers (Iwan, 1997; Miranda, 1999; Miranda and Taghavi, 2005).

Finite element models became widespread due to the developments in computer technology and needs for advanced methodologies (Clough, 1980). By the help of finite element method, shear wall models could be solved in great detail with acceptable accuracy.

For walls two main modeling approaches are used as macro and micro modeling depending on element technology in finite element method. Micro modeling is a continuum mechanics based approach and consist of two or three dimensional solid or shell finite elements. Non – linear behavior of concrete and steel can be applied in the model on the basis of material constitutive relationship and numerical techniques that approach the theoretical and experimental results (Ile and Reynouard 2003, 2005; Kazaz et al, 2006; Ile et al., 2008; Fischinger and Isakovic, 2000). Micro modeling is suitable for obtaining the local behavior in the structure. ANSYS, ABAQUS, ADINA and DIANA are some of the finite element software that includes a variety of element and material models in their libraries for micro modeling.

Many researchers have used micro modeling approach to simulate the experimental measurements (Kwak and Kim, 2004; Palermo and Vecchio, 2007). On the other hand, non – linear micro modeling of a full structure (with all its components such as beam, column, foundation etc.) with non – linear time – history analyses is impractical in terms of the time consumed and the output obtained.

Application of macro models are more practical and easy, however, a need exists in calibration for, in terms of flexure, shear or combined effects of shear – flexure conditions in the systems to obtain accurate results. Despite these limitations, macro models are widely used in models which have dominant modes. Equivalent beam model, equivalent frame model and wide column analogy are examples for macro modeling.

Nowadays, wide column analogy is extensively used especially for the design of shear walls in the elastic range (Sözen and Moehle, 1993; Beyer et al., 2008). This method can be used in the analyses of slender multi – storey walls but is not applicable in short shear dominant wall analysis. Despite the fact that shear walls are commonly related to shear forces, the effects that dominate their behavior are actually flexural in character. Kabeyasawa et al (1983), Fishinger and Isakovic (2000), Orakcal and Wallace (2004; 2006) developed multi-vertical-line-element models for structural analyses. However, the accuracy of all these models was tested under flexural forces and models did not give very good results especially for shear dominant walls. Defining the spring parameters for shear and flexural effects is the biggest problem in the macro models. Research that had been done using different modeling techniques in previous years indicated that equivalent beam models and vertical-line-element models may have drawbacks in performance estimates (OECD /NEA /CSNI, 1996; IAEA-TECDOC, 2008). On the other hand, micro models that use the solid continuum mechanics techniques are indicated as giving good results only if they are modeled in a realistic way for material models and element displacement approximations.

Pushover analysis became popular with the concept of performance based engineering in recent years (Kwak and Kim, 2004). The main aim of the performance based engineering is to ensure that the structure remain within the desired safety and deformation limits under a given seismic hazard effect. As noted in the chapter for retrofitting and assessment in the current Turkish Earthquake Code (TEC 2007), simplified shear wall models used in engineering applications is vertical-line-element model based on stacked hinge assumption because they are much simpler. There is not enough research in literature for the use of bar element methods for the non - linear behavior of shear walls. That is the reason that there is a need, especially for U and L shaped walls, for simplified models mimicking non – linear behavior.

Limit state design, is the one of the major developments in seismic design over the past 10 years. Priestley (2000) indicates the importance and advantages of direct displacement – based design by comparing forced – based design.

Performance – based design is a powerful tool for the assessment of buildings under earthquake effects. In performing a seismic risk analysis of a structural system, the vulnerability information in the form of fragility curves is a widely practiced approach. In recent decades, the probabilistic approaches have become much more popular than deterministic approaches for the determination of fragility curves of structures. Shinozuka et al. (2000) empirically developed the fragility curves associated with different states of damage of bridges under the 1995 Kobe earthquake event. They introduced the uncertainty and statistical interpretation of randomness through the notation of combined and composite fragility curves.

It is important to define the appropriate and valid criteria for the performance assessment of buildings besides accurate modeling of the structural behavior. The first that comes to mind in determining the earthquake performance of structures is the FEMA 356 (2000) documentation that sets limits for plastic hinge rotations in the components of structures. These limits generally are given according to empirically based “expert” opinion unlike in TEC 2007. It is obvious that experimental and analytical results are necessary for determining the validity of the criteria specified in specifications and codes.

Choi et al. (2003) searched the vulnerability information of bridges according to the HAZUS 97 damage states for bridges and obtained fragility curves under synthetic ground motions for Central and Southeastern United States to obtain a good bridge type for design.

Rota et al. (2008) used advanced nonlinear regression methods to be able to obtain the typological fragility curves according to the post – earthquake survey data, collected in the areas affected by the most relevant Italian earthquakes of the last three decades.

Shear wall building behavior under earthquake effects and their performance should be observed from past earthquakes and experimental results. It has been noted that there is almost no collapse under earthquake effects. However, despite the inadequate number of researches done on the performance limits of shear wall, indicates different results (Wallace and Moehle, 1992; Moehle, 1996).

Ay and Erberik (2008) investigated seismic safety of the low- and mid – rise structures, which is approximately 75 percent of the total building stock in

Turkey by generating the fragility curves. They used moment resisting reinforced concrete frames with different numbers of stories. The Latin Hypercube Sampling was used for the selection of suitable data for whole population in general and attenuation relationships used for near fault, far fault effects.

The vulnerability analysis of buildings that undergo three dimensional seismic effects such as torsion is another topic of current interest. The main problem of these types of buildings is the assessment criteria, namely damage indexes. Jeong and Elnashai (2006a, 2006b) proposed a new three dimensional damage index which takes into account the bidirectional and torsional response effects. The main purpose in their study is to estimate three dimensional damage capacity indexes, namely the global response of a structure under earthquake effects by its simple frame systems. Aziminejad and Moghadam (2009), investigate the different configurations of centers of stiffness and strength to generate the fragility curves. They also indicated that these configurations can be used as a new reference point for identifying acceptable limits of eccentricity.

Akkar et al. (2005) derived the fragility curves for most vulnerable building types in Turkey. Their study indicates also the limit state determination for the vulnerability analysis that will be discussed in detail in the following chapter.

1.3.Object and Scope

The main purpose of this study is to understand the behavior of the torsion effects in a scaled shear wall structure that has been tested in France.

Initially, the response of the numerical model is verified through comparisons with experimental results. Then, a parametric study is conducted to examine the goodness of the fit of the predictions and to identify the parameters that effect nonlinearity for reinforced concrete shear wall structure. This part of the study is a validation case. Eventually, the vulnerability analysis is done according to the given data in the SMART 2008 Phase 2 report.

The fragility analysis of the frame systems are studied by many researchers, however, the suitable fragility curve fitting for the shear wall structures is a current issue.

The fragility analyses were done for different seismic ground motion indicators under bi-axially loaded seismic excitations.

To give a brief introduction to this thesis, it is necessary to mention the contents of each chapter. Chapter 2 is devoted to information about the modeling specifications and experimental results of the SMART 2008 specimen.

In Chapter 3, the results of numerical model prepared in ANSYS are compared with experimental results in terms of displacement values at different points on the same floor level.

In Chapter 4, sensitivity analysis is investigated to understand which parameter affects the behavior most.

In Chapter 5, fragility curves of the specimen are calculated for different seismic ground motion indicators such as PGA, PGV, PGD and CAV. Maximum inter-story drifts are used in fragility analysis as damage indicator.

In Chapter 6, the summary of the results is discussed and the conclusions obtained from this study are recaptured. Finally, the recommendations are listed to make this study much more relevant to practice.

CHAPTER 2

MODEL BUILDING AND ITS SPECIFICATIONS

2.1. SMART 2008 Experimental Program

In the interest of assessing the seismic three dimensional effects (such as torsion) and non-linear response of reinforced concrete buildings, Commissariat à l'Energie Atomique (CEA) and Electricité de France (EDF) has launched in 2008 the "*SMART-2008*" international project (*Seismic design and best-estimate Methods Assessment for Reinforced concrete buildings subjected to Torsion and non-linear effects*).

The main purpose of this project is to compare various modeling methods proposed by researchers or engineers to approach a reliable prediction and assessment for the behavior of a reinforced concrete building designed according to the French nuclear practices by testing a mock up representation.

A reduced scaled model (scale of 1/4th) of a nuclear reinforced concrete building was tested on the AZALEE shaking table at Commissariat à l'Energie Atomique (CEA Saclay, France).

The loadings on the model ranged from very low seismic motions to five times the design level.

There were two phases for the SMART-2008 project. The first one consisted of two separate parts, Phase 1A and Phase 1B (RAPPORT DM2S, 2007 and RAPPORT DM2S, 2009). Phase 1A was a contest open to teams from practicing structural engineering as well as the academic and research community worldwide. Phase 1B was related only with the benchmark study. The main aim was to allow the participants to improve their best estimate predictions by updating their model with information available for some of the seismic runs, so as to perform new analyses at higher loading levels.

The second phase of the project was dedicated to the variability, sensitivity and vulnerability analysis, by using numerical models of the SMART specimen carried out in the previous stages.

In this thesis, Phase 1B and Phase 2 of the SMART-2008 project are studied. The Phase 1B is only used for validation of the mathematical model by comparing with experimental results. This is not done in all of its details. The main scope of this thesis is Phase 2 and the details of the two parts will be given in the following pages.

2.1.1. Geometric and Material Properties and Additional Loadings

2.1.1.1. Geometric Properties

The model building, which was studied is a 1/4 scale trapezoidal-plan, three-story reinforced concrete structure. It is composed of three walls forming a U shape, a column and a beam dividing the slab in two parts.

The height of the floor levels are, accordingly, 1.25 m, 2.45m, and 3.65 m from the basement. The thickness of the slab is 10 cm. The geometrical details of column and walls are shown in Figure 2.1 - 2.2 and given in the Table 2.1.

Table 2-1 Dimension of Structural Elements

	Length (m)	Thickness (m)	Height (m)
Wall (#V01+#V02)	3.1	0.1	3.65
Wall #V03	2.55	0.1	3.65
Wall #V04	1.05	0.1	3.65
Beam	1.45	0.15	0.325
Column	3.8	0.2	0.2

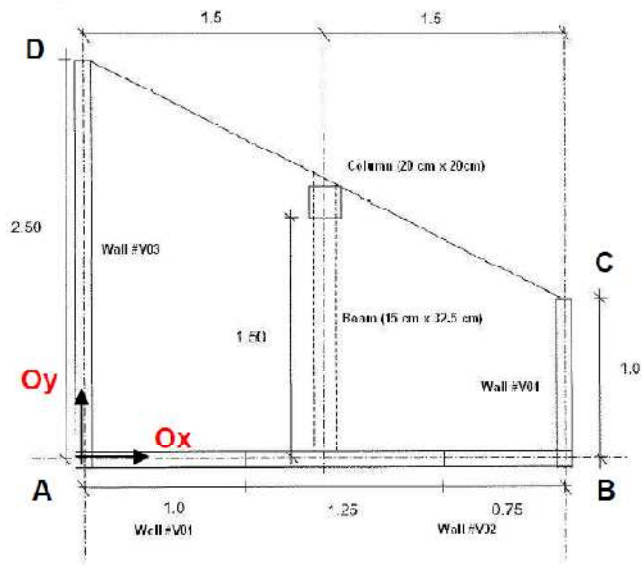

Figure 2-1 Plan drawing of the SMART-2008 Specimen

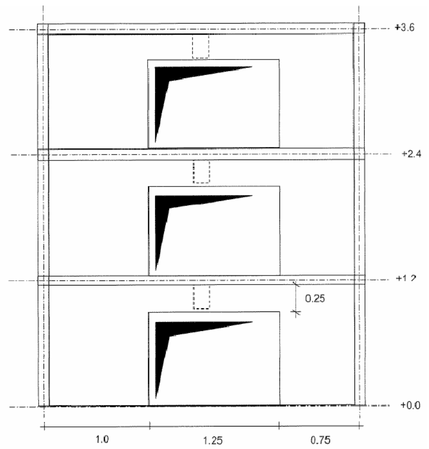

Figure **2**-2 Elevation of wall #V01 & #V02

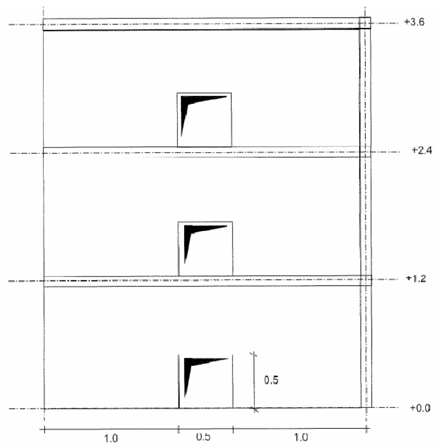

Figure 2-3 Elevation of wall #V03

The wall's foundations were made of a continuous reinforced concrete footing. The footing was 38 cm wide, 15 cm high and lay on a 62*2 cm high steel plate. The reinforced concrete column was directly anchored on a 62 by 62 cm steel plate. The steel plates were bolted on AZALEE shaking table with M36 bolts. In the analysis, the effect of the shaking table will be ignored

2.1.1.2. Material Properties

The following information was given for the blind predictive benchmark. Compressive and tensile strength of the concrete, elasticity modulus of concrete and Poisson's ratio are given in Table 2.2.These values were representative for the French Nuclear Plants.

Table 2-2 Materials characteristics

f_{cj} (MPa)	f_{tj} (MPa)	E_c (MPa)	ν_c	ν_s
30	2.4	32000	0.2	0.3

The steel reinforcement has been defined according to the European design codes (EC2). Steel reinforcement FeE500-3 is used in details and its yielding stress is 500 MPa.

2.1.1.3. Additional Loading

To reproduce the structural and additional masses of the real structure; additional loads were applied on the slab at each level. The total mass of the specimen was estimated at about 44.29 T in the SMART 2008-Phase 2 Contest Report (RAPPORT DM2S, 2009). Additional loadings on the floor levels are given below.

Additional loading on the 1st slab ~ 11.60 T

Additional loading on the 2nd slab ~ 12.00 T

Additional loading on the 3rd slab ~ 10.25 T

The average density of the reinforced concrete of the structure was taken 2460 kg/ m3 as given in the SMART 2008 Phase 2 report (RAPPORT DM2S, 2009).

2.1.2. Shaking Table

The Azalée shaking table can be considered as a rigid block with a total mass of 25 t fixed to eight hydraulic jacks (4 in the horizontal direction and 4 in the vertical direction –Figure 2.4).

The actuators controlling the horizontal motion of the table are located at 1.02 m below the upper face of the shaking table, while the centre of gravity is 0.60 m below this level.

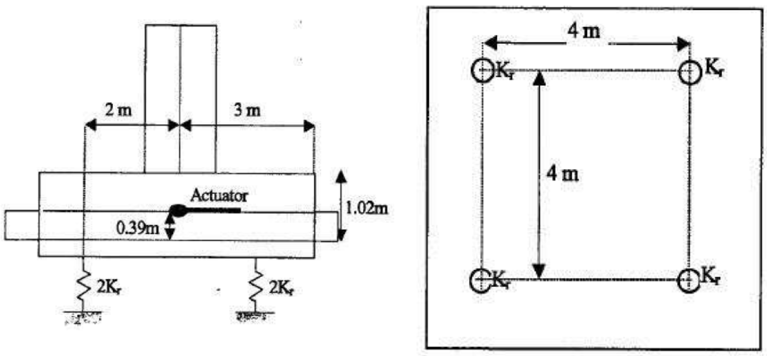

Figure 2-4 Simplified model of the shaking table AZALEE (elevation and top view)

All the jacks are active systems, which means that they are controlled during the experiment. The spring constant value of 215 MN/m could be used for each vertical jack to simulate the foundation- shaking table connection. The centers of gravity of the table and the model are given in Table 2.2.

Table 2-3 Centre of gravity for the system coordinates presented in Figure 2.5

	x_g (m)	y_g (m)
Table	1.50	0.94
Model	1.28	0.92

Because of the complexity of the hydraulic jack system used (active system), it is difficult to predict the shaking table behavior and therefore it is not recommended to consider the model/table interaction at this stage. Therefore shaking table is not modeled. Position of the model on the shaking table is represented in Figure 2.5.

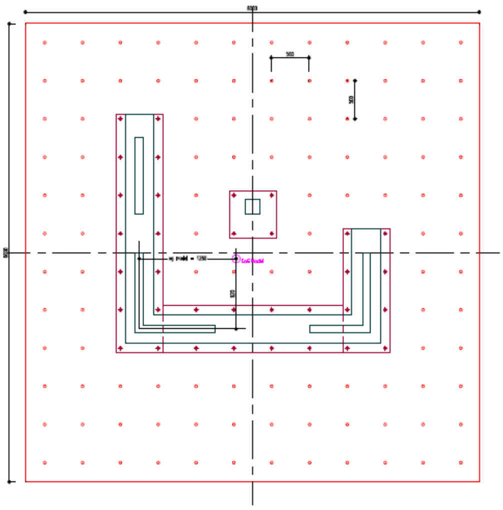

Figure 2-5 Position of the specimen on the shaking table

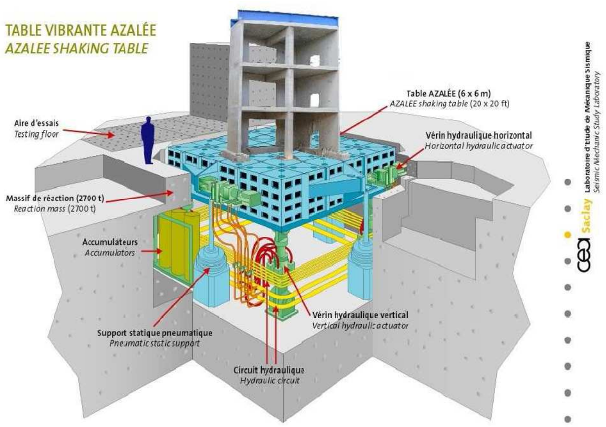

Geometry and performances of table Azalée	
Dimensions of table	6x6 m
Mass of table	25 tons
Maximum mass of specimen	100 tons
Maximum height of the specimen	12 m
Excitement axis	Tri-axial
	X-Y-Z
	6 degrees of freedom
Strength of actuators	X: 2 x 1000 kN
	Y: 2 x 1000 kN
	Z: 4 x 1000 kN
Maximum displacement	X ± 125 mm
	Y ± 125 mm
	Z ± 100 mm
Maximum speed	Seism: 1 m/s
	Sinus: 0.7 m/s
Maximum acceleration (specimen: 100 tons)	1 g
Excitement frequencies	0 to 100 Hz

Figure 2-6 Position of the specimen on the shaking table (3D) and detailed information about the shaking table.

2.1.3. Experimental Program and The Summary of Results

In Phase 1 (RAPPORT DM2S, 2007), three real and 10 synthetic accelograms were used. The details of the accelerogram sets are given in Table 2.4 and Figure 2.7. The earthquake motions were applied in both orthogonal directions.

Table 2-4 Real and synthetic accelerogram sets

No		Real Earthquakes	M	Dist.	Acc .(g)
1	REA1	UMBRO-MARCH(AS)	5.2	23	0.05
2	REA2	MANJIL(AS)	4.4	14	0.05
3	REA3	UMBRO-MARCHIGIANO	5.9	81.4	0.05
		Synthetic Earthquakes			
4-13	Derived according to the response spectrum and scaled from 0.1 g to 1.0 g				

The specimen was a reproduction of a typical nuclear building sub-component at a scale of ¼. Thus, some assumptions were made to perform the experiments. In order to keep the same acceleration (gravity load cannot be changed) as well as the same material properties, the scaling of ¼ of the structure’s dimension implies to scale the mass by 1/16 and the time by ½. The other scaling factors of parameters are given in Table 2.5.

Table 2-5 Scaling factors of the parameters

	Scaling factor
Length (m)	4= (λ)
Mass (kg)	16=(λ^2)
Time (sec)	2=($\lambda^{1/2}$)
Acceleration (g*)	1
Stress (MPa)	1
Frequency (Hz)	0.5
Force (N)	16
Steel reinforcement area (m^2)	16
* 1 g = 9.81 m/s^2	

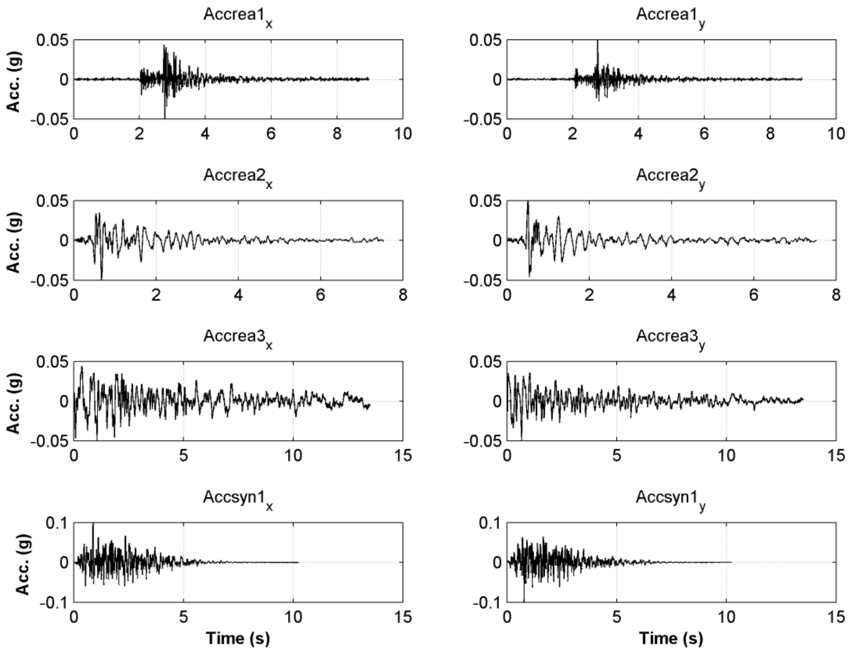

Figure 2-7 Ground motion data used in the experiments

2.1.3.1. The Summary of Results

The experimental results of specimen were given at predetermined points (Figure 2.8). The results proposed in this study are the summary of experimental studies which is part of Phase 1 of the SMART 2008 project.

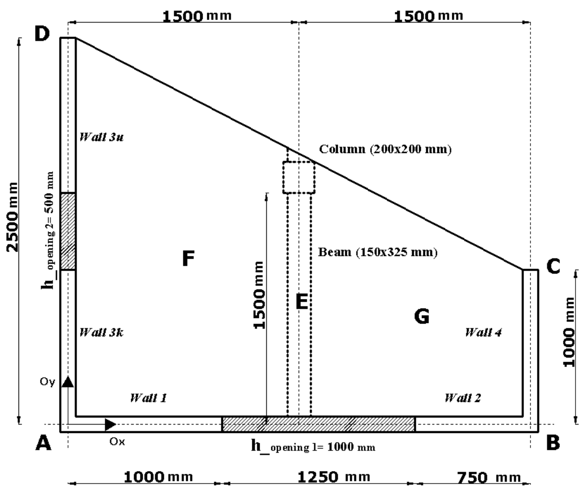

Point	X (m)	Y (m)
A	0	0
B	3	0
C	3	1
D	0	2.5
E	1.5	0.75
F	0.75	1.03
G	2.25	0.65

Figure 2-8 TheIdentification of locations where results have to be computed and result locations in the system coordinates

Figure 2-9 SMART Specimen, unloaded and fully loaded (Lermitte et al., 2008)

Figure 2-10 Examples of local instrumentation of SMART specimen

The experimental results were obtained from transducers and gages (Figure 2.10). Local behavior of the specimen was monitored at several locations. In all 42 steel gages were placed on bars at the foundations, walls and lintels. 42 concrete gages were placed at the base of walls and on lintels of the 1st level, 55 displacement transducers were placed on walls and lintels and 6 crack opening transducers were placed at the base of walls #3 and #4.

Time histories of the measured displacement responses at 3rd floor level for Run 9 and Run 11 are represented as given in Figure 2.11. The measured maximum displacement is in Point D and 15 mm in Run 9 and 17 mm in Run 11. In the X direction, A-B, and C-D; in the Y direction, A-D and B-C were close to each other.

Ground motion sets applied to the mock – up consecutively. Thus, the damage increased cumulatively. The graphs represented in Figure 2.12 to 2.14 are the maximum measured values from the experimental study.

Not only the measured maximum acceleration, but also the measured maximum displacement magnitudes increase with the increasing run-levels. Building response is dominant in the X direction. The measured floor acceleration magnitudes are closely similar at specified points in X direction for low seismicity. However, increase in acceleration level of the applied seismic excitation results in separation on the responses of the points at the same floor level.

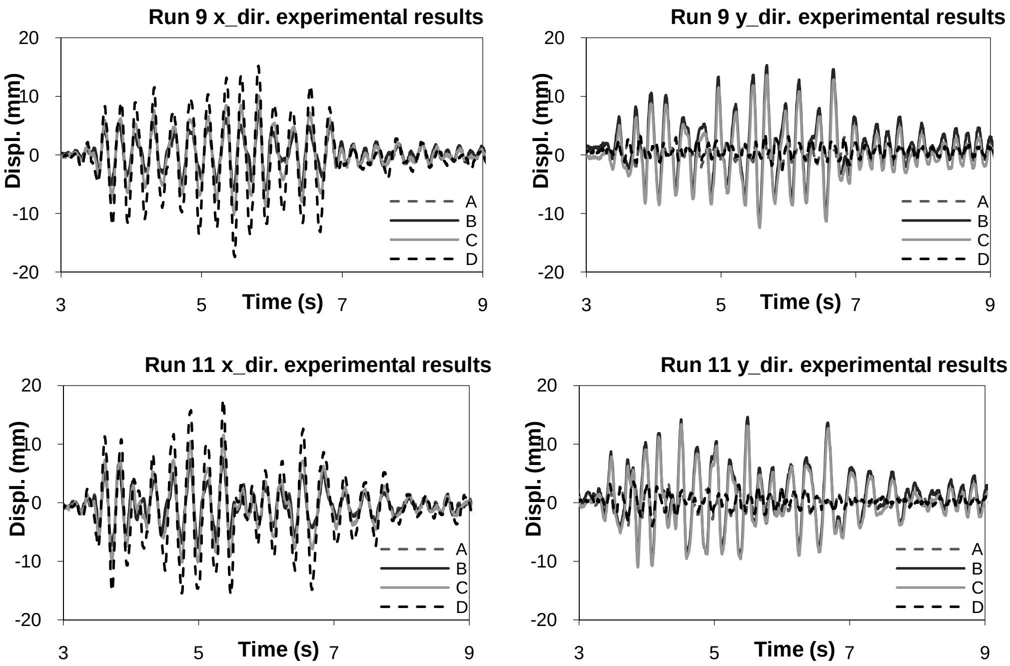

Figure 2-11 Run 9 and Run 11 displacement response at 3rd Floor

The displacement response also increased in a similar way as the acceleration response and changes at different points on the same floor level (Figure 2.11 – 2 .13). In Run 5, the highest response is measured at Point D at the first floor level for the X and Y directions. The difference is so much when the results compared with the other points defined in the same floor level. In Run 13, transducers measured the highest response in the Point D for Y direction similarly at first floor level.

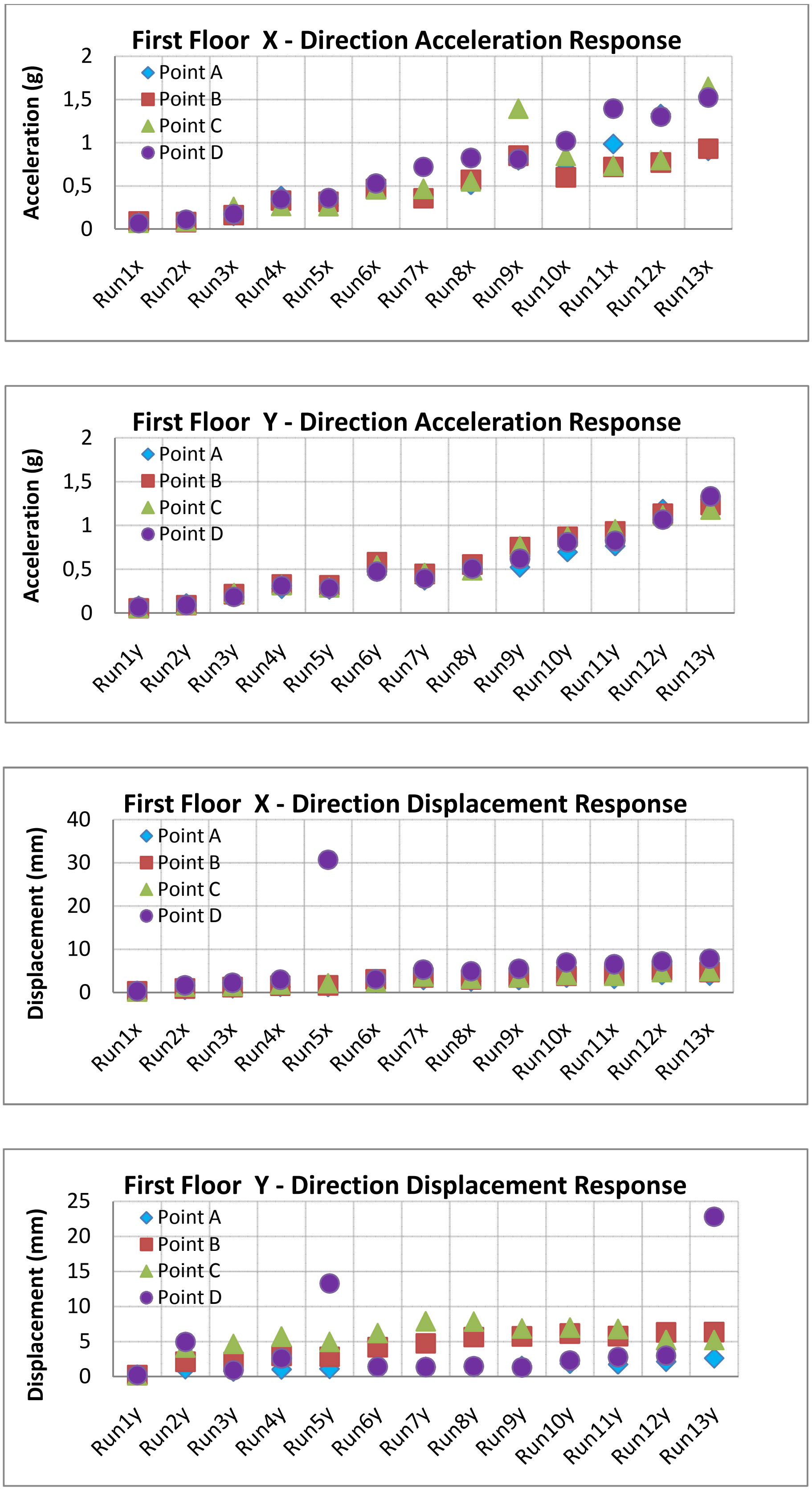

Figure 2-12 Maximum measured relative acceleration and displacement response at first floor

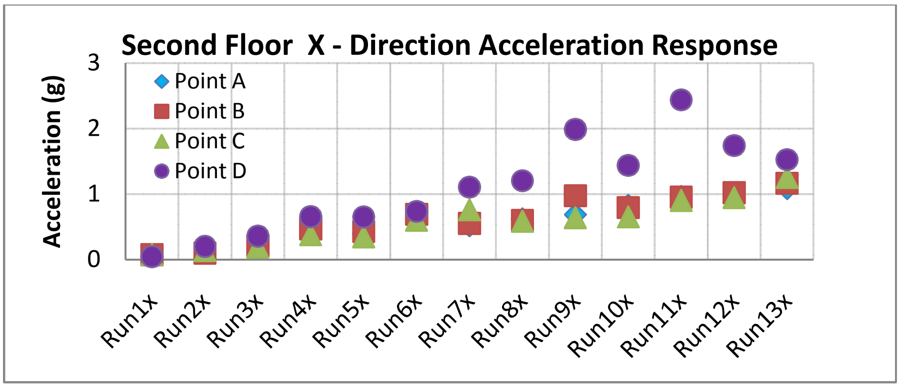

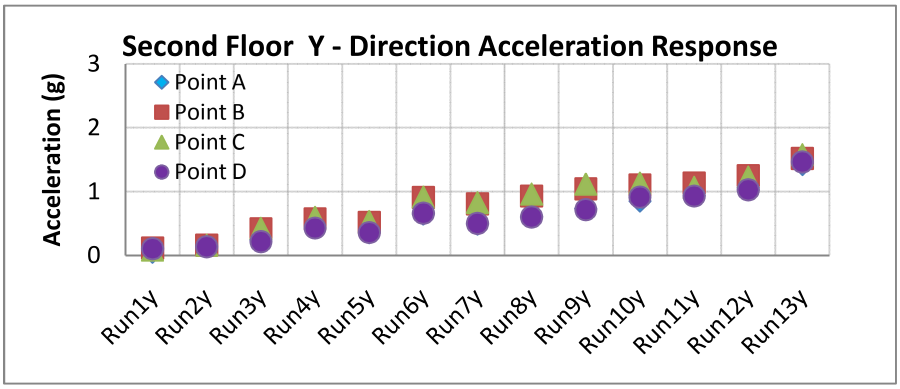

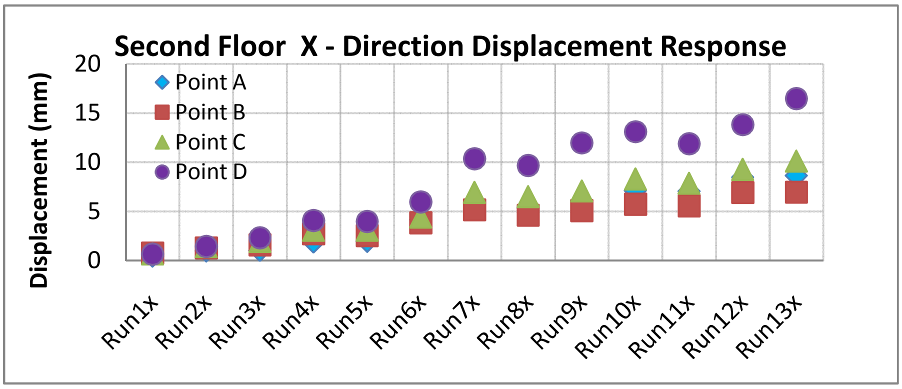

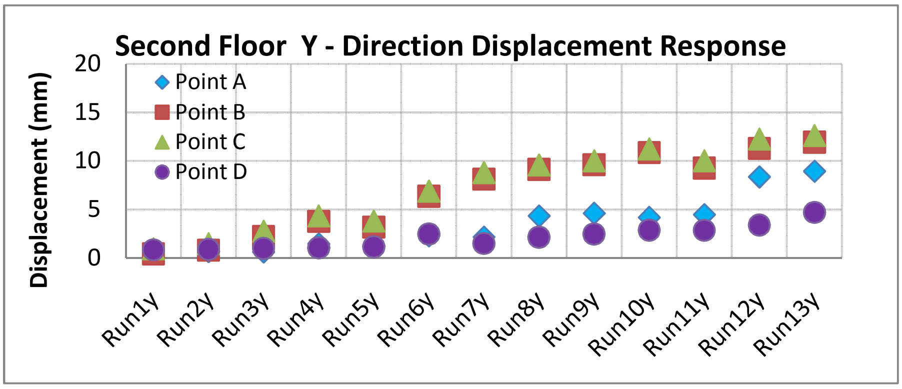

Figure 2-13 Maximum measured relative acceleration and displacement response at second floor

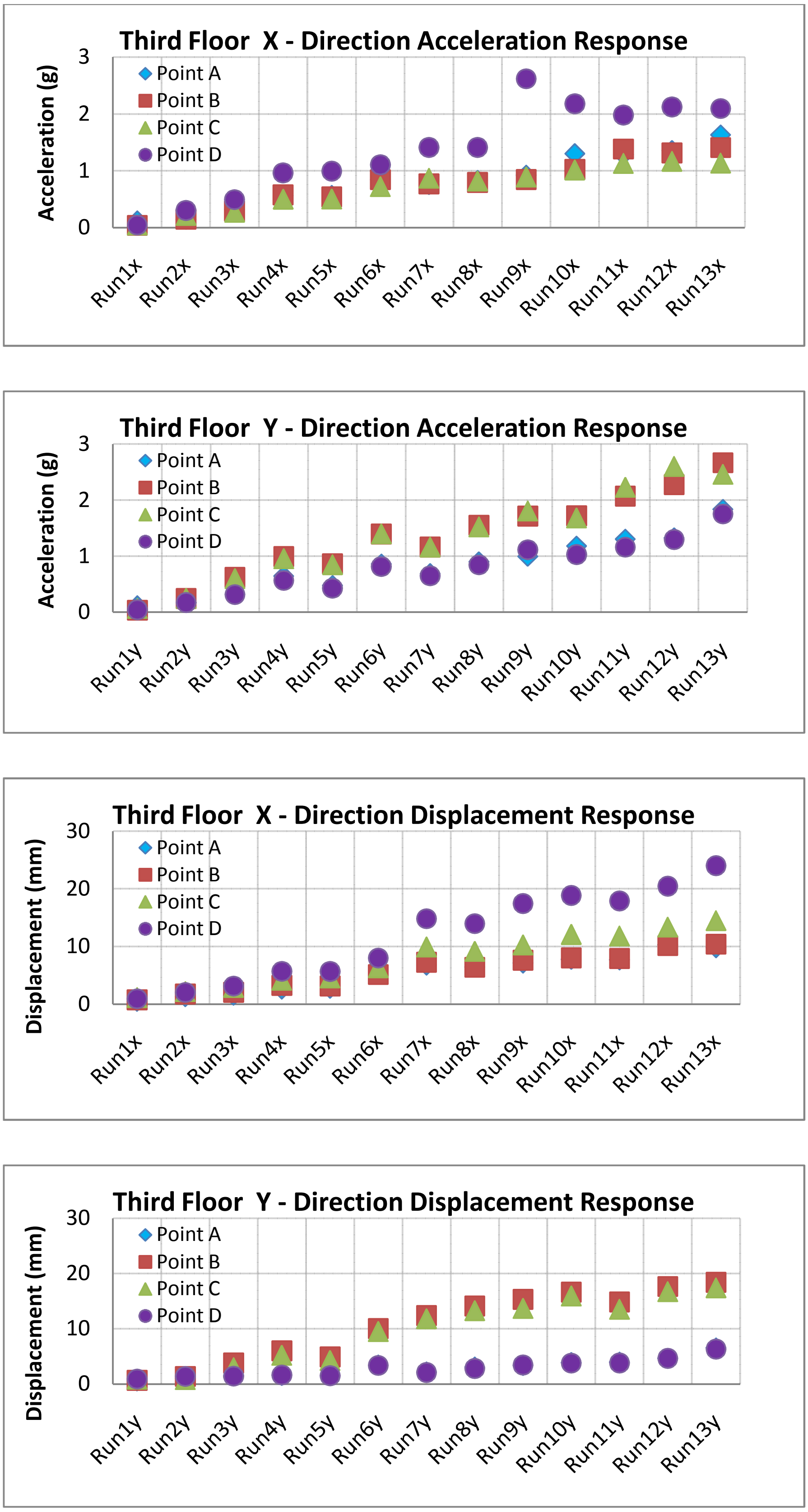

Figure 2-14 Maximum measured relative acceleration and displacement response at third floor

Figure 2.15 represents the relative horizontal displacements of each corner of the structure at 3rd floor under 0.1 g seismic test. Displacements have been scaled to exhibit the structure behavior. Mass center and shear center are located on the figure (Lermitte et al., 2008). Blue data clouds represent the top floor horizontal displacement time history data under 0.1g (Run 4) seismic test.

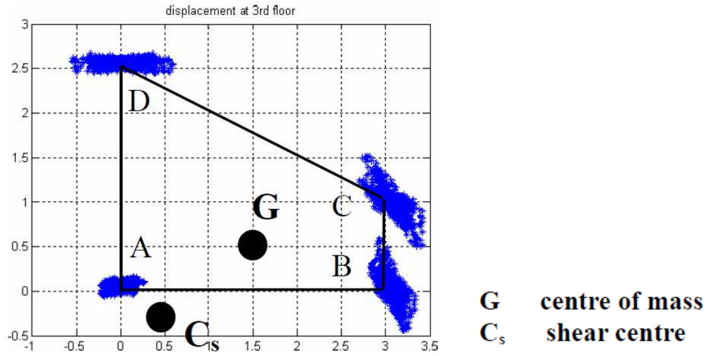

Figure 2-15 Top floor horizontal displacement – 0.1 g (Run 4) seismic test (Lermitte et al., 2008)

The modal analysis result obtained from the first seismic test in which PGA = 0.05 g (Table 2.6).

Table 2-6 Initial natural frequencies (Lermitte et al., 2008)

	f (Hz)	Type
Mode 1	6.24	Bending (Ox)
Mode 2	7.86	Bending (Oy)
Mode 3	15	Torsion

The structure did not suffer damage from the first 5 seismic tests (Run1-5). One of these tests was the design level. No crack openings were observed. The condition after the last run of the structure is shown in Figure 2.16. Crack patterns during the seismic excitation are given in Figure 2.17. It can be observed from the Figure 2.17 that the relatively wide cracks in the structure were obtained after 0.5 g seismic excitation level.

Figure 2-16 Two figure from the last condition of the specimen

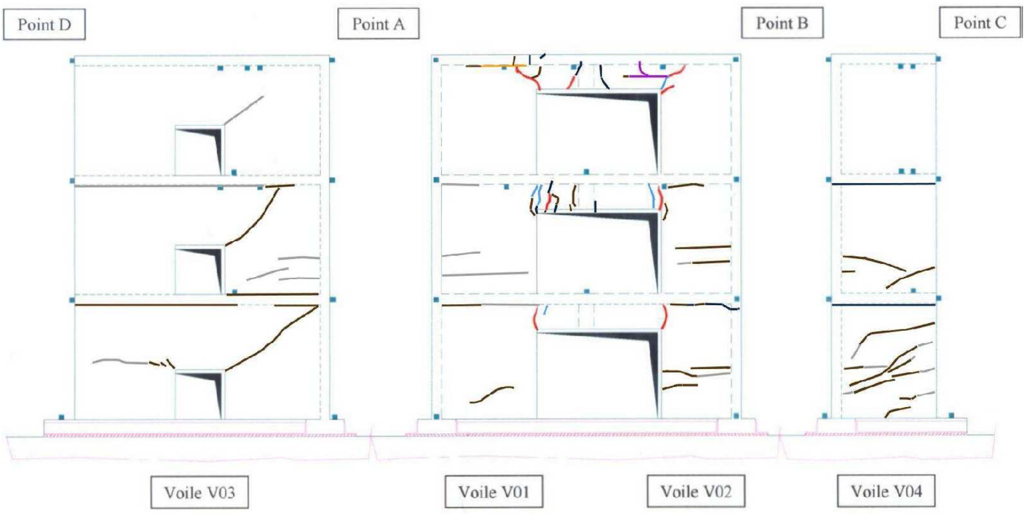

Legend	Red	Green	Blue	Black	Pink	Orange	Brown	Grey
Cracks	Before	During	During	During	During	During	During	During
Acc (g)	0.3	0.35	0.55	0.56	0.67	0.77	1.06	1.13

Figure 2-17 Cracks after the seismic tests

2.2. Experimental Results and Comparison with TEC 2007

Experimental results were compared with strain values and torsional irregularity coefficient defined in the TEC 2007. In Figures 2.18-2.21, measured strain values from the experimental results were compared with the TEC 2007 Immediate Occupancy strain values for both compression and tensile damages and none of them surpassed these damage levels. Calculated strains were the average values of these points. Because there were no measured strain values from the experiments, only displacements and acceleration time-histories were available. According to the TEC 2007, the absolute displacements ratio between cross two points in the plan of the structure is a measure of torsional irregularity. If these values passes the 1.2 critical value means that system includes torsion behavior. In Figures 2.22, torsional irregularity coefficients were investigated and most of the results passed the 1.2 critical value.

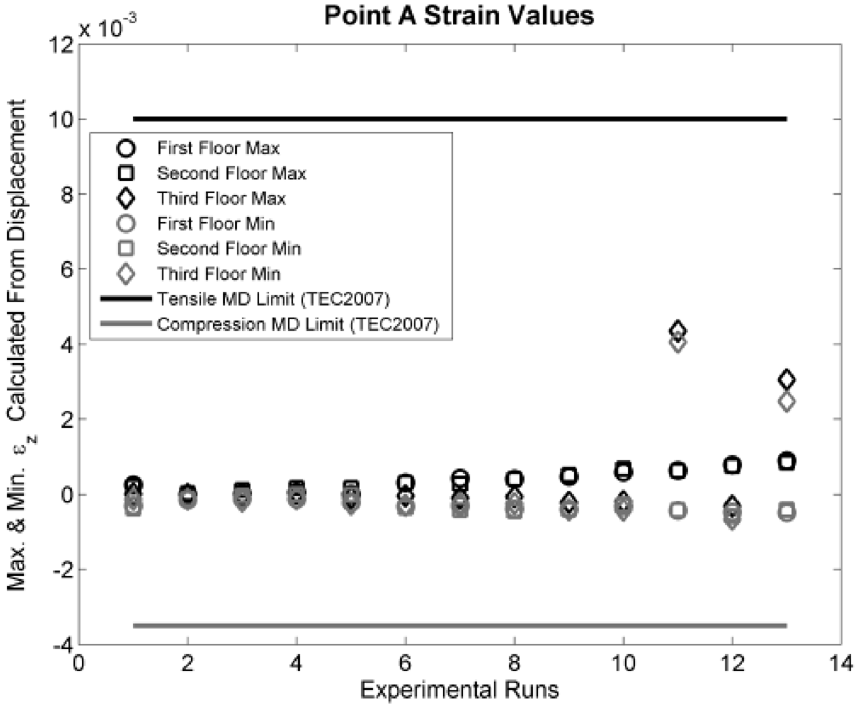

Figure 2-18 Calculated strain values from the experimental results compared with the TEC 2007 compression and tension strain values for Point A

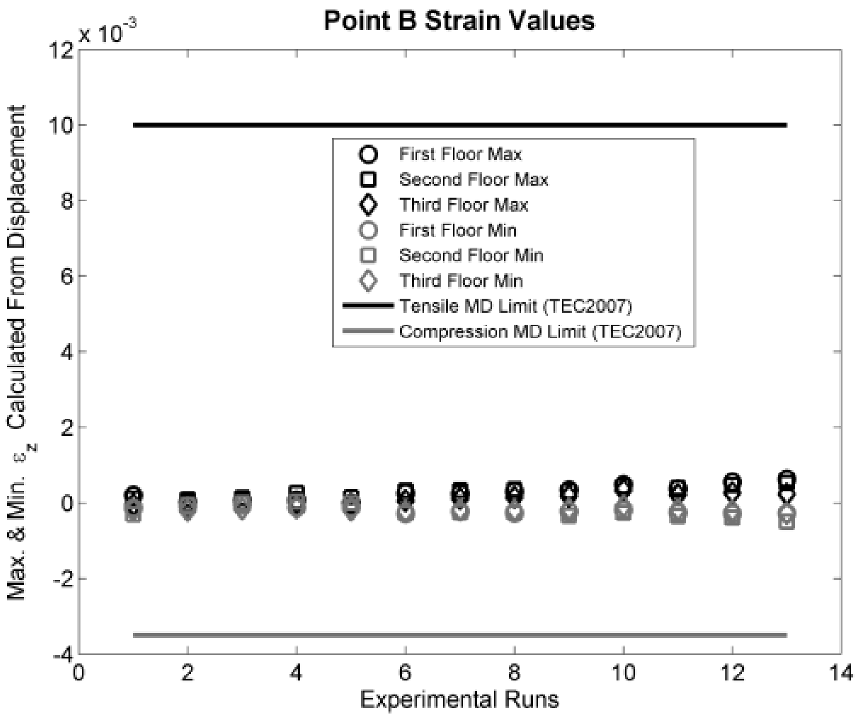

Figure 2-19 Calculated strain values from the experimental results compared with the TEC 2007 compression and tension strain values for Point B

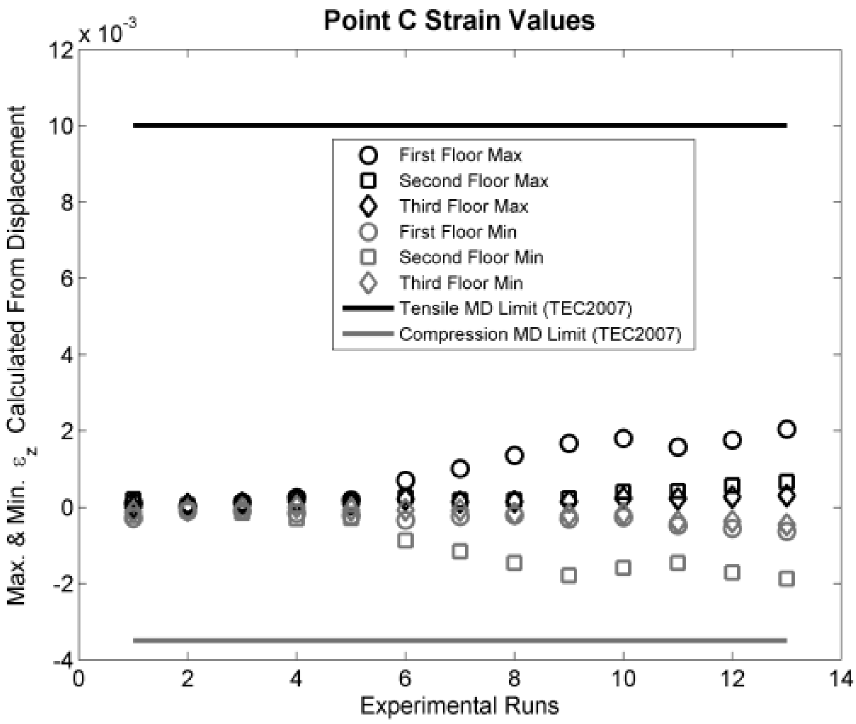

Figure 2-20 Calculated strain values from the experimental results compared with the TEC 2007 compression and tension strain values for Point C

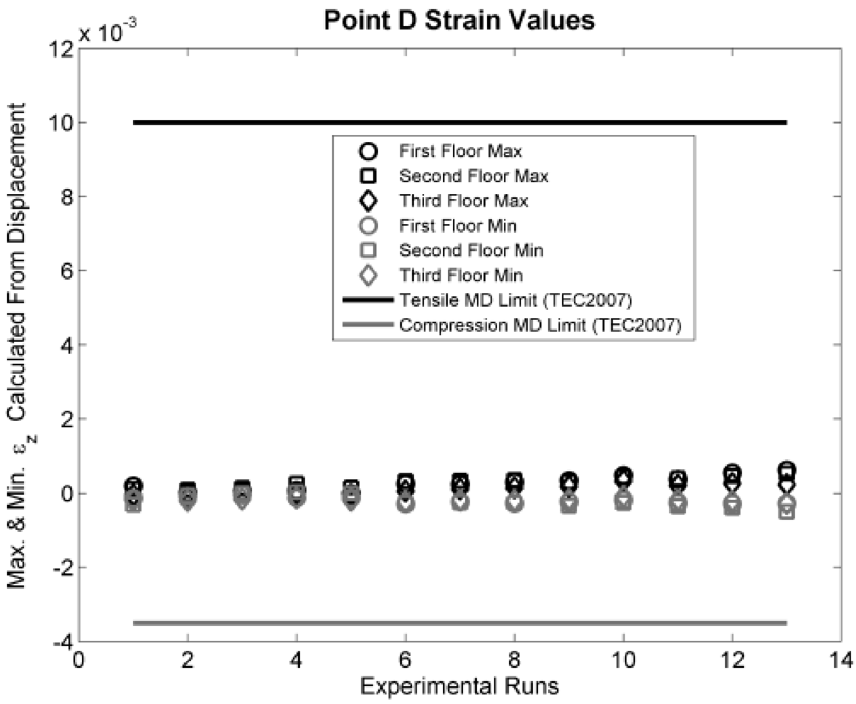

Figure 2-21 Calculated strain values from the experimental results compared with the TEC 2007 compression and tension strain values for Point

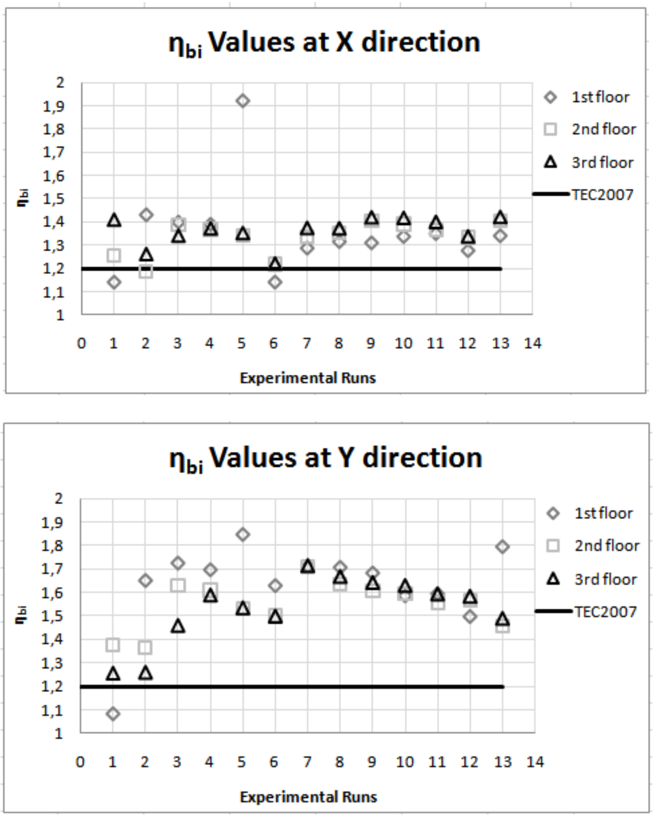

Figure 2-22 Torsional Irregularity check according to TEC 2007

2.3. Modeling of the Specimen

In the interest of obtaining a reasonably accurate result from the analytical model, the system was modeled using the procedures of finite element method. The ANSYS software was used (ANSYS R 12.0). ANSYS is a widespread tool for research.

2.3.1. Element Types Used in the Analysis

2.3.1.1. 3-D Reinforced Concrete Element

Three–dimensional–modeling approach was chosen for analyzing the specimen. The element type chosen for this purpose is SOLID 65 (3-D Reinforced concrete element). It was preferred for the modeling of concrete solids with or without reinforcing bars. Element specifications are explained in detail in ANSYS manual. The element is defined by an eight node solid having three translational degrees of freedom at each node. Up to three different rebar specifications may be defined. Reinforcement in concrete can be added to the model by the "Smeared" approach for SOLID 65 or using the LINK 8, three dimensional truss elements. In this study, the smeared reinforcement method was used (Figure 2.23).

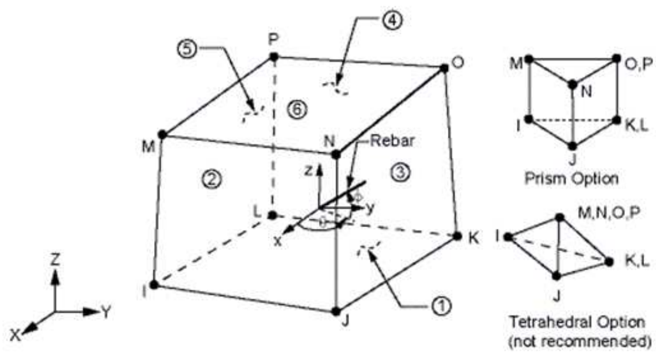

Figure 2-23 SOLID 65 (3-D Reinforced Concrete Element) (ANSYS R12.0)

The most important aspect of this element is the treatment of nonlinear material properties. The concrete is capable of cracking (in three orthogonal directions), crushing, plastic deformation, and creep. The rebar are capable of tension and compression, but not shear. They are also capable of plastic deformation and creep. (ANSYS R 12.0)

2.3.1.1.1. The Mathematical Description of SOLID 65 Element

SOLID 65 is an eight-noded isoparametric brick element. Linear interpolation functions are used for the geometry and the displacements with the eight integration points (2x2x2). The interpolation function is given as below:

$$N_i = \frac{1}{8}(1 \pm \xi)(1 \pm \eta)(1 \pm \zeta) , \qquad \text{where } i \in 1, \dots, 8 \qquad (2.1)$$

According to the given interpolation function, the nodal displacements (u_i, v_i, w_i,) calculated at the nodes are interpolated at any point (ξ, η, ζ) within the element as

$$u = u_1 N_1 + u_2 N_2 + \dots + u_8 N_8$$

$$v = v_1 N_1 + v_2 N_2 + \dots + v_8 N_8 \qquad (2.2)$$

$$w = w_1 N_1 + w_2 N_2 + \dots + w_8 N_8$$

Using the Gauss integration scheme of 2x2x2 the displacement field in the element is calculated.

2.3.1.1.2. Assumptions and Restrictions for SOLID 65 Element

Cracking is permitted in three orthogonal directions at each integration point. The orientation of the reinforcement and local coordinates are defined in Figure 2.24. If cracking occurs at an integration point, the cracking is modeled through an adjustment of material properties which effectively treats the cracking as a “smeared band” of cracks, rather than as discrete cracks.

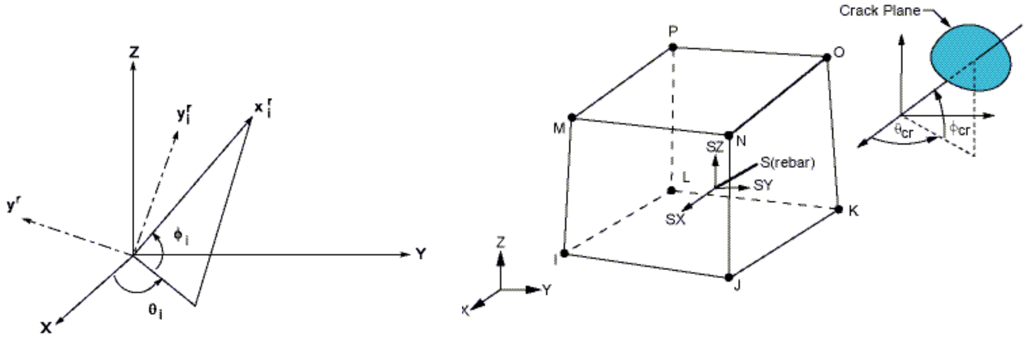

Figure 2-24 Reinforcement Orientation in SOLID 65

In addition to cracking and crushing, the concrete may also deform plastically, with the Drucker-Prager failure surface being most commonly used. In this case, the plasticity check is done before the cracking and crushing checks.

2.3.1.1.3. Linear Behavior of Concrete for SOLID 65 Element

The stress – strain relationship for this material is given in Equation (2.3).

$$[D] = \left(1 - \sum_{i=1}^{N_r} v_i^R\right)[D^c] + \sum_{i=1}^{N_r} v_i^R \ [D^r]_i \tag{2.3}$$

N_r = number of reinforcing materials (maximum of three, all reinforcement is ignored if M_1 is zero. Also, if M_1, M_2, or M_3 equals the concrete material number, the reinforcement with that material number is ignored)

v_i^R = ratio of volume of the reinforcing material I to the total volume of element

$[D^c]$ = stress-strain matrix for concrete,

$[D^r]_i$ = stress-strain matrix for reinforcement i,

M_1, M_2, M_3 = material numbers associated of reinforcement (input as MAT_1, MAT_2, and MAT_3 as real constants

The $[D^c]$ matrix is derived by specializing and inverting the orthotropic stress-strain relations defined by Equation (2.4) to the case of an isotropic material, Equation (2.5).

$$[D]^{-1} = \begin{bmatrix} 1/E_x & -v_{xy}/E_x & -v_{xz}/E_x & 0 & 0 & 0 \\ -v_{yx}/E_y & 1/E_y & -v_{yz}/E_y & 0 & 0 & 0 \\ -v_{zx}/E_z & -v_{zy}/E_z & 1/E_z & 0 & 0 & 0 \\ 0 & 0 & 0 & 1/G_{xy} & 0 & 0 \\ 0 & 0 & 0 & 0 & 1/G_{yz} & 0 \\ 0 & 0 & 0 & 0 & 0 & 1/G_{zx} \end{bmatrix} \tag{2.4}$$

$$[D^c] = \frac{E}{(1+v)(1-2v)} \begin{bmatrix} (1-v) & v & v & 0 & 0 & 0 \\ v & (1-v) & v & 0 & 0 & 0 \\ v & v & (1-v) & 0 & 0 & 0 \\ 0 & 0 & 0 & \frac{(1-2v)}{2} & 0 & 0 \\ 0 & 0 & 0 & 0 & \frac{(1-2v)}{2} & 0 \\ 0 & 0 & 0 & 0 & 0 & \frac{(1-2v)}{2} \end{bmatrix} \tag{2.5}$$

E = Young's modulus for concrete

ν = Poisson's ratio for concrete

2.3.1.1.4. Linear Behavior of Reinforcement in the SOLID 65 Element

The orientation of reinforcement in ANSYS (ANSYS R 12.0) is defined in Figure 2.24. The element coordinate system is denoted by (X, Y, Z) and (x_i^r, y_i^r, z_i^r) are defined for the coordinate system for reinforcement type *i* (Equation (2.6)).

$$\begin{pmatrix} \sigma_{xx}^r \\ \sigma_{yy}^r \\ \sigma_{zz}^r \\ \sigma_{xy}^r \\ \sigma_{yz}^r \\ \sigma_{xz}^r \end{pmatrix} = \begin{bmatrix} E_i^r & 0 & 0 & 0 & 0 & 0 \\ 0 & 0 & 0 & 0 & 0 & 0 \\ 0 & 0 & 0 & 0 & 0 & 0 \\ 0 & 0 & 0 & 0 & 0 & 0 \\ 0 & 0 & 0 & 0 & 0 & 0 \\ 0 & 0 & 0 & 0 & 0 & 0 \end{bmatrix} \begin{pmatrix} \varepsilon_{xx}^r \\ \varepsilon_{yy}^r \\ \varepsilon_{zz}^r \\ \varepsilon_{xy}^r \\ \varepsilon_{yz}^r \\ \varepsilon_{xz}^r \end{pmatrix} = [D^r]_i \begin{pmatrix} \varepsilon_{xx}^r \\ \varepsilon_{yy}^r \\ \varepsilon_{zz}^r \\ \varepsilon_{xy}^r \\ \varepsilon_{yz}^r \\ \varepsilon_{xz}^r \end{pmatrix} \tag{2.6}$$

E_i^r = Young modulus of the reinforcement type *i*.

The only nonzero component in Equation 2.5 is σ_{xx}^{r} in the axial stress in the x_i^r direction. The relationship between the (X, Y, Z) coordinate system (Figure 2.24) is indicated in the Equation (2.7).

$$\begin{pmatrix} X \\ Y \\ Z \end{pmatrix} = \begin{pmatrix} \cos\theta_i \cos\varphi_i \\ \sin\theta_i \cos\varphi_i \\ \sin\theta_i \end{pmatrix} x_i^r = \begin{pmatrix} e_1^r \\ e_2^r \\ e_3^r \end{pmatrix} x_i^r \qquad (2.7)$$

θ_i = Angle between the projection of the x_i^r axis on XY plane and the X axis

φ_i = Angle between the x_i^r axis and the XY plane

e_i^r = Direction cosines of x_i^r and element X, Y, Z axis

Transformation of the reinforcement material is done according to Equation (2.8).

$$[D^R]_i = [T^r]^T [D^r]_i [T^r] \qquad (2.8)$$

Transformation matrix for D^r is used in ANSYS was proposed by Schnobrich (1973).

2.3.1.1.5. Non - linear Behavior of Concrete for SOLID 65 Element

The material matrix is capable of plasticity, cracking, creep and crushing with the CONCRETE material type and multi-linear hardening models.

The cracks in the elements are arranged with the β_t and β_c are the open and closed shear transfer coefficients for the plasticity model and ANSYS has 16 possible combinations for the rearrangement of the cracked section stress – strain relationship (Figure 2.25). After cracking, a certain amount of stress relaxation is included in the element formulation with the constant T_c. R_t is the secant slope. It diminishes to zero when it converges to solution.

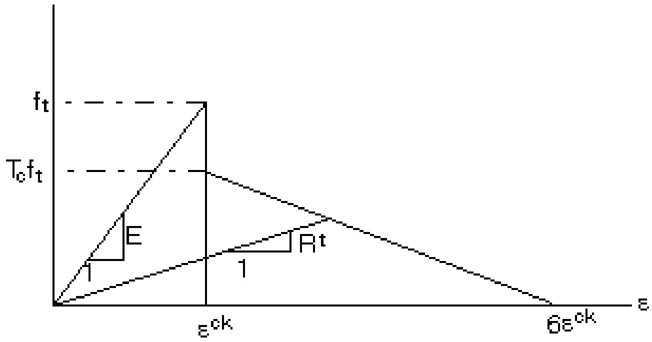

Figure 2-25 Strength of Cracked Condition

The superscript “ck” is used for the stress strain relation that refers to a coordinate system parallel to principal stress directions with the x^{ck} axis perpendicular to the crack face. f_t is the uniaxial cracking tensile stress and T_c is the multiplier for tensile stress relaxation (default to 0.6) Example for the stress-strain relations for concrete, if it has cracked in all three directions:

$$[D_c^{ck}] = E\begin{bmatrix} \frac{R^t}{E} & 0 & 0 & 0 & 0 & 0 \\ 0 & \frac{R^t}{E} & 0 & 0 & 0 & 0 \\ 0 & 0 & 1 & 0 & 0 & 0 \\ 0 & 0 & 0 & \frac{\beta_t}{2(1+v)} & 0 & 0 \\ 0 & 0 & 0 & 0 & \frac{\beta_t}{2(1+v)} & 0 \\ 0 & 0 & 0 & 0 & 0 & \frac{\beta_t}{2(1+v)} \end{bmatrix} \tag{2.9}$$

If both directions reclose,

$$[D_c^{ck}] = \frac{E}{(1+v)(1-2v)}\begin{bmatrix} (1-v) & v & v & 0 & 0 & 0 \\ v & (1-v) & v & 0 & 0 & 0 \\ v & v & (1-v) & 0 & 0 & 0 \\ 0 & 0 & 0 & \beta_c\frac{(1-2v)}{2} & 0 & 0 \\ 0 & 0 & 0 & 0 & \frac{(1-2v)}{2} & 0 \\ 0 & 0 & 0 & 0 & 0 & \beta_c\frac{(1-2v)}{2} \end{bmatrix} \tag{2.10}$$

The other combinations for cracking are given the ANSYS manual (ANSYS R 12.0).

Crushing in concrete is defined in ANSYS solvers. The material is assumed to crush at that point, if the material at an integration point fails in uniaxial, biaxial, or triaxial compression. In SOLID 65, crushing is defined as the complete deterioration of the structural integrity of the material such as material spalling. Under conditions where crushing has occurred, material strength is assumed to have degraded to an extent such that the contribution to the stiffness of an element at the integration point in question can be ignored.

For reinforcement; one-dimensional plasticity and creep behavior is modeled for SOLID 65 in ANSYS.

2.3.1.2. MASS21 (Structural Mass)

MASS21 is a point element that have up to six degrees of freedom (DOF). These DOFs are translations in the nodal x, y, and z directions and rotations about the nodal x, y, and z axes (Figure 2.26). A different mass and rotary inertia may be assigned to each nodal coordinate direction.

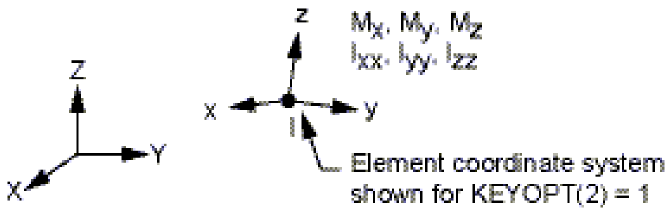

Figure 2-26 MASS21 Geometry

2.3.2. Material Properties

Density of the concrete is used as 2460 kg/ m^3 and Young Modulus of concrete is 32000 MPa as (a reference case) according to the SMART 2008 Phase 2 report given by CEA as described in 2.2.1.1 (RAPPORT DM2S, 2009).

MKIN and CONCRETE are used for the concrete in the model. MKIN (Multi linear kinematic hardening), rate-depended plasticity is used (Figure 2.27).

CONCRETE is a defined material model in ANSYS for Willam – Warnke material model. For this material type open shear transfer coefficient, 0.2 and closed shear transfer coefficient, 0.8, are used. Uniaxial cracking stress is 2.4 MPa.

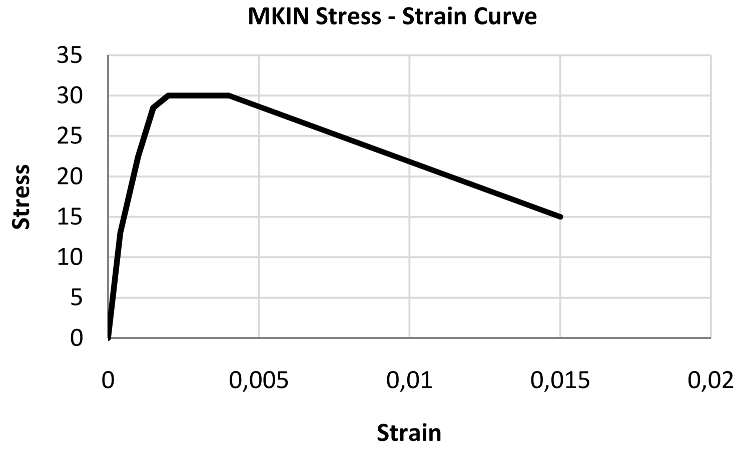

Figure 2-27 MKIN stress- strain curve

2.3.3. Meshing

One of the important aspects of the finite element modeling is the meshing type. The model building walls are meshed by mapping with hexahedral shapes. The important point in mapping in this study is that to keep the element dimension ratio smaller than the 1.5. The slabs and the connections between the column-slab and column- beam meshed with the sweep option in ANSYS (ANSYS R 12.0). The model representation is given in Figure 2.28. The thickness of the walls and the slabs depth divided into two pieces to be able to capture the behavior under seismic activity.

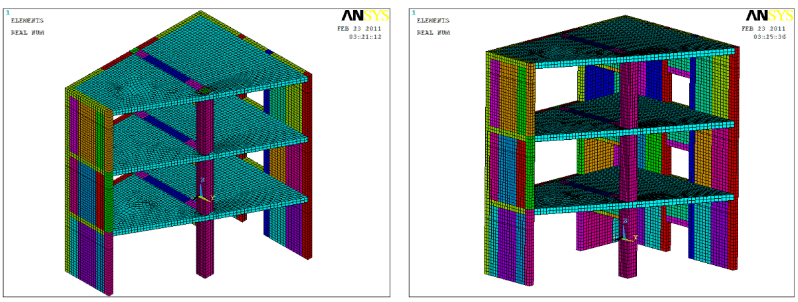

Figure 2-28 Representations of the model building

2.3.4. General Information for the simulation

The model developed for this study consists of 28740 SOLID65 (3-D Reinforced concrete elements) and 5282 MASS21 (Structural mass) element types. Also, the model has 43179 nodes for calculations.

Shaking table and foundation is not modeled and basement is assumed as fixed supported as proposed in SMART 2008 –Phase 1 report (RAPPORT DM2S, 2007) (Figure 2.28). Seismic excitations applied at basement level in the analytical model.

The given figures of the model (Figure 2.28) were chosen for their real constant change. In other words, different colors in the model represent the change in the reinforcement ratios in concrete elements. 74 real constants were defined in the model for the reasonably accurate simulation of the real structure with smeared modeling approach of the reinforcement.

CHAPTER 3

MODEL VERIFICATION CRITERIA

Before starting the sensitivity and fragility analysis, the response of the model will be compared in this chapter with the experimental results according to Phase1 specifications. The details of sensitivity and fragility analysis will be given in the following chapter.

3.1. Frequency Domain Error (FDE) Calculations

For obtaining reasonably accurate results from fragility curves the analytical model results compared with the experimental results to satisfy the accuracy of the numerical model. This comparison was done according to the method developed by Dragovich and Lepage (2009). In this method, Fourier transformations were taken for both measured and calculated data and amplitudes taken into account to calculate the frequency domain error (FDE). FDE is a new method, which has been proposed by Dragovich and Lepage (2009), giving an idea about the accuracy of the estimate by comparing measured and calculated response.

This method makes available comparison about how signals for time response analysis and records match each other by using the fast Fourier transformations of both signals. Error between two signals can be determined from Equations 3.1-3.4. Figure 3.1 presents the frequency domain error calculation. A_m and A_c are the amplitude values of measured and calculated values obtained by their real and imaginary parts. In Equation 3.3, the error amplitude is calculated from the square root of sum of the squares of the difference between real and the difference between imaginary parts of the amplitudes.

$$A_m = \sqrt{(R_m^2 + I_m^2)} \tag{3.1}$$

$$A_c = \sqrt{(R_c^2 + I_c^2)} \tag{3.2}$$

$$A_e = \sqrt{((R_m - R_c)^2 + (I_m - I_c)^2)} \tag{3.3}$$

A_m, A_c = the amplitude of the measured and calculated signals

R_m, R_c = the real parts of the amplitude of the measured and calculated signals

I_m, I_c = the imaginary parts of the amplitude of the measured and calculated signals

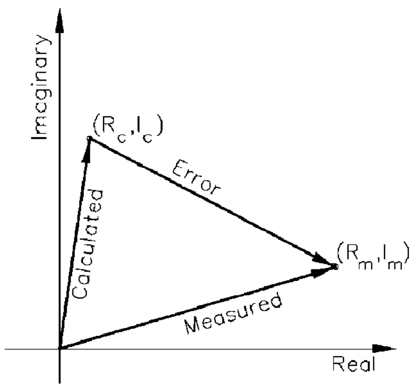

Figure 3-1 FDE representations (Dragovich and Lepage, 2009)

According to the triangle inequality that the sum of any two sides of a triangle is greater than the third side from Figure 3.4, it follows that $A_e < A_m + A_c$. When the measured and calculated signals are 180 degrees out–of–phase of each other, the error vector is equal to the sum of the $A_m + A_c$. Thus, 0 means that the signals are identical and 1 means that there is no fit between the signals as shown in Equation 3.4.

$$FDE = 0 < \frac{A_e}{A_m + A_c} < 1 \tag{3.4}$$

The frequency domain error is calculated according to Equation 3.5.

$$FDE = \frac{\sum_{i=f_1}^{f_2} A_{e_i}}{\sum_{i=f_1}^{f_2} A_{m_i} + \sum_{i=f_1}^{f_2} A_{c_i}} \tag{3.5}$$

3.2. Comparisons of Analytical and Experimental Response

The mock-up was modeled in ANSYS according to the specifications described in the SMART 2008 Phase 1 report (ANSYS R 12.0). The excitations used in experimental runs were used in the time history analysis and the results were compared with the experimental results. The objective here was not to develop a model that produces experimental results accurately but to show that analytical model was reasonable and could generally reflect the behavior obtained experimentally. The main use of the model will be for the development of fragility curves.

As mentioned in Chapter 2, all seismic excitations to the model were applied consecutively. This means that, following response in the elastic range, plastic deformations had been increased cumulatively. The first 3 seismic excitations were in elastic range and therefore, they were not presented in here. The numerical and experimental results of synthetic accelerograms are given in Table 3.1-3.2. The relative error percentages ((calculated-measured)/measured) were calculated according to the measured data and the results were given in Table 3.3. Dp30xA defines third floor displacement in X direction at Point A.

Table 3-1 Numerical results in terms of absolute maximum displacement

Name: **Unit:**	**Dp30xA (mm)**	**Dp30xB (mm)**	**Dp30xC (mm)**	**Dp30xD (mm)**	**Dp30yA (mm)**	**Dp30yB (mm)**	**Dp30yC (mm)**	**Dp30yD (mm)**
Accsyn1	0.40	0.38	0.51	0.83	0.18	0.55	0.56	0.18
Accsyn2	1.63	1.64	2.41	4.10	0.78	4.63	4.64	0.77
Accsyn3	1.90	1.99	2.40	2.63	0.88	3.16	3.16	0.86
Accsyn4	6.42	6.97	8.95	11.88	2.84	13.04	13.02	2.82
Accsyn5	7.73	8.39	9.92	12.04	3.60	14.97	14.95	3.61
Accsyn6	8.50	9.31	12.86	16.86	4.23	17.90	17.86	4.24
Accsyn7	9.21	9.98	12.53	18.35	4.94	21.55	21.52	4.98
Accsyn8	10.28	11.03	14.26	20.06	5.69	22.73	22.60	5.78
Accsyn9	11.08	11.93	15.61	21.13	6.51	23.45	23.32	6.65
Accsyn10	11.39	11.57	16.43	25.87	7.50	24.58	24.56	7.84

Table 3-2 Experimental results in terms of absolute maximum displacement

Name: Unit:	Dp30xA (mm)	Dp30yA (mm)	Dp30xB (mm)	Dp30yB (mm)	Dp30xC (mm)	Dp30yC (mm)	Dp30xD (mm)	Dp30yD (mm)
Accsyn1	2.47	1.38	3.11	5.85	4.02	5.03	5.65	1.51
Accsyn2	2.72	1.28	3.00	4.77	4.41	4.06	5.55	1.33
Accsyn3	5.39	3.46	5.10	10.04	6.38	9.56	7.99	3.35
Accsyn4	6.78	2.14	7.30	12.41	9.94	11.86	14.83	2.07
Accsyn5	6.58	2.86	6.19	14.01	9.29	13.13	14.10	2.69
Accsyn6	6.84	3.21	7.39	15.13	10.49	13.51	17.61	3.19
Accsyn7	7.57	3.61	7.81	16.45	11.91	15.77	18.99	3.63
Accsyn8	7.42	4.12	7.75	14.65	11.55	13.38	17.62	4.02
Accsyn9	10.02	4.88	10.40	17.42	13.10	16.47	20.68	4.94
Accsyn10	9.74	6.70	10.70	18.19	14.73	17.17	24.25	6.52

Table 3-3 Relative Error Percentages between calculated and measured data according to absolute maximum displacements

	Ax	Ay	Bx	By	Cx	Cy	Dx	Dy
Accsyn1	-0.84	-0.87	-0.88	-0.91	-0.87	-0.89	-0.85	-0.88
Accsyn2	-0.40	-0.39	-0.45	-0.03	-0.46	0.14	-0.26	-0.42
Accsyn3	-0.65	-0.75	-0.61	-0.69	-0.62	-0.67	-0.67	-0.74
Accsyn4	-0.05	0.33	-0.05	0.05	-0.10	0.10	-0.20	0.36
Accsyn5	0.18	0.26	0.36	0.07	0.07	0.14	-0.15	0.34
Accsyn6	0.24	0.32	0.26	0.18	0.23	0.32	-0.04	0.33
Accsyn7	0.22	0.37	0.28	0.31	0.05	0.36	-0.03	0.37
Accsyn8	0.39	0.38	0.42	0.55	0.23	0.69	0.14	0.44
Accsyn9	0.11	0.33	0.15	0.35	0.19	0.42	0.02	0.35
Accsyn10	0.17	0.12	0.08	0.35	0.12	0.43	0.07	0.20

Negative values mean that calculated values are smaller than the experimental results in Table 3.3. Table 3.3 figures out that increase in the level of the seismic excitation, results in decrease in error percentages.

The main conclusion drawn from the Phase 1 was that the finite element model cannot replicate the behavior under the low seismic excitation. This difference may come from many reasons such as the connection problem of mock–up to the shaking table, element inadequacy of finite model or assumptions made for the basement nodes. Furthermore, there are many other unknown variables that may affect this behavior, and should be taken up in another research. Acceptable results were obtained under the stronger seismic excitations (Figure 3.2-3.3).

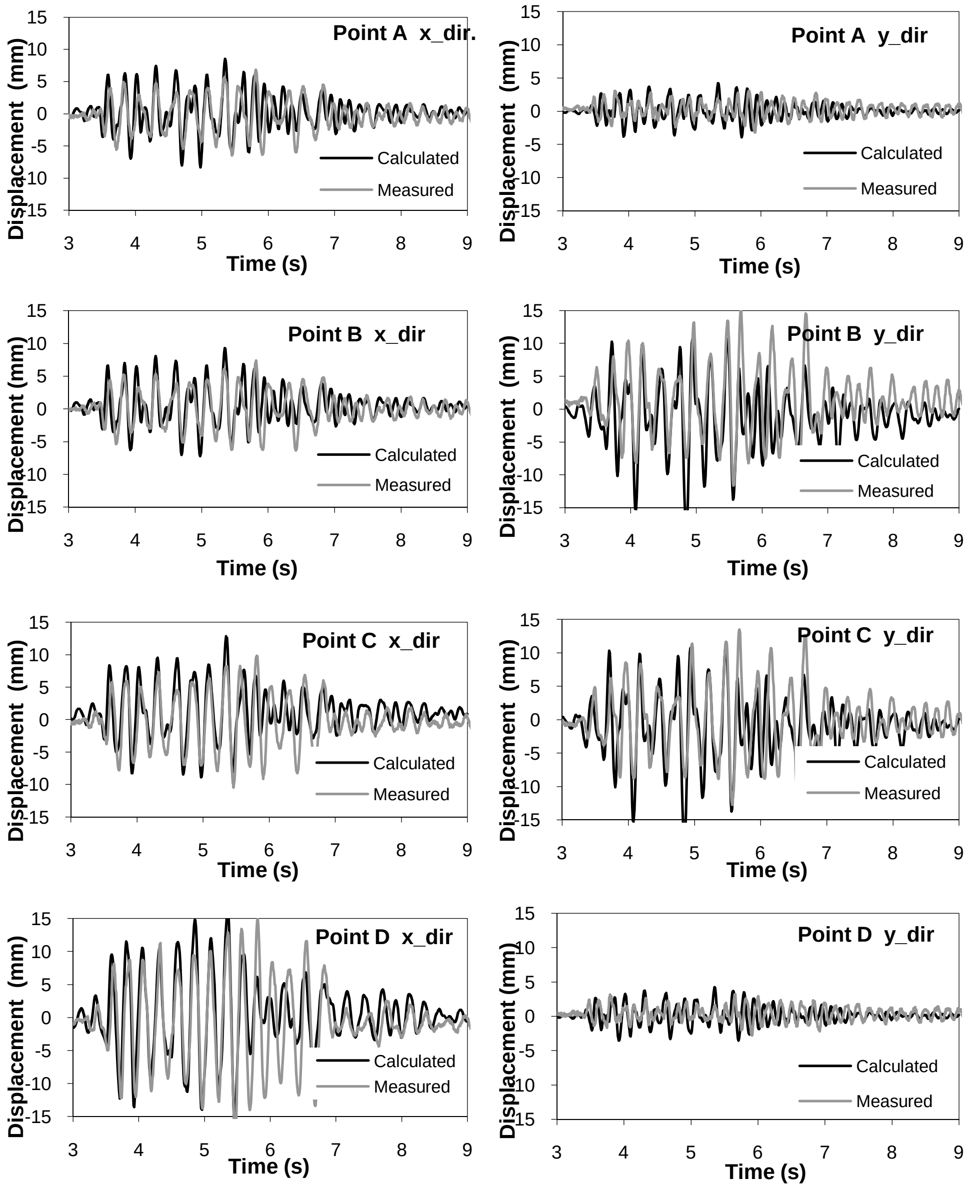

Figure 3-2 Displacement comparisons of the experimental results and analytical results at the 3rd floor level for Run 9 (Accsyn-0.6g)

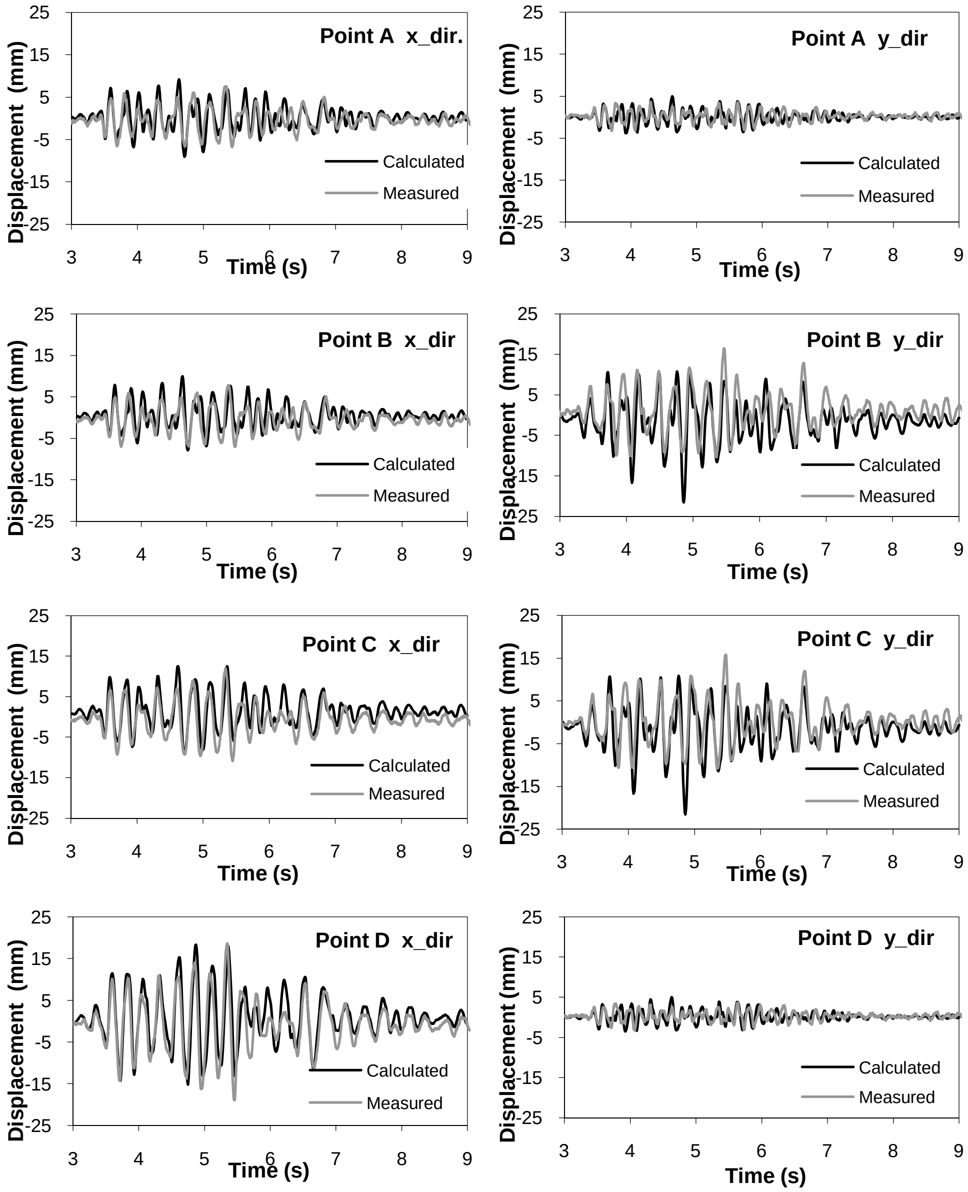

Figure 3-3 Displacement comparisons of the experimental results and analytical results at the 3rd floor level for Run 10 (Accsyn-0.7 g)

This problem was also experienced by other researchers who participated in SMART 2008 Phase 1- Benchmark Study (SMART Workshop, 2010,). It is believed that more accurate results can be obtained if the shaking table is included in the model. However, due to the inadequate information about the properties of the table and significant increase in the computation time for the nonlinear time-history analysis the shaking table modeling was not included in this study.

Furthermore, the main scope of this thesis is the SMART 2008 project Phase 2 and the first assumption in this phase is to ignore the shaking table because of its unknown behavior. Thus, the given figures for the comparison reflect the general behavior of the structure.

In Figures 3.2 and 3.3, the match between the measured and calculated response improves a better representation of the experimental behavior is achieved. The comparisons are quantified in the following section.

Table 3.4 shows that FDE decreases when the seismic excitation level increases. For Accsyn- 0.7 g the values become smallest. Especially for X direction these values decrease significantly.

FDE comparison is totally depended on the time history results which mean that dt (time step) term between the compared data should effect the results. In analysis of the Phase 1 Runs, all loadings had to be applied consecutively, thus, some limitations had to be considered. For example, In ANSYS (ANSYS R 12.0), each converged step for time history analysis are kept in a monitoring file (extension of the file is ".MNTR") in the memory. This file is only capable of 10000 line limitation to keep the converged data and ANSYS cannot solve the problem if this file exists 10000 lines. Due to this limitation, some precautions were taken into account.

Table 3-4 FDE Calculations for some of the SMART 2008 Phase 1b Runs at specified points at 3rd floor level

Accsyn 0.3 g		Accsyn 0.6 g		Accsyn 0.7 g	
Points	**FDE**	**Points**	**FDE**	**Points**	**FDE**
A3X	0.868007	A3X	0.544477	A3X	0.461273
B3X	0.825244	B3X	0.518019	B3X	0.461138
C3X	0.795348	C3X	0.488837	C3X	0.395757
D3X	0.838212	D3X	0.45666	D3X	0.308891
A3Y	0.864505	A3Y	0.63732	A3Y	0.541903
B3Y	0.847194	B3Y	0.565943	B3Y	0.474089
C3Y	0.837387	C3Y	0.562192	C3Y	0.457174
D3Y	0.874332	D3Y	0.685665	D3Y	0.597971

The time step in the acceleration data was 0.025 s and time duration for each Run was approximately 6 s (if only we take active duration of the pulses into consideration). Thus, the length of the loading file becomes 31200 lines, which was not applicable.

Therefore, a script is written to keep the converged steps in monitoring file once in every four steps. This way, all experimental runs can be solved numerically in ANSYS. But, as a result of this intervention FDE should increase a bit because of being directly related to the time versus response data.

As a result, the numerical model is thought to have reasonably enough accuracy for the Phase 2 of the SMART 2008 Project.

CHAPTER 4

SENSITIVITY STUDY

4.1. SENSITIVITY STUDY AND RESULTS

The response of a structure that includes a wall is controlled by many parameters that interact with one another. The purpose of this chapter is to determine the importance and impacts of the chosen predefined parameters on the complete structural behavior. One parameter was changed in each step to be able to identify the change in the system response. Then, the uncertain parameters were ranked to figure out their relative importance. By drawing on the calculated response that combines many parameters, it becomes possible to generalize the results for fragility curves.

4.1.1. Predefined Variables

The predefined variables were chosen in order to determine the importance and impact of the chosen structural properties. These are the elastic modulus of concrete (E_c), steel yield stress (F_y), overall damping coefficient of the system and additional loading effects on the structural response.

The ranges of these parameters are coherent with the experimental results (Table 4.1). The mass variation was the same at each floor level. The values prescribed in this section are not always representative of common practice. They have been chosen to define the importance of those parameters on the structural response under seismic loading.

Table 4-1 Range of the parameters

Concrete Elastic Modulus E_c	
25600 MPa 28800 MPa 32000MPa (Mean) 35200 MPa 38400 MPa	(± 20% coherent with experimental results)
Steel yielding stress F_y	
425 MPa 500 MPa (Mean) 575 MPa 650 MPa	(-15/+30% coherent with experimental results)
Damping	
From 0.5% to 5% according to damage level: ~2% at design level (experimental results) 0.5%, 2%, 5% corresponding to the viscous elastic and numerical damping (not accounting for cracking, friction, yielding …)	

Table 4-2 Additional Masses

Case	***1***	***2***	***3***
RC structure mass	10.44 T	10.44 T	10.44 T
Additional loading on the 1st slab	10.44 T	11.60T	12.76 T
Additional loading on the 2nd slab	10.80 T	12.00 T	13.20 T
Additional loading on the 3rd slab	9.22 T	10.25 T	11.20 T
TOTAL ADDITIONAL MASSES	30.46 T	33.85 T	37.23 T

The SMART 2008 Phase 2 project team derived two sets of horizontal synthetic accelerograms from white noise in order to study the impact of parameter uncertainty (RAPPORT DM2S, 2009).

Both of the accelerograms, design level (0.2 g) and over-design level (0.6 g), were applied at X and Y direction simultaneously. This way, the torsion behavior has been taken into the consideration. The length of all signals was fixed to 5 sec, with a time step of 0.005 sec. Both the design and the over- design level acceleration graphs are represented in Figure 4.1.

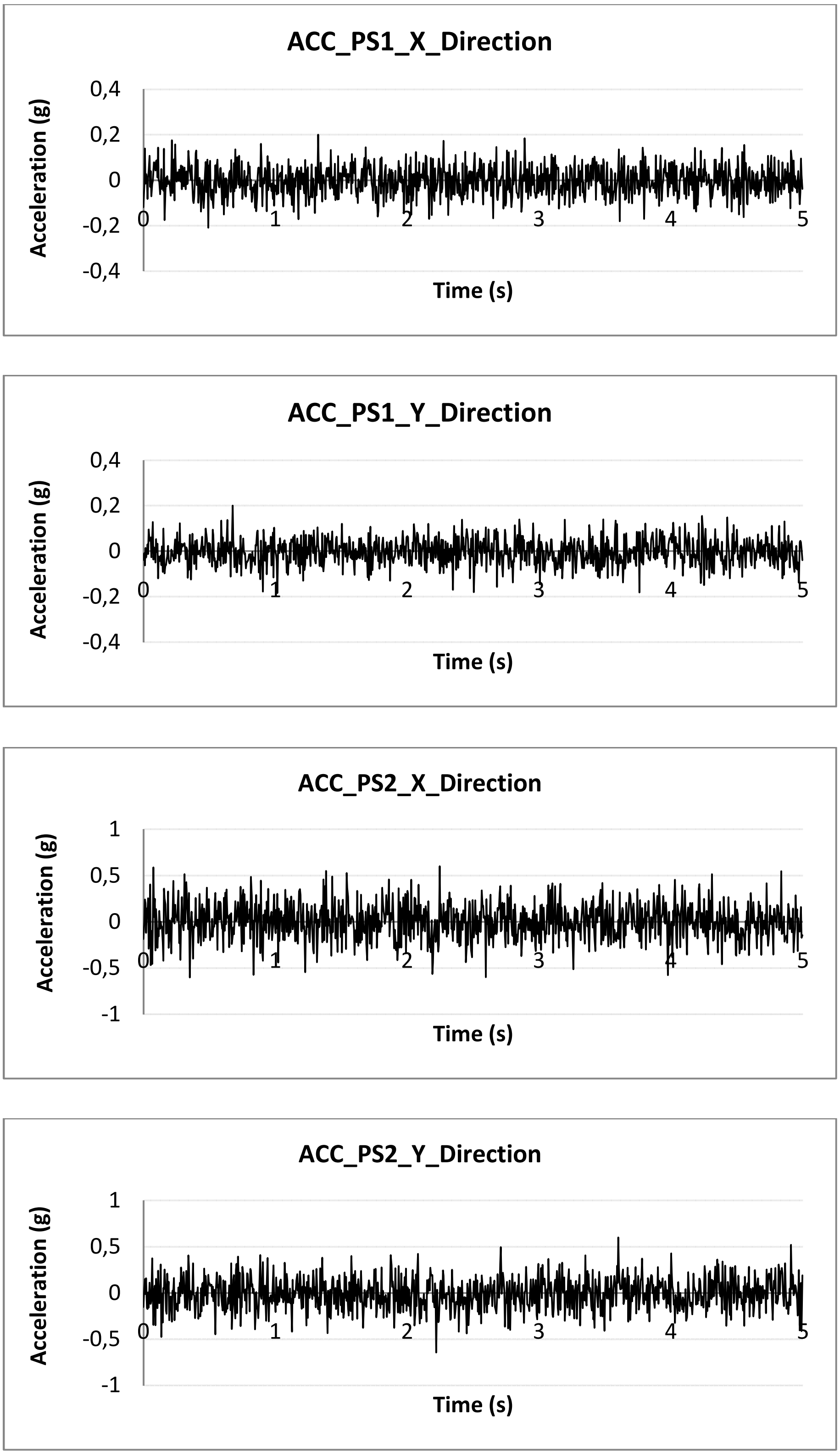

Figure 4-1 Design and Over - Design Level (0.6 g) X and Y Directions Accelerograms

4.1.2. Sensitivity Cases

Only time-history analyses were performed using the two provided sets of accelerograms. For each accelerogram set 12 cases were studied. These cases described in Table 4.3. The model was built using the ANSYS platform.

Table 4-3 Sensitivity Study Cases

CASE	E_c (MPa)	F_y (MPa)	Damping (%)	Additional Masses (T)
1-Reference	**32000**	**500**	**2**	**33.85**
2	25600	500	2	33.85
3	28800	500	2	33.85
4	35200	500	2	33.85
5	38400	500	2	33.85
6	32000	425	2	33.85
7	32000	575	2	33.85
8	32000	650	2	33.85
9	32000	500	0.5	33.85
10	32000	500	5	33.85
11	32000	500	2	30.46
12	32000	500	2	37.23

According to Table 4.3, the first five cases reflect the change in the Elastic modulus of concrete. The latter three cases, between 6 and 8, are the changes in the steel yielding force. Cases 9 and 10 are about the damping coefficient change. The last two cases are additional mass variations.

4.1.3. Modal Analysis

It is fundamental to do the modal analysis to start the nonlinear time history analysis. In Figure 4.2, first three modes of the SMART 2008 specimen given for the Reference Case specified in Table 4.3. The frequencies for all cases are tabulated in Table 4.4.

The highest frequency values observed at Case 5 in which the highest modulus of elasticity was assumed. The stiffer structures have higher frequency values.

When the structure was exposed to the highest additional loadings, the frequency values obtained from the modal analysis decreased.

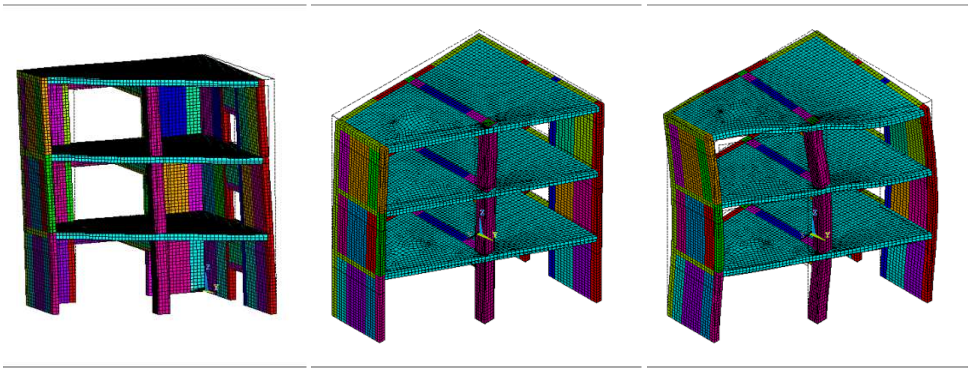

Figure 4-2 First three modes of the SMART 2008 specimen calculated from the ANSYS for the Reference Case given in Table 4.3

Table 4-4 Modal analysis results for Sensitivity analysis cases

	Sensitivity Analysis Cases											
Mode (Hz)	1	2	3	4	5	6	7	8	9	10	11	12
1	9.23	8.26	8.76	9.68	10.11	9.23	9.23	9.23	9.23	9.23	9.64	8.87
2	15.93	14.25	15.11	16.70	17.44	15.93	15.93	15.93	15.93	15.93	16.62	15.31
3	32.76	29.31	31.08	34.35	35.87	32.76	32.76	32.76	32.76	32.76	34.20	31.48
4	34.58	30.94	32.81	36.26	37.87	34.58	34.58	34.58	34.58	34.58	36.22	33.14
5	35.94	32.16	34.10	37.69	39.36	35.94	35.94	35.94	35.94	35.94	37.43	34.61
6	37.24	33.32	35.33	39.06	40.79	37.24	37.24	37.24	37.24	37.24	39.01	35.70
7	40.46	36.19	38.38	42.43	44.31	40.46	40.46	40.46	40.46	40.46	42.42	38.74
8	41.46	37.10	39.34	43.48	45.41	41.46	41.46	41.46	41.46	41.46	43.45	39.72

Table 4-5 Damping Parameters

Cases	alpha	beta
1	1.4690	2.530E-04
2	1.3146	2.827E-04
3	1.3938	2.667E-04
4	1.5404	2.413E-04
5	1.6085	2.311E-04
6	1.4690	2.530E-04
7	1.4690	2.530E-04
8	1.4690	2.530E-04
9	0.3672	6.326E-05
10	3.6724	6.326E-04
11	1.5333	2.424E-04
12	1.4119	2.632E-04

In Table 4.5, damping parameters are given. These values were used in the time history analysis as mass and stiffness multiplier. Damping parameters were calculated according to the Rayleigh method (Chopra, 2000). First and second mode frequency values were used to calculate the Rayleigh damping coefficients.

4.1.4. Results

The results of sensitivity analyses were observed in the Points A, B, C, D, E, F, and G in the Figure 2.8. To figure out the importance or impact of parameters in the whole behavior; maximum displacements, maximum inter-story drifts, maximum inter-story drifts ratios, floor response spectrums at 3rd floor and base shears at walls were investigated and given in detail in the following parts.

4.1.4.1. Maximum displacements

Displacement graphs are drawn for both design and over-design level in Figure 4.2 and 4.3. In each graph, absolute maximum displacements are represented in both x and y directions. At design level, change in the parameters can represent the impacts on the response. In Figure 4.2, higher displacement values occurred at points A and D in the x direction. At points C and D, motion in the y direction is dominant. Structural response is highly sensitive to increase in the Elastic modulus and damping coefficient at 0.2 g design level for all points. Absolute maximum displacement values are given in the Table 4.4 and Table 4.5. The cells with maximum displacements are filled with grey in Table 4.6.

Table 4-6 SA PS1 Cases X Direction Absolute Maximum Displacements (mm)

	Case 1	Case 2	Case 3	Case 4	Case 5	Case 6	Case 7	Case 8	Case 9	Case 10	Case 11	Case 12
A	1.081	0.98	1.108	0.97	0.77	1.101	1.098	1.098	0.994	0.533	0.7337	1.0412
B	1.128	1.009	1.164	1.028	0.795	1.151	1.149	1.149	1.032	0.5165	0.7265	1.0884
C	1.604	1.558	1.698	1.461	1.109	1.637	1.634	1.634	1.738	0.8832	0.9942	1.5833
D	2.515	2.418	2.557	2.32	1.814	2.576	2.576	2.576	2.895	1.4922	1.6393	2.378
E	1.393	1.347	1.493	1.274	0.961	1.419	1.416	1.416	1.476	0.7932	0.9229	1.3618
F	1.579	1.518	1.653	1.449	1.083	1.602	1.601	1.602	1.68	0.9098	1.0201	1.529
G	1.34	1.286	1.431	1.2	0.933	1.379	1.377	1.376	1.39	0.737	0.883	1.3004

Table 4-7 SA PS1 Cases Y Direction Absolute Maximum Displacements (mm)

	Case 1	Case 2	Case 3	Case 4	Case 5	Case 6	Case 7	Case 8	Case 9	Case 10	Case 11	Case 12
A	0.423	0.417	0.434	0.392	0.31	0.426	0.424	0.424	0.4	0.2217	0.3324	0.395
B	2.206	1.857	1.849	1.934	1.408	2.162	2.152	2.157	2.833	1.0503	1.3189	1.9333
C	2.217	1.869	1.861	1.942	1.415	2.171	2.161	2.166	2.844	1.0606	1.3268	1.9459
D	0.414	0.408	0.423	0.383	0.302	0.416	0.414	0.414	0.39	0.216	0.3275	0.3809
E	0.978	0.917	0.879	0.892	0.675	0.951	0.945	0.947	1.231	0.4394	0.6653	0.8529
F	0.514	0.549	0.55	0.491	0.382	0.508	0.507	0.507	0.573	0.2463	0.4213	0.5182
G	1.602	1.366	1.399	1.408	1.029	1.569	1.562	1.565	2.079	0.7565	1.0214	1.3751

It is clear that Case 3 and Case 9 have maximum displacements on different points at design levels. These values can be read from Tables 4.6 and 4.7. From Figure 4.3, it can be concluded that, concrete Elastic modulus, damping coefficient and additional loading variables have visible impacts at design level (In which spectrum the SMART 2008 building was designed). However, steel yielding stress has no impact on the structural response in terms of absolute maximum displacement.

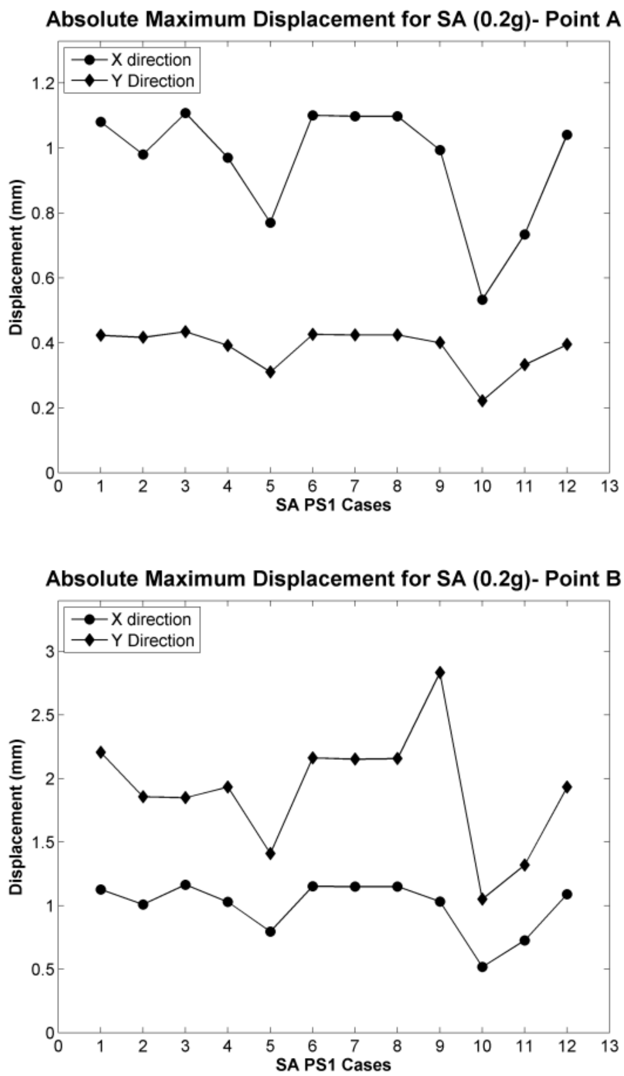

Figure 4-3 Design Level (0.2 g) Absolute maximum displacement values on the 3rd Floor

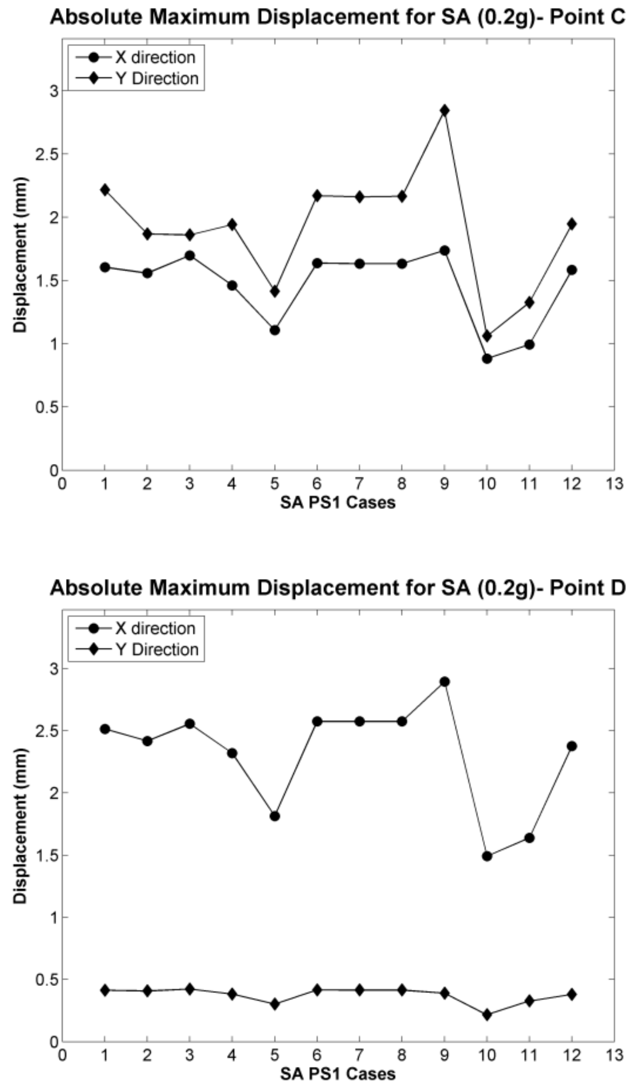

Figure 4.3 (Continue) Design Level (0.2 g) Absolute maximum displacement values on the 3rd Floor

At higher acceleration levels, such as in the curves in Figure 4.4, the most dominant variable is the damping coefficient that affects the structural response at different points of the structure distinctly. Displacements at points in X and Y directions are close to each other as seen in the curves. Absolute maximum displacement values change at different points. At over-design cases low damping results in maximum displacement. The responses are approximately the same for other variables of the parametric study at over-design level.

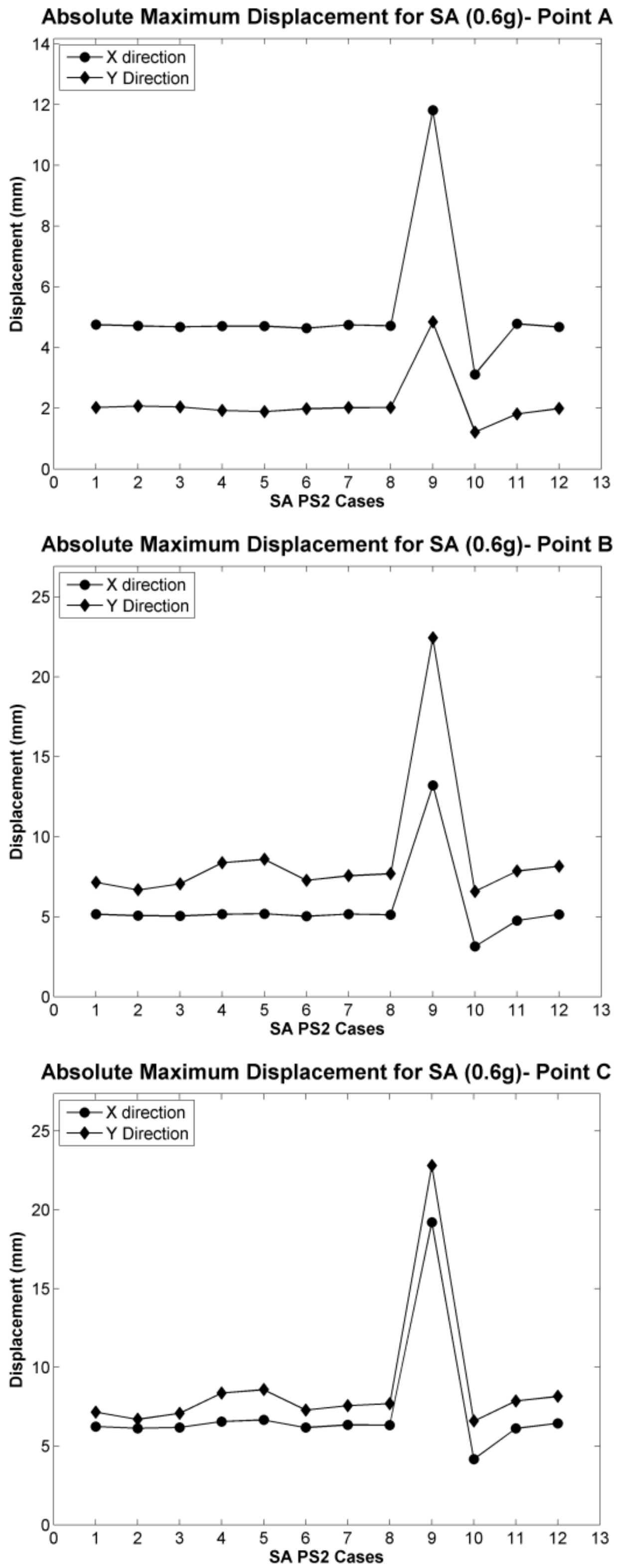

Figure 4-4 Over-Design Level (0.6 g) Absolute maximum displacement values at 3rd Floor

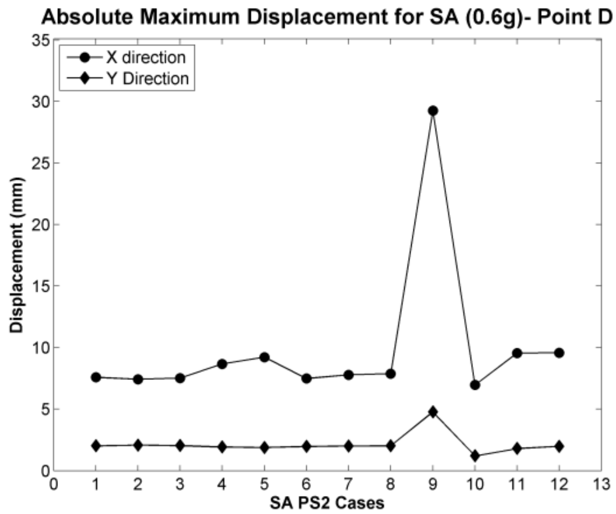

Figure 4.4 (Continue) Over-Design Level (0.6 g) Absolute maximum displacement values at 3rd Floor

The absolute maximum displacement values for over-design level cases are represented in Tables 4.8 4.9 for the X and Y directions. All points have different drift values. This is a clue for the torsion response of the structure.

Figures 4.5 and 4.6 show the relationship in terms of displacement response at the third floor level between the specified points (Figure 2.8). The relationship between the A and D are linear in the y direction due to the high stiffness of Wall 3. However, it is hard to say that there is a linear relationship between A-D in X direction and B-D in X and Y directions. Especially in X direction dispersion is much higher.

Table 4-8 SA PS2 Cases - X Direction Absolute Maximum Displacements

	Case 1	**Case 2**	**Case 3**	**Case 4**	**Case 5**	**Case 6**	**Case 7**	**Case 8**	**Case 9**	**Case 10**	**Case 11**	**Case 12**
A	4.755	4.716	4.684	4.706	4.709	4.638	4.752	4.716	11.82	3.1199	4.7831	4.6765
B	5.157	5.067	5.049	5.161	5.183	5.027	5.17	5.117	13.21	3.1372	4.7594	5.1434
C	6.234	6.13	6.184	6.553	6.657	6.171	6.344	6.334	19.21	4.1657	6.1197	6.4417
D	7.591	7.433	7.527	8.68	9.232	7.487	7.793	7.886	29.26	6.969	9.5643	9.5903
E	5.67	5.559	5.58	5.901	5.966	5.567	5.727	5.724	16.97	4.0176	5.9412	5.5973
F	5.969	5.856	5.881	6.257	6.343	5.841	6.043	6.063	18.59	4.4805	6.5185	6.0658
G	5.647	5.535	5.555	5.816	5.892	5.524	5.697	5.681	16.48	3.7217	5.5474	5.6663

Table 4-9 SA PS2 Cases- Y Direction Absolute Maximum Displacements

	Case 1	Case 2	Case 3	Case 4	Case 5	Case 6	Case 7	Case 8	Case 9	Case 10	Case 11	Case 12
A	2.029	2.074	2.047	1.929	1.893	1.985	2.02	2.025	4.841	1.2156	1.8159	1.9943
B	7.15	6.681	7.058	8.37	8.584	7.271	7.558	7.686	22.43	6.5739	7.8558	8.1572
C	7.153	6.696	7.073	8.368	8.577	7.279	7.564	7.69	22.8	6.5809	7.8635	8.1455
D	2.021	2.07	2.039	1.918	1.884	1.973	2.008	2.013	4.772	1.2019	1.8031	1.9765
E	3.46	3.445	3.64	4.059	4.236	3.563	3.79	3.815	11.69	3.0247	3.7525	4.3027
F	2.057	2.119	2.189	2.362	2.451	2.111	2.257	2.267	5.923	1.4828	1.8152	2.4881
G	5.413	5.06	5.355	6.221	6.314	5.441	5.7	5.759	18.35	4.8883	5.9566	6.3121

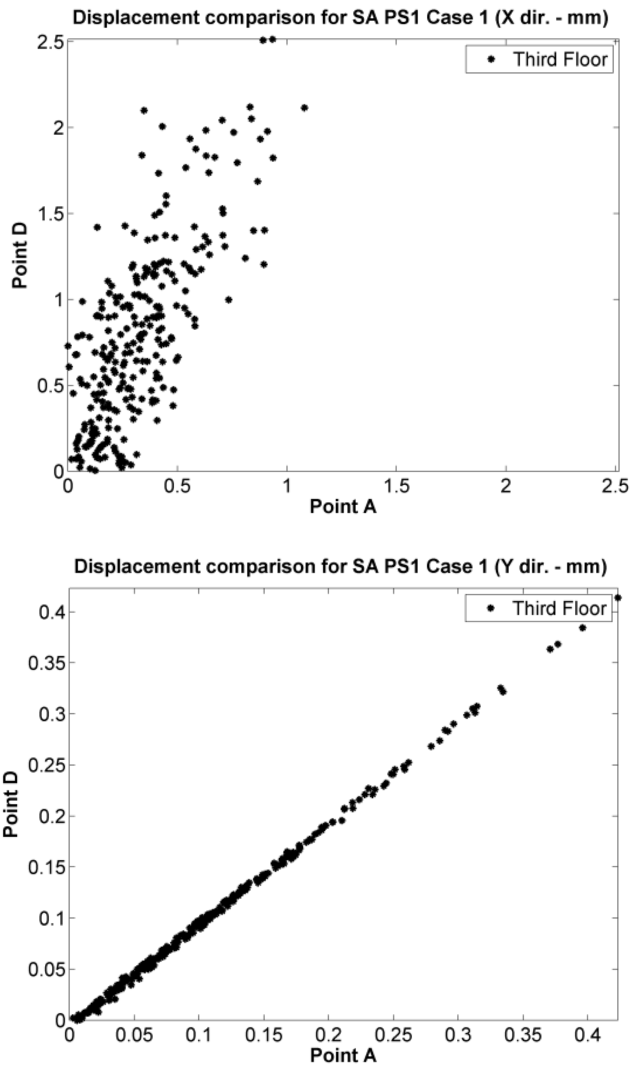

Figure 4-5 Points A and D displacement comparisons for X and Y directions at 3rd floor

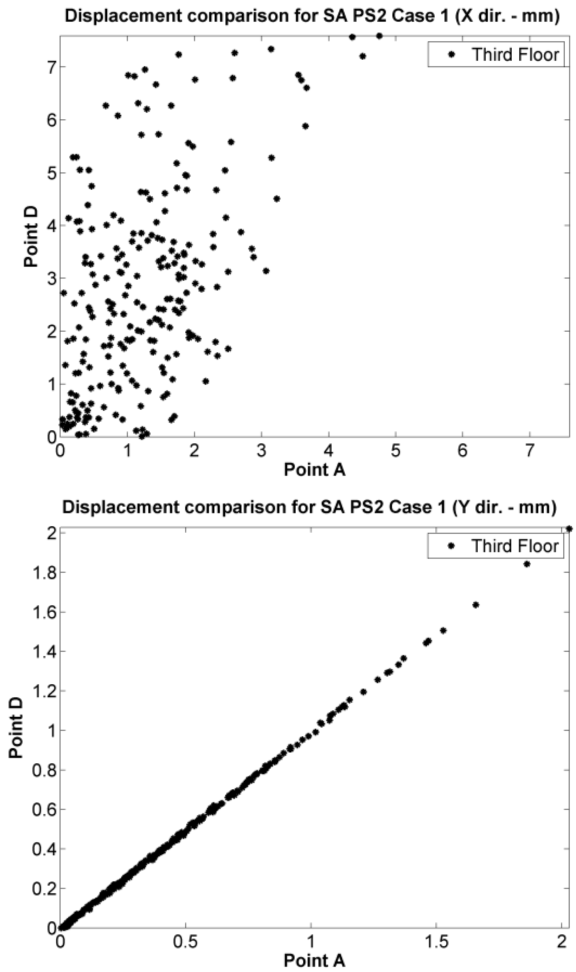

Figure 4.5 (Continue) Points A and D displacement comparisons for X and Y directions at 3rd floor

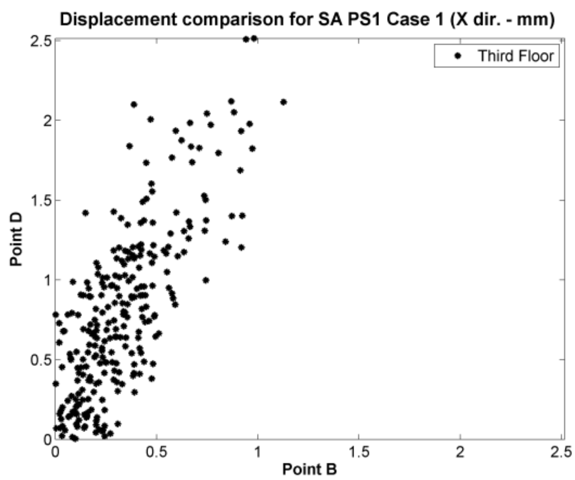

Figure 4-6 Points B and D displacement comparisons for X and Y directions at 3rd floor

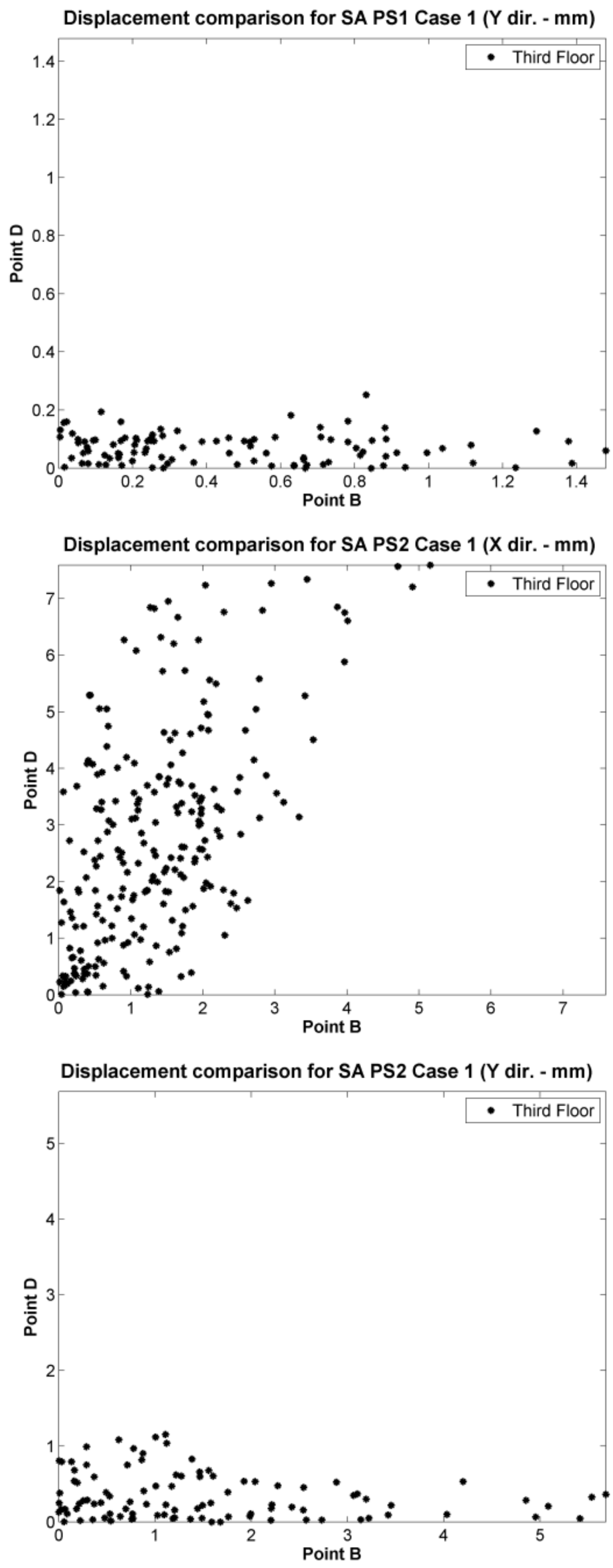

Figure 4.6 (Continue) Points B and D displacement comparisons for X and Y directions at 3rd floor

4.1.4.2. Maximum inter-story drifts

The response of the structure is also investigated in terms of the absolute maximum inter-story drifts at the specified points on the floor level (Figure 2.8). In Figure 4.7, the curves indicate that A and D, and B and C show similar behavior in terms of the inter-story drifts. At all points, second and third floor drift values are close to each other in the Y direction at design level. Elastic moduli of concrete, damping coefficient and additional loading have important effects on structural response. Change in the elastic modulus of concrete alters the drifts, but this change is not very high. Damping coefficient and additional loading parameters change the drift values.

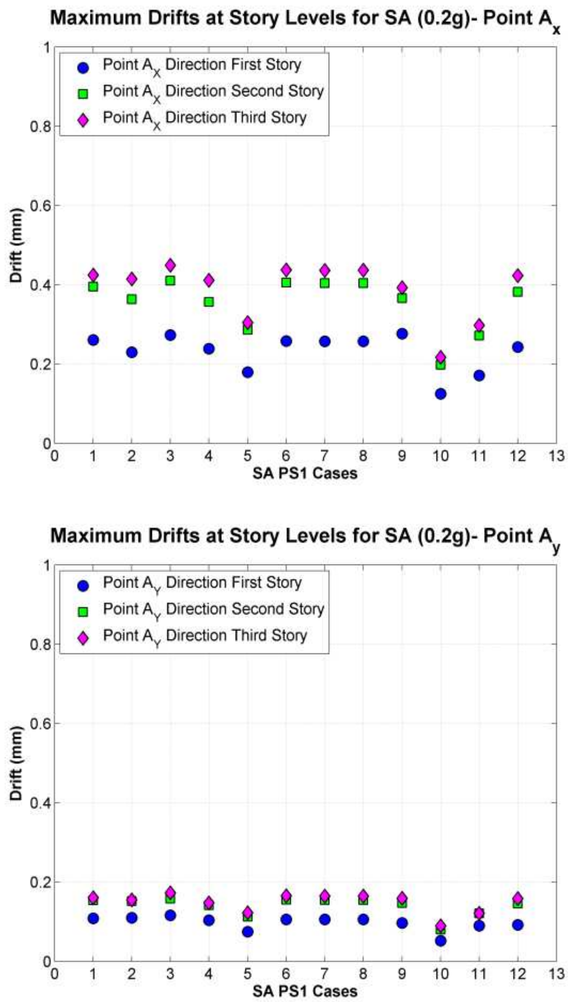

Figure 4-7 Design Level (0.2 g) - Maximum Inter-Story Drifts

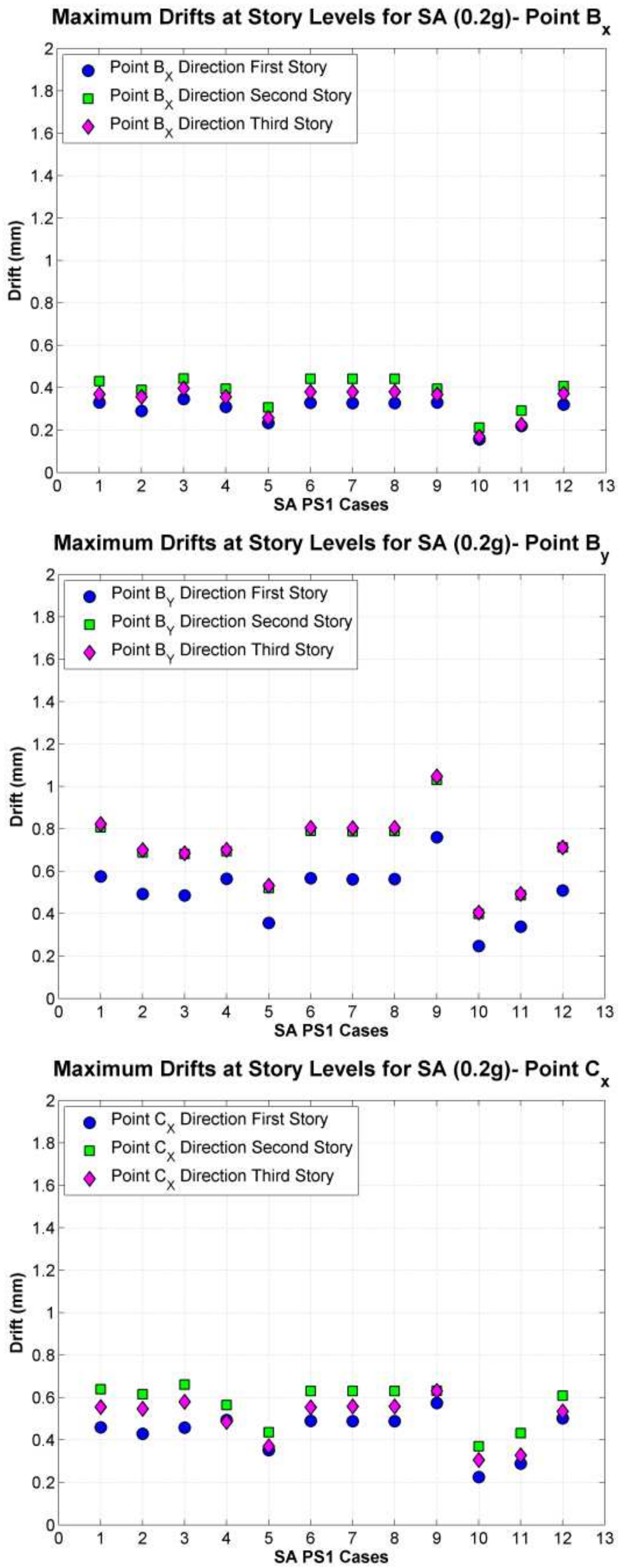

Figure 4.7 (Continue) Design Level (0.2 g) - Maximum Inter-Story Drifts

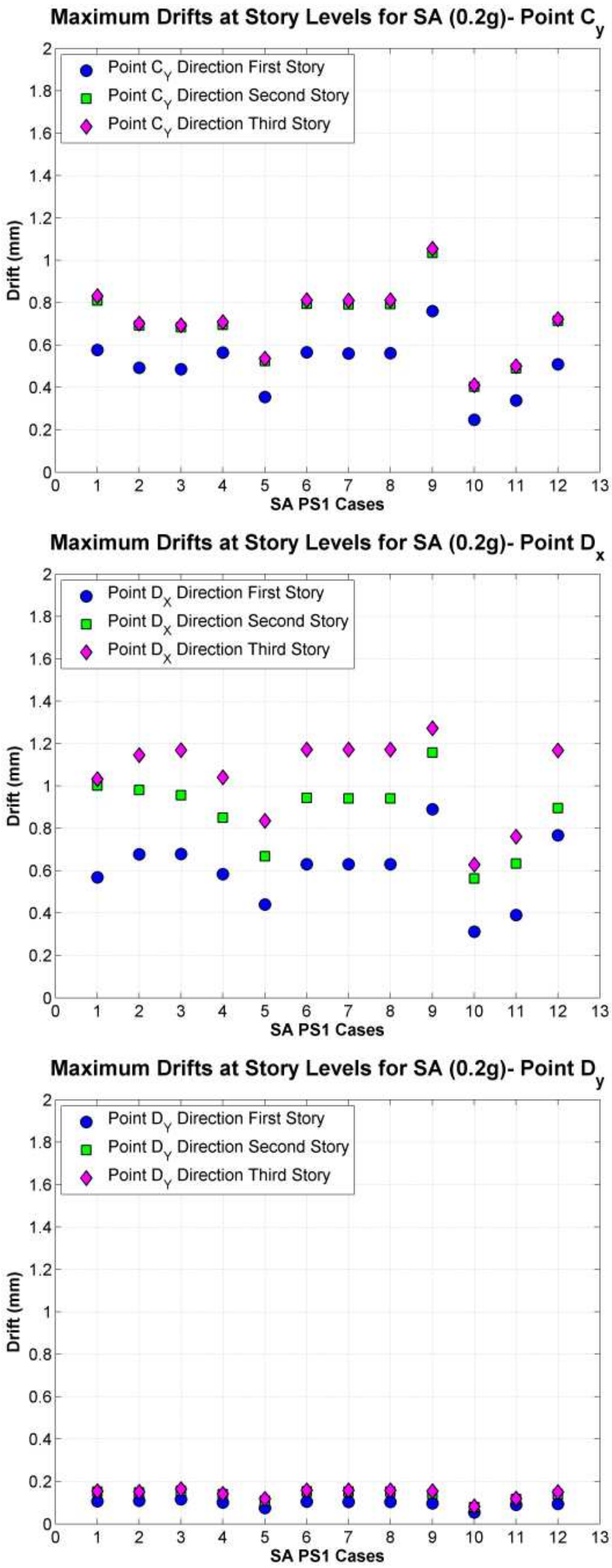

Figure 4.7 (Continue) Design Level (0.2 g) - Maximum Inter-Story Drifts

Figure 4.8 represents over-design absolute maximum inter-story drifts. In all directions at over-design cases, second and third floor drifts are close to each other. Furthermore, points B and C have approximately the same drifts except Case 9, in which the damping coefficient is (0.5%).

At over-design cases, damping coefficient variable seems to be an important parameter. The additional loading parameter may also be taken into consideration, however, not as crucial as damping coefficient according to increment in additional loading as given in Table 4.3.

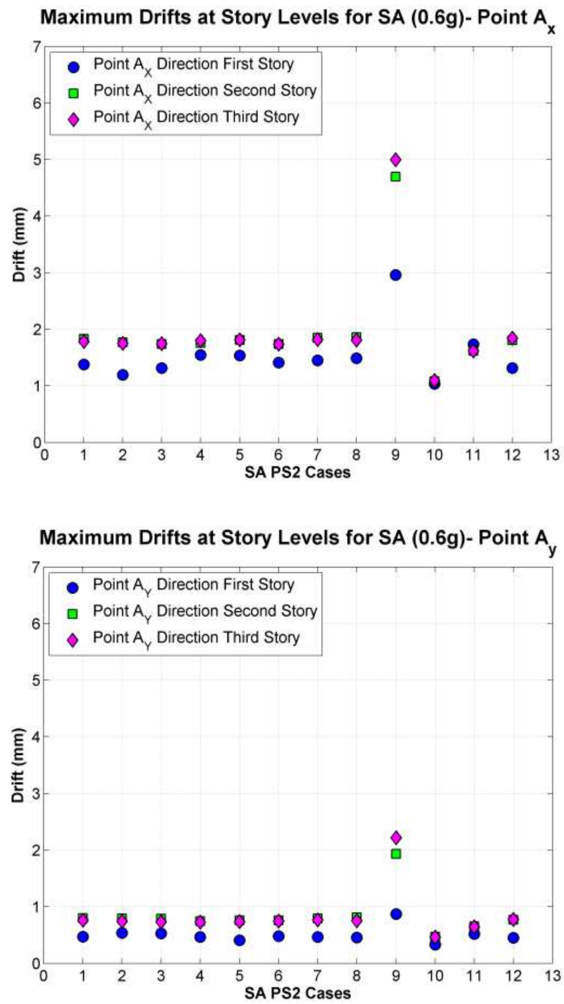

Figure 4-8 Over-Design Level (0.6 g) - Maximum Inter-Story Drifts

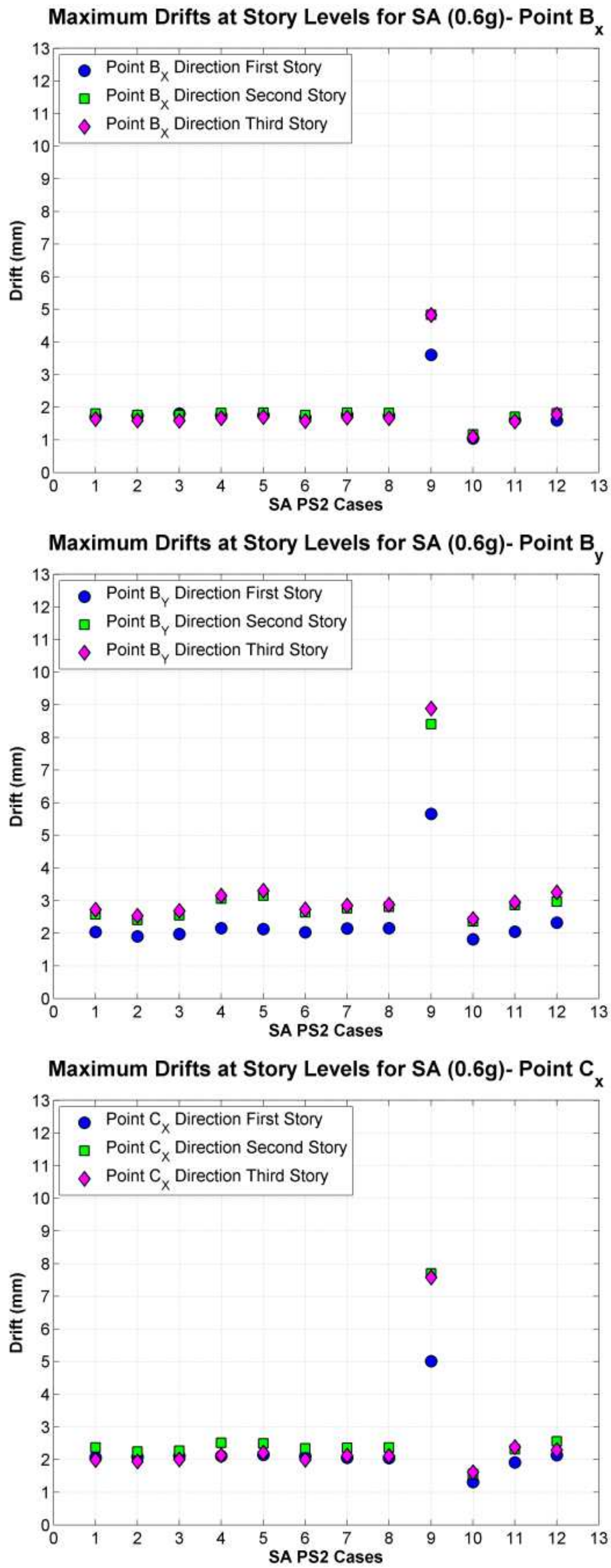

Figure 4.8 (Continue) Over-Design Level (0.6 g) - Maximum Inter-Story Drifts

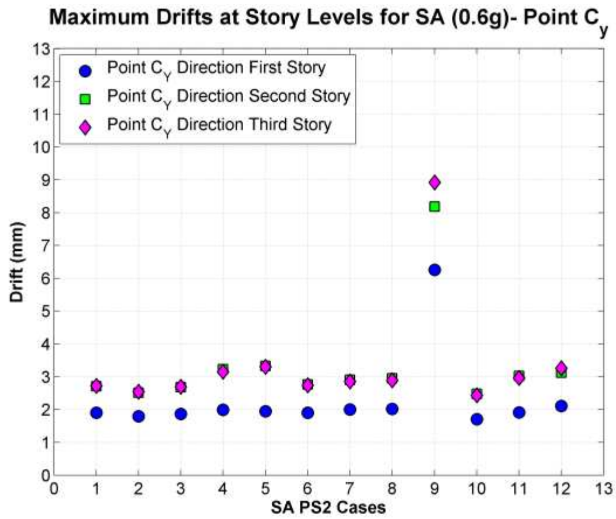

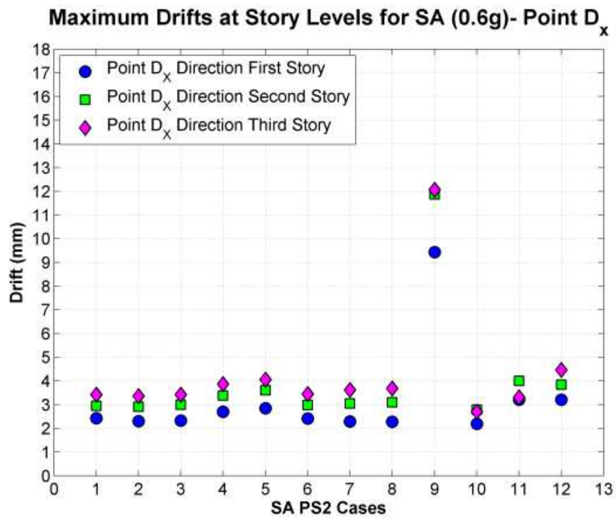

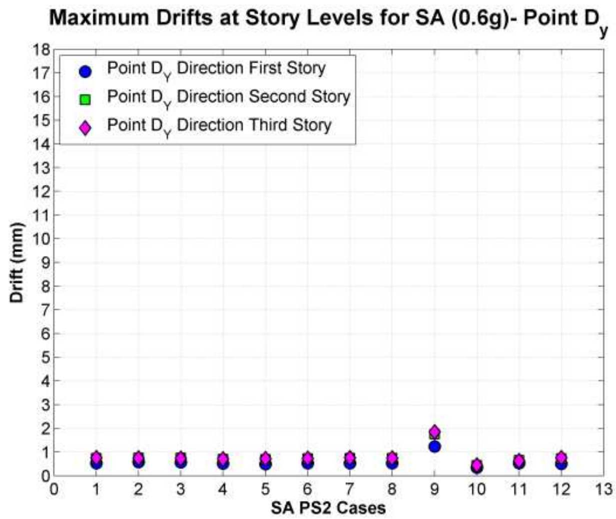

Figure 4.8 (Continue) Over-Design Level (0.6 g) - Maximum Inter-Story Drifts

Maximum drifts at over-design cases in parametric study changes between 2 and 3 mm except Case 9. Decrease in damping coefficient not only increase the drifts but also increase the time needed to solve. Case 9 took more than two weeks on a computer with a high performance (3.33 GHz) processor.

4.1.4.3. Maximum inter-story drift ratios

To see the effects of the parameters on the soft stories, the drift ratios are investigated in Figures 6.4.3 and 6.4.4 for both design and over-design levels accordingly.

In Figure 4.9, for point A (Points are represented in Figure 2.7.), both in X and Y directions, the largest difference in drift ratios takes place in the first floor – second floor interface. In the X direction drift ratios changes in range of 1e-4 – 3.6e-4. In the Y direction, it changes between 0.4e-4 and 1.4e-4, which is approximately 2.5 times lower than X direction values. For point B, maximum drift ratio change occurs in first floor, especially in Y direction. Drift ratios ranges for X and Y directions are accordingly 1.3e-4 – 3.6e-4 and 2e-4 – 8e-4. Point C displays the same trend as point B. In X direction first floor-second floor connection has more drift ratio change than second floor - third floor connection. In Y direction the difference in drift ratio is small between second and third floor connection. Drift ratios ranges for X and Y directions are 1.8e-4 – 5.5e-4 and 2e-4 – 8e-4. For point D, in both X and Y directions first and second floor connection has the most drift ratio change. Ranges for X and Y directions are 2.5e-4 – 10.5e-4 and 2.5e-4 – 14e-4, respectively.

To sum up for design level, damping coefficient and additional loading parameters (Table 4.3) make difference on results at design level. Case 10 in which the damping coefficient is 5 percent, the drift ratios seem to decrease. Cases 5 and 11, which are related with the elastic modulus of the concrete and additional loadings, make the similar change in the structural behavior. Increase in concrete elastic modulus and decrease in additional loadings reduce the drift ratios. Case 9, in which the damping coefficient is 0.5%, increase the drift ratio. However, it is close to the other cases except Cases 5, 10 and 11.

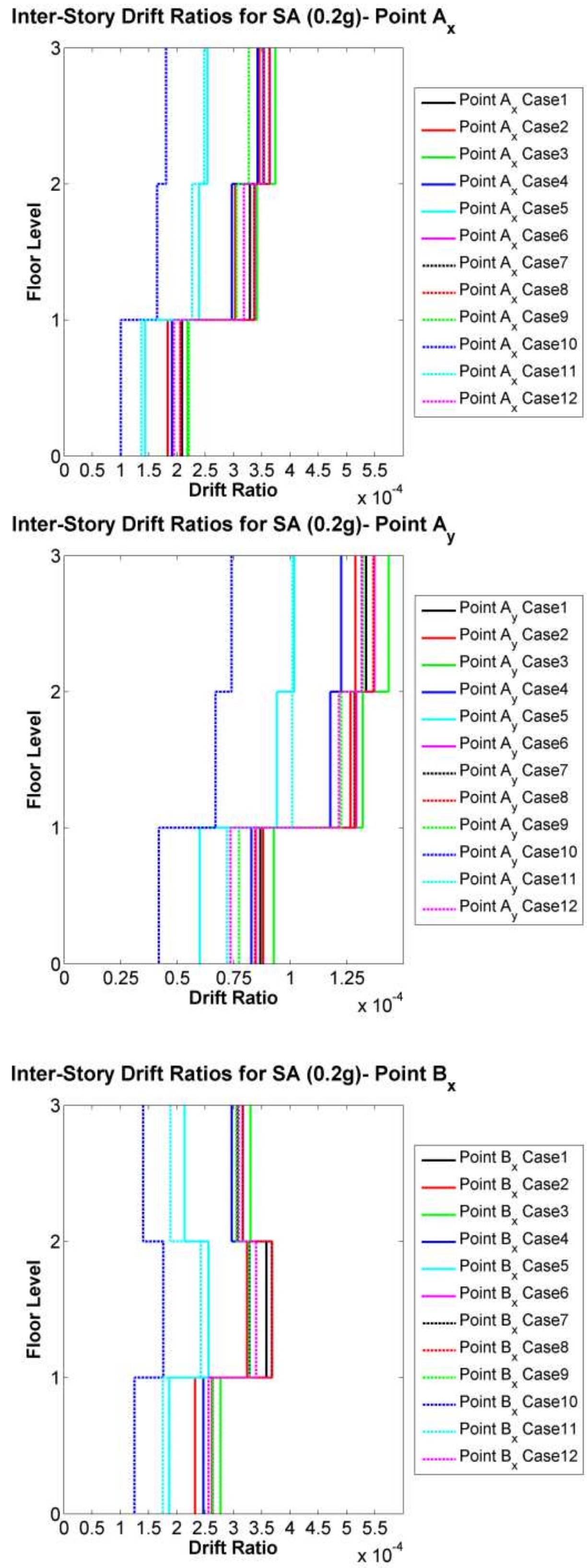

Figure 4-9 Design Level (0.2 g) - Maximum Inter-Story Drift Ratios

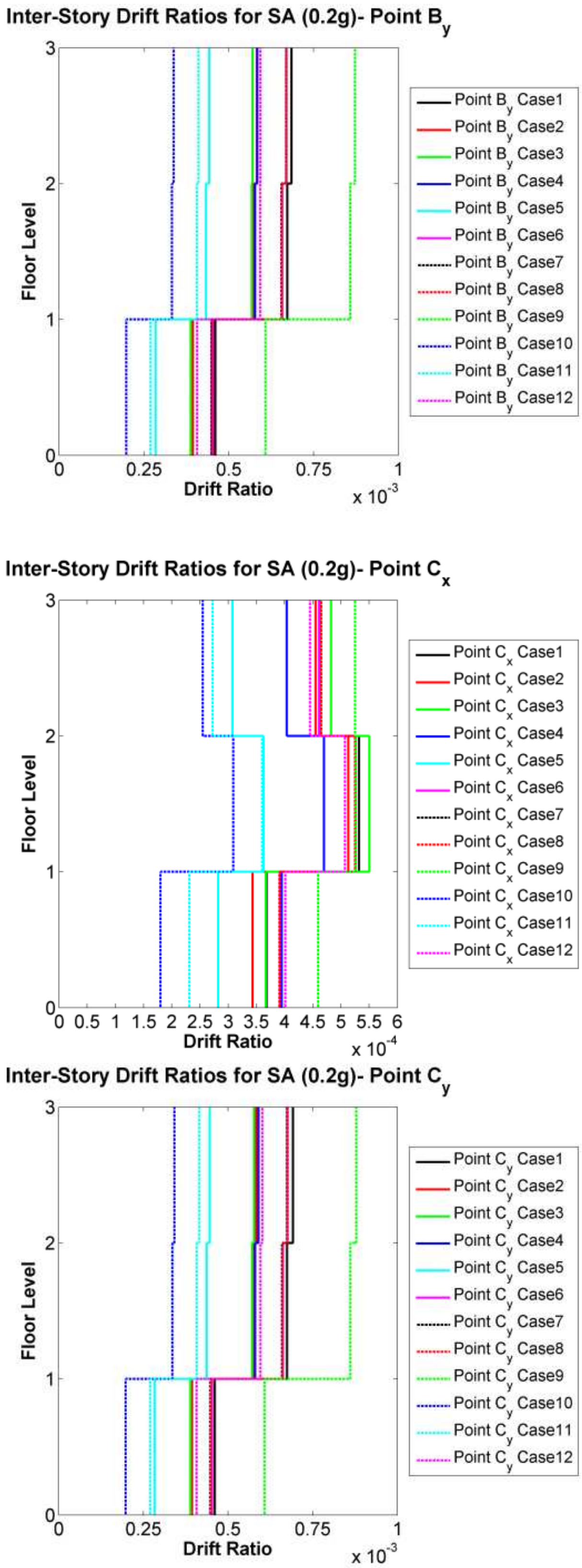

Figure 4.9 (Continued) Design Level (0.2 g) - Maximum Inter-Story Drift Ratios

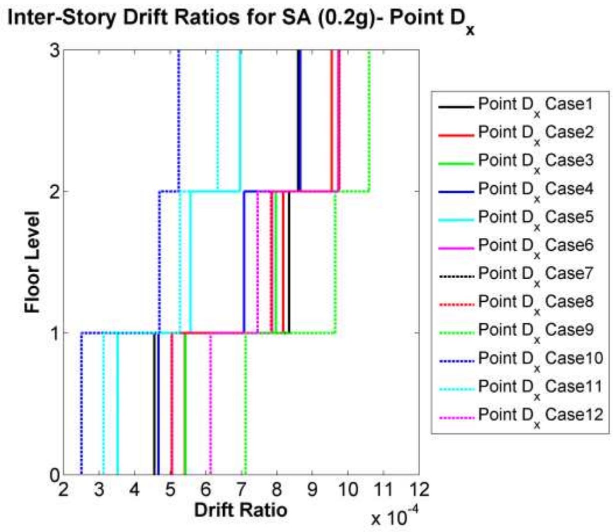

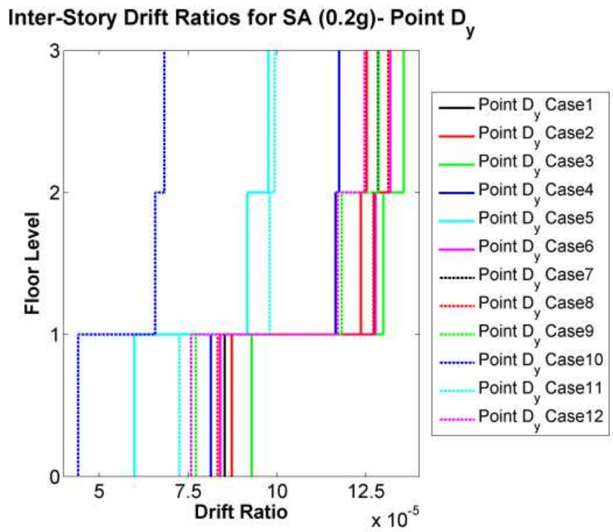

Figure 4.9 (Continued) Design Level (0.2 g) - Maximum Inter-Story Drift Ratios

Figure 4.10 represents the drift ratios for over – design cases as mentioned before. For point A, in X and Y directions at over-design level, the ranges of the drift ratios are accordingly 0.8e-3 – 1.7e-3 and 0.25e-3 – 0.75e-3 except Case 9. Case 9, in which the damping coefficient is 0.5%, changes between 2.3e-3 – 4.2e-3 and 0.7e-3 – 1.8e-3 in ranges accordingly for X and Y directions.

For point B, the ranges of drift ratios for X and Y directions are 0.8e-3 – 1.5e-3 and 1.4e-3 – 3e-3 except Case 9. Connection between first floor – second floor and second floor – third floor have approximately the same drift ratio change in X direction except Case 9. In Case 9, the maximum drift ratio change, 1e-3, occurs in first floor – second floor inter-connection both in X and Y direction.

Point C behaves like point B in terms of displacement response. The ranges of the drift ratios are 1e-3 – 2.2e-3 and 1.2e-3 – 3e-3 accordingly for X and Y directions except Case 9. Case 9 has the same behavior as in point B. The ranges of the drift ratios for Case 9 in X and Y directions are 4e-3 – 6.5e-3 and 5e-3 – 7.2e-3 accordingly.

For point D, the ranges of the drift ratios for X and Y directions are 2e-3–3.2e-3 and 0.25e-3 – 0.6e-3 except Case 9. In Case 9 for point D, the ranges of drift ratios are 7e-3 – 10.5e-3 and 1e-3 – 1.6e-3 in X and Y directions accordingly.

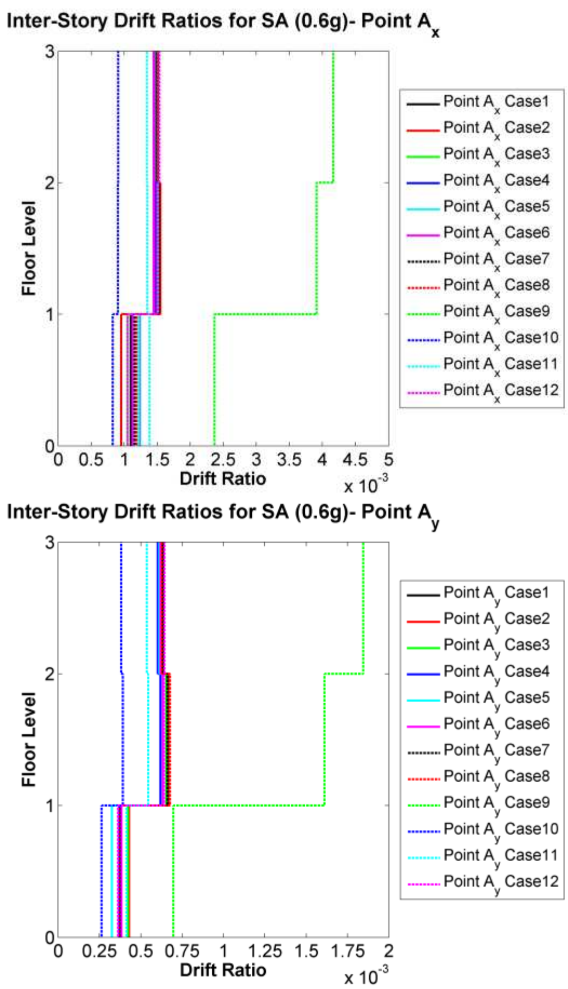

Figure 4-10 Over-Design Level (0.6 g) - Maximum Inter-Story Drift Ratios

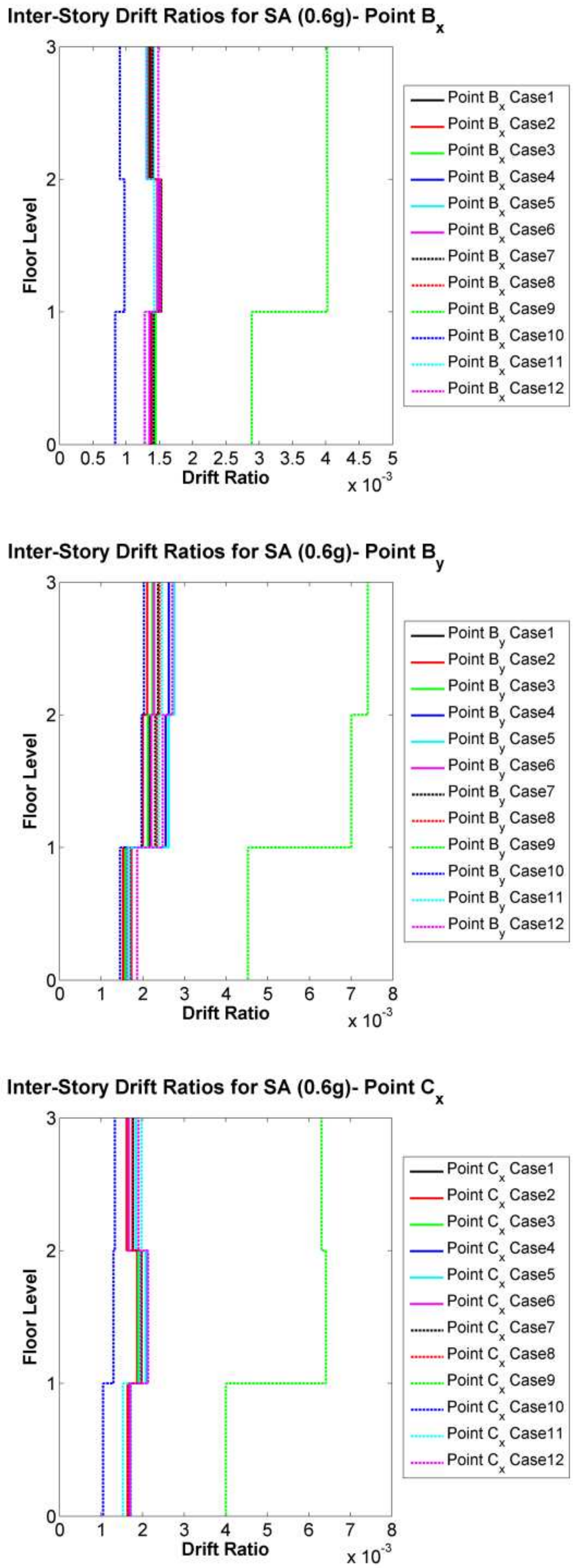

Figure 4.10 (Continued) Over-Design Level (0.6 g) - Maximum Inter-Story Drift Ratios

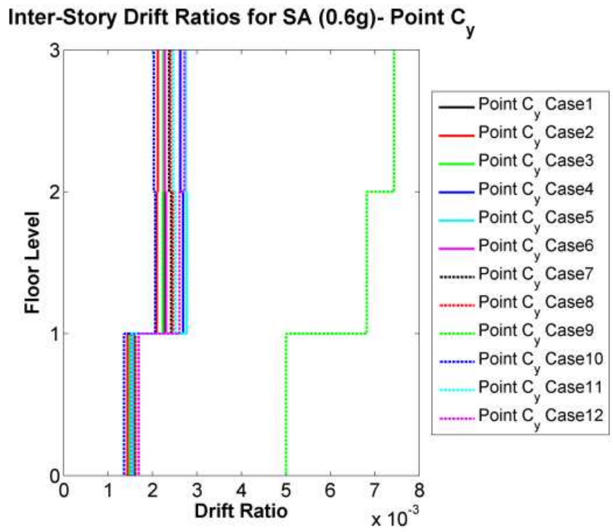

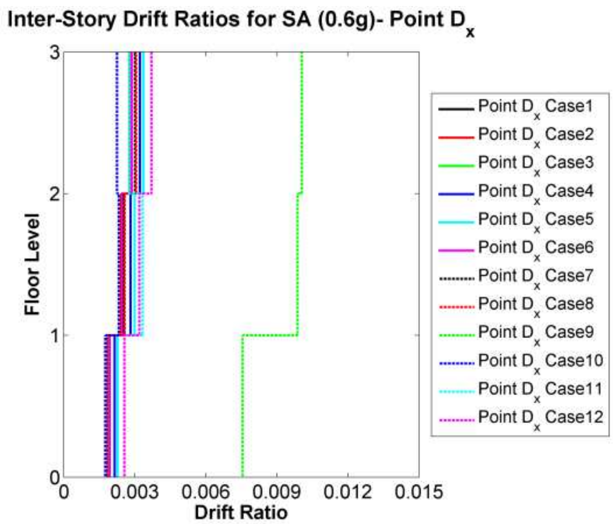

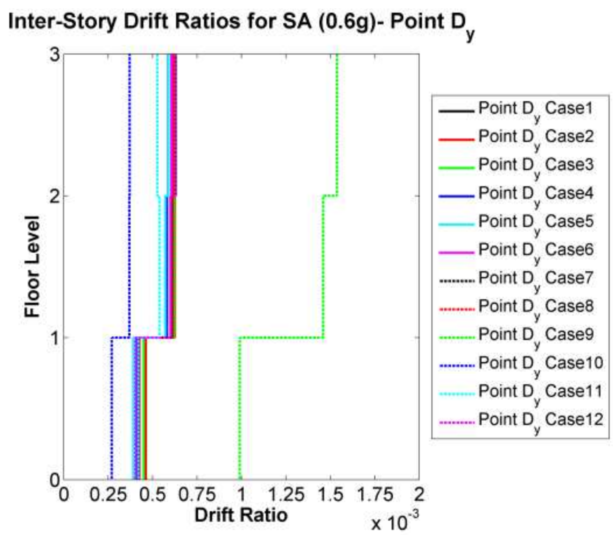

Figure 4.10 (Continued) Over-Design Level (0.6 g) - Maximum Inter-Story Drift Ratios

It is necessary to summarize the over-design level parametric study cases. At over- design level the damping coefficient parameter seems to be the most important one. Additional loading parameter loses its impact on response at over-design level, because its results are close to the other cases except for Case 9 and Case 10, which are related with the damping coefficient changes in the system.

4.1.4.4. Floor Response Spectrums

To figure out the effects of amplification of accelerations at upper levels of the building when subjected to the earthquakes the floor response spectrums were investigated. The Figure 4.11 and Figure 4.12 represent floor response spectrums at specified points of the building (Figure 2.7) for design and over-design parametric study cases at third floor.

In Figure 4.11, floor response spectrums at design level cases for third floor are represented.

For design level cases (Table 4.3) at point A (Figure 4.11), maximum spectral acceleration in the X direction occurs at period 0.07053 s with 2.32 g amplitude in Case 5. In Y direction maximum spectral acceleration occurs at first peak and period 0.033 s with 2.23 g amplitude in Case 11.

For point B (Figure 4.11), maximum spectral acceleration occurs at period 0.0746 s in second peak with amplitude of 2.08 g in X direction at Case 4. In Y direction, maximum spectral acceleration occurs again in second peak with 3.79 g amplitude at period 0.071 s in Case 11.

Maximum spectral acceleration at point C (Figure 4.11) occurs at period 0.04 s, which is the first peak, with 2.35 g amplitude in Case 9 for X direction. In Y direction it occurs at second peak with 3.78 g amplitude in Case 11 at a period of 0.071 s.

For point D, maximum spectral acceleration takes place in Case 9 with 4.23 g amplitude at second peak and period of 0.1035 s in X direction. In Y direction, it occurs at first peak with 2.24 g amplitude in Case 11 at period 0.033 s at first peak.

To sum up the general behavior at design level cases for floor response spectrums, the maximum peaks occurs approximately at the same periods. However, maximum spectral acceleration values changes at specified points. For points A, B and D, maximum spectral accelerations take place in second peaks in figures (Figure 4.10). For point C, maximum spectral acceleration takes place at the first peak.

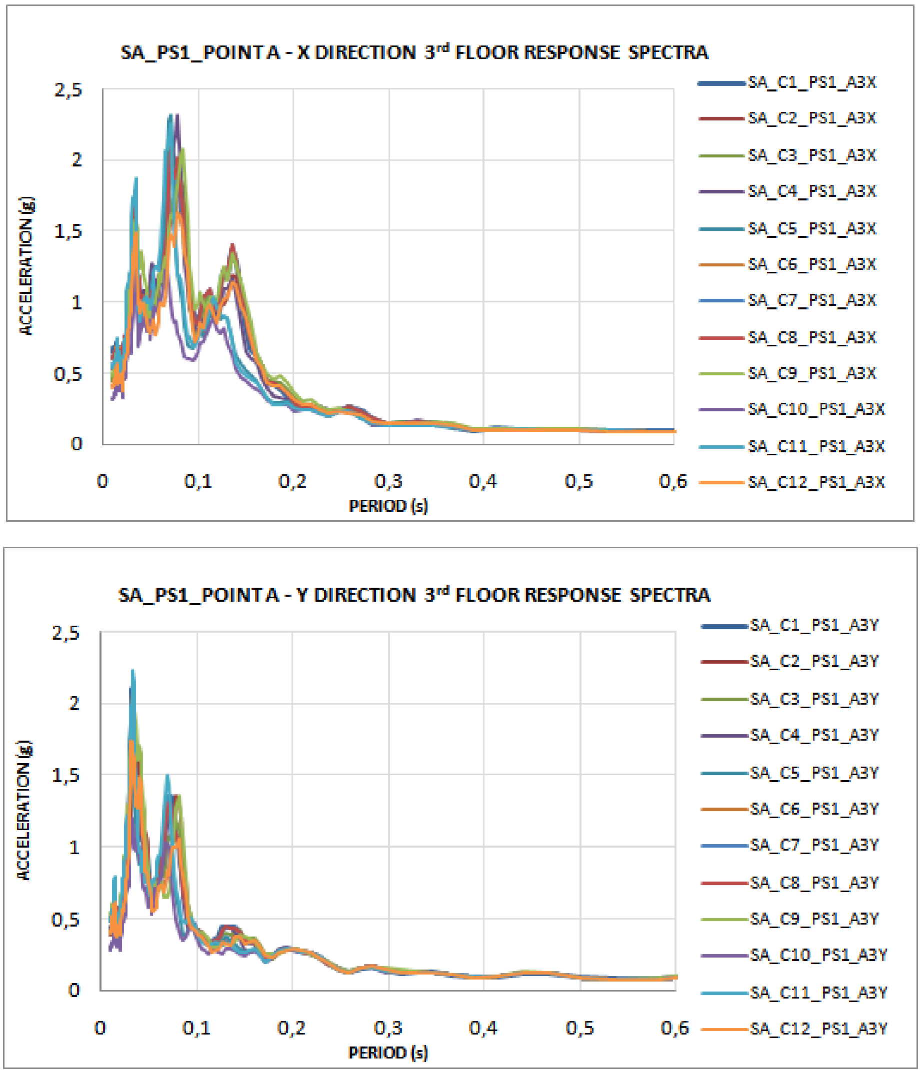

Figure 4-11 Design Level (0.2 g) – Third Floor, Floor Response Spectrums

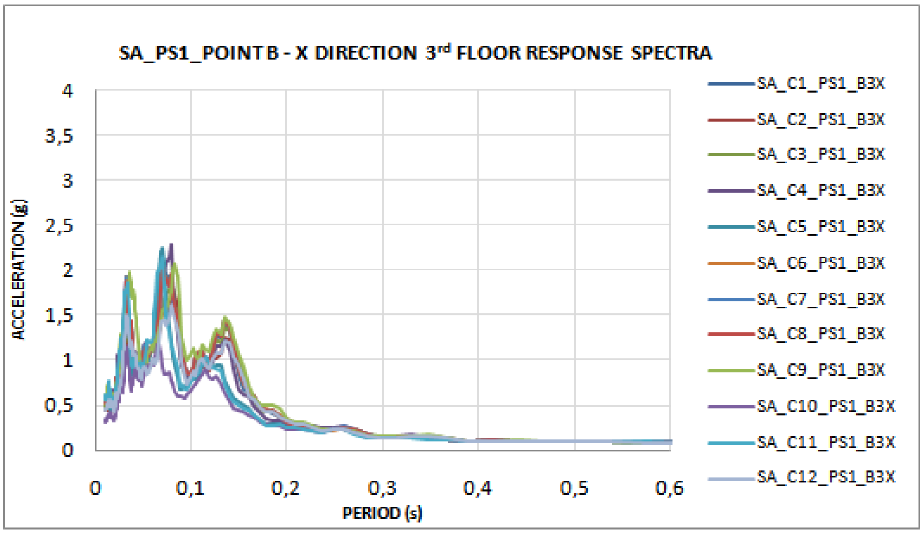

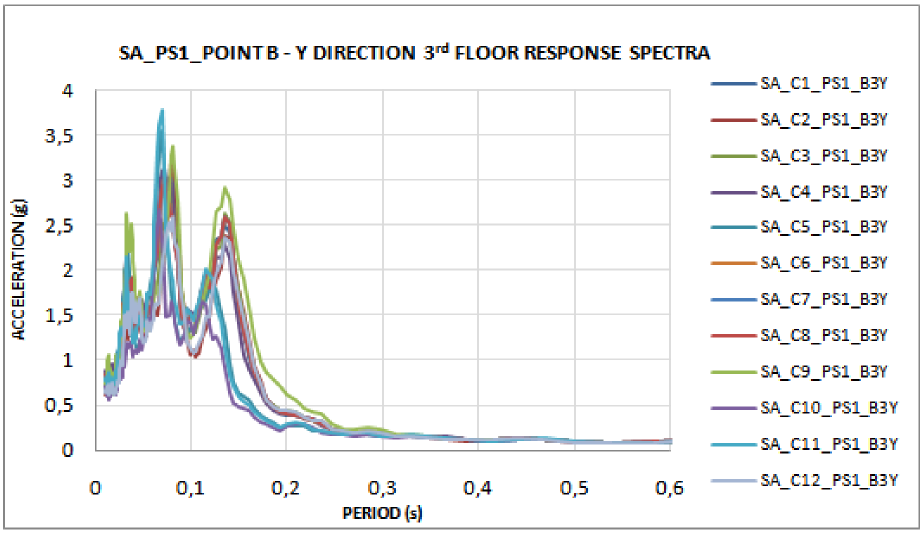

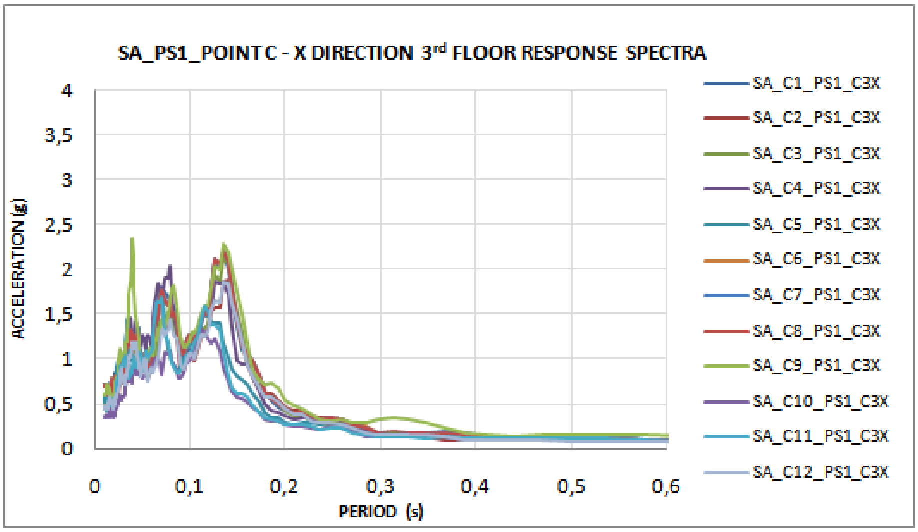

4.11 (Continue) Design Level (0.2 g) – Third Floor, Floor Response Spectrums

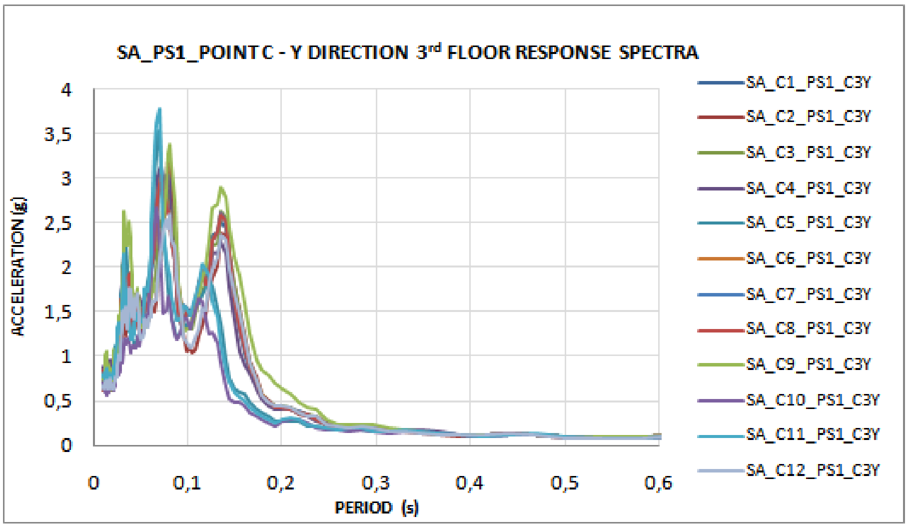

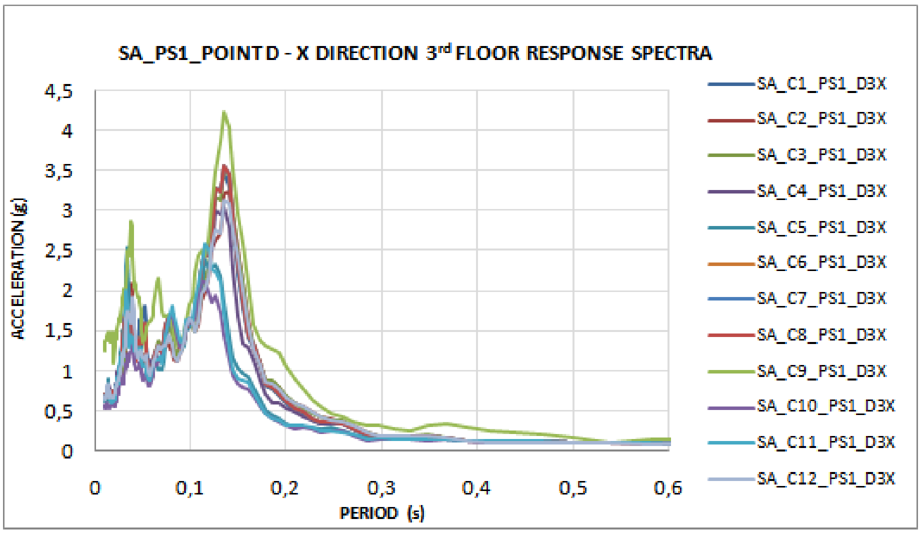

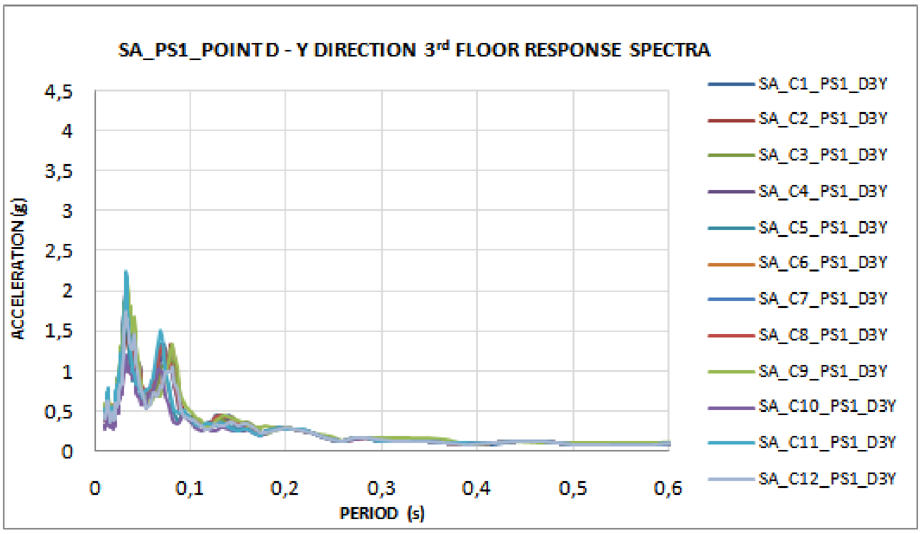

4.11 (Continue) Design Level (0.2 g) – Third Floor, Floor Response Spectrums

The cases also change in which the maximum spectral acceleration occurred. Case 11 seems to be the dominant case in design level cases. Case 11 is related with the decrease in additional loadings (Table 4.3)

Additionally, Case 12 also affects the spectrum. Thus it should be concluded that additional loading parameter is the most effective parameter at design level. Furthermore, at point D, which is the outer point on the floor level, maximum spectral acceleration is affected by damping coefficient in Case 9.

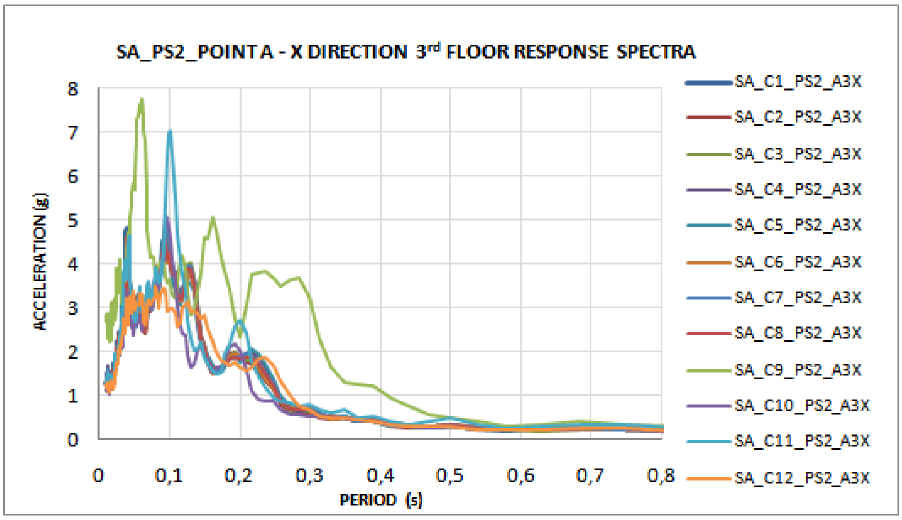

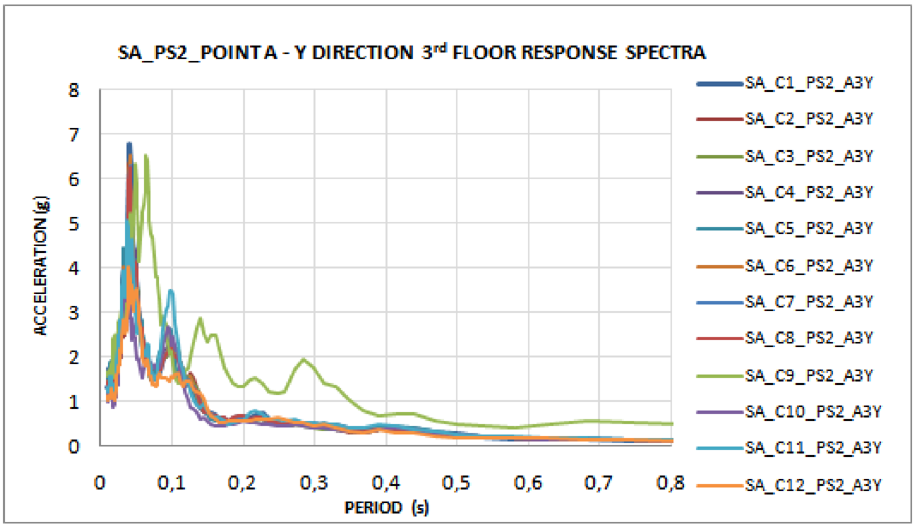

Figure 4-12 Over - Design Level (0.6 g) – Third Floor, Floor Response Spectrums

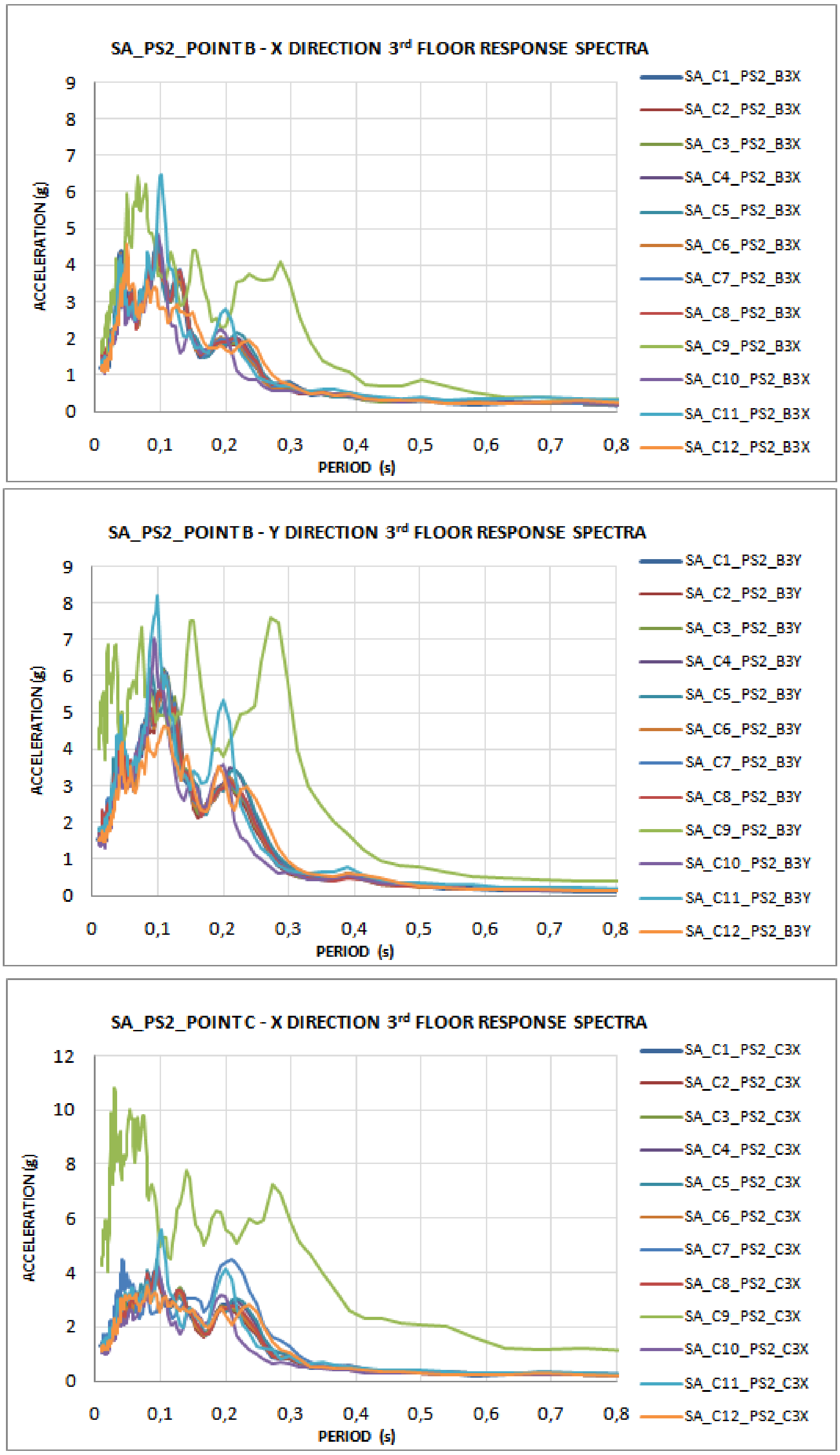

Figure 4.12 (Continue) Over - Design Level (0.6 g) – Third Floor, Floor Response Spectrums

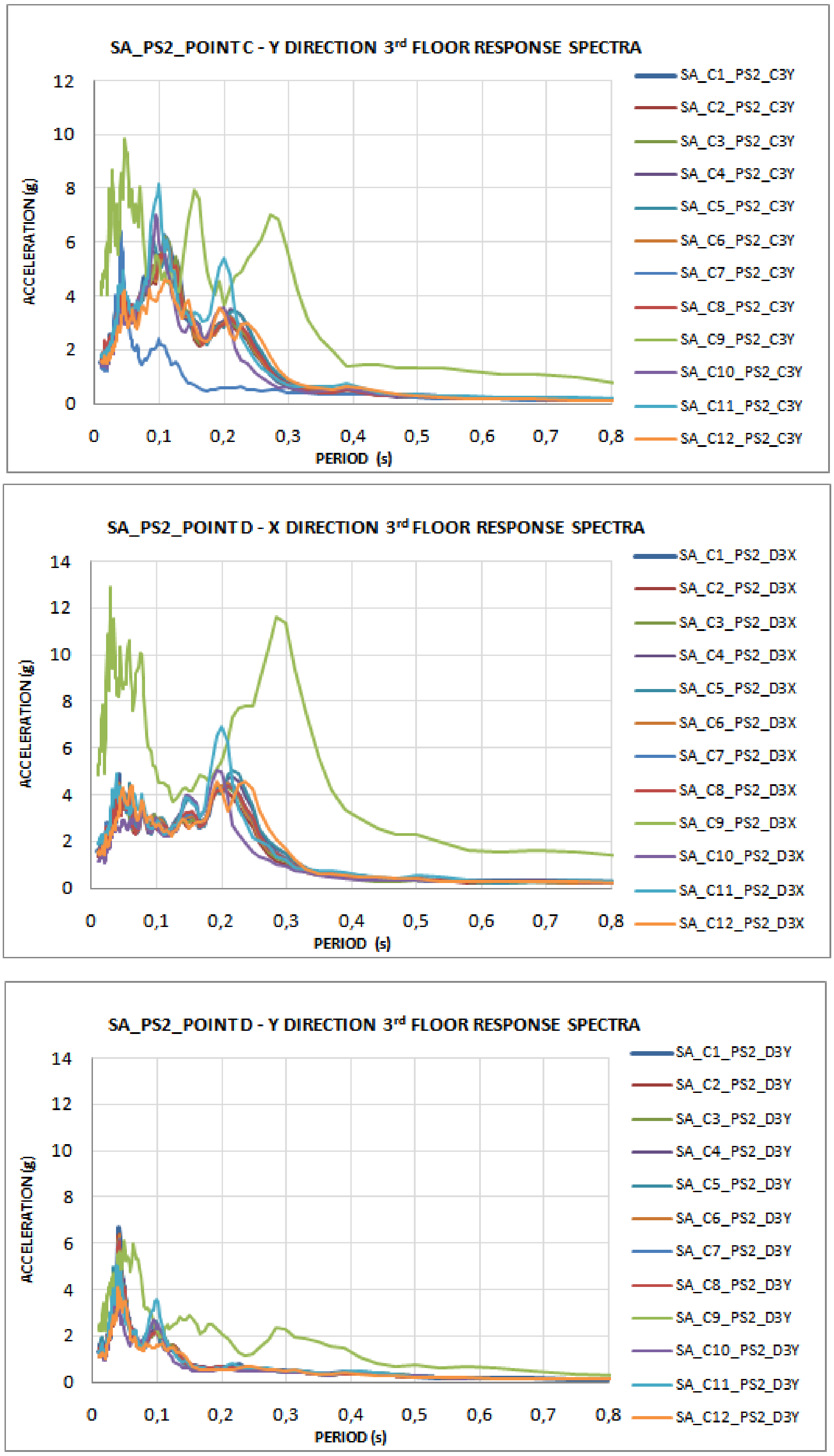

Figure 4.12 (Continue) Over - Design Level (0.6 g) – Third Floor, Floor Response Spectrums

In Figure 4.12, over-design level, floor response spectrums at third floor are represented. In all over- design cases, Case 9 has the maximum spectral acceleration values. However, due to the low damping ratio it seems to be not admissible. Thus, the maximum spectral accelerations are given for Case 9 and among the others.

For point A (Figure 4.12), at over-design level, maximum spectral acceleration occurs at period of 0.0603 s with 7.76 g amplitude in Case 9 in X direction. In Y direction, 6.77 g spectral acceleration occurs at period 0.041 s in Case 1. In X direction, if the case 9 is omitted, the maximum spectral acceleration occurs at period 0.102 s with 7.03 g amplitude in Case 11.

For point B (Figure 4.12), maximum spectral acceleration occurred at period 0.102 s with 6.48 g amplitude in Case 11 in X direction. In Y direction, it occurs at period 0.099s with 8.2 g amplitude in Case 11.

For point C (Figure 4.12), maximum spectral accelerations occurred at period 0.03 s with 10.81 g amplitude at first peak in X direction. The other maximum spectral acceleration in X direction occurs in Case 11 with 5.58 g amplitude at period 0.102s at second peak. In Y direction, maximum spectral acceleration occurred at period 0.047s with 9.86 g amplitude in Case 9. Again, if the Case 9 is omitted, maximum spectral acceleration in Y direction occurs at period 0.099 s with 8.18 g amplitude in Case 11.

For point D (Figure 4.12), maximum spectral acceleration is occurred in X direction at period 0.029 s with 12.86 g amplitude in Case 9. The second maximum spectral acceleration in X direction is at period 0.201 s with 6.92 g amplitude in Case 11. In Y direction, the maximum spectral acceleration occurs in Case 1 with 6.67 g amplitude at period 0.041 s.

To conclude the results of the parametric study for the over-design level, low damping ratio is the parameter that has the largest effect for the over-design level. Decrease in the damping ratio changes the floor response spectrum. Additional loading is another parameter affects the behavior of the structure as well. Increase in the additional loading on the structure decrease the floor response spectrum. Reverse is also true. Decrease in the additional loading result in increase in the floor response spectrum. It should be observed from the Figure 4.12 that, Case 11 has the maximum spectral acceleration amplitude in all when Case 9 is ignored.

4.1.4.5. Base Shear at Walls

Base shear forces for walls are calculated from the nodes at the basement level of each wall. Figure 4.13 and Figure 4.14 are displayed from the max base shears calculated from the basement nodes to figure out the system in an easy way.

At the design level, for all cases maximum base shear is carried by Wall 1 (Figure 2.7) which has the legend of max_1Fx in Figure 4.13 for X direction. In Y direction, this changes and Wall 4, the outer corner wall, takes the maximum base shear. In both directions at design level, Wall 3k takes base shear.

Elastic modulus of concrete, damping ratio and additional loading parameters seem to be effective, especially on walls that have greater part of the base shear.

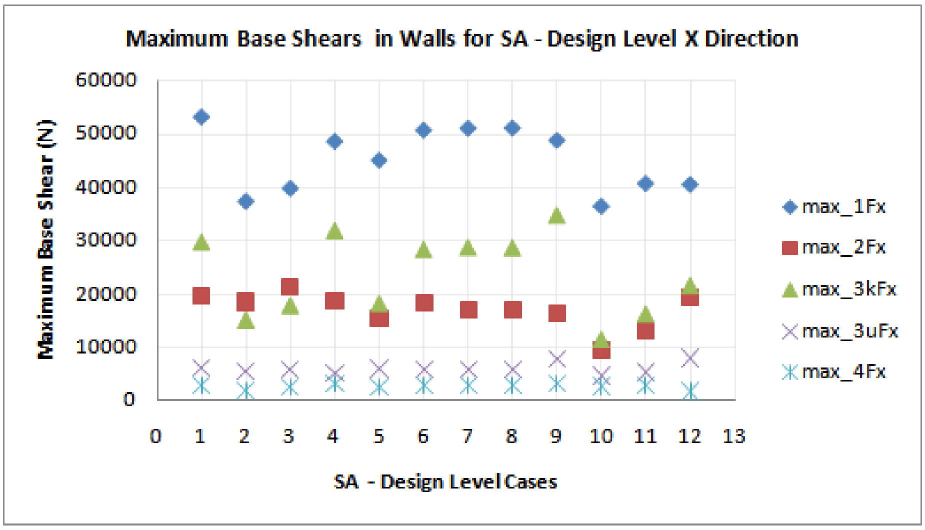

Figure 4-13 Design Level (0.2 g)–Maximum Base Shears of the Walls

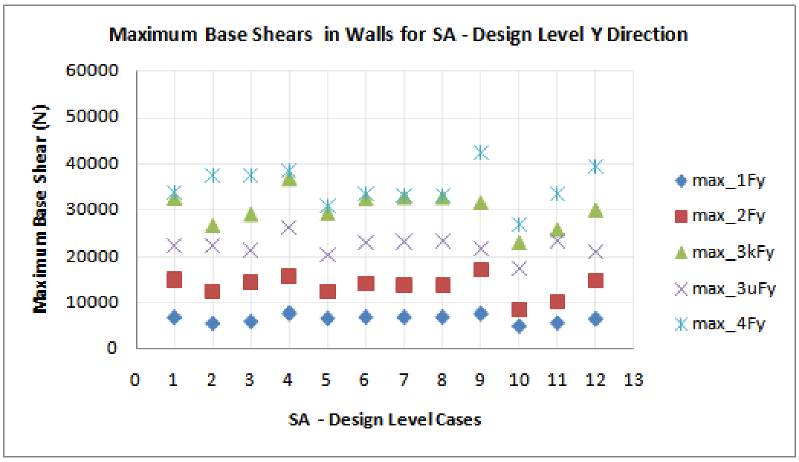

Figure 4.13 (Continue) Design Level (0.2 g)–Maximum Base Shears of the Walls

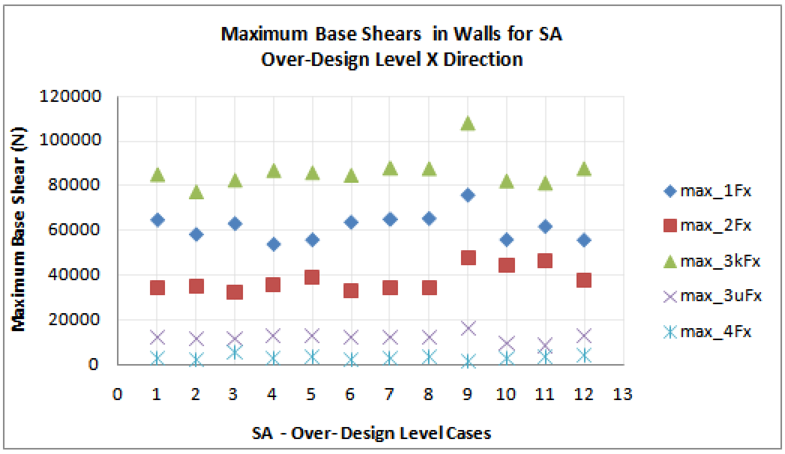

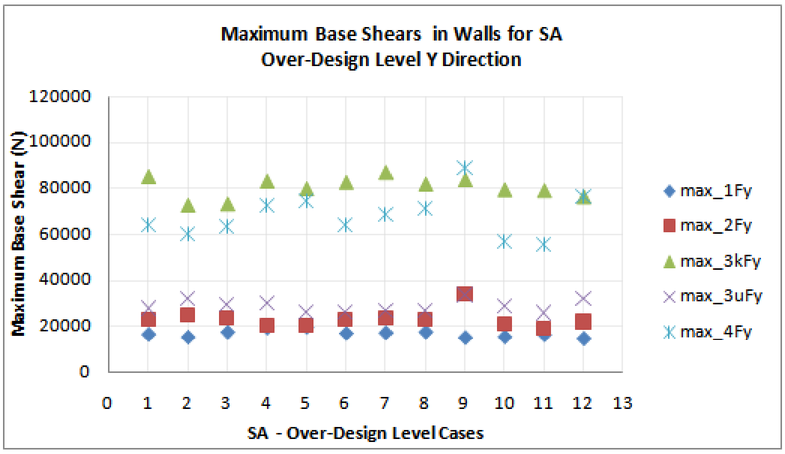

Figure 4-14 Over- Design Level (0.6 g)–Maximum Base Shears of the Walls

At over-design level, in both X and Y directions, maximum base shear is “carried” by Wall3k. Separation is visible for base shear capacities at over-design level in Figure 4.13. In the X direction; Wall 1, Wall 2, Wall 3k and Wall 3u and Wall 4 are separated as shown in Figure 4.14 in terms of base shear. In the Y direction, Wall 4 has reached maximum base shear in Case 9 in which the damping coefficient is the minimum.

As a conclusion, Elastic modulus affects the response in terms of displacement based results, especially in design level. However, it loses its importance at over – design level. Damping and additional loading parameters are the most effective ones in the parametric study cases as mentioned in design and over-design levels.

CHAPTER 5

FRAGILITY CURVES

One of the main objectives of this study is to obtain the fragility curves of this structure to develop an idea about the behavior of shear wall buildings under different seismic excitations with torsion effects. The main difficulty in the determination of fragility curves is the determination of limit states for the damage levels. In this chapter, the SMART- 2008 (RAPPORT DM2S, 2009) damage limits will be used for the limit states and compared with HAZUS limits.

5.1. Damage Indicators and threshold for failure criteria

All damage indicators and failure criteria thresholds are stated by SMART 2008 Project (RAPPORT DM2S, 2009) team as explained below.

Maximum inter-story drifts were used as a damage detector. To investigate the local effects of the damage, the fragility curves were calculated at specified points shown in Figure 2.8. The thresholds are given in Table 5.1. These damage levels are used as the criteria for the fragility analysis. H is the story height and equals to 1.2 m.

Table 5-1 Damage levels defined for maximum inter-story drifts

Damage Levels	(mm)
Light Damage	H/400 = 3
Controlled Damage	H/200 = 6
Extended Damage	H/100 =12

5.2. Seismic Motion Characterization for Fragility Analysis

A total of 30 sets of bi-directional horizontal accelerograms were used for the vulnerability analysis. The accelerograms chosen in this database were synthetic accelerograms, with a spectrum similar in shape with the one used to design the SMART specimen and a PGA of 0.2 g.

The amplitudes of the accelerograms had been chosen arbitrarily in order to cause visible damage in the structure and were not realistic, because they are much higher than an expected earthquake in France. All acceleration data for seismic excitation are applied bi-directionally and simultaneously in the analyses. The acceleration database is given in Appendix C.

5.2.1. Seismic Motion Indicators

Peak ground acceleration (PGA), cumulative absolute velocity (CAV), peak ground spectral displacement (PGD) and peak ground velocity (PGV) ground motion indicators were used in the vulnerability analysis. These indicators are given in Table 5.2 for the selected ground motion records.

Table 5-2 Seismic Motion Indicators for the Fragility Analysis

Accelerograms (ms-2)	**PGA** (g)	**PGV** (ms-1)	**PGD** (m)	**CAV** (ms-1)	**Accelerorgrams** (ms-2)	**PGA** (g)	**PGV** (ms-1)	**PGD** (m)	**CAV** (ms-1)
ACC_VA_1X_a	0.6361	0.4640	0.2340	4.4840	ACC_VA_1Y_a	0.6707	0.3000	0.1900	3.7340
ACC_VA_2X_a	0.0754	0.0260	0.0060	1.0520	ACC_VA_2Y_a	0.1713	0.0640	0.0080	2.2100
ACC_VA_3X_a	0.6157	0.3660	0.0740	4.8880	ACC_VA_3Y_a	0.4506	0.4340	0.1520	5.6680
ACC_VA_4X_a	0.4179	0.2920	0.1300	3.9740	ACC_VA_4Y_a	0.4404	0.3960	0.1500	3.5120
ACC_VA_5X_a	0.6646	0.4380	0.1420	5.4560	ACC_VA_5Y_a	0.9276	0.5740	0.1940	6.4220
ACC_VA_6X_a	0.3833	0.1460	0.0300	10.6560	ACC_VA_6Y_a	0.5158	0.1660	0.0780	11.0540
ACC_VA_7X_a	0.1814	0.0880	0.0280	1.7680	ACC_VA_7Y_a	0.2120	0.1360	0.0300	3.6840
ACC_VA_8X_a	0.3609	0.2260	0.0460	6.8040	ACC_VA_8Y_a	0.4363	0.2100	0.0780	7.0480
ACC_VA_9X_a	0.1346	0.0440	0.0100	4.2800	ACC_VA_9Y_a	0.1142	0.0580	0.0220	3.8940
ACC_VA_10X_a	0.2671	0.4020	0.3620	2.1300	ACC_VA_10Y_a	0.2100	0.2760	0.1080	3.3080
ACC_VA_11X_a	0.2895	0.1460	0.0580	2.0320	ACC_VA_11Y_a	0.2181	0.2740	0.1720	3.9000
ACC_VA_12X_a	0.3282	0.2020	0.0640	8.6460	ACC_VA_12Y_a	0.7339	0.3780	0.2720	16.3240
ACC_VA_13X_a	0.8583	0.2320	0.1620	9.7440	ACC_VA_13Y_a	0.4404	0.1060	0.0280	5.6200
ACC_VA_14X_a	0.2222	0.2700	0.0640	2.8320	ACC_VA_14Y_a	0.2059	0.2120	0.0960	3.5880
ACC_VA_15X_a	0.3384	0.1460	0.0360	3.9880	ACC_VA_15Y_a	0.2936	0.1380	0.0420	2.6320
ACC_VA_16X_a	1.0296	0.2300	0.0860	16.4220	ACC_VA_16Y_a	0.9827	0.3300	0.2920	12.0500
ACC_VA_17X_a	1.1254	0.3440	0.2580	25.3440	ACC_VA_17Y_a	1.2049	0.3160	0.2740	19.7380
ACC_VA_18X_a	0.4098	0.4380	0.2360	13.9280	ACC_VA_18Y_a	0.9235	0.4460	0.2480	26.4360
ACC_VA_19X_a	0.2120	0.1100	0.0420	2.8560	ACC_VA_19Y_a	0.0734	0.1140	0.1100	1.9560

Table 5.2 (Continued) Seismic Motion Indicators for the Fragility Analysis

Accelerograms (ms-2)	**PGA** (g)	**PGV** (ms-1)	**PGD** (m)	**CAV** (ms-1)	**Accelerorgrams** (ms-2)	**PGA** (g)	**PGV** (ms-1)	**PGD** (m)	**CAV** (ms-1)
ACC_VA_20X_a	0.2426	0.1560	0.0240	6.1020	ACC_VA_20Y_a	0.3751	0.1300	0.0200	10.3900
ACC_VA_21X_a	0.3344	0.1380	0.0720	5.8940	ACC_VA_21Y_a	0.2487	0.0920	0.0100	5.0520
ACC_VA_22X_a	0.3874	0.2280	0.1920	19.9440	ACC_VA_22Y_a	0.7339	0.3160	0.1860	16.2160
ACC_VA_23X_a	0.9113	0.3560	0.0820	14.3900	ACC_VA_23Y_a	0.8277	0.5260	0.3160	6.6240
ACC_VA_24X_a	0.8155	0.2060	0.0260	17.0900	ACC_VA_24Y_a	0.7258	0.1780	0.0460	14.5260
ACC_VA_25X_a	1.1682	0.4040	0.1160	22.9060	ACC_VA_25Y_a	0.6381	0.4600	0.4480	8.5000
ACC_VA_26X_a	0.2243	0.1860	0.0860	2.1340	ACC_VA_26Y_a	0.2406	0.1960	0.1220	2.6420
ACC_VA_27X_a	0.2141	0.0680	0.0100	5.0480	ACC_VA_27Y_a	0.2875	0.0800	0.0300	5.5140
ACC_VA_28X_a	0.8705	0.4240	0.1300	11.7700	ACC_VA_28Y_a	0.4771	0.3560	0.0460	7.4380
ACC_VA_29X_a	0.5280	0.1680	0.0320	9.1900	ACC_VA_29Y_a	0.5362	0.1480	0.0300	12.3640
ACC_VA_30X_a	1.0805	0.3800	0.1140	16.9720	ACC_VA_30Y_a	1.0663	0.2880	0.1280	11.5080

5.3. Structural Properties and Limitations

The parameters used in the fragility analysis were established according to the reference case presented in Table 4.3. This way, E_c= 32000 MPa, F_y= 500 MPa, damping coefficient is 2 percent and additional loading is 33.85 t.

In the fragility analysis part, the base boundary conditions have been taken as fixed according to the SMART 2008 report (RAPPORT DM2S, 2009). Shaking table was not modeled due to many unknown variables in its physical characterization.

5.4. Analyses Performed for the Fragility Curves

Time – history analyses were performed for the fragility analysis. In this way, fewer assumptions were made for the simulation of the building behavior under seismic excitations. The nonlinear material models were used as stated in Chapter 2.

According to the results of the fragility analysis, the log – normal distribution was assumed for the distribution of the structural response indicators and then the fragility curves were obtained according to median capacity and standard deviation of this distribution.

5.4.1. Log-normal Distribution for Fragility Curves

Fragility curves express the conditional probability of failure of a structure or component for a given seismic input motion parameter, such as PGA, PGV, CAV and PGD.

The fragility of a structure or component is determined with respect to its capacity, denoted by "A". Capacity is defined as the limit seismic load before failure occurs and is modeled by a random variable. The limit seismic load can be characterized by a parameter related to the ground motion level, such as PGA or others. For instance, if PGA has been chosen to characterize seismic ground motion level, then capacity is also expressed in terms of PGA. The probability of failure P_f of a structure or component conditioned on seismic ground motion level "a" is expressed by fragility curves as given in Equation (5.1).

$$P_f \equiv P(Failure|a) = P(A < a) \tag{5.1}$$

Failure occurs, if the actual capacity of the structure is inferior to the seismic demand, that is the given ground motion level "a".

In a general way, fragility curves can be derived by statistical estimation of failure probabilities. An alternative approach is the very commonly used lognormal model. The log – normal distribution was defined by Hahn and Saphiro (1967).

In this study, log-normal distribution was assumed for fragility model and the fragility curves were entirely defined by the median capacity, A_m and a log standard deviation, β. The failure probability conditioned on ground motion parameter "a" given by the cumulative distribution function of capacity A can be calculated from Equation 5.2.

$$P_f = \Phi(\frac{\ln(a) - A_m}{\beta}) \tag{5.2}$$

If a random variable $\ln(a)$ is normally distributed with median A_m and standard deviation β, the random variable a becomes log – normally distributed. Cumulative distribution function for random variable $ln\, a$ is of normal type:

$$F(ln\, a) = \frac{1}{\sqrt{2\pi}}.\frac{1}{\beta}.\int_{-\infty}^{\ln a} e^{-\frac{1}{2}\left(\frac{\ln v - \mathrm{A_m}}{\beta}\right)^2} d(\ln v) = \frac{1}{\sqrt{2\pi}}.\frac{1}{\beta}.\int_{-\infty}^{X} e^{-\frac{1}{2}\left(\frac{\ln v - \mathrm{A_m}}{\beta}\right)^2} \frac{1}{v}\, dv \qquad (5.3)$$

Since:

$$F(ln\, a) = \int_{-\infty}^{a} f(v)dv \qquad (5.4)$$

The probability density function will be defined by Equation 5.5.

$$f(a) = \frac{1}{\sqrt{2\pi}}.\frac{1}{\beta}.\frac{1}{x} e^{-\frac{1}{2}\left(\frac{\ln x - \mathrm{A_m}}{\beta}\right)^2} \qquad (5.5)$$

If one uses the reduced variable $(\ln(v) - \mathrm{A_m})/\beta = u$, $du/dv = 1/(v\beta)$ and one must integrate from $-\infty$ to $z = (\ln(a) - \mathrm{A_m})/\beta$ then from Equation 5.3;

$$\Phi\left(\frac{\ln(a) - A_m}{\beta}\right) = \Phi(z) = \frac{1}{\sqrt{2\pi}}.\int_{-\infty}^{z} e^{-\frac{u^2}{2}}\, du \qquad (5.6)$$

Probability density function for reduced variable can be obtained from Equation 5.6.

5.4.2. Regression analysis

To obtain the fragility curves from the probability density functions, we need to define the acceptable median capacity and standard deviations for the limit states defined in Table 5.1 under different seismic excitations.

One of the well known methods used to determine the median capacity and the standard deviation is the regression analysis.

For a given data set $\{y_i, x_{i\,1}, x_{i\,2}, x_{i\,3}, \dots, x_{i\,p}\}_{i=1}^{n}$ of n statistical units, linear regression model assumes that the relationship between the dependent variable y_i and independent variable $x_{i\,p}$ vectors is linear. There is also an error term, ε_i , which is an unobserved random variable that adds a noise to the linear relationship between the dependent and independent variables.

$$y_i = b_i\, x_{i\,1} + b_i\, x_{i\,2} + \cdots + b_i\, x_{i\,p} + \alpha_i, \qquad i = 1, \ldots, n \tag{5.7}$$

In vector form:

$$y = bX + \alpha \qquad \underline{b} = n \times 1;\ X = n \times p \tag{5.8}$$

$$y = \begin{bmatrix} y_1 \\ y_2 \\ \vdots \\ y_n \end{bmatrix}, X = \begin{bmatrix} x_{11} & \cdots & x_{1p} \\ x_{21} & \cdots & x_{2p} \\ \vdots & \ddots & \vdots \\ x_{n1} & \cdots & x_{np} \end{bmatrix}, b' = \begin{bmatrix} b_1 \\ b_2 \\ \vdots \\ b_n \end{bmatrix}, \alpha = \begin{bmatrix} \alpha_1 \\ \alpha_2 \\ \vdots \\ \alpha_n \end{bmatrix} \tag{5.9}$$

When dealing with two or more variables, the mathematical relationship between the variables is often of interest. In Equation 5.10, given by Ang and Tang (1975), α and b are constants and the variance of Y may be independent or a function of x. This is known as the linear regression of Y on X as given in Equation (5.10).

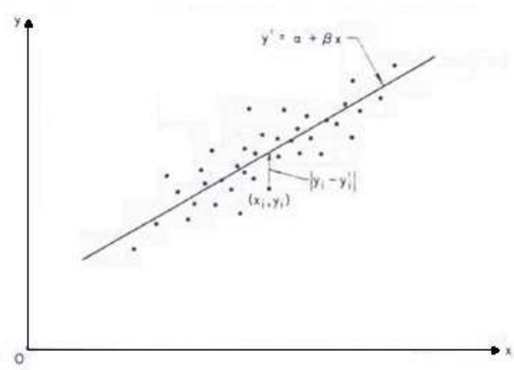

Figure 5-1 Linear analyses of data for two variables (Ang and Tang, 1975)

$$E(Y|X = x) = \alpha + bx \tag{5.10}$$

Depending on the values of α and b constant terms, there could be many straight lines that might qualify as the mean- value function of Y in the light of the data. According to Ang and Tang (1975), the "best" line is the one that passes through the data points with the least error. Figure 5.1 gives notation used in least squares method.

To obtain the least error, the method of least squares is applied to the data in this study. According to the least squares method, the line with the least total error can be obtained by minimizing the sum of the squared errors as given in equation 5.12 and 5.13.

$$\Delta^2 = \sum_{i=1}^{n} (y_i - y_i')^2 = \sum_{i=1}^{n} (y_i - \alpha + bx_i)^2 \tag{5.11}$$

$$\frac{\partial \Delta^2}{\partial \alpha} = \sum_{i=1}^{n} 2(y_i - \alpha + bx_i)(-1) = 0 \tag{5.12}$$

$$\frac{\partial \Delta^2}{\partial \beta} = \sum_{i=1}^{n} 2(y_i - \alpha + bx_i)(-x_i) = 0 \tag{5.13}$$

5.4.3. Results of Regression and Fragility Analyses

Linear regression with least squares method was applied to the log-normal distribution according to the indicators given in the SMART 2008 Phase-2 report (RAPPORT DM2S, 2009). For log-normal distribution linear regression is still applicable because, since Y is supposed to be log-normally distributed, ln(Y) is a normally distributed (Gaussian) random variable (Figure 5.2). This is the reason that linear regression is performed for ln(Y) and ln(X) by virtue of Equation 5.14.

$$ln(Y) = \alpha + bln(X) + \varepsilon \tag{5.14}$$

In this expression, parameters α and b are to be determined from the least squares method and ε is a centered normally distributed random variable with standard deviation $\sigma_{ln\varepsilon}$. In consequence, Y and X were linked by the Equation 5.15.

$$Y = \tilde{\alpha} X^b \tilde{\varepsilon} \tag{5.15}$$

Where $\tilde{\alpha} = exp(\alpha)$ and $\tilde{\varepsilon} = exp(\varepsilon)$ was log-normally distributed random variable with median equal to one and logarithmic standard deviation σ_{ε}.

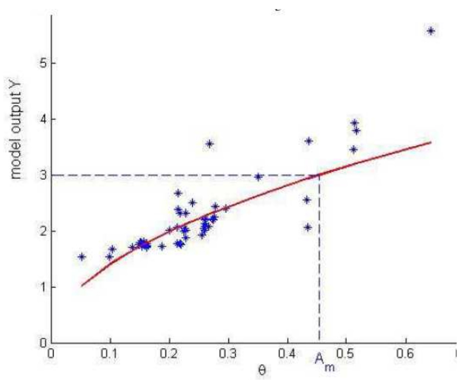

Figure 5-2 Regression analyses for model output Y (SMART 2008 Phase 2 Report, 2009)

After regression analyses the needed median seismic capacity, A_m and log-standard deviation, β can be evaluated. For the evaluation of A_m, Y_{crit} value can be used as shown in Equation 5.16.

$$ln\ (A_m) = \frac{\ln(Y_{crit}) - \alpha}{b} \tag{5.16}$$

In Equation 4.16, Y_{crit} values were defined in the SMART 2008 Phase-2 report (RAPPORT DM2S, 2009) as damage levels which were given in Table 5.1.

As mentioned in Section 4.2.1., damage indicators for the fragility analysis are given as maximum inter-story drift results for the time-history analyses. Regression analyses done for both X and Y directions for seismic ground motion indicators (SGMI) and maximum inter-story drift (MISD) results were obtained from time history analyses on points A, B, C, D, E, F and G (Figure 2.8) with respect to the given damage indicators.

The regression analyses results are given in Appendix A. The median seismic capacity, A_m and log-standard deviation, β values are given in Tables 5.3 and 5.4, respectively for the damage indicators under seismic ground motion indicators. In Table 5.5, the linear relationship between the MISD and SGMI are examined.

A probabilistic distribution of the damage levels according to the MISD values at different points on the building with respect to the given damage levels are given in Table 5.6 for both X and Y directions. Points A, D and F have no extended damage level according to the calculated probabilistic distribution in Table 5.6.

Table 5-3 β (Log-standard deviation) coefficients for data

	PGA_x	PGA_y	PGV_x	PGV_y	PGD_x	PGD_y	CAV_x	CAV_y
Point A	0.46	0.46	0.44	0.44	0.74	0.74	0.69	0.69
Point B	0.45	0.41	0.43	0.45	0.74	0.81	0.69	0.65
Point C	0.45	0.42	0.43	0.46	0.74	0.82	0.72	0.65
Point D	0.43	0.50	0.46	0.55	0.80	0.76	0.70	0.68
Point E	0.46	0.41	0.45	0.49	0.73	0.80	0.73	0.62
Point F	0.45	0.42	0.44	0.53	0.73	0.80	0.74	0.58
Point G	0.47	0.42	0.46	0.47	0.73	0.81	0.73	0.64

Table 5-4 A_m –Seismic median capacity coefficients for data

		Point A	Point B	Point C	Point D	Point E	Point F	Point G
	LD	0.53	0.53	0.41	0.27	0.45	0.40	0.46
	CD	0.96	0.95	0.73	0.47	0.80	0.72	0.82
PGA_x	ED	1.73	1.71	1.29	0.81	1.42	1.28	1.46
	LD	0.26	0.26	0.21	0.14	0.22	0.20	0.23
	CD	0.46	0.45	0.35	0.23	0.39	0.35	0.39
PGV_x	ED	0.80	0.79	0.61	0.39	0.66	0.60	0.68
	LD	0.10	0.10	0.08	0.05	0.08	0.08	0.08
	CD	0.17	0.17	0.13	0.09	0.14	0.13	0.15
PGD_x	ED	0.30	0.30	0.23	0.15	0.25	0.22	0.25
	LD	8.84	8.73	6.32	3.67	7.09	6.26	7.29
	CD	18.78	18.54	13.22	7.49	14.91	13.11	15.34
CAV_x	ED	39.87	39.40	27.67	15.28	31.36	27.44	32.27
	LD	0.53	0.30	0.29	1.03	0.46	0.69	0.33
	CD	0.96	0.52	0.51	1.91	0.82	1.26	0.58
PGA_y	ED	1.73	0.92	0.90	3.54	1.48	2.30	1.02
	LD	0.26	0.15	0.15	0.50	0.23	0.34	0.17
	CD	0.46	0.26	0.25	0.89	0.40	0.60	0.29
PGV_y	ED	0.80	0.44	0.43	1.59	0.70	1.07	0.49
	LD	0.10	0.06	0.05	0.18	0.09	0.13	0.06
	CD	0.17	0.10	0.09	0.33	0.15	0.22	0.11
PGD_y	ED	0.30	0.17	0.16	0.59	0.26	0.40	0.18
	LD	8.84	4.21	4.10	20.55	7.32	12.19	4.76
	CD	18.78	8.64	8.40	45.00	15.37	26.13	9.82
CAV_y	ED	39.87	17.75	17.22	98.56	32.27	56.03	20.23

Table 5-5 Correlation coefficients for MISD versus SGMI

	PGA_x	PGA_y	PGV_x	PGV_y	PGD_x	PGD_y	CAV_x	CAV_y
Point A	0.80	0.81	0.83	0.78	0.76	0.71	0.69	0.77
Point B	0.80	0.81	0.83	0.79	0.77	0.69	0.68	0.64
Point C	0.82	0.81	0.86	0.79	0.77	0.69	0.63	0.65
Point D	0.81	0.78	0.83	0.78	0.71	0.71	0.60	0.75
Point E	0.82	0.85	0.85	0.77	0.77	0.70	0.63	0.76
Point F	0.83	0.82	0.85	0.73	0.76	0.70	0.60	0.82
Point G	0.82	0.83	0.85	0.78	0.77	0.70	0.64	0.70

Table 5-6 Probabilities of the data passes the damage levels

	X Direction			Y Direction		
	LD	CD	ED	LD	CD	ED
Point A	0.58	0.26	0.16	0.77	0.23	0.00
Point B	0.58	0.26	0.16	0.32	0.23	0.45
Point C	0.52	0.13	0.35	0.32	0.16	0.52
Point D	0.32	0.23	0.45	0.77	0.23	0.00
Point E	0.55	0.13	0.32	0.45	0.26	0.29
Point F	0.52	0.06	0.42	0.65	0.35	0.00
Point G	0.55	0.16	0.29	0.35	0.19	0.45

LD = Light Damage; CD = Controlled Damage; ED = Extended Damage

The points that intersect the damage levels in Figure 5.3 graphs are the seismic median capacities for the given seismic ground motion indicators.

The fragility curves were obtained according to the calculated seismic median capacity and log-standard deviation coefficients (Table 5.3 and Table 5.4). The fragility curves obtained according to these parameters are given in Appendix B.

For Point A, (Figure A.1), in Y direction regression analyses did not give a good fit for the seismic motion indicators such as PGA, PGV, PGD and CAV. Standard deviation were used twice as error term (ε_{lnx}) for the analyses to capture reasonably good fit for data. This is the lower limit of the fitted curve for Point A data.

Due to torsion in the building, specified points (Figure 2.8) on the same floor level have different responses. In this study, Point E is taken into account so as to represent the structural behavior. This point is close to the mass center of the system and, has the high correlation coefficients when the time history data is compared with the fitted curves as a result of the regression analysis. The correlation coefficients of fitted curves and time history analyses are given in Table 5.7.

Table 5-7 Correlation coefficients for time history data versus fitted curves

	PGA_x	PGA_y	PGV_x	PGV_y	PGD_x	PGD_y	CAV_x	CAV_y
Point A	0.87	0.86	0.90	0.86	0.85	0.82	0.97	0.98
Point B	0.88	0.88	0.91	0.89	0.86	0.81	0.97	0.89
Point C	0.89	0.88	0.92	0.89	0.86	0.81	0.94	0.88
Point D	0.89	0.84	0.90	0.86	0.81	0.82	0.83	0.99
Point E	0.89	0.91	0.92	0.87	0.86	0.82	0.94	0.97
Point F	0.89	0.88	0.92	0.85	0.85	0.82	0.93	0.99
Point G	0.88	0.90	0.92	0.88	0.86	0.82	0.95	0.92

The regression analysis results for Point E are given in Figure 5.3 and fragility curves are shown in Figure 5.4. The highest correlation coefficients are obtained from the time history analyses for the CAV (Cumulative Absolute Velocity) seismic ground motion indicator and the lowest correlation coefficients for the PGD seismic motion indicator. The correlation coefficient for PGA parameter for X and Y directions are respectively 0.89 and 0.91. These results were thought to have reasonably enough accuracy for the fragility curves.

The scatter of the fragility curves for the given damage levels changes under different seismic ground motion indicators as shown in Figure 5.4. PGA and PGV have similar trends in shape; however the CAV and PGD differ.

The probabilistic scatters between the damage levels were slightly wider and the structure behaves well even under relatively higher seismic motions. In Figure 5.4, the probability of failure at the damage levels under PGA seismic motion indicator were nominal till 0.5 g.

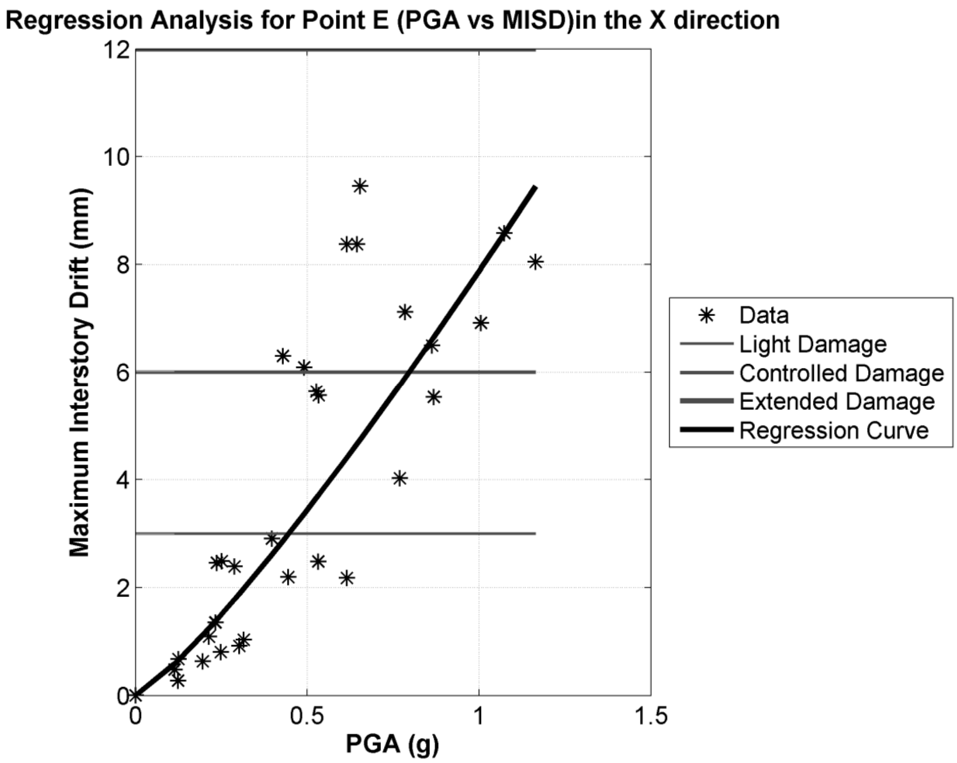

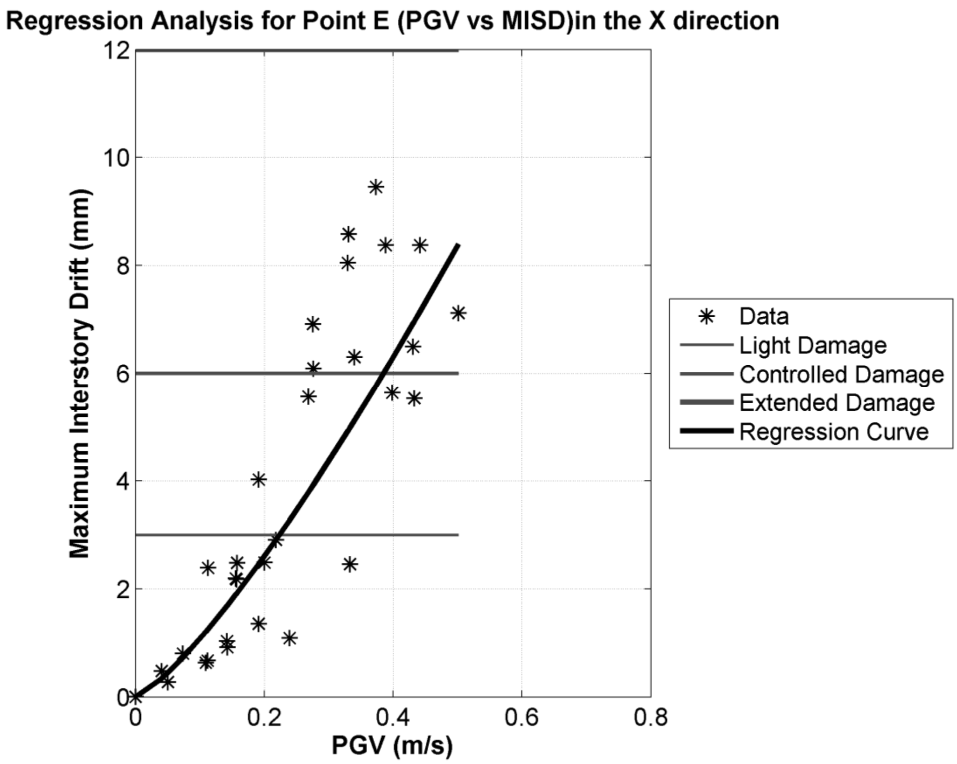

Figure 5-3 Regression Analysis for Point E for seismic motion indicators

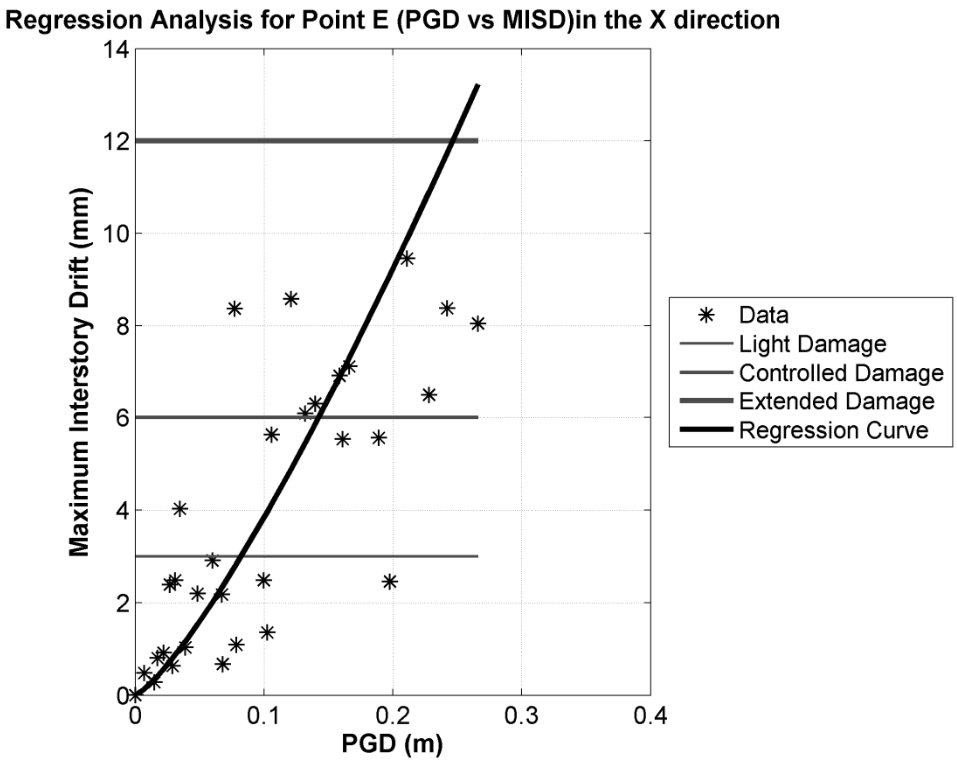

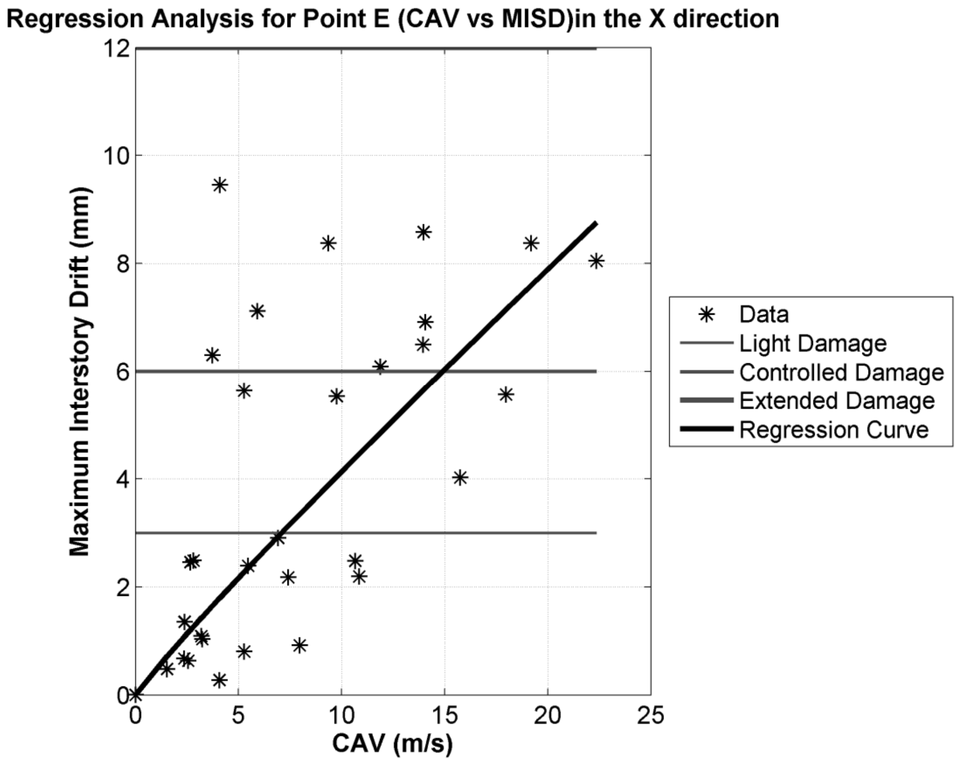

Figure 5.3 (Continued) Regression Analysis for Point E for seismic motion indicators

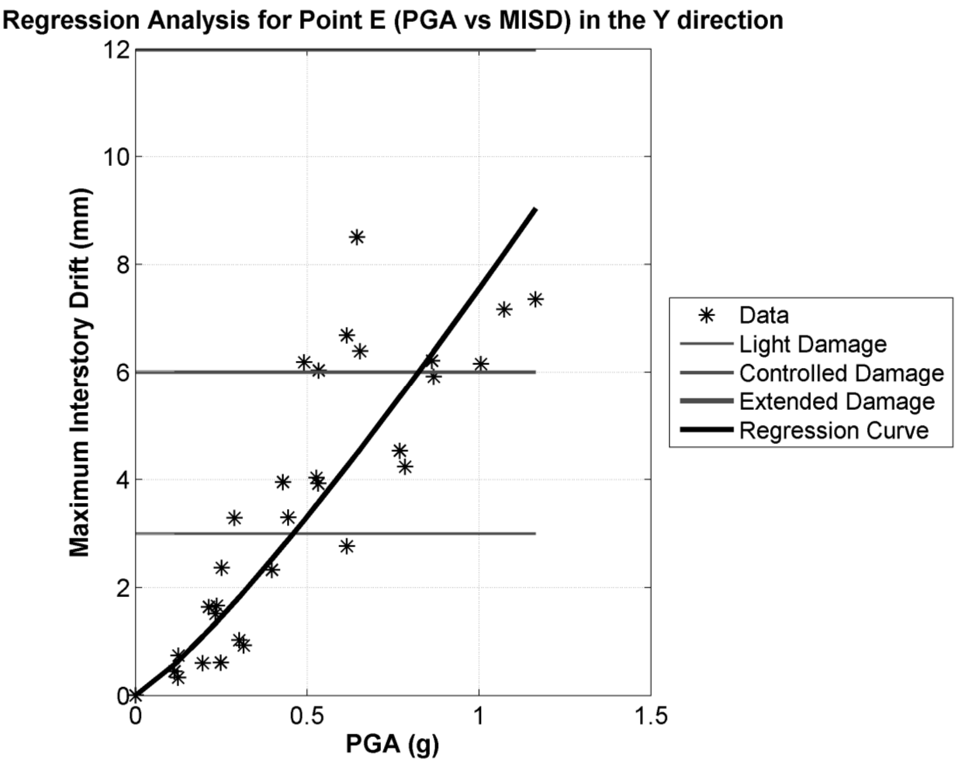

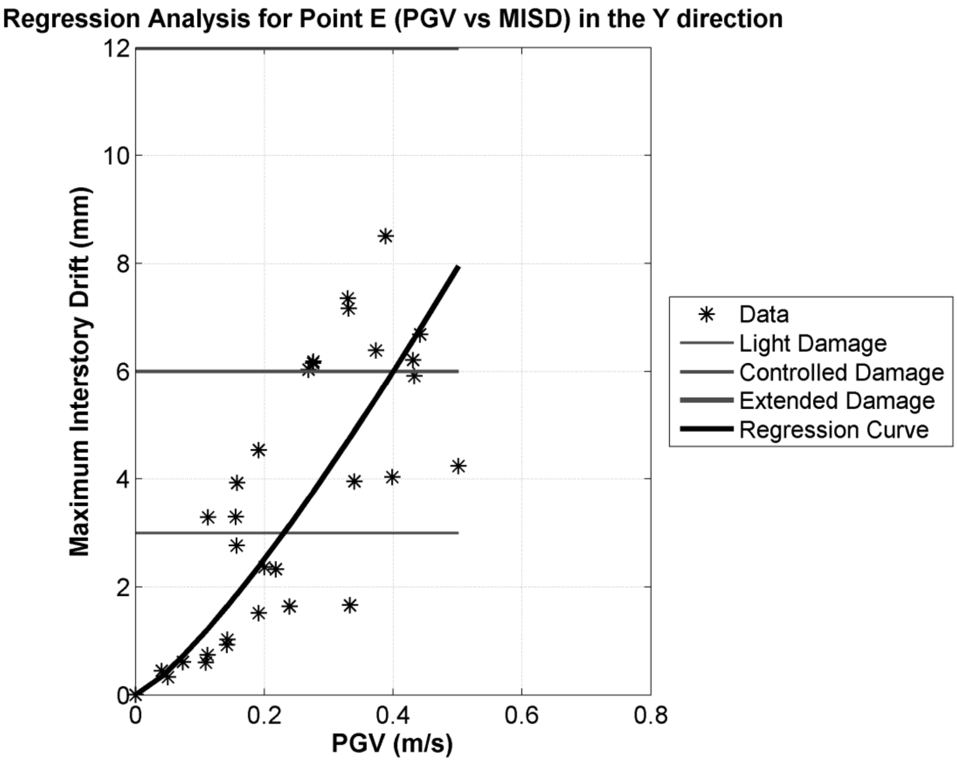

Figure 5.3 (Continued) Regression Analysis for Point E for seismic motion indicators

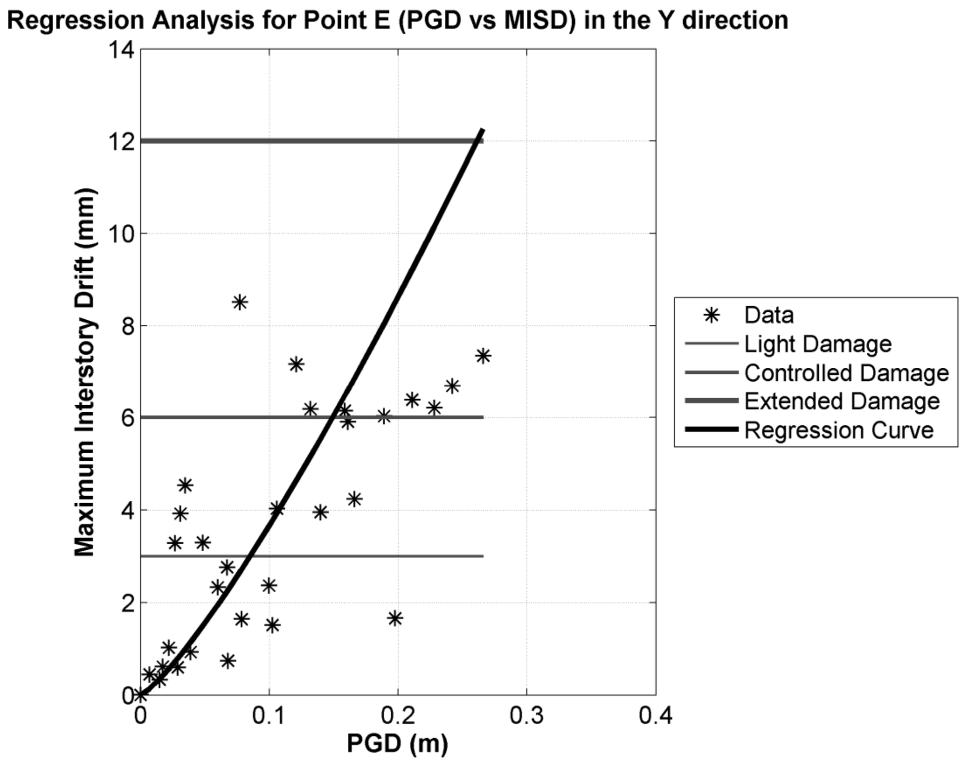

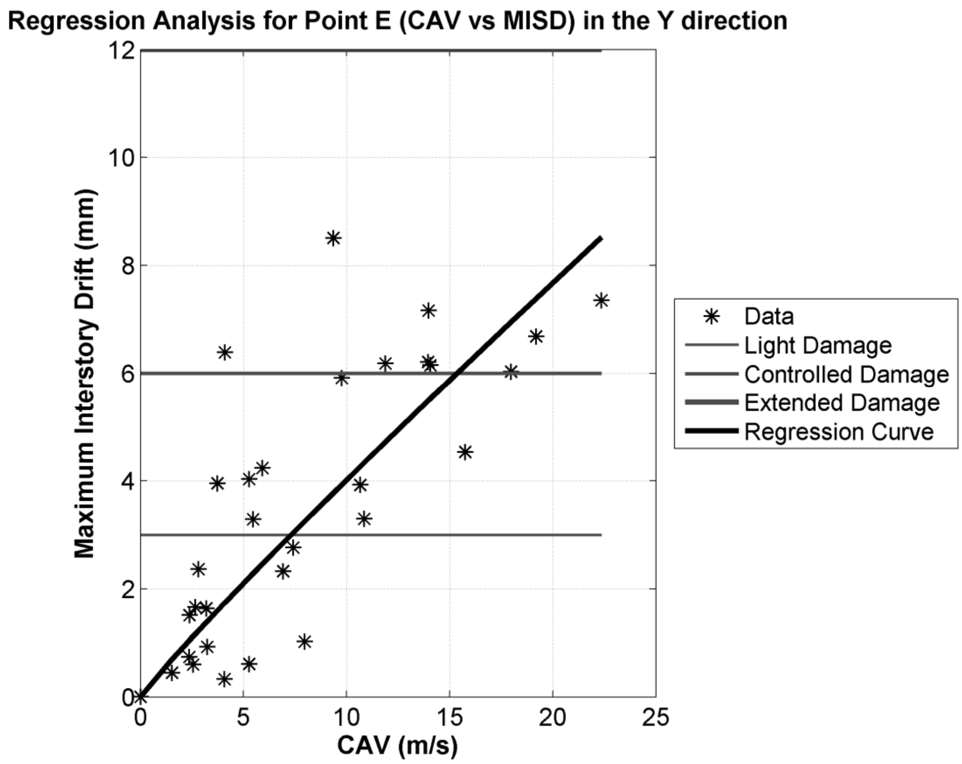

Figure 5.3 (Continued) Regression Analysis for Point E for seismic motion indicators

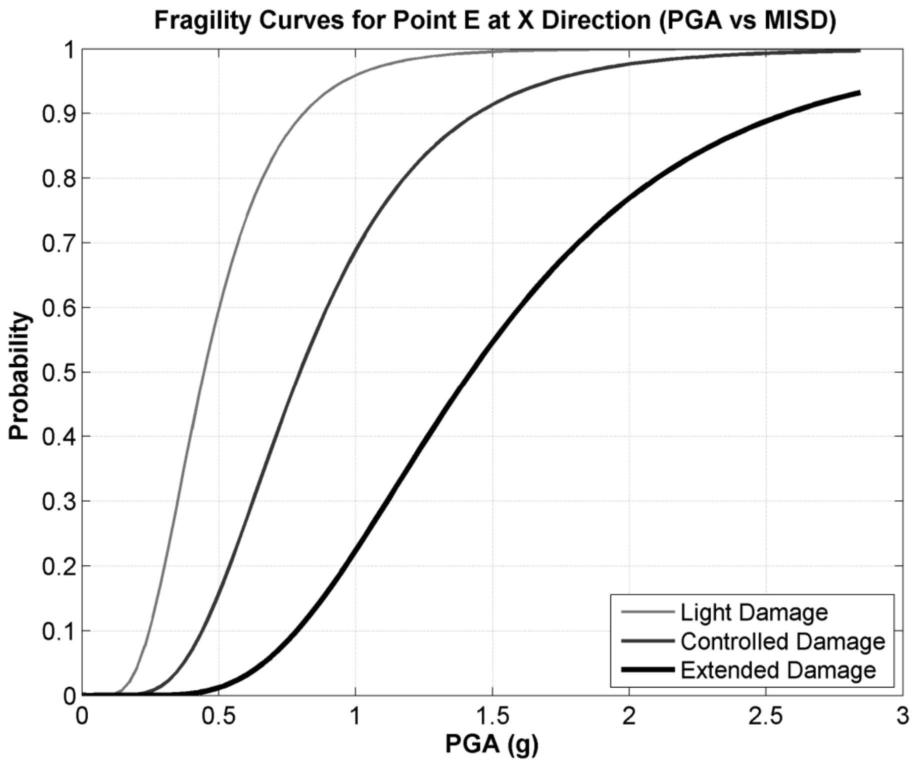

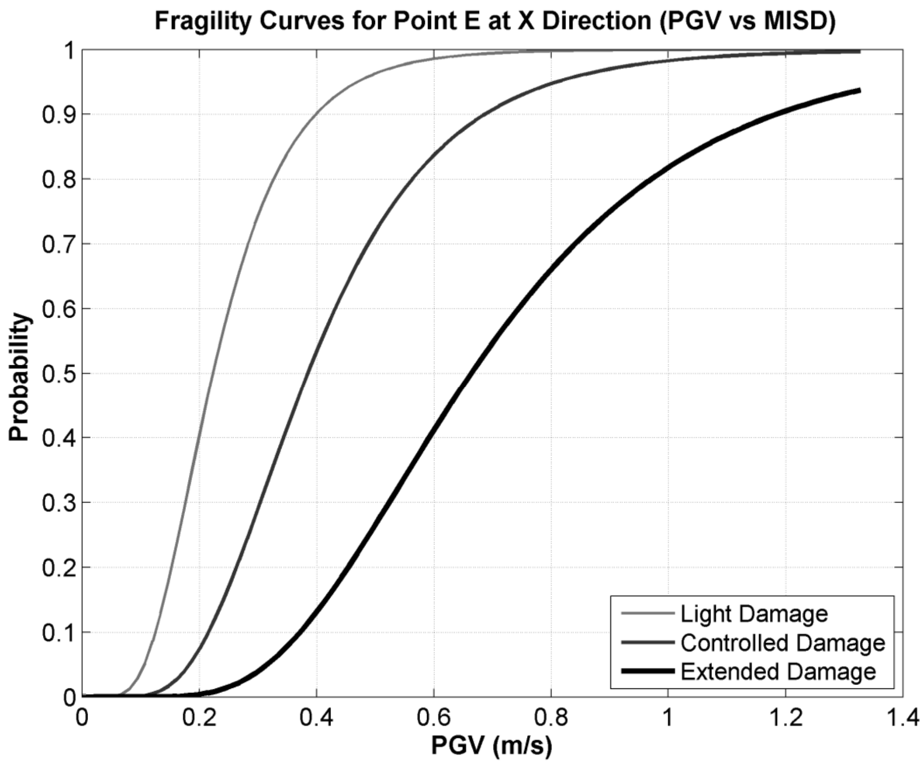

Figure 5-4 Fragility Curves for Point E for various seismic motion indicators

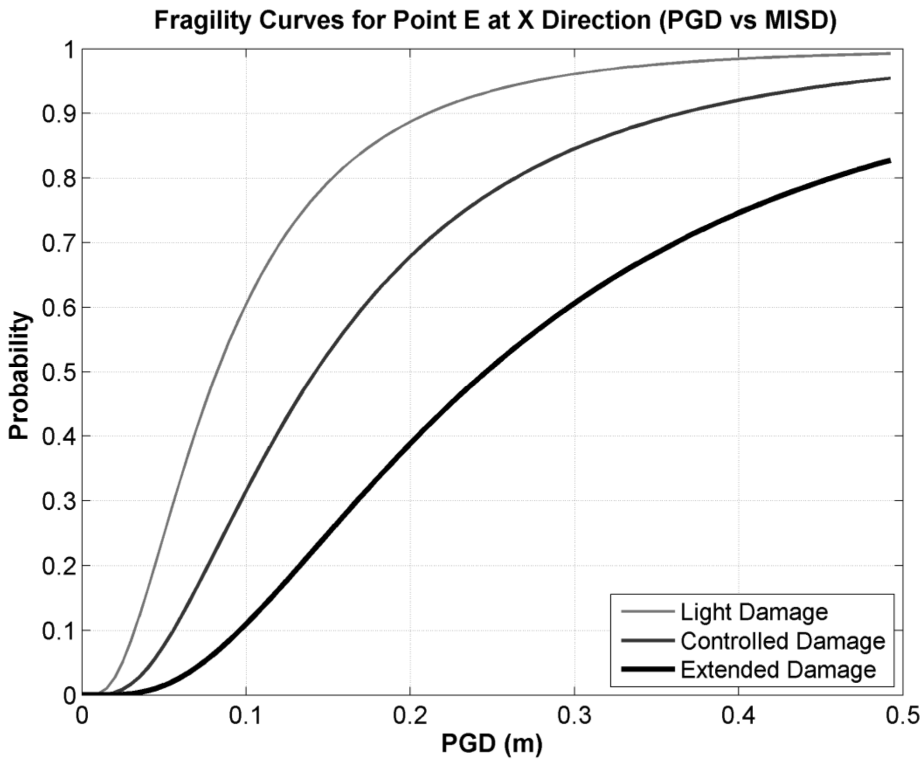

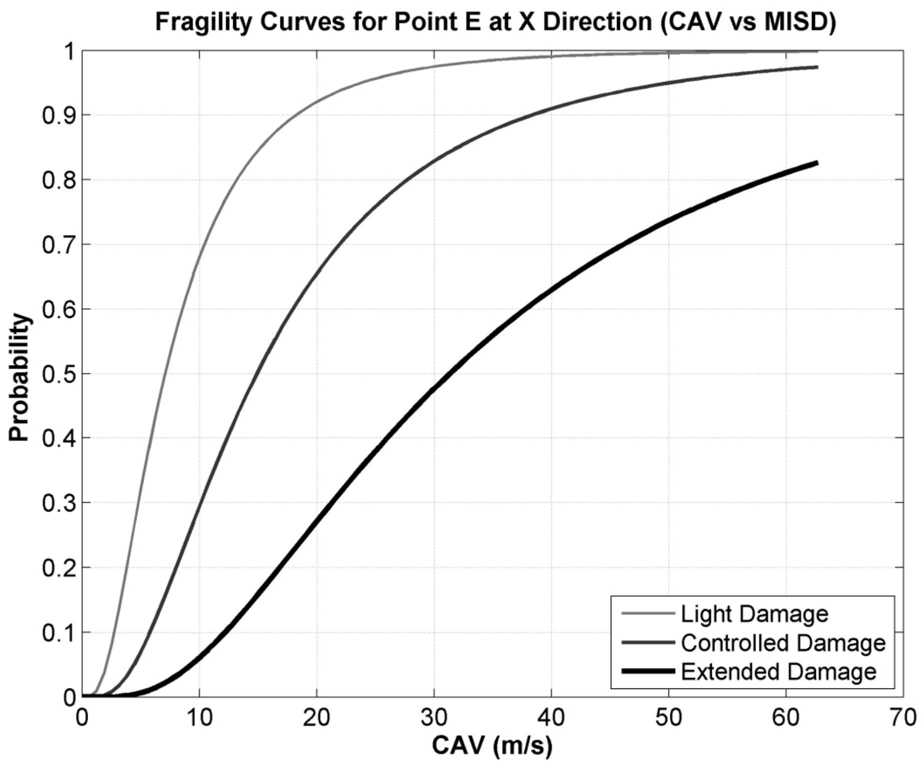

Figure 5.4 (Continued) Fragility Curves for Point E for various seismic motion indicators

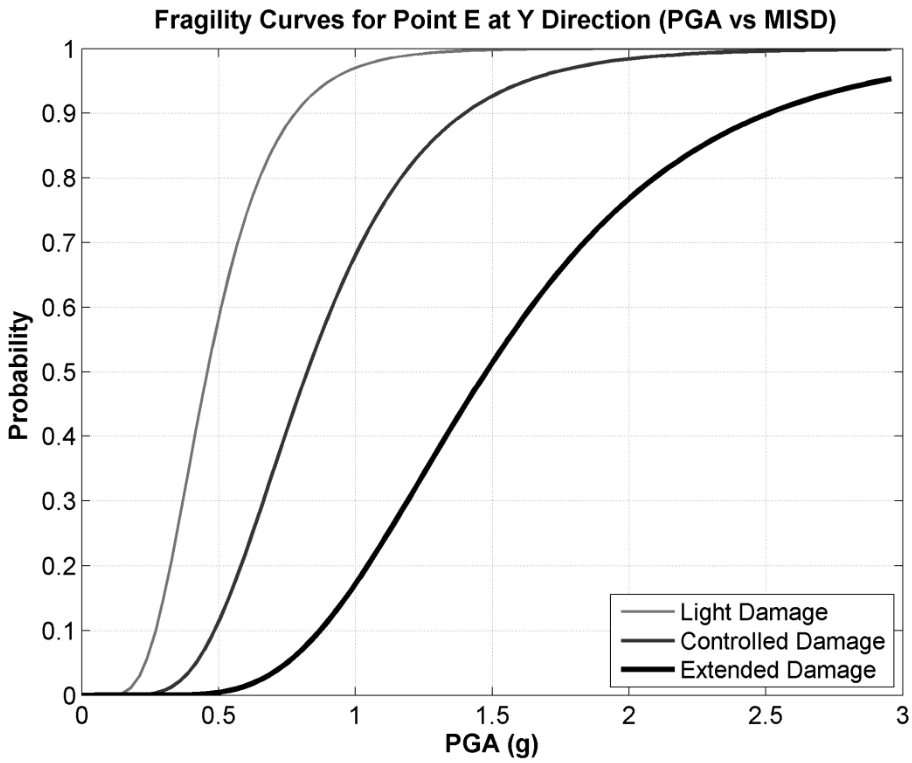

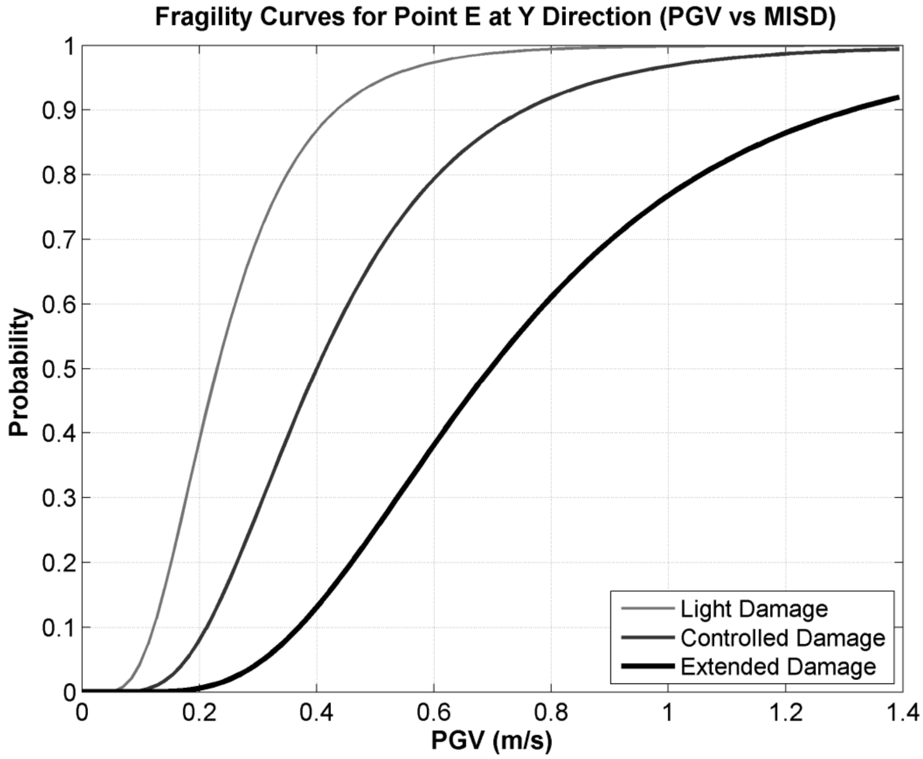

Figure 5.4 (Continued) Fragility Curves for Point E for various seismic motion indicators

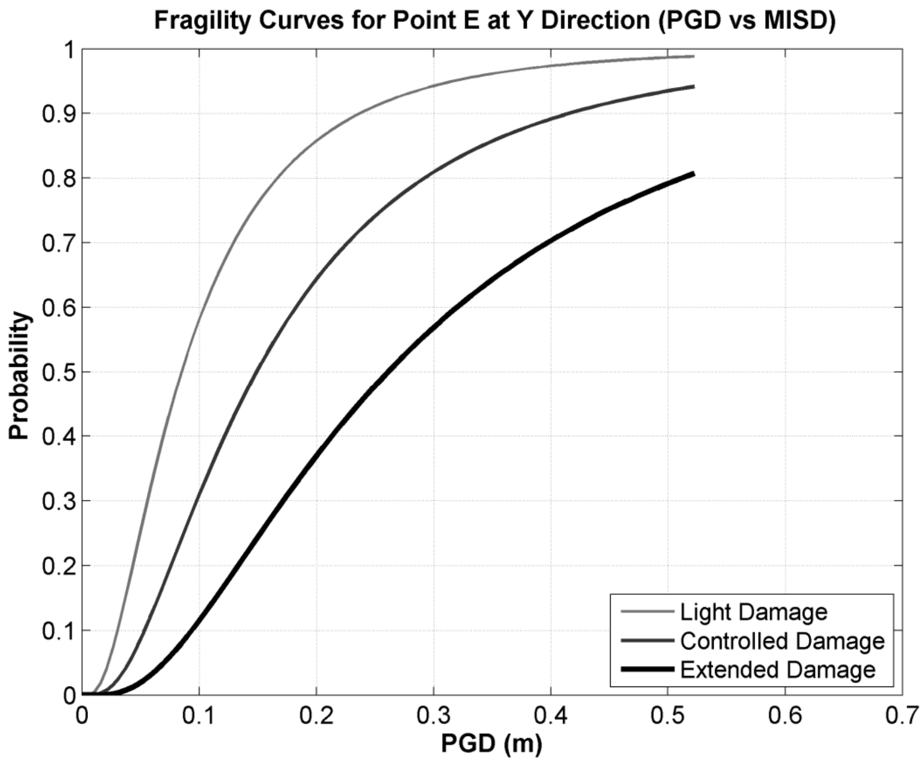

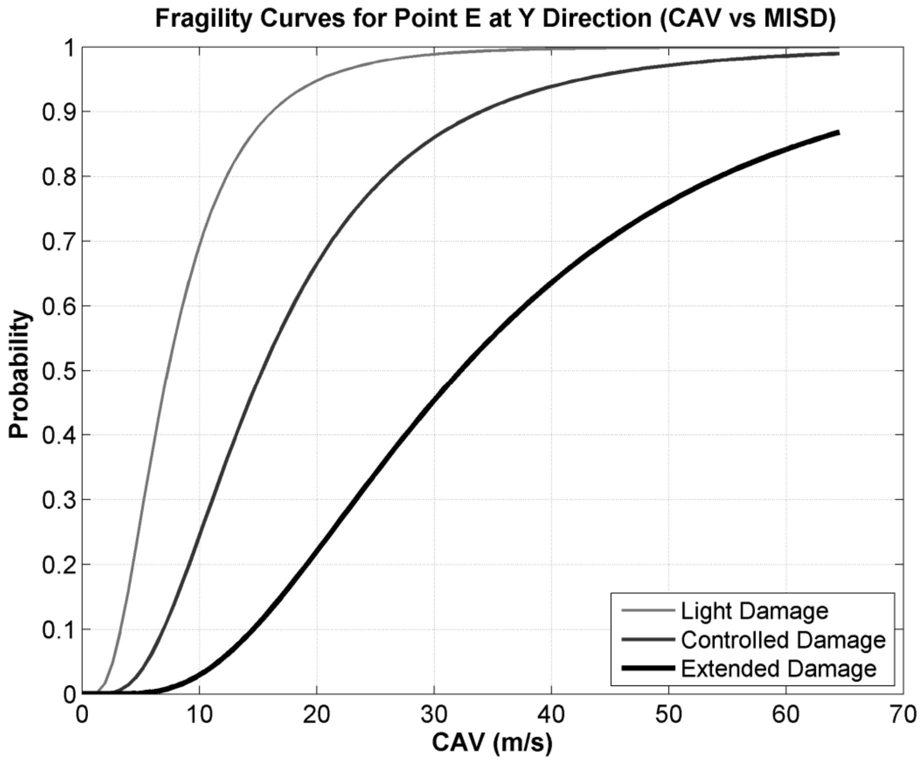

Figure 5.4 (Continued) Fragility Curves for Point E for various seismic motion indicators

5.5. Fragility Analysis according to the HAZUS damage limits

HAZUS (The Hazards U. S.) is a nationally applicable standardized methodology that estimates potential losses. HAZUS-MH is a multi hazard methodology that takes into account earthquakes, hurricane winds, and floods. The Federal Emergency Management Agency (FEMA) developed HAZUS- MH under contract with the National Institute of Building Sciences (NIBS). HAZUS damage limits were used for comparison purposes to obtain fragility curves for these limits.

HAZUS-MH damage limits vary from "None" to "Complete" for building conditions. The HAZUS damage limits for the concrete shear wall structures are defined as given below.

- *Slight Structural Damage:* Diagonal hairline cracks on most concrete shear wall surfaces; Minor concrete spalling at few locations.
- *Moderate Structural Damage:* Most shear wall surfaces exhibit diagonal cracks; some shear walls have exceeded yield capacity indicated by larger diagonal cracks and concrete spalling at wall ends.
- *Extensive Structural Damage:* Most concrete shear walls have exceeded their yield capacities; some walls have exceeded their ultimate capacities indicated by large, through-the wall diagonal cracks, extensive spalling around the cracks and visible buckled wall reinforcement or rotation of narrow walls with inadequate foundations. Partial collapse may occur due to failure of non-ductile columns not designed to resist lateral loads.
- *Complete Structural Damage:* Structure has collapsed or is in imminent danger of collapse due to failure of most of the shear walls and failure of some critical beams or columns.

HAZUS damage states are based on the drift index for different grades of design (Figure 5.5).

Moderate code design level for mid-rise concrete shear wall building was used (Mieses et. al, 2007). In Table 5.8, the inter-story drift ratio limits for each damage state proposed by HAZUS-MH MR1 (2003) for medium rise reinforced concrete shear wall structures are given.

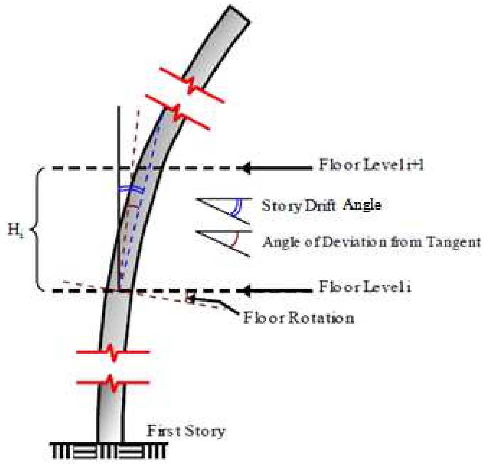

Figure 5-5 Parameters related to damage of structural walls (Mieses et. al., 2007)

Table 5-8 HAZUS Average Inter-Story Drift Ratio of Structural Damage States (HAZUS-MH MR1 2003)

Damage Levels	Slight	Moderate	Extensive	Complete
Drift Angle	0.003	0.005	0.015	0.040
Drift (H=1200 mm)	3.6	6	18	48

Log-normal distribution was used for the derivation of the fragility curves. Least squares method was preferred for regression analyses to determine the median capacities of the distributions and the standard deviations. The curves obtained from the regression analyses were the same because of having the same data. However, seismic median capacity coefficients for the damage states change. First three damage states of the HAZUS were taken into consideration for the comparison with the SMART damage states. The median capacity coefficients are given in Table 5.9. The seismic median capacity coefficients calculated according to the HAZUS damage states are higher than the SMART 2008 ones.

In Table 5.10, the probabilities of the data exceeding the damage levels according to the HAZUS damage limits are shown. Controlled damage and moderate damage levels were similar because of having same damage state values and small increase in the slight damage. Extended and extensive damage level probabilities of the data exceeding these levels did not change.

Table 5-9 Am –Seismic median capacity coefficients for data according to HAZUS

		Point A	Point B	Point C	Point D	Point E	Point F	Point G
	LD	0.62	0.61	0.47	0.31	0.52	0.47	0.53
	CD	0.96	0.95	0.73	0.47	0.80	0.72	0.82
PGA_x	ED	2.45	2.42	1.81	1.13	2.00	1.79	2.05
	LD	0.30	0.30	0.24	0.16	0.26	0.24	0.26
	CD	0.46	0.45	0.35	0.23	0.39	0.35	0.39
PGV_x	ED	1.11	1.10	0.83	0.54	0.91	0.83	0.93
	LD	0.11	0.11	0.09	0.06	0.10	0.09	0.10
	CD	0.17	0.17	0.13	0.09	0.14	0.13	0.15
PGD_x	ED	0.41	0.41	0.31	0.20	0.34	0.31	0.35
	LD	10.78	10.64	7.67	4.43	8.63	7.61	8.87
	CD	18.78	18.54	13.22	7.49	14.91	13.11	15.34
CAV_x	ED	61.95	61.23	42.63	23.18	48.43	42.28	49.87
	LD	0.62	0.34	0.34	1.21	0.54	0.81	0.38
	CD	0.96	0.52	0.51	1.91	0.82	1.26	0.58
PGA_y	ED	2.45	1.28	1.25	5.08	2.08	3.28	1.43
	LD	0.30	0.18	0.17	0.58	0.27	0.39	0.19
	CD	0.46	0.26	0.25	0.89	0.40	0.60	0.29
PGV_y	ED	1.11	0.61	0.59	2.23	0.96	1.49	0.67
	LD	0.11	0.06	0.06	0.21	0.10	0.15	0.07
	CD	0.17	0.10	0.09	0.33	0.15	0.22	0.11
PGD_y	ED	0.41	0.23	0.22	0.83	0.36	0.57	0.25
	LD	10.78	5.08	4.95	25.25	8.89	14.89	5.76
	CD	18.78	8.64	8.40	45.00	15.37	26.13	9.82
CAV_y	ED	61.95	27.04	26.21	155.91	49.80	87.54	30.88

Table 5-10 Probabilities of the data exceeding the damage levels according to HAZUS

	X Direction			Y Direction		
	LD	CD	ED	LD	CD	ED
Point A	0.58	0.26	0.16	0.87	0.13	0.00
Point B	0.58	0.26	0.16	0.35	0.19	0.45
Point C	0.55	0.10	0.35	0.35	0.13	0.52
Point D	0.32	0.23	0.45	0.94	0.06	0.00
Point E	0.55	0.13	0.32	0.52	0.19	0.29
Point F	0.55	0.03	0.42	0.71	0.29	0.00
Point G	0.55	0.16	0.29	0.39	0.16	0.45

LD = Light Damage; CD = Controlled Damage; ED = Extended Damage

Fragility curves derived for the HAZUS damage states are given in Appendix B. In this chapter, only the comparisons of fragility curves for Point E are given in detail.

5.5.1. Comparison of the Fragility Curves

In Figure 5.6, the fragility curves calculated for both SMART 2008 damage states and HAZUS damage states are compared. According to this comparison, the HAZUS damage states gives lower probability of failure especially for the extensive damage. The scatter between the damage states increased when the HAZUS damage states were taken into account.

Controlled damage and moderate damage levels were similar to each other because of having the same damage limit value as 6 mm and the difference between the slight damage and light damage is only 0.6 mm and did not affect the curves so much.

The fragility curves obtained from the SMART 2008 damage states are more conservative than the HAZUS ones. This difference could be admissible when the SMART 2008 structure is thought to be designed according to nuclear plant specifications. The biggest difference came from the Extended Damage and Extensive Damage.

Another important point is that HAZUS damage states are defined to represent a large scale of buildings that have no torsional irregularity. However, the fragility curve obtained in this study is only for one structure. That could be a reason for the huge difference in the fragility curves between the Extended and the Extensive damage states.

In Figure 5.6, it can also be observed that fragility curves give low probabilities of failure for Controlled-Moderate and Extended-Extensive damage limits even for high level of ground motion excitations. This means that this kind of shear wall building structures behave well when subjected to earthquakes.

To examine one of the fragility figures, Point E in the X direction and PGA as seismic ground motion indicator was chosen. For the fragility curves calculated for SMART 2008 damage states, under 0.52 g of PGA, the model has 36.4 % of probability of no damage, 45.24 % of probability of light damage and 16.79 % of probability of controlled damage and 1.57 % of probability of extended damage. For the fragility curves calculated for HAZUS 2008 damage states, under 0.52 g of PGA, the model has 49 % of probability of no damage, 32.64 % of probability of slight damage and 18.16 % of probability of moderate damage and 0.2% of probability of extensive damage. The influence of damage state limits is observed to be significantly affecting the fragilities.

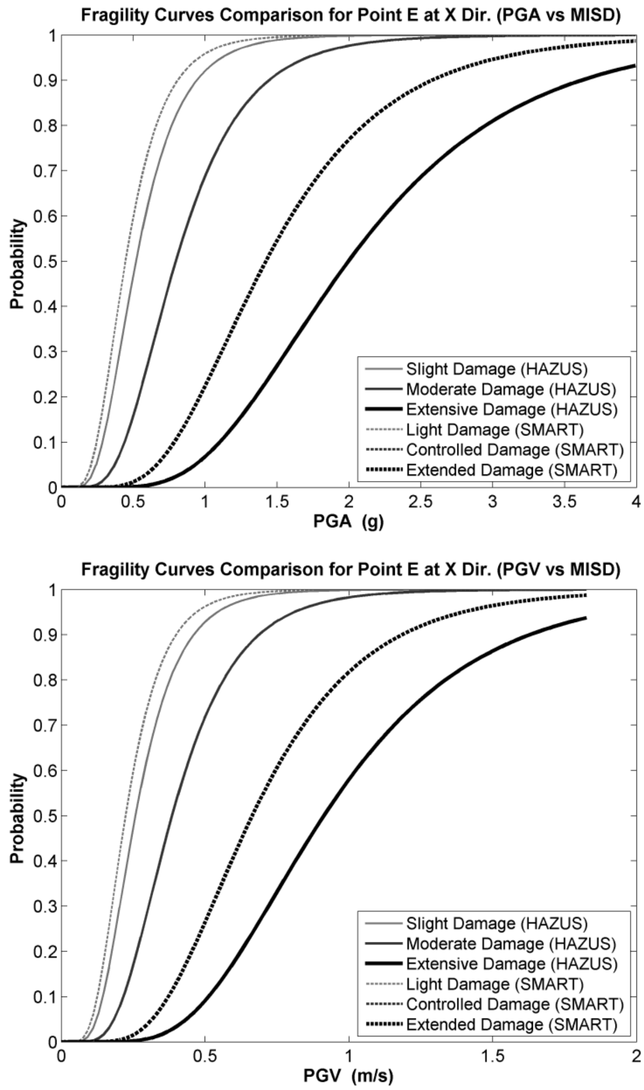

Figure 5-6 Fragility Curves Comparisons of Point E for various seismic motion indicators

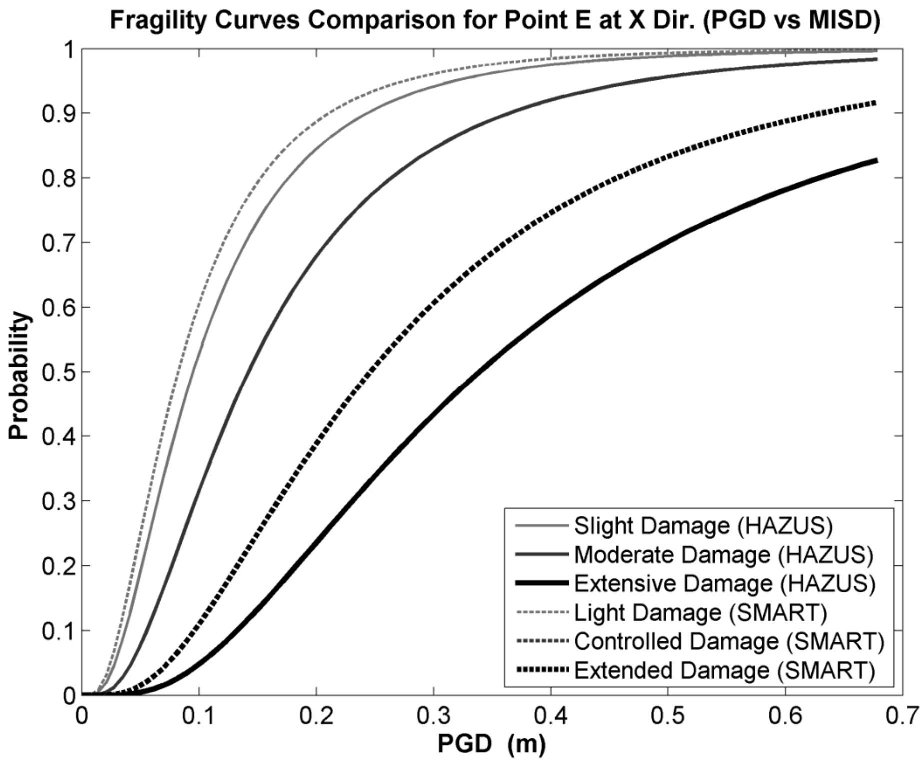

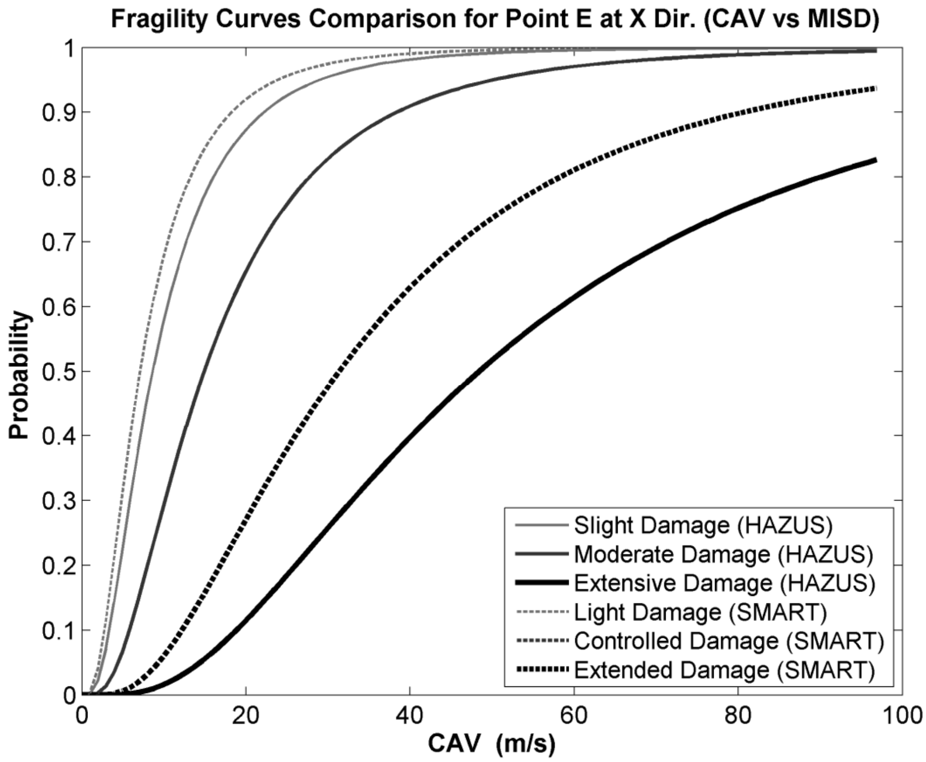

Figure 5.6 (Continued) Fragility Curves Comparisons of Point E for various seismic motion indicators

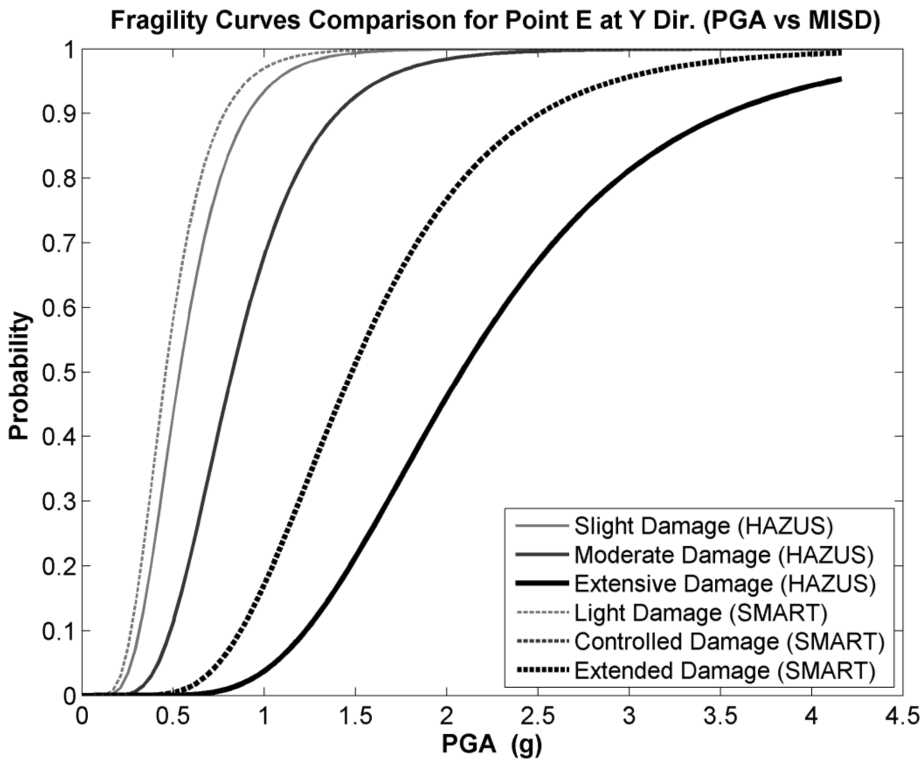

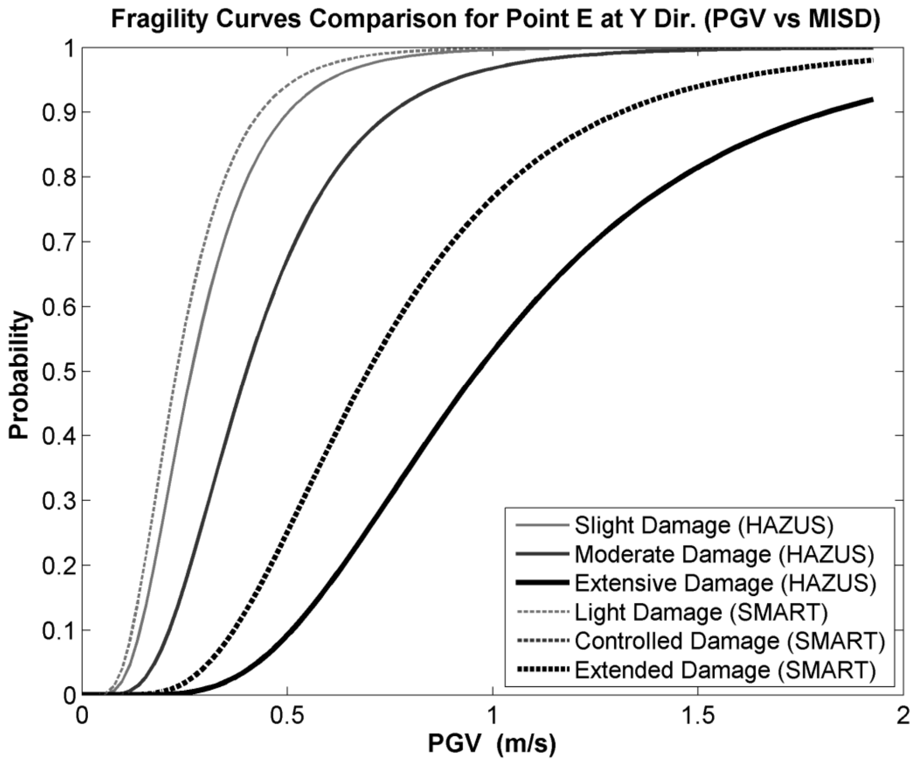

Figure 5.6 (Continued) Fragility Curves Comparisons of Point E for various seismic motion indicators

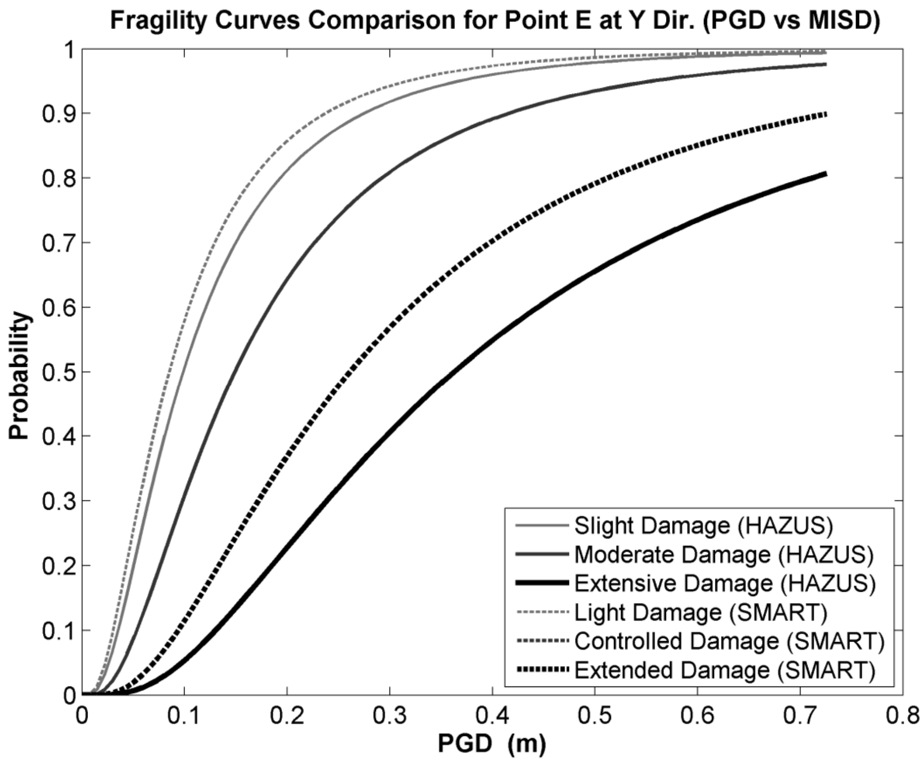

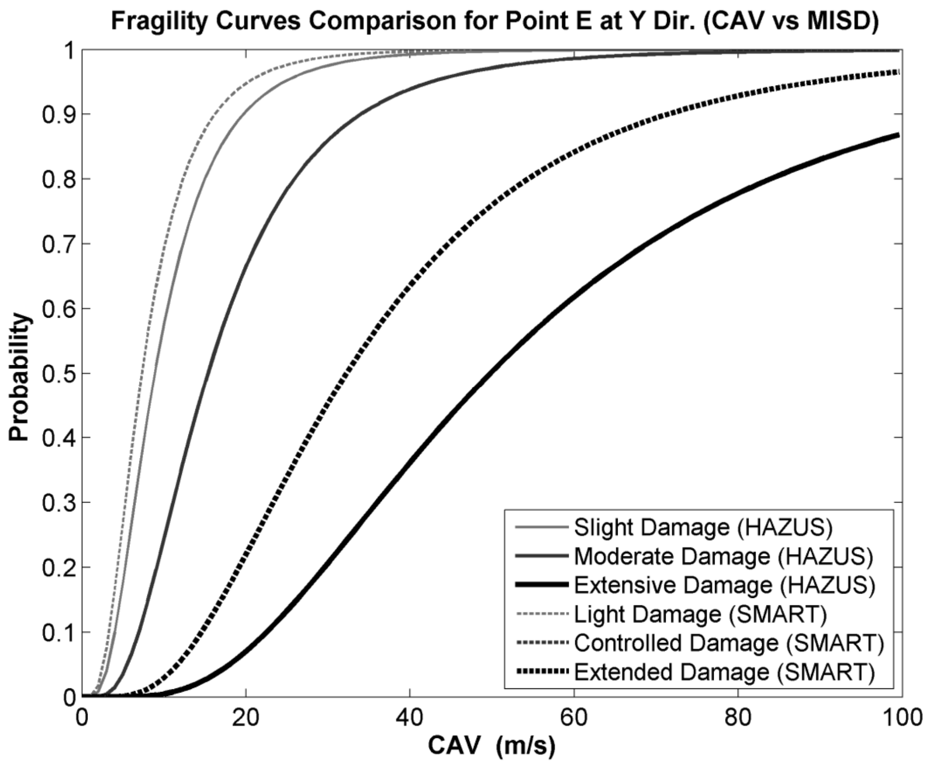

Figure 5.6 (Continued) Fragility Curves Comparisons of Point E for various seismic motion indicators

CHAPTER 6

SUMMARY, CONCLUSIONS AND RECOMMENDATIONS FOR FURTHER STUDIES

6.1. SUMMARY AND CONCLUSIONS

A shear wall structure that is a typical part of nuclear power plants was modeled numerically according to the SMART 2008 project specifications. The model structure has a plan torsional irregularity that makes its seismic response more complicated as compared to a symmetric one. SMART 2008 project was initiated to understand behavior of these structures and to develop relevant tools needed for their evaluation. The main scope of this thesis is to use the experimental measurements and generalize them to understand the behavior of the torsionally irregular shear wall structures with different properties under earthquake forces and to obtain the fragility curves of the structure for different seismic indicators.

Since the primary objective of the study was to simulate the experimental behavior, SMART 2008 Project Team did not want the shaking table to be included in the numerical model for sensitivity and fragility analyses, because of also uncertainties in the modeling of the shaking table. For fragility analysis there were 30 bi-directional time history analyses and 24 time history analyses for the sensitivity study.

There were two phases in SMART 2008 project. The First Phase (RAPPORT DM2S, 2007) was related with the benchmark study. In this thesis, Phase 1 was used for verification of the model response with the experimental results and it was observed that numerical model results were reasonably accurate and managed to capture the displacement response measured from the experimental runs under high amplitude seismic ground motions. For comparison of the Phase 1 results with the experimental results, frequency domain error (FDE) methodology was preferred. According to the FDE analyses, the error becomes smaller when the seismic ground motion amplitudes increased.

It is observed that modal analysis results were higher than the experimental results. Similar results were also obtained by other researchers in the SMART 2008 Project. It is thought that the fixed- based modeling may increase the modal frequencies in the numerical model.

Phase 2 consists of two parts designated as sensitivity study and fragility analysis. In sensitivity study, 12 parametric cases were taken into account under two different seismic ground motions. Ground motions were derived from white noise by SMART 2008 project team. One of the ground motion sets was design level which has max amplitude of 0.2 g and the other one was over-design level which has amplitude of 0.6 g as mentioned in SMART 2008 Phase 2 Report (RAPPORT DM2S, 2009).

The main scope of the sensitivity study was to understand which parameters of the building properties affects the response of a structure under two different ground motion levels. In the sensitivity study, damping coefficient was observed as the most important parameter for the response. Elasticity modulus of concrete and additional loading on the structure also seemed effective on the response. However, change in the steel yielding stress did not affect the results. Furthermore, differences on the results were observed to be more significant in design level than the over-design level. In over-design level analyses only damping seemed to be effective on results.

In the second part of the Phase 2, fragility curves for different types of seismic indicators were obtained. An improved methodology was used for the calculation of fragility curves. This methodology was applied a special building which was a mock up of a nuclear power plant structure and the fragility curves obtained only applicable for this stereotypes.

The most important issue for the fragility curves is that the determination of the limit states for the damage indicators or detectors. In this study, maximum inter-story drift was used as damage indicator and damage limits were used as given in SMART 2008 Phase 2 Report (RAPPORT DM2S, 2009). Log-normal distribution assumption was used for the fragility curves. Regression analyses were performed using the least squares method to obtain median capacities and standard deviations of the distributions. The correlation coefficients for time history data versus fitted curves changes from 0.80 to 0.99 for different points. The lower correlation coefficients occurred at PGD seismic indicators. Some fragility curves end with less than 100 percent probability. These curves give idea about the damage and failure probability of the shear wall structure under different seismic ground motion indicators.

Fragility curves were also obtained for HAZUS MH MR1 (2003) damage states for mid rise concrete shear walls. This comparison was done only to evaluate the relationship of the fragility curves of SMART 2008 building with the limits of HAZUS which was developed for a group of buildings for general purpose. The fragility curves compared and it was observed that moderate and controlled damage level fragility curves were same, slight and light damage level fragility curves were close to each other but there was a bit huge difference between the extended and extensive damage levels fragility curves. This difference is considered to arise from the definition of the damage states of HAZUS and SMART 2008. HAZUS damage states represent a family of buildings. However, SMART 2008 damage limits were only demonstrated for one structure.

6.2. RECOMMENDATIONS FOR FURTHER STUDIES

This study can also be improved in the future to increase the accuracy of the fragility curves and to increase the goodness of fit of the numerical data to the experimental data.

- Shaking table should be modeled to investigate the effects on the modal and time history analyses results. Phase 1 can be used for this purpose.
- Fragility analyses should be extended to the vulnerability analysis by including other cases given in sensitivity study. Other cases should also be added such as geometrical effects to increase the accuracy. However, this kind of extended study totally depends on higher computer technology; otherwise ANSYS cannot be suitable software for this purpose.
- As another further study, damage limits should be investigated and will be. The most important parameter for fragility curves is that the determination of the true damage levels for more accurate results. This study will be extended in future for the check of Turkish Earthquake Code (TEC 2007) strain limits. Another code or specifications also can be checked.

REFERENCES

Akkar S., Sucuoğlu H. and Yakut A., 2005, “Displacement – based fragility functions for low- and mid – rise ordinary concrete buildings”, Earthquake Spectra, Vol. 21, No. 4, pp. 901-927.

Ang A. H-S. and Tang W. H., 1975, “Probability concepts in engineering planning and design ”,John Wiley and Sons, Canada.

ANSYS R 12.0, Swanson Analysis System, 2011.

Ay B.Ö. and Erberik M.A., 2008, “Vulnerability of Turkish low – rise and mid – rise reinforced concrete frame structures”, Journal of Earthquake Engineering, 12 (S2), pp. 2-11.

Aziminejad A. and Moghadam A. S., 2009, “Performance of asymmetric multistory shear buildings with different strength distributions”, Journal of Applien Science Vol.9, No.6, pp. 1080-1089

Beyer K., Dazio A. and Priestley M.J.N., 2008, “Inelastic wide – column models for U – shaped reinforced concrete walls”, Journal of Earthquake Engineering, 12 (S1):1-33.

Chopra A., 2000, “Dynamics of structures: Theory and application to earthquake engineering”, Prentice – Hall, 3rd edition.

Clough R. W. and Penzien J., 1993, “Dynamics of Structures”, McGraw-Hill, New York.

Clough R. W., 1980, “The finite element method after twenty – five years: A personal view”, Computers & Structures, Vol. 12, pp. 361-370.

Cook R.D., Malkus D.S., Plesha M.E., Witt R.J., 2001, “Concepts and applications of finite element analysis”, Fourth Edition, John Willey and Sons, New York.

Dragovich J.J. and Lepage A., 2009. “FDE index for goodness – of – fit between measured and calculated response signals”. Earthquake Engineering and Structural Dynamics, 38:1751-1758.

Fischinger M. and Isakovic T., 2000, “Benchmark analysis of a structural wall”, 12th World Conference on Earthquake Engineering, 0416

Gülkan P. and Sözen M., 1974, “Inelastic responses of reinforced concrete structures to earthquake motions”, Proceedings of the ACI, Vol. 54, No. 5, pp. 333-345

IAEA-TECDOC, 2008, “Safety significance of a type of seismic input motions and consequences on nuclear industry practice”, International Atomic Energy Egency, Vienna, Austria.

Ile N. and Reynouard J.M., 2003, “Lightly reinforced walls subjected to multi – directional seismic excitations: Interpretation of CAMUS 2000-1 dynamic tests”, Vol. 40, No. 2-4, pp. 117-135.

Ile N. and Reynouard J.M., 2005, “Behaviour of U-shaped walls subjected to uniaxial and biaxial cyclic lateral loading”, Journal of Earthquake Engineering, Vol. 9, No. 1, pp. 67-94.

Ile N., Nguyen X. H., Kotronis P., Mazars J. M., 2008, “Shaking table tests of lightly RC walls”, Journal of Earthquake Engineering, 12:6, pp. 849-878.

Iwan W. D., 1997, “Drift spectrum: Measure of demand for earthquake ground motions”, Journal of Structural Engineering, Vol. 123, No. 4, pp. 397-404.

Jeong S. –H. and Elnashai A. S., 2006a, “New three- dimensional damage index for RC buildings with planar irregularities”, Journal of Structural Engineering, Vol. 132, No.9, pp. 1482-1490.

Jeong S. –H. and Elnashai A. S., 2006b, “Fragility analysis of buildings with plan irregularities”, 4.th International Conference on Earthquake Engineering, Taipei, Taiwan

Kabeyasawa T., Shiohara H., Otani S. and Aoyama, H., 1983, “Analysis of the full – scale seven story reinforced concrete test structure”, Vol.37, No. 2, pp. 432-478

Kazaz İ., Yakut A. and Gülkan P., 2006, “Numerical simulation of dynamic shear wall tests: A benchmark study”, Computers and Structures, Vol. 84, pp. 549-562.

Kazaz İ., 2010, “Dynamic characteristics and performance assessment of reinforced concrete structural walls”, Phd Thesis, Middle East Technical University, February

Khan, F.R. and Sbarounis, J.A., 1964, “Interaction of Shear Walls and Frames”, ASCE Journal of Structural Division, Vol.90, No.3, 285-335.

Kwak H.–G. and Kim D.–Y., 2004, “FE analysis of RC shear walls subjected to monotonic loading”, Magazine of Concrete Research, 56, No. 7, pp. 387-403.

Lermitte S. Chaudat T., Payen T., Vandeputte D. and Viallet E., 2008, “SMART 2008: Experimental tests of a reinforced concrete building subjected to torsion”, The 14th World Conference on Earthquake Engineering.

Lermitte S. Chaudat T., Payen T., Vandeputte D. and Viallet E., 2007, “SMART 2008 Project: Seismic design and best – estimate methods for reinforced concrete buildings subjected to torsion and non – linear effects, Earthquake blind prediction contest and fragility assessment”, Transactions, SMiRT 19, Toronto, K 15/ 4.

Mieses L.A., Lopez R. and Saffar A., 2007, “Development of fragility curves for medium rise reinforced concrete shear wall residential buildings in Puerto Rico”, Mecanica Computacional, Vol. XXVI, pp, 2712-2727.

Miranda E. and Taghavi, S., 2005, “Approximate floor acceleration demands in multistory buildings. I: Formulation”, Journal of Structural Engineering, Vol. 131, No. 2, pp. 203-211.

Miranda E., 1999, “Approximate seismic lateral deformation demands in multistory buildings”, Journal of Structural Engineering, Vol. 125, No. 4, pp. 417-425.

Moehle J. P., 1996. “Displacement – based seismic design criteria”. 11th World Conference on Earthquake Engineering, 2125, ISBN: 0 08 042822 3.

Newmark N. M. and Hall, W. J., 1982, “Earthquake spectra and design”, Engineering monographs on earthquake criteria, structural design, and strong motion records, Earthquake Engineering Research Institute, Oakland, California.

OECD/NEA/CSNI, 1996, “Seismic shear wall ISP NUPEC's seismic ultimate dynamic response test -Comparison Report”, NEA/CSNI/R(96)10, OECD/GD(96)188.

Orakcal K. and Wallace J.W., 2004, “Modeling of slender reinforced concrete walls”, 13th World Conference on Earthquake Engineering, 555

Orakcal K. and Wallace J.W., 2006, “Flexural modeling of reinforced concrete walls – experimental verification”, ACI Structural journal, 103(2):196-206

Palermo D. and Veccihio F.J., 2007, "Simulation of cyclically loaded concrete structures based on the finite element method", Journal of Structural Engineering, Vol. 33, No. 5, pp. 728-738

Park R. and Paulay T.,1975, "Reinforced concrete structures", New York: Wiley.

Priestley M. J. N., 2000, "Performance Based Seismic Design", 12th World Conference on Earthquake Engineering, 2831.

RAPPORT DM2S, 2007, "Presentation of blind prediction contest", COMMISSARIAT A L' ÉNERGIE ATOMIQUE, SEMT/EMSI/PT/07-003/C.

RAPPORT DM2S, 2009, "Presentation of the Benchmark Contest –Phase 2 Project SMART 2008", COMMISSARIAT A L'ÉNERGIE ATOMIQUE, SEMT/EMSI/PT/09-011/A

Rosman, R., 1968, "Statik und dynamic der scheibensysteme des hochbaues,", Springer-Verlag, Berlin, West Germany, pp. 88-183, 260-302.

Shimazaki, K. and Sözen, M. A., 1984, "Seismic drift of reinforced concrete structures", Res. Reports, Hazama – Gumi, Tokyo, Japan

Shinozuka M., Feng M. Q. Lee J. and Naganuma T., 2000, "Statistical analysis of fragility curves", Journal of Structural Engineering, Vol. 126, No.12, pp. 1224-1231.

SMART – 2008 Workshop, Saclay, Paris,France.

Sözen M.A., 1989, "Earthquake response of buildings with robust walls", Fifth Chilian Conference on Earthquake Engineering, Santiago, Chile.

Taghavi S. and Miranda E., 2005, "Approximate floor acceleration demands in multistory buildings. II: Applications", Journal of Structural Engineering, Vol. 131, No. 2, pp. 212-220.

TSC 2007, 2007, "Turkish Seismic Design Code for Buildings", Ministry of Public Works and Resettlement, Ankara, Turkey.

Vulcano A., Bertero V. V., Colloti V., 1988, "Analytical modeling of R/C structural walls", Proceedings of Ninth World Conference on Earthquake Engineering, 9-1-7

Wallace J. W. and Moehle J. P., 1992, "Ductility and detailing requirements of bearing wall buildings", Journal of Structural Engineering, Vol. 118, No.6, ASCE, ISSN 0733-9445/92/0006-1625.

Willam, K. J. and Warnke, E. D., "Constitutive Model for the Triaxial Behavior of Concrete", Proceedings, International Association for Bridge and Structural Engineering, Vol. 19, ISMES, Bergamo, Italy, p. 174. 1975.

Yun S. Y., Hamburger R. O., 2002, Cornell and Foutch, A., “Seismic performance evaluation for steel moment frames”, Journal of Structural Engineering, Vol. 8, No.4, pp. 534-545.

APPENDIX A

Regression Analyses and Fragility Curves according to SMART damage states

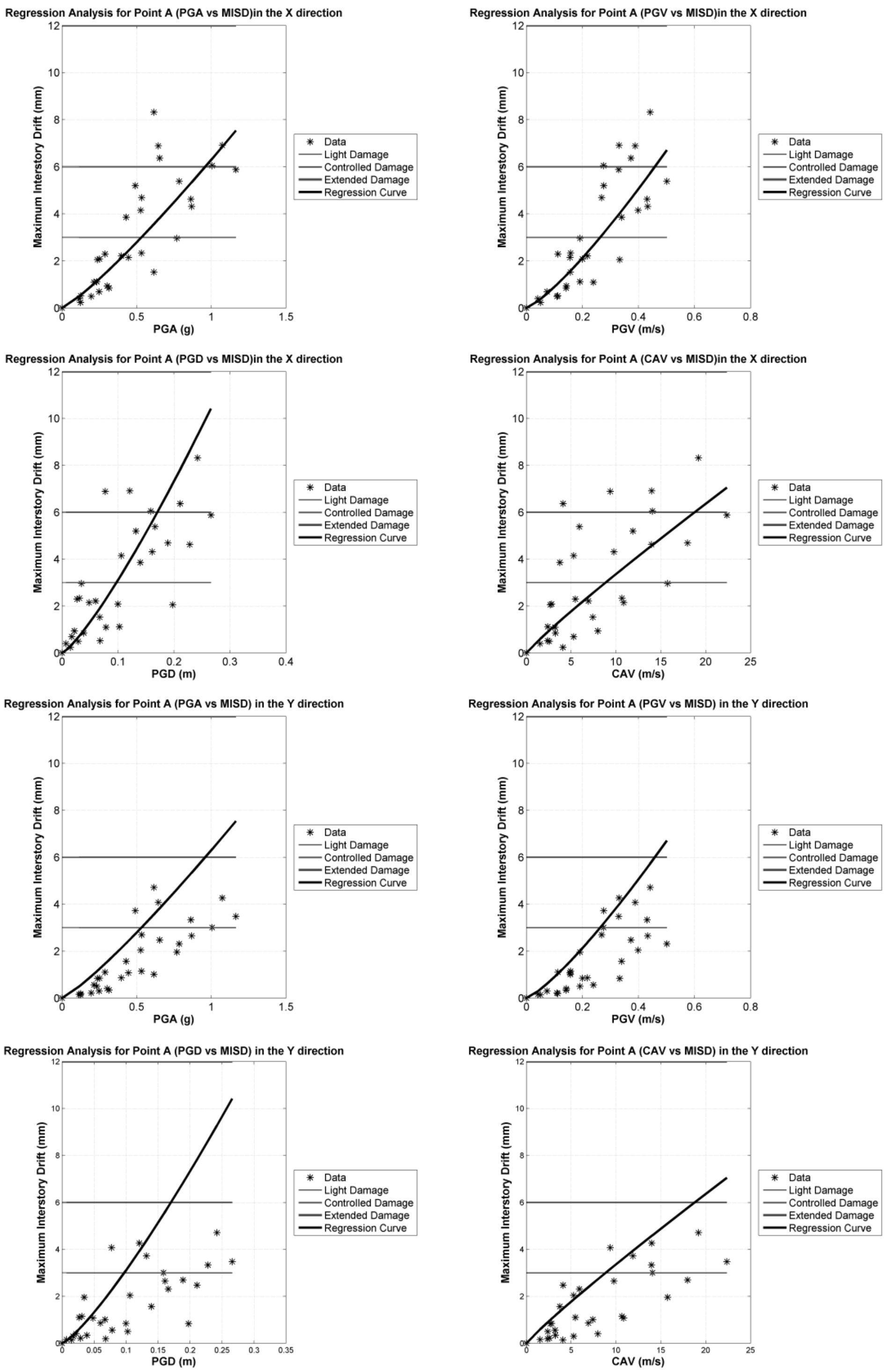

Figure A.1 Regression Analysis for Point A for seismic motion indicators

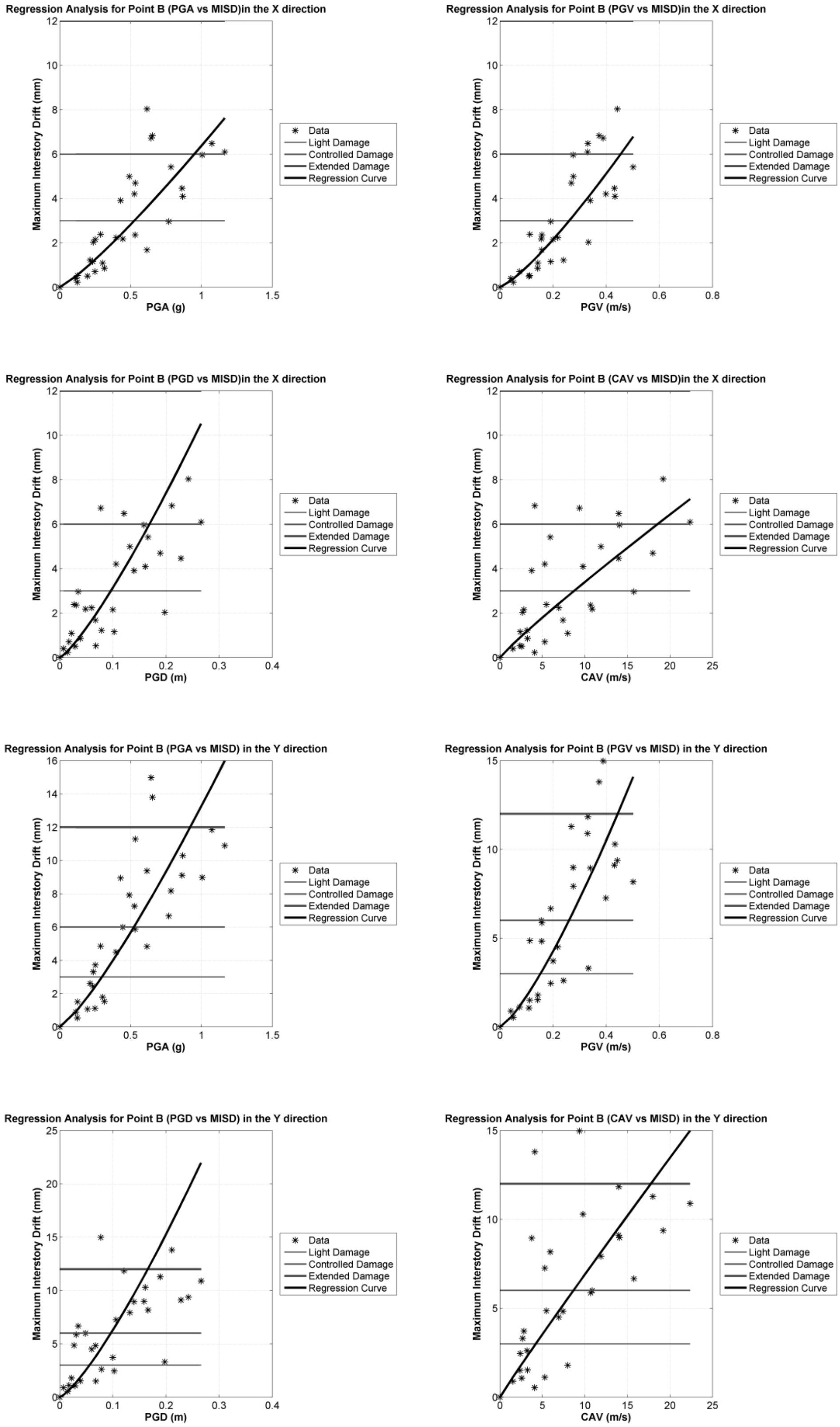

Figure A.2 Regression Analysis for Point B for seismic motion indicators

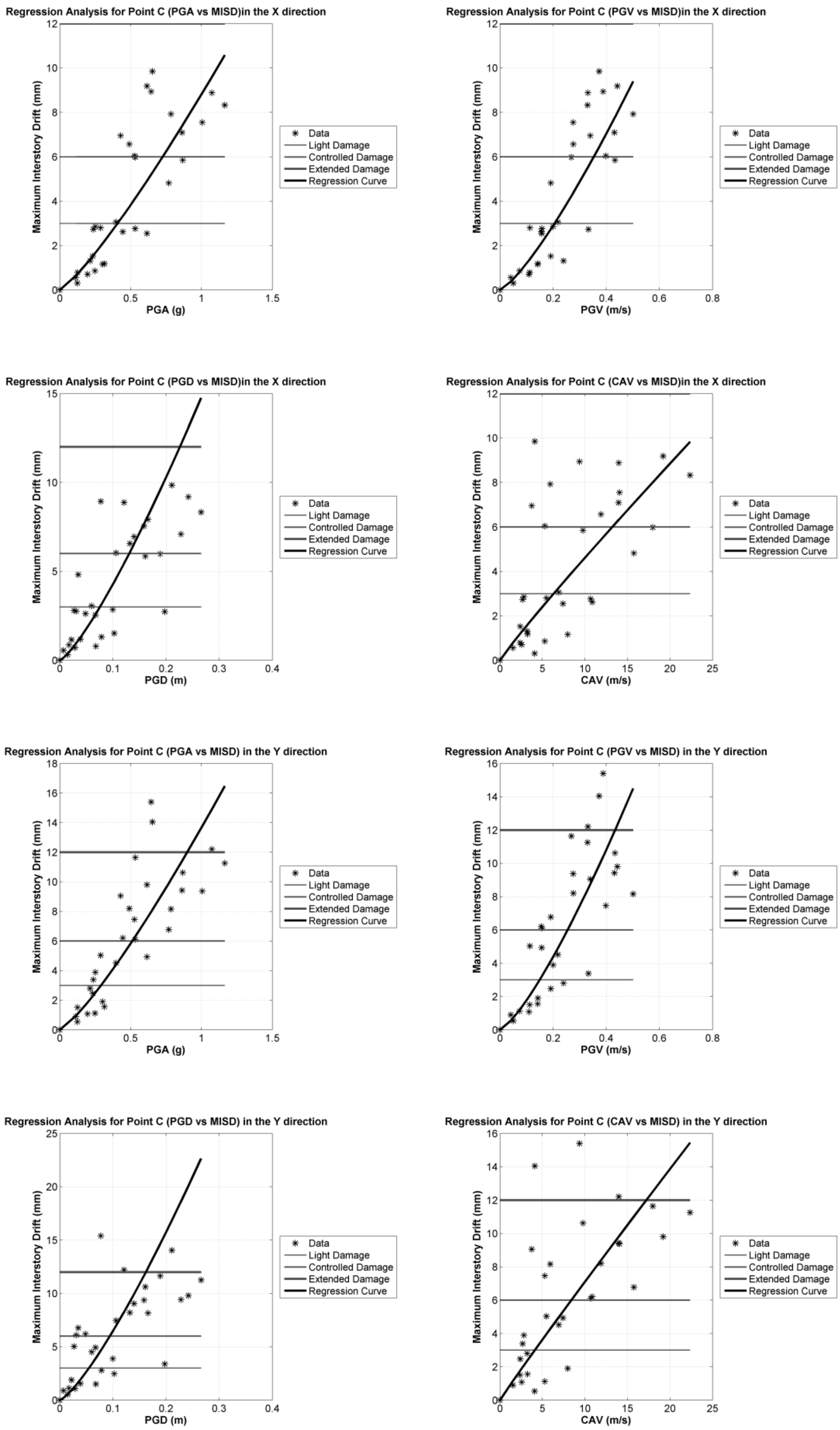

Figure A.3 Regression Analysis for Point C for seismic motion indicators

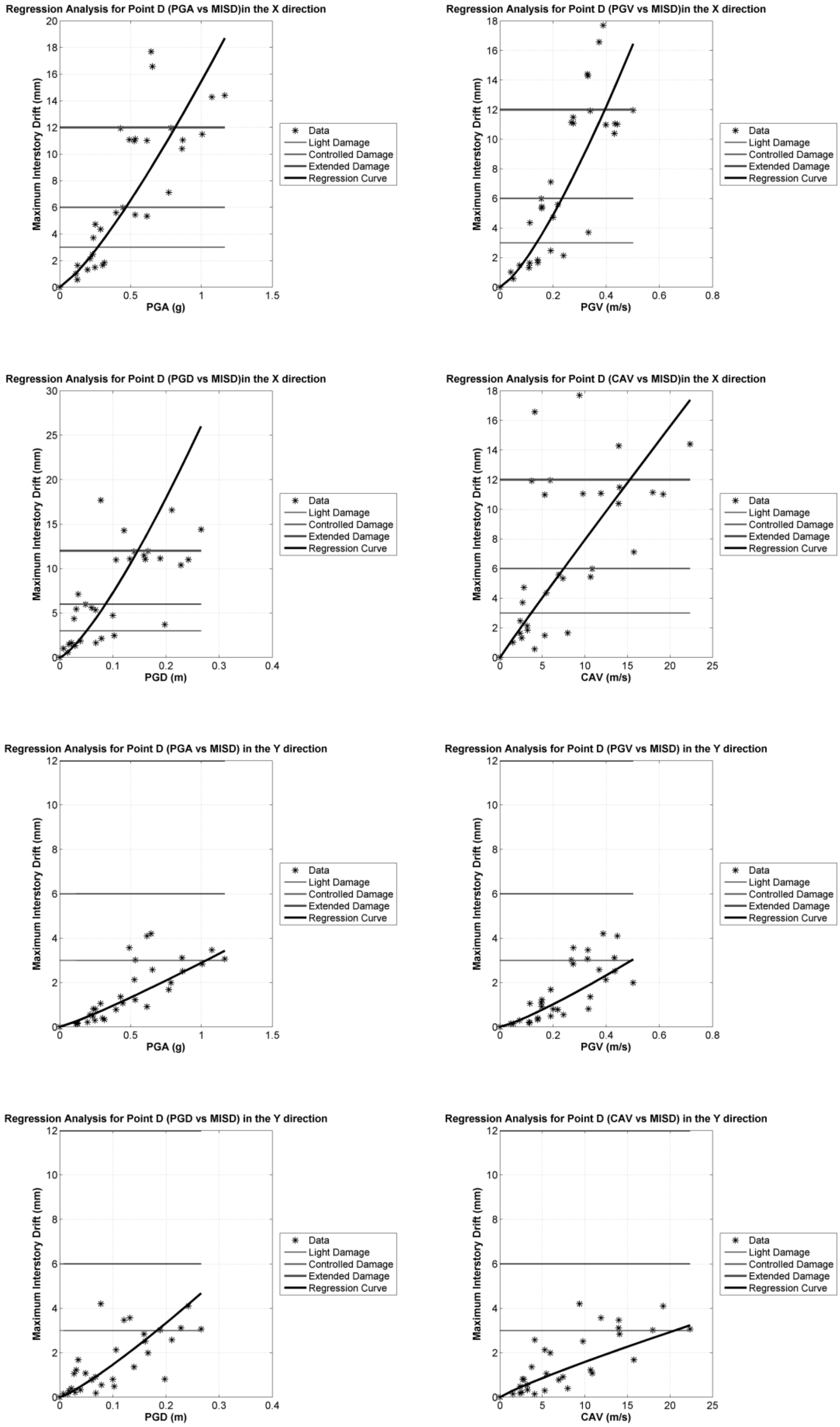

Figure A.4 Regression Analysis for Point D for seismic motion indicators

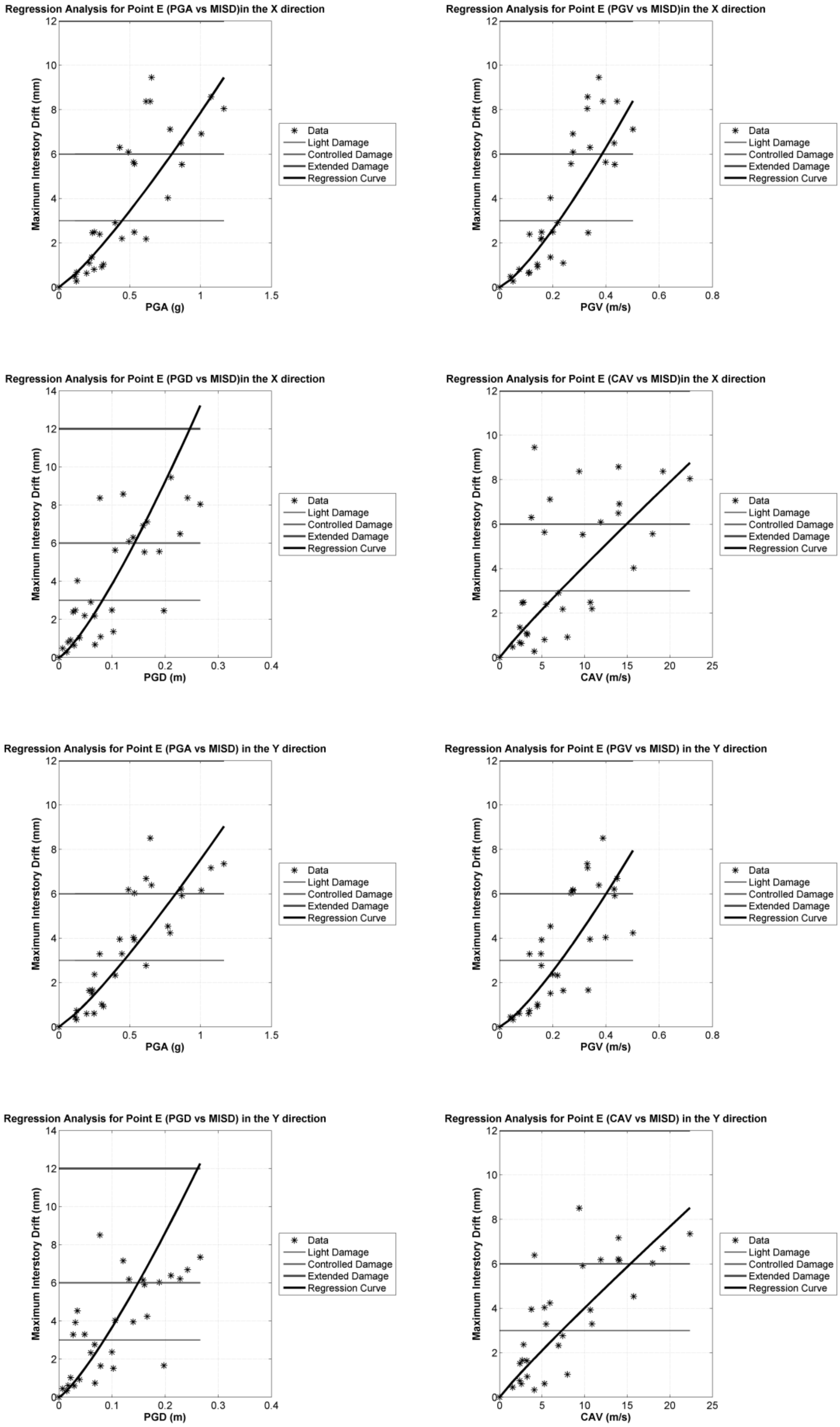

Figure A.5 Regression Analysis for Point E for seismic motion indicators

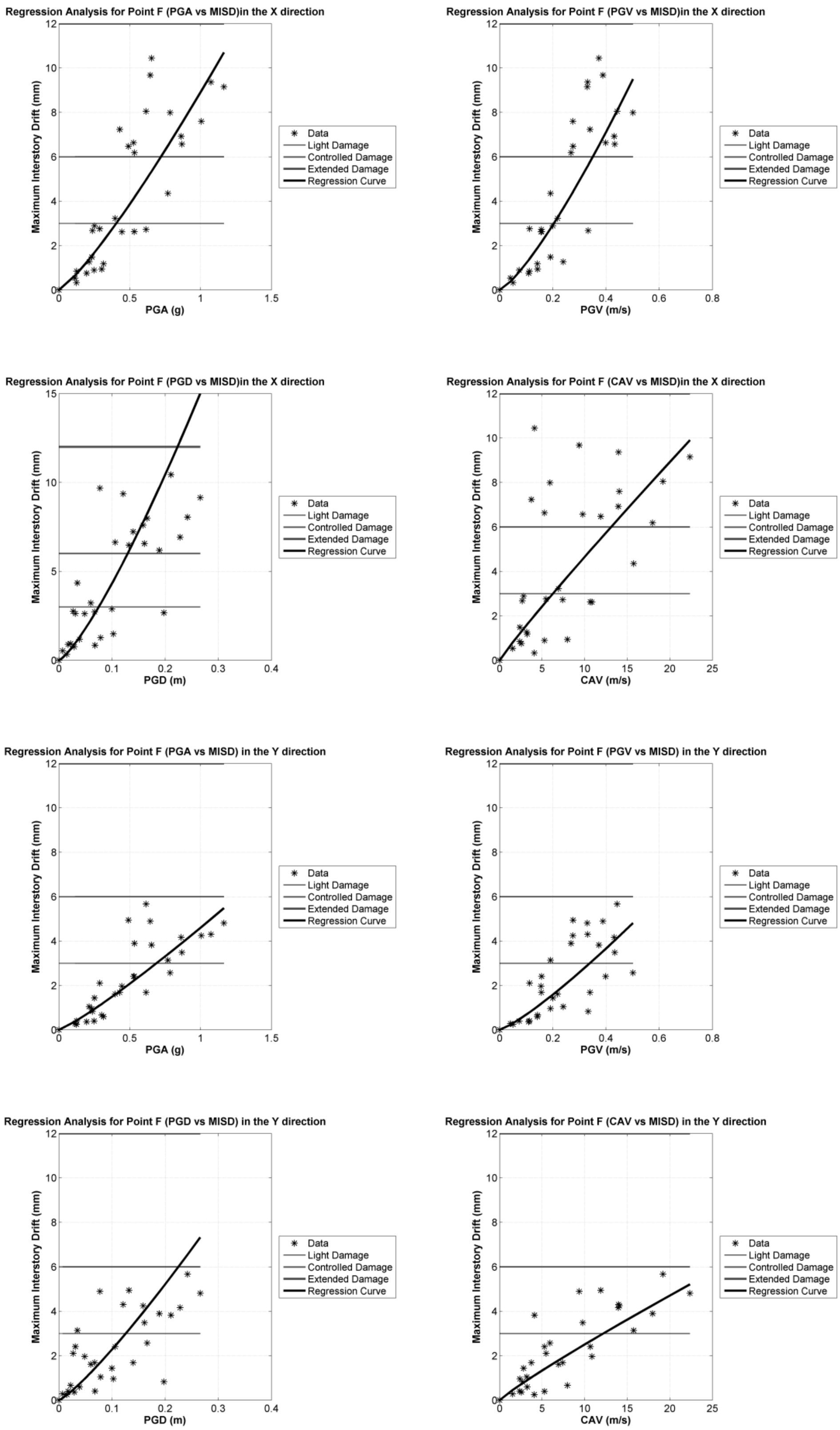

Figure A.6 Regression Analysis for Point F for seismic motion indicators

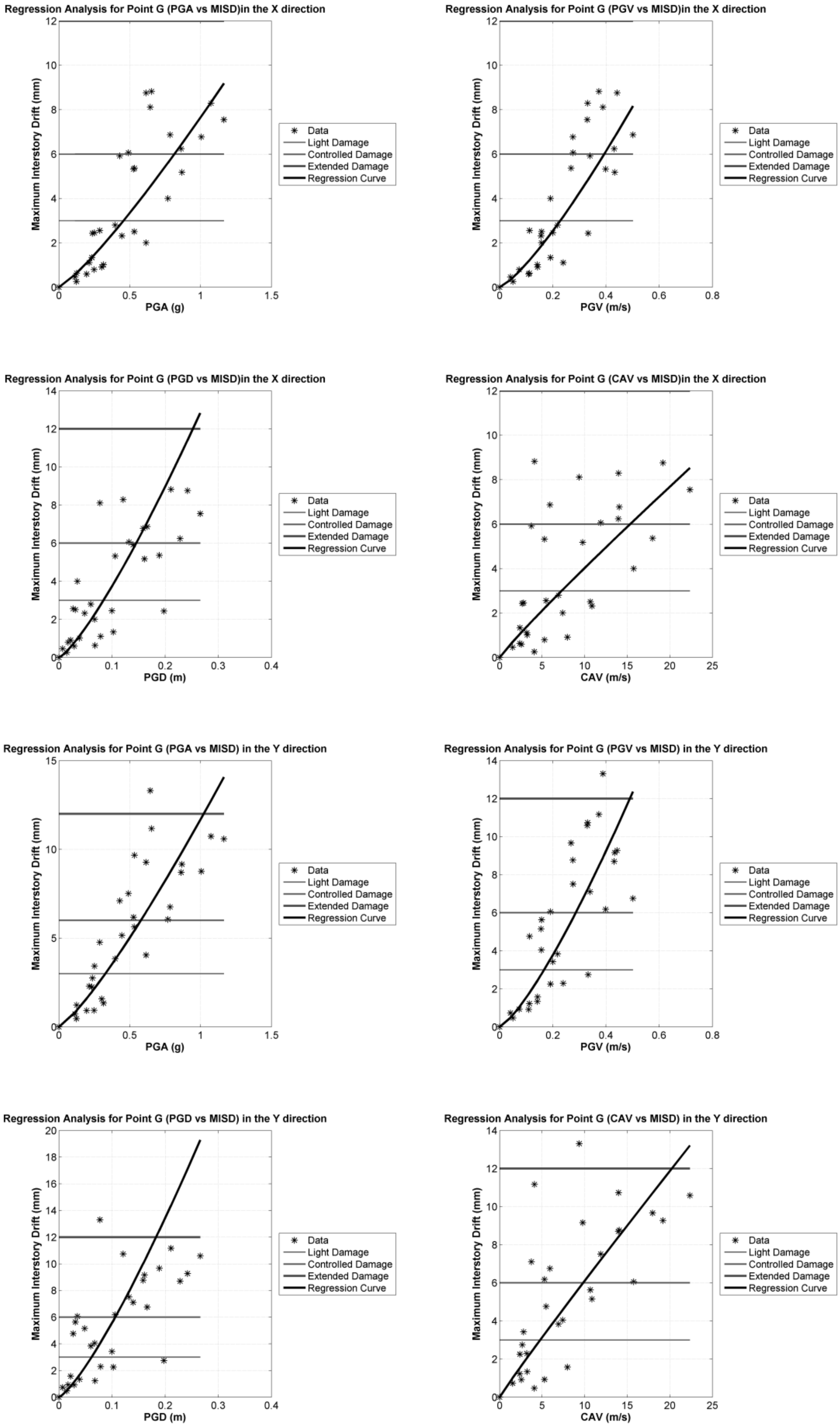

Figure A.7 Regression Analysis for Point G for seismic motion indicators

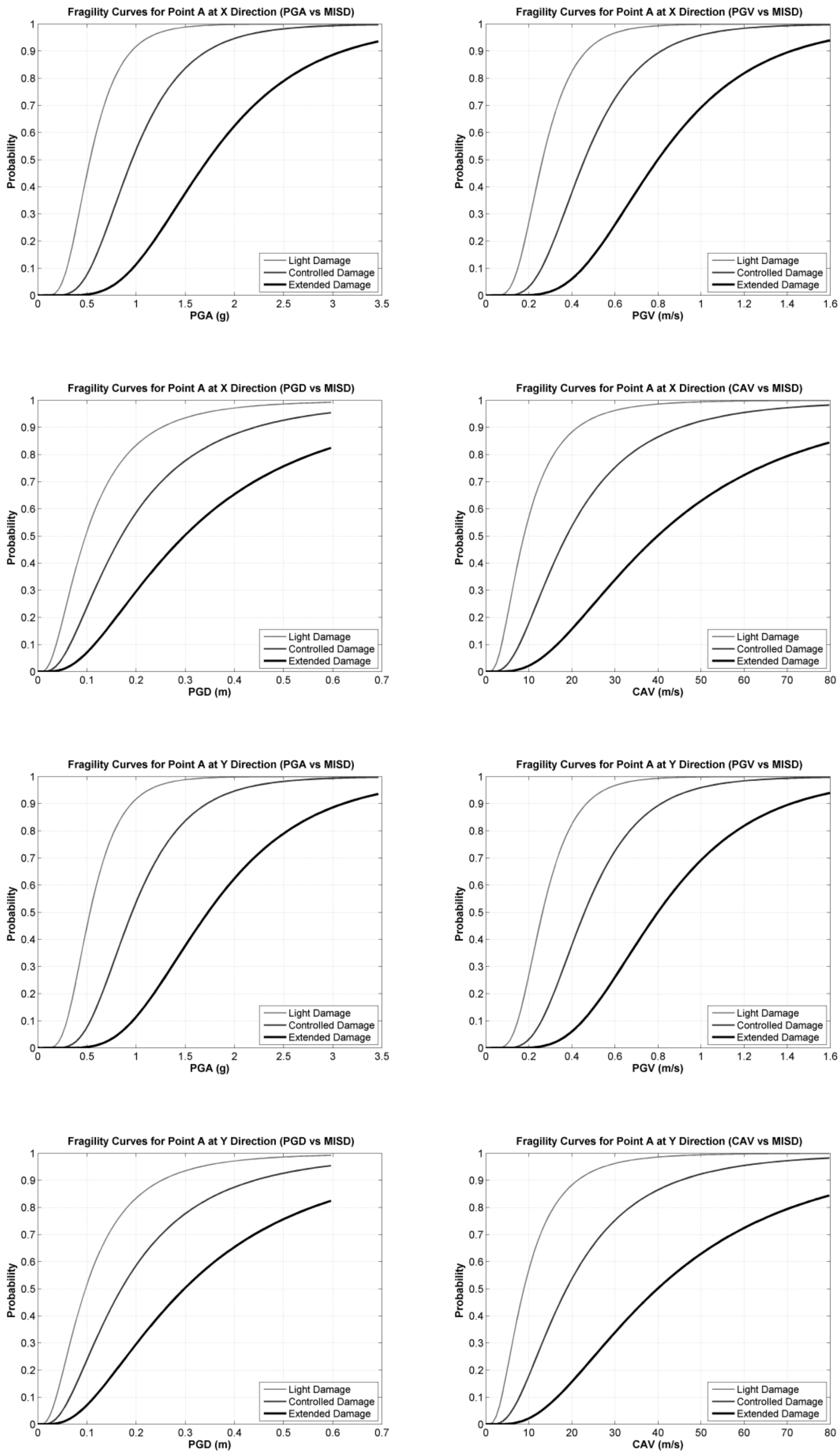

Figure A.8 Fragility Curves for Point A for various seismic motion indicators

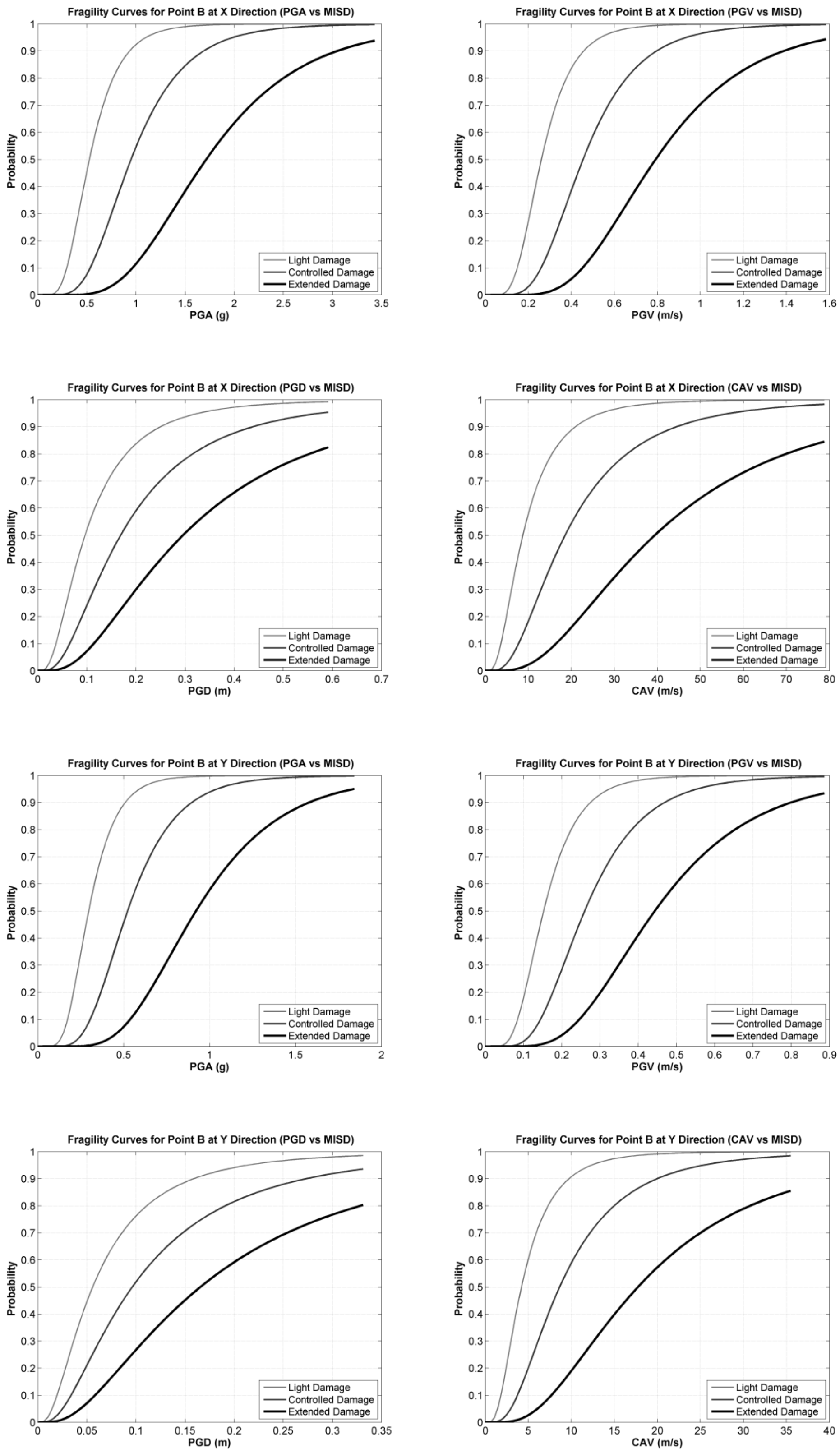

Figure A.9 Fragility Curves for Point B for various seismic motion indicators

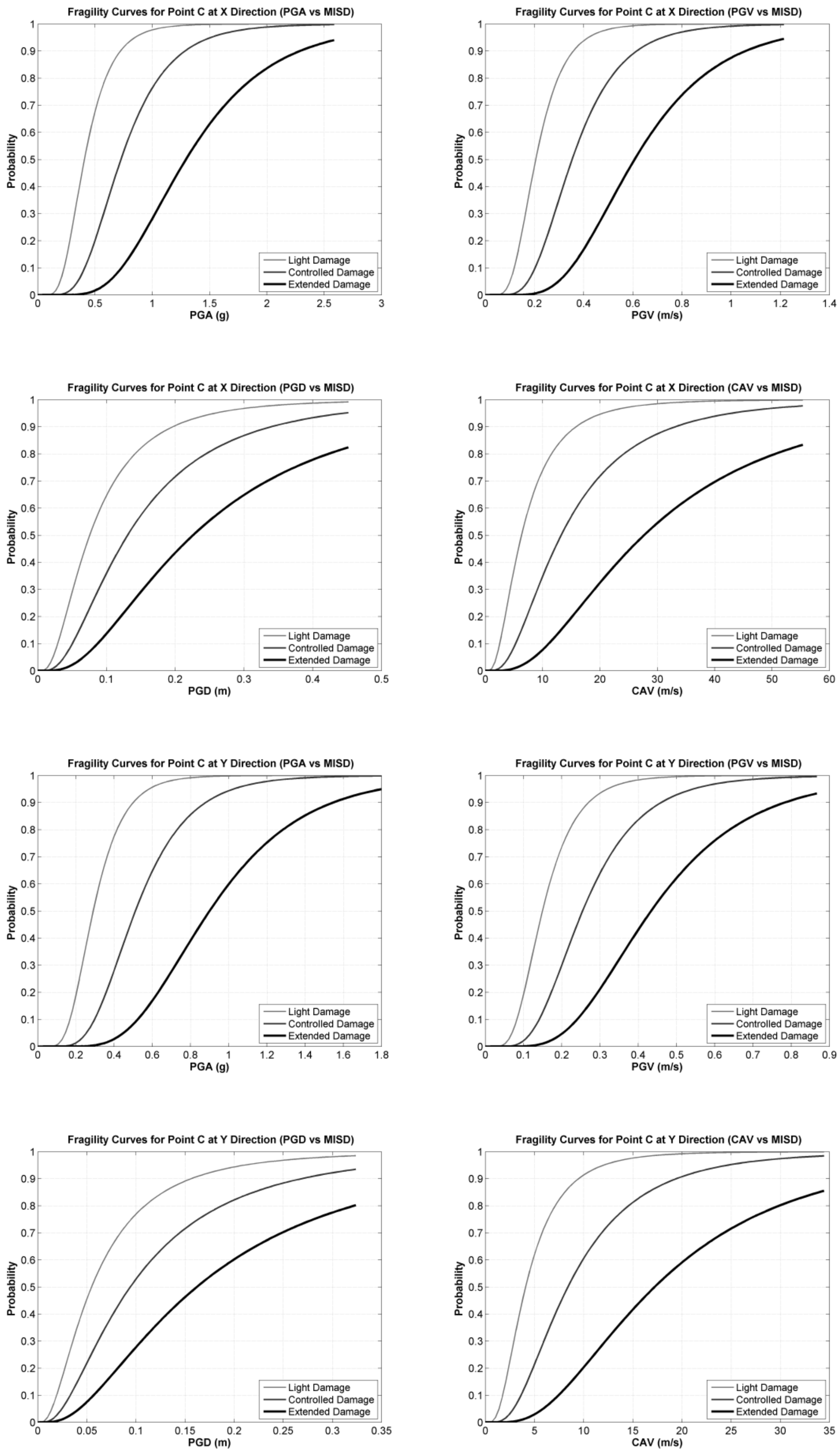

Figure A.10 Fragility Curves for Point C for various seismic motion indicators

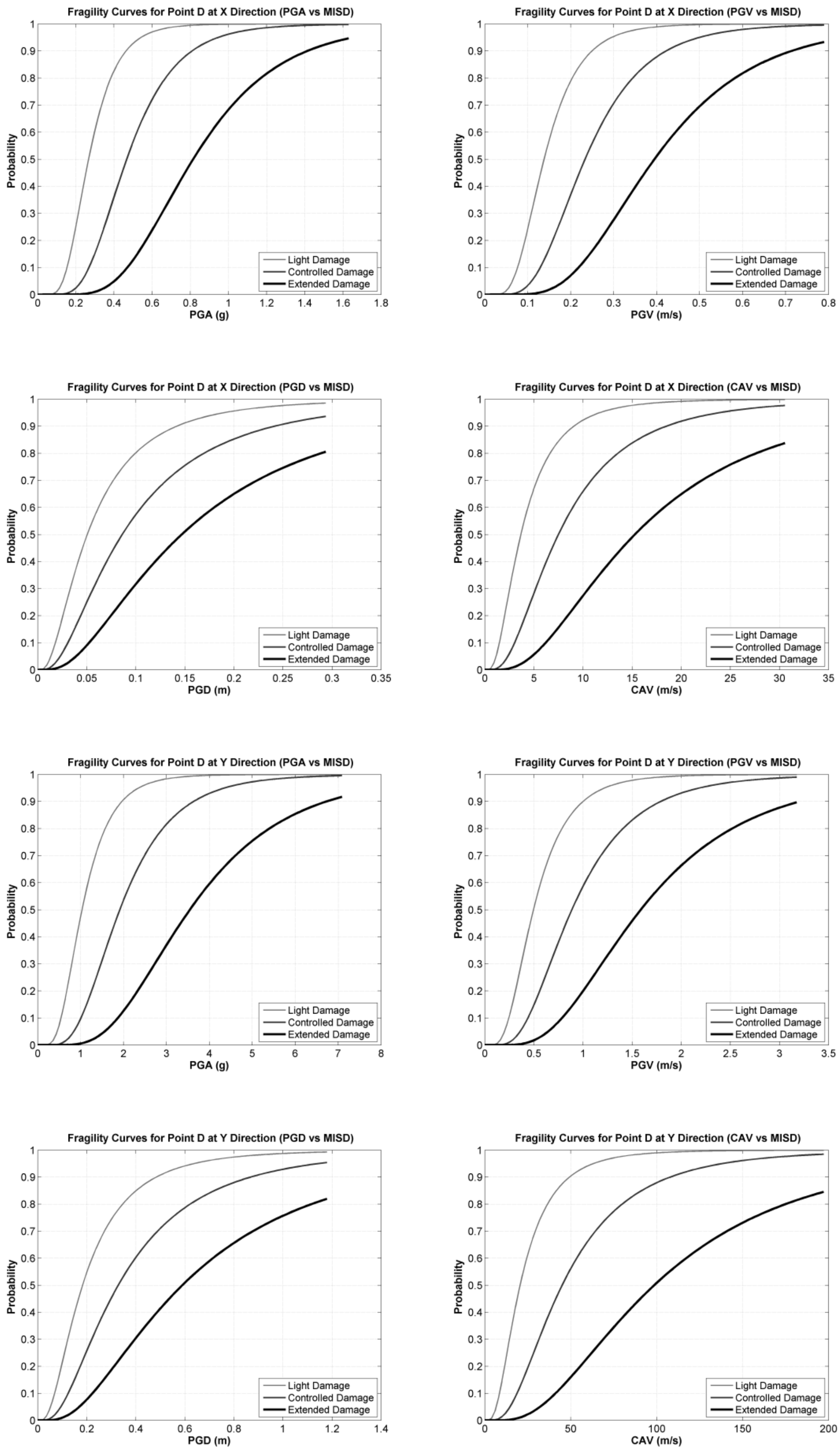

Figure A.11 Fragility Curves for Point D for various seismic motion indicators

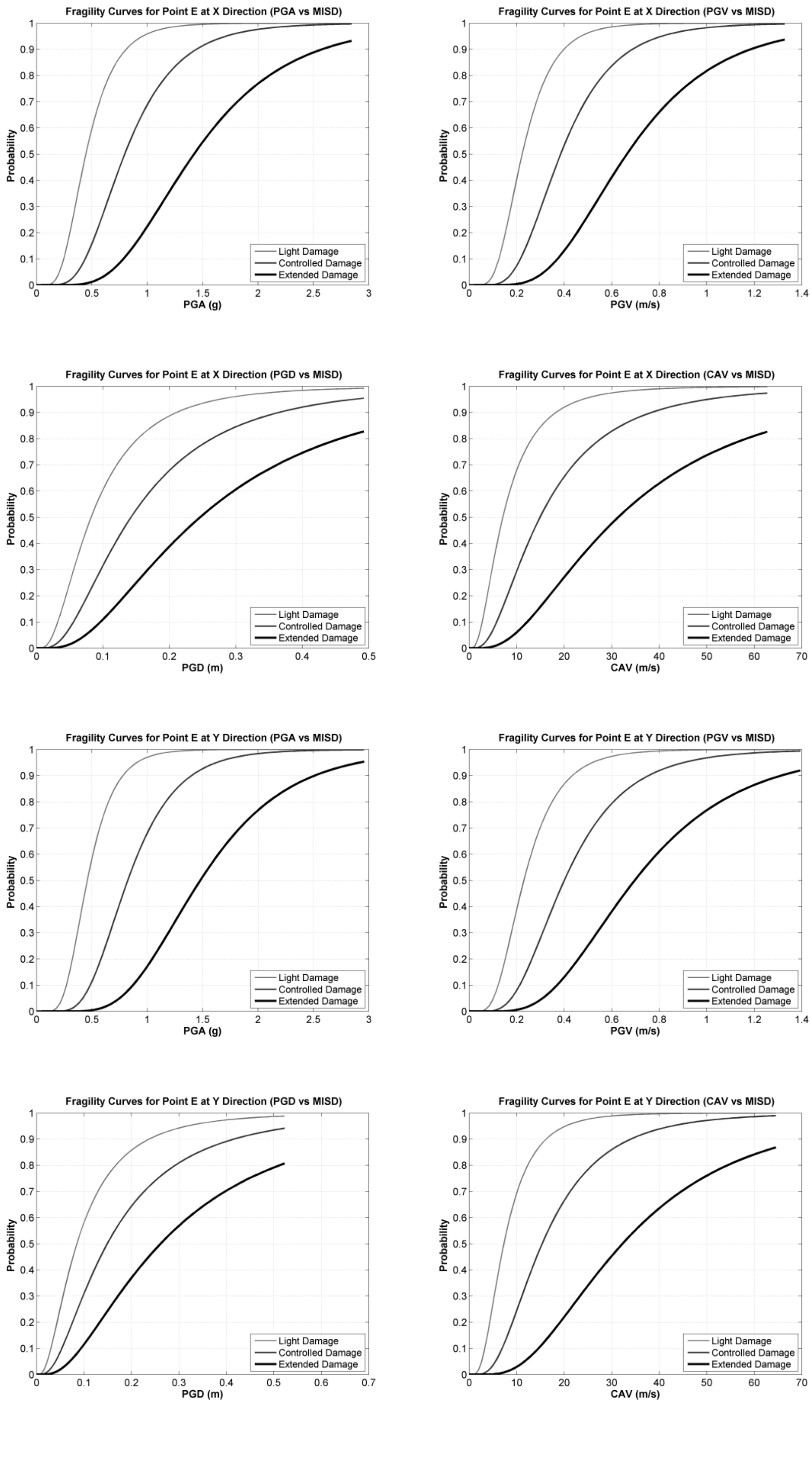

Figure A.12 Fragility Curves for Point E for various seismic motion indicators

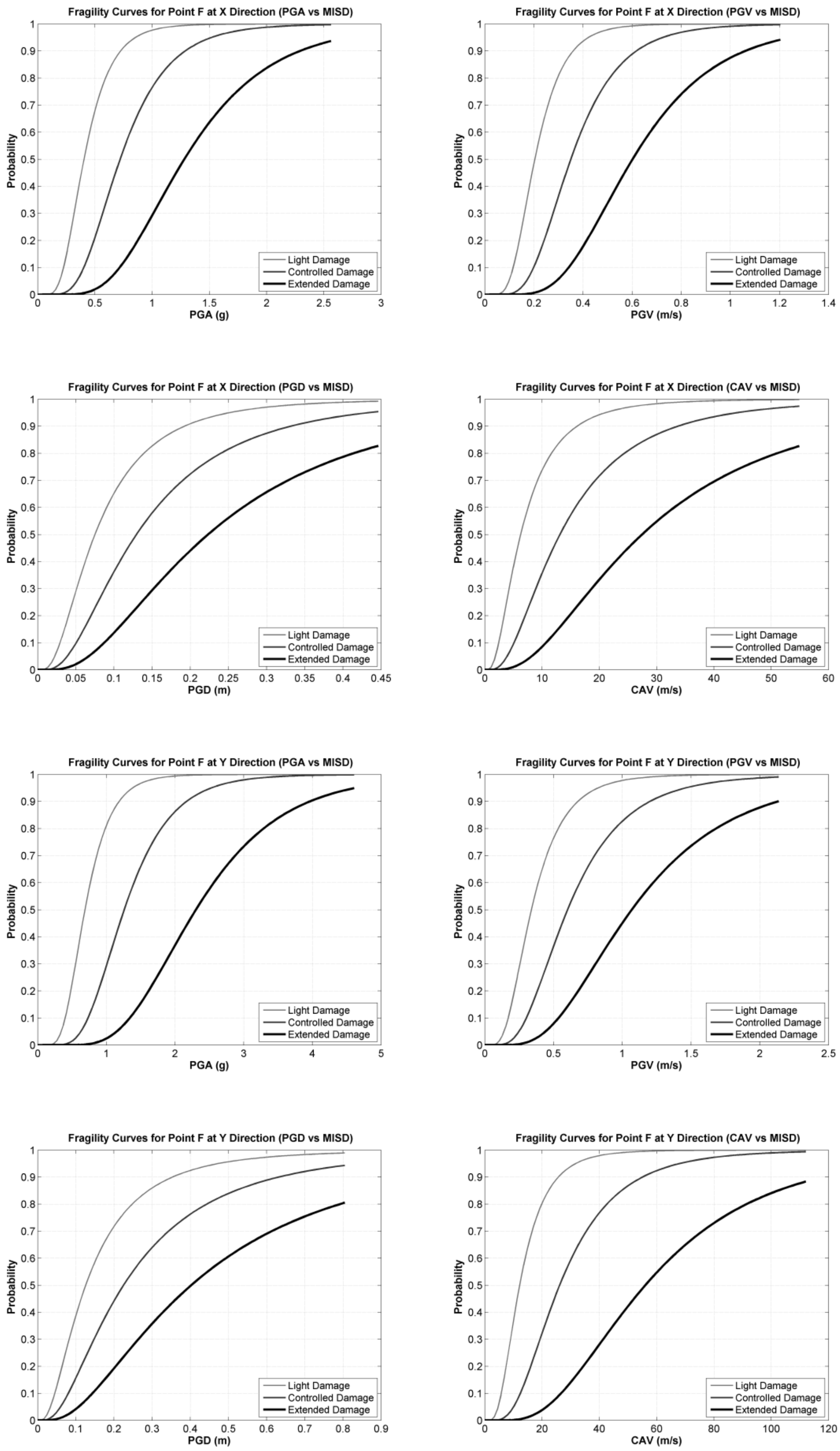

Figure A.13 Fragility Curves for Point F for various seismic motion indicators

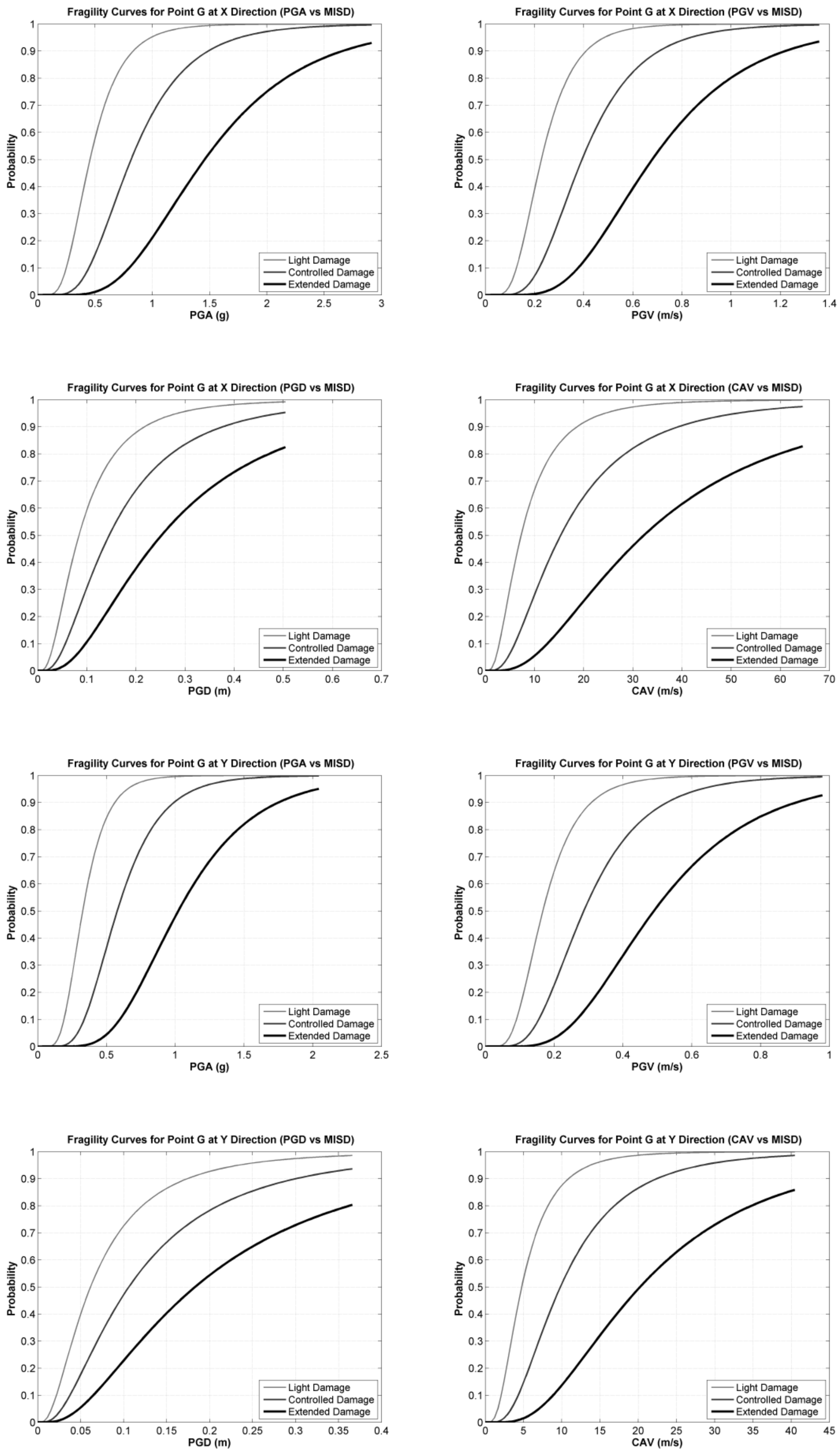

Figure A.14 Fragility Curves for Point G for various seismic motion indicators

APPENDIX B

Regression Analyses and Fragility Curves according to HAZUS-MH MR1 (2003) damage states

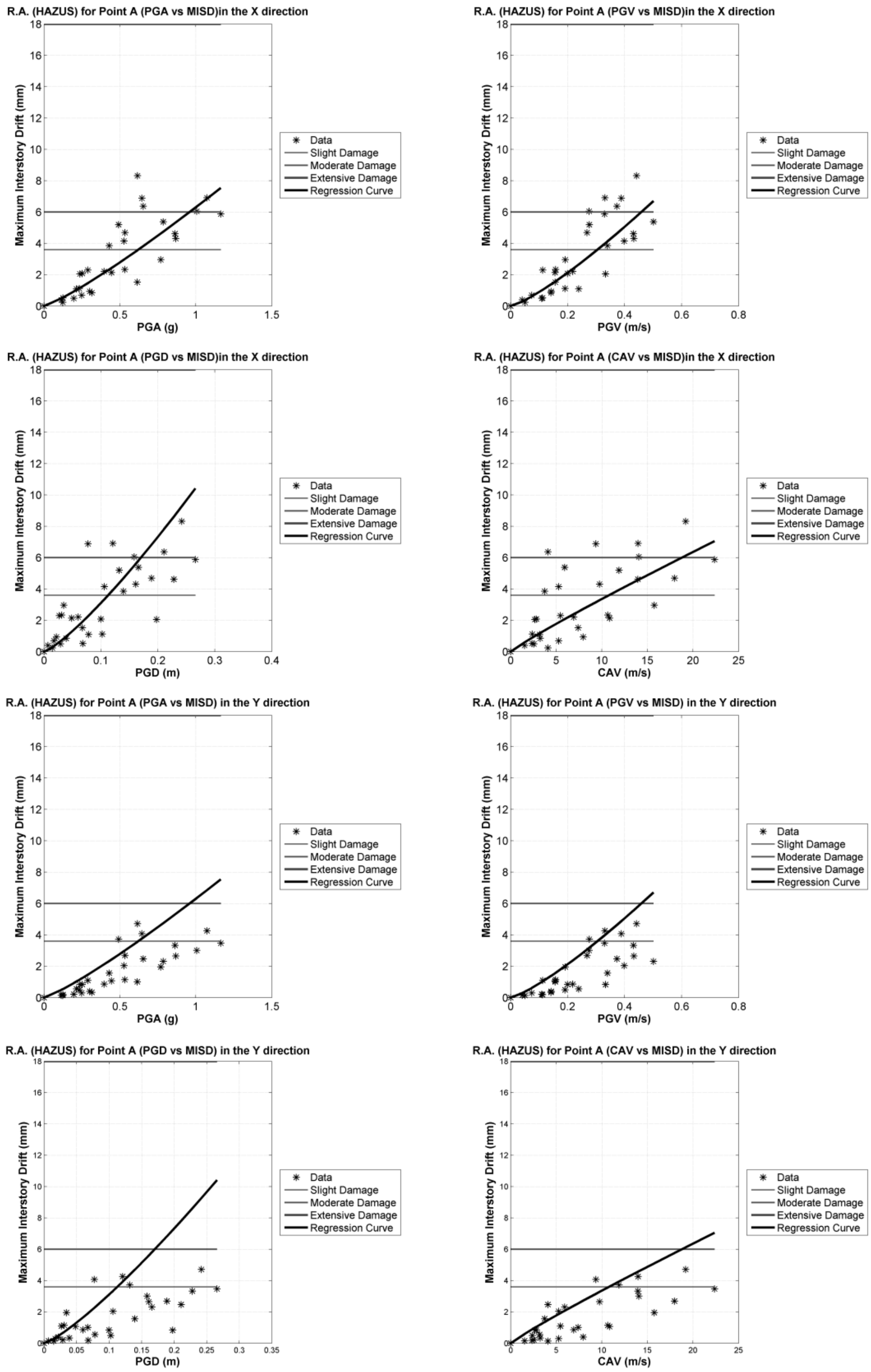

Figure B.1 Regression Analysis for Point A for seismic motion indicators according to HAZUS damage states

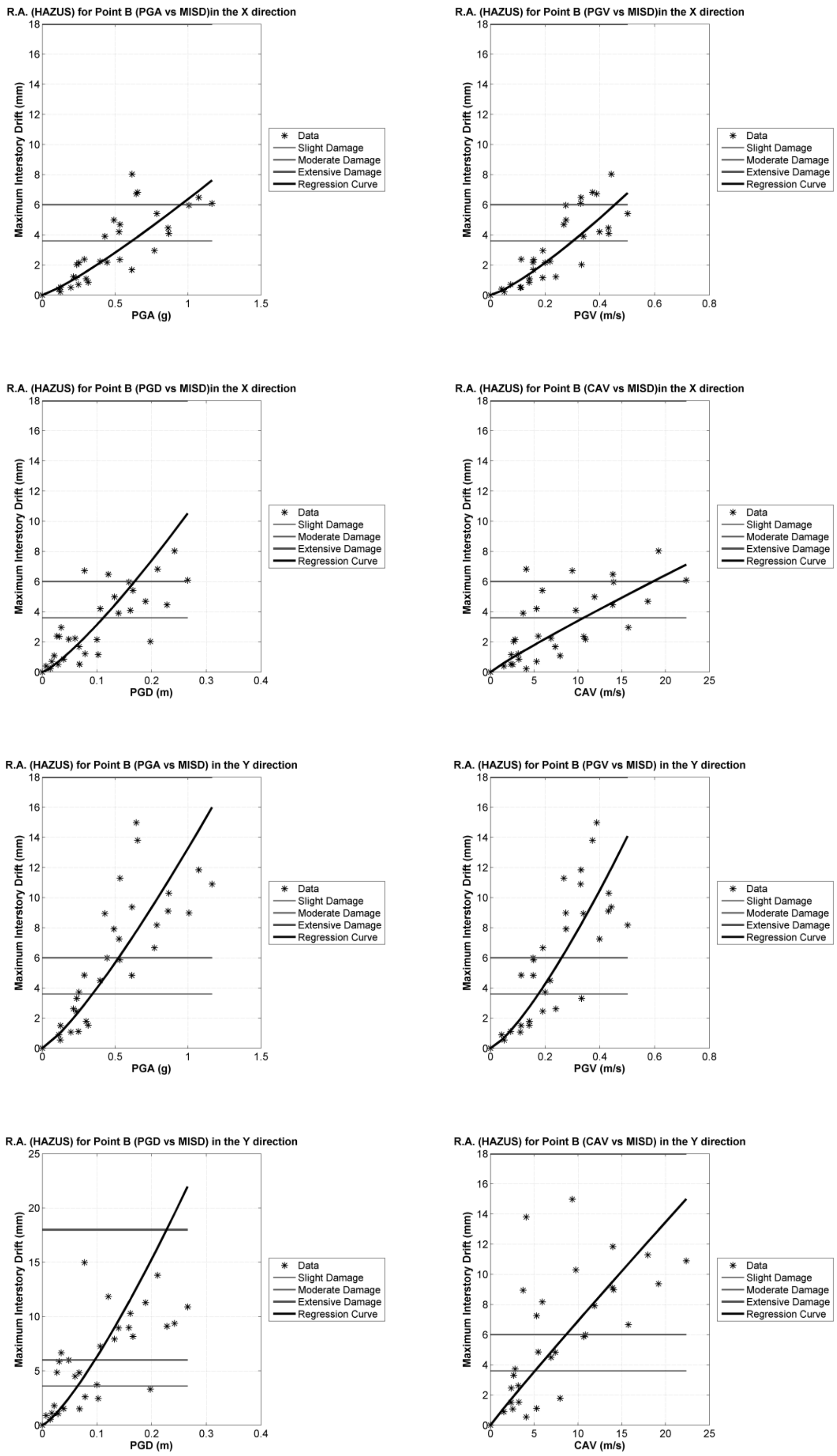

Figure B.2 Regression Analysis for Point B for seismic motion indicators according to HAZUS damage states

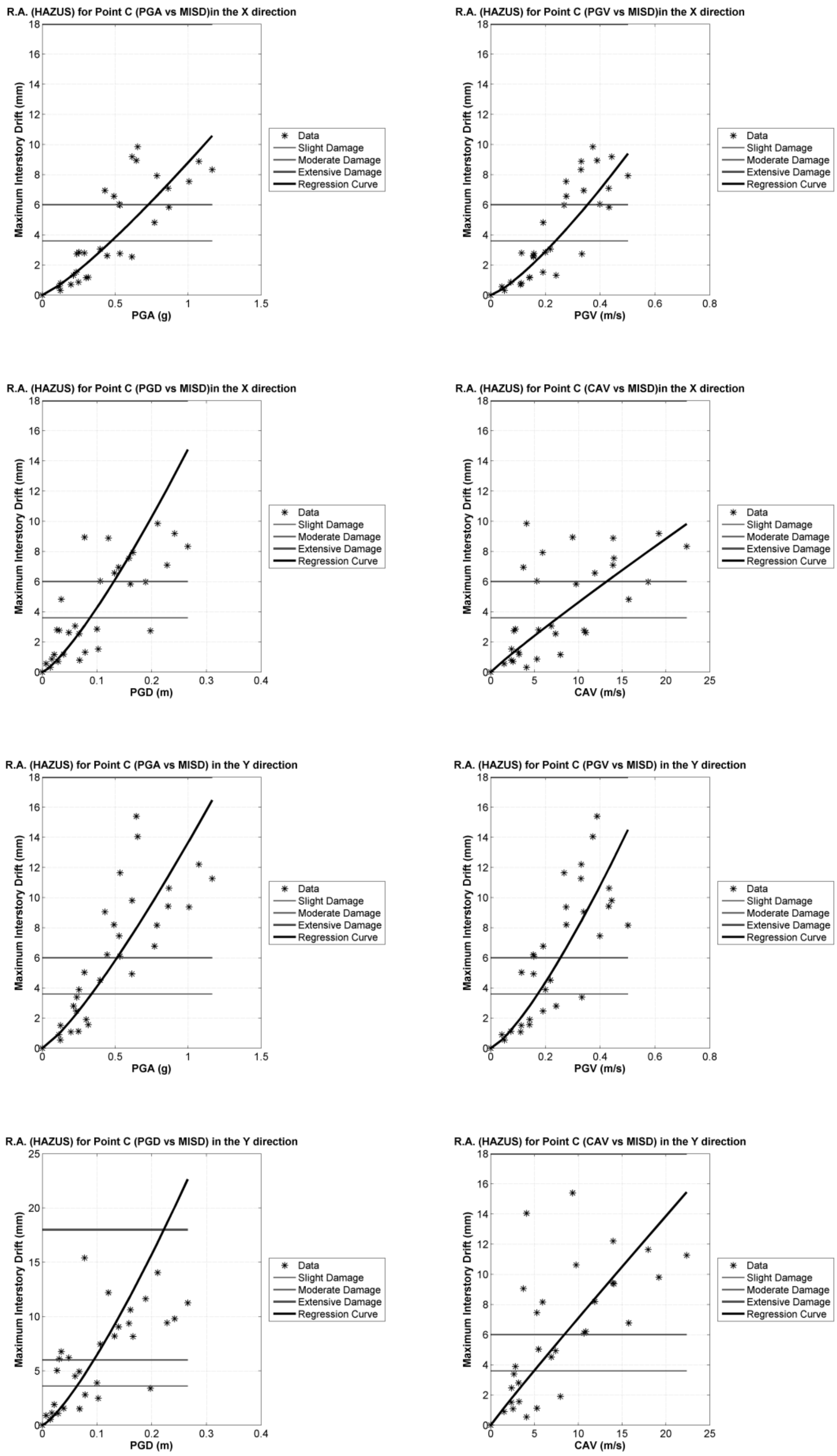

Figure B.3 Regression Analysis for Point C for seismic motion indicators according to HAZUS damage states

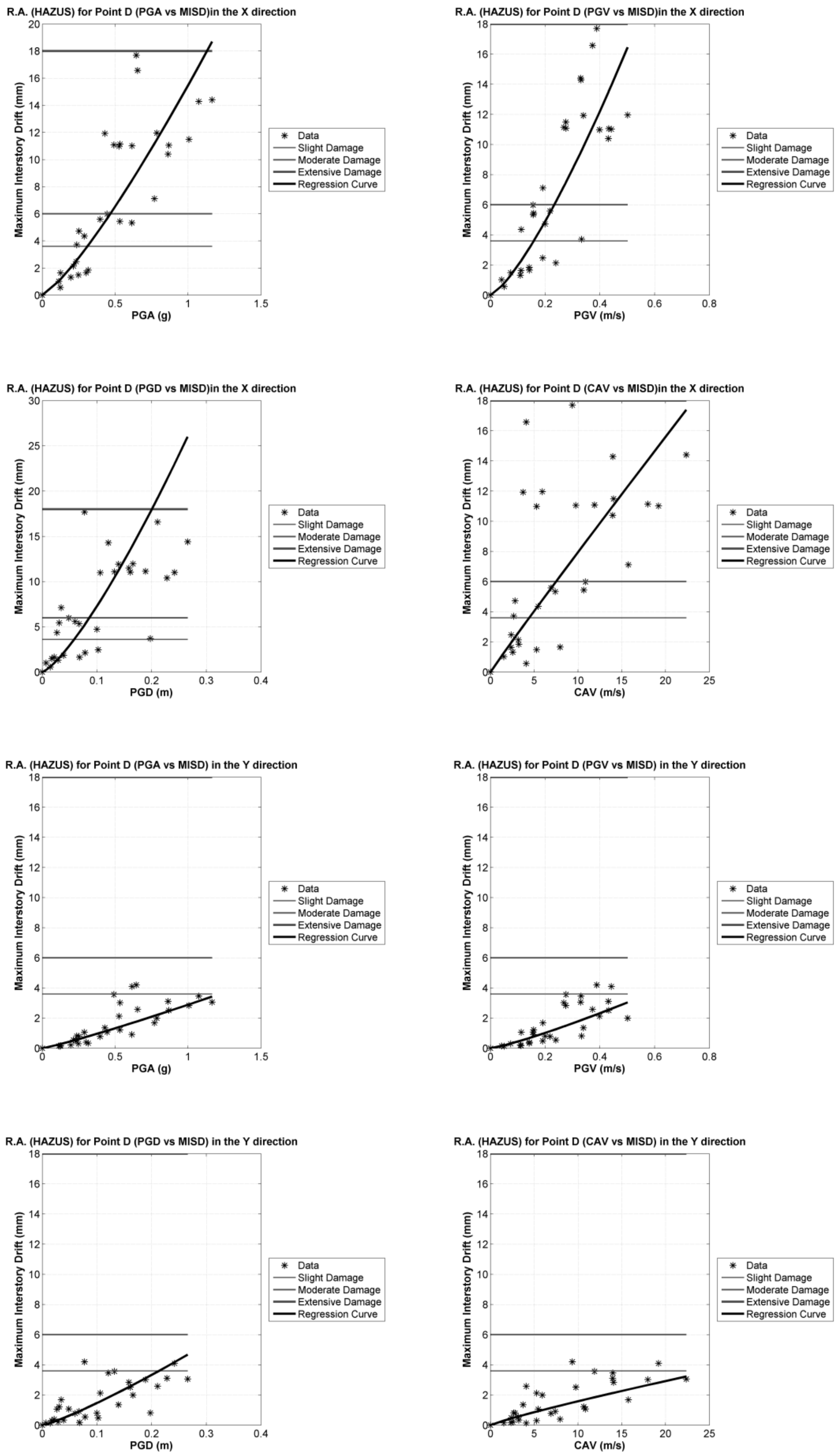

Figure B.4 Regression Analysis for Point D for seismic motion indicators according to HAZUS damage states

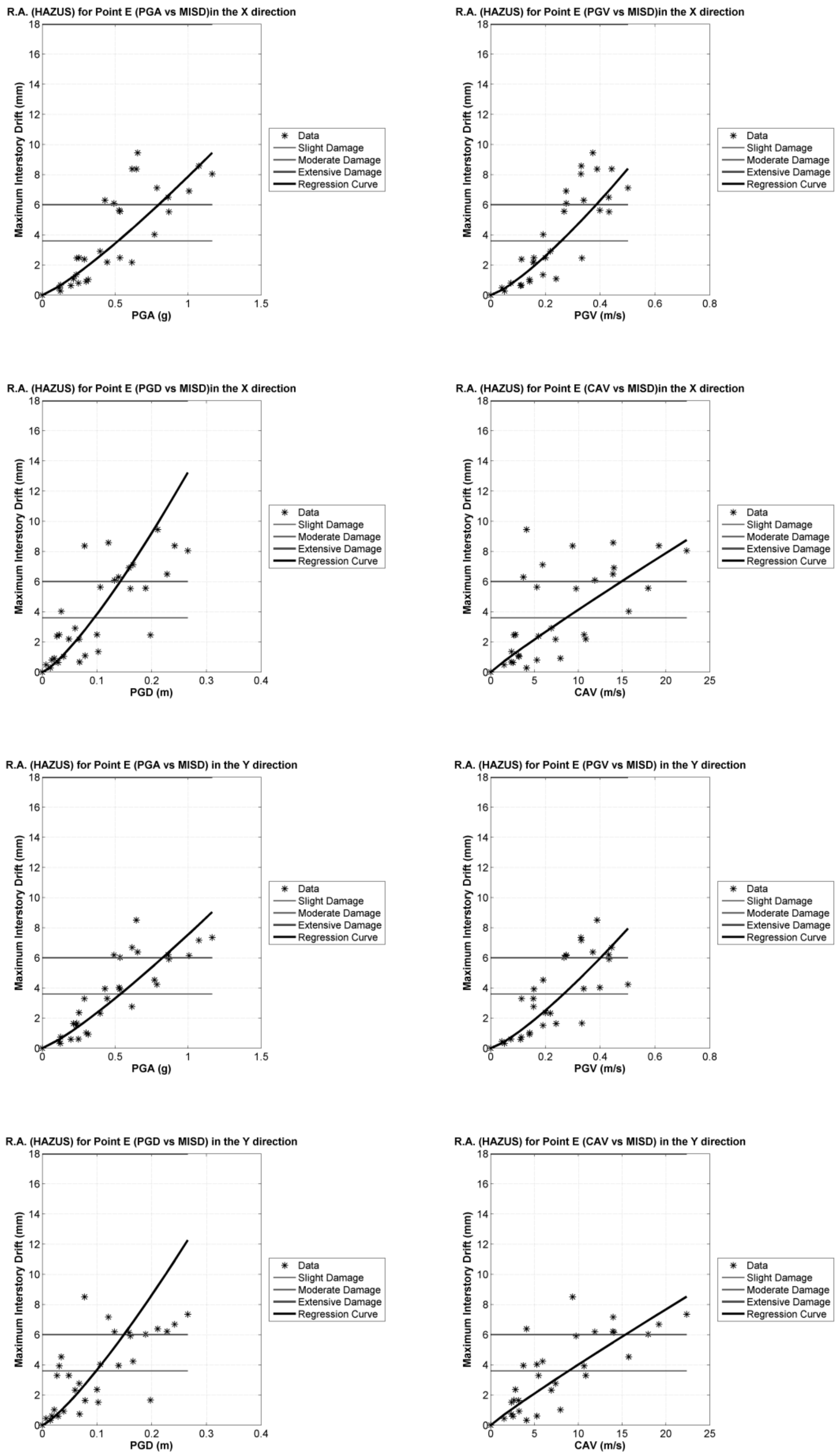

Figure B.5 Regression Analysis for Point E for seismic motion indicators according to HAZUS damage states

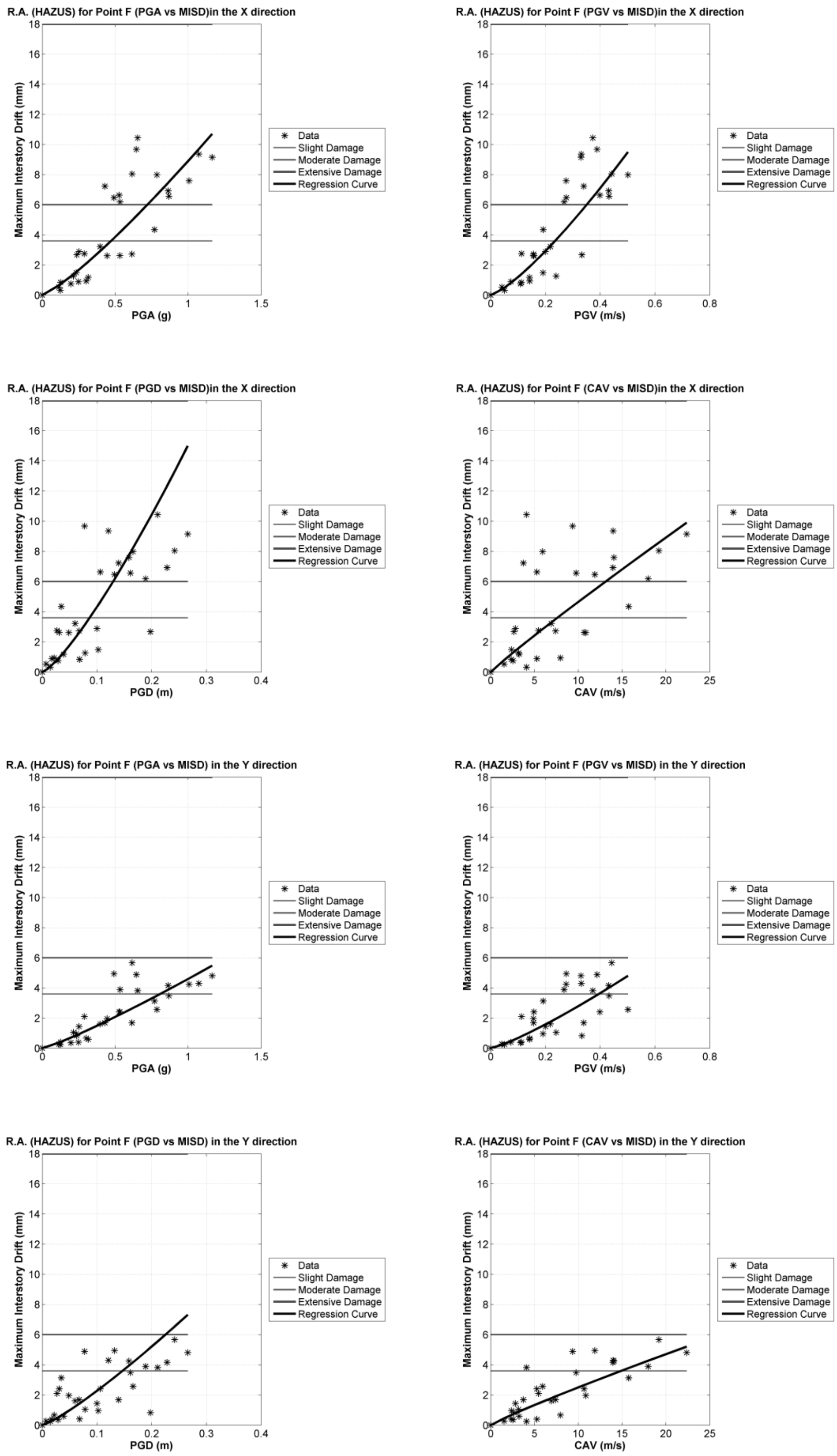

Figure B.6 Regression Analysis for Point F for seismic motion indicators according to HAZUS damage states

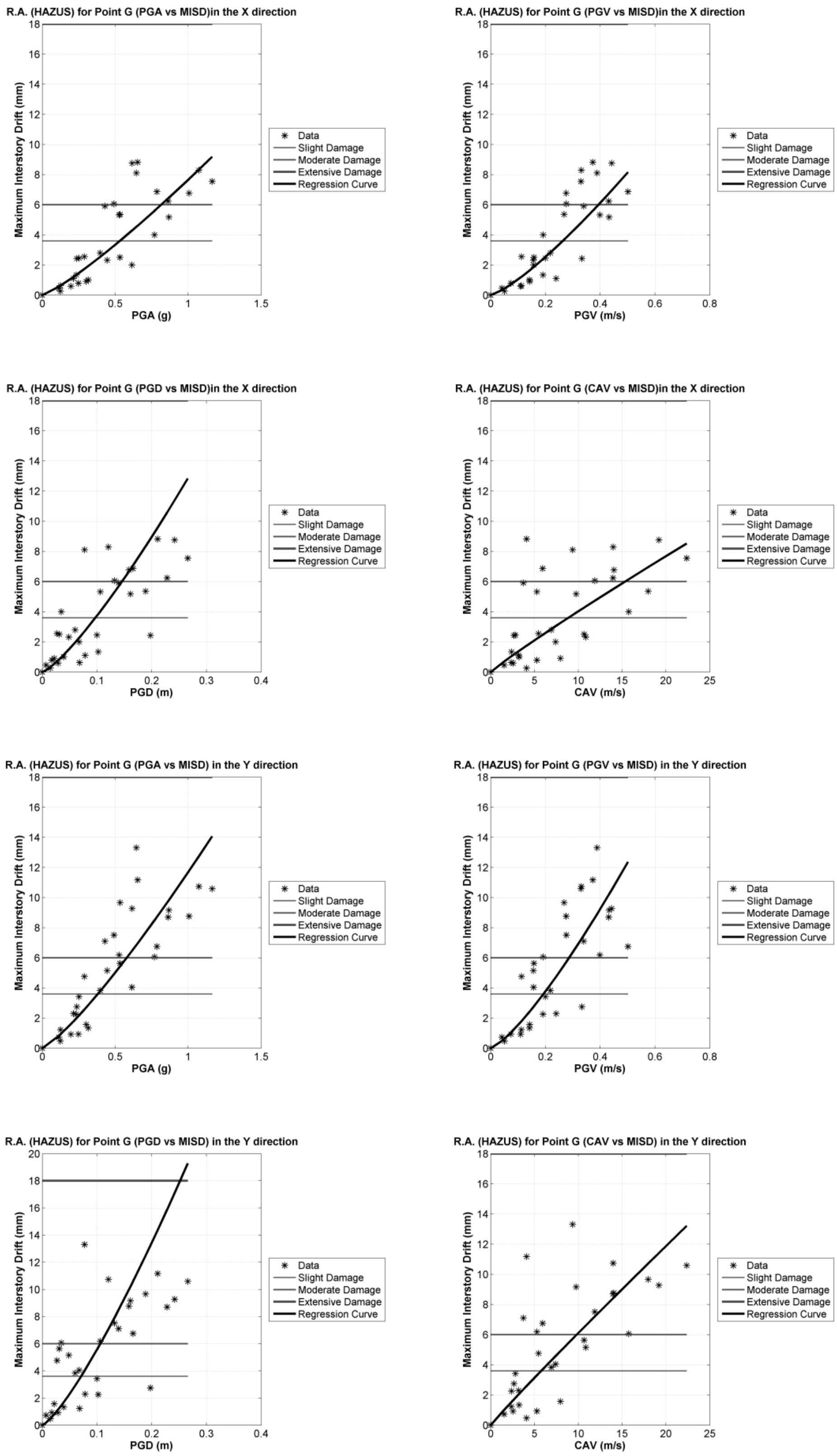

Figure B.7 Regression Analysis for Point G for seismic motion indicators according to HAZUS damage states

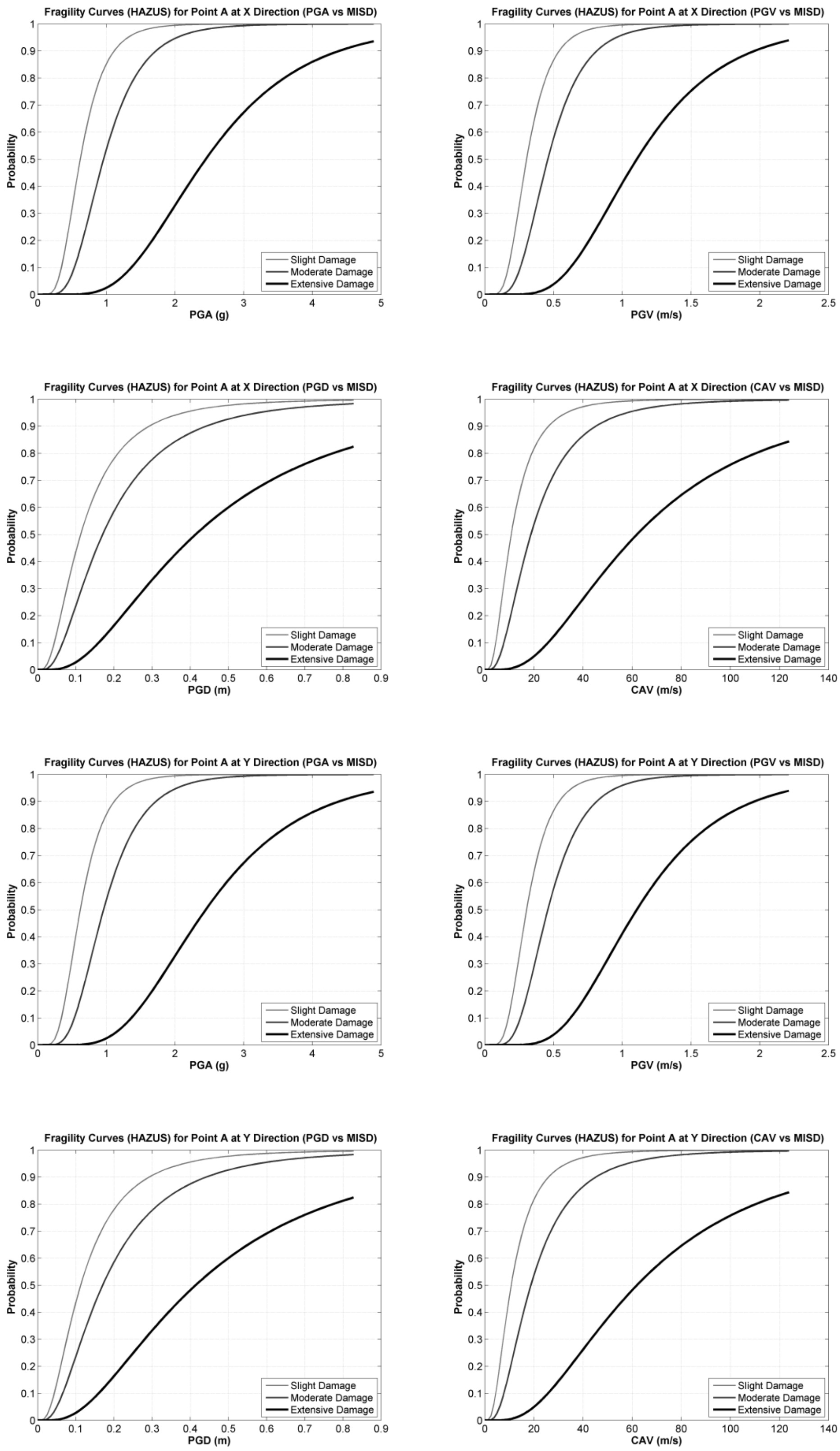

Figure B.8 Fragility Curves for Point A for various seismic motion indicators according to HAZUS damage states

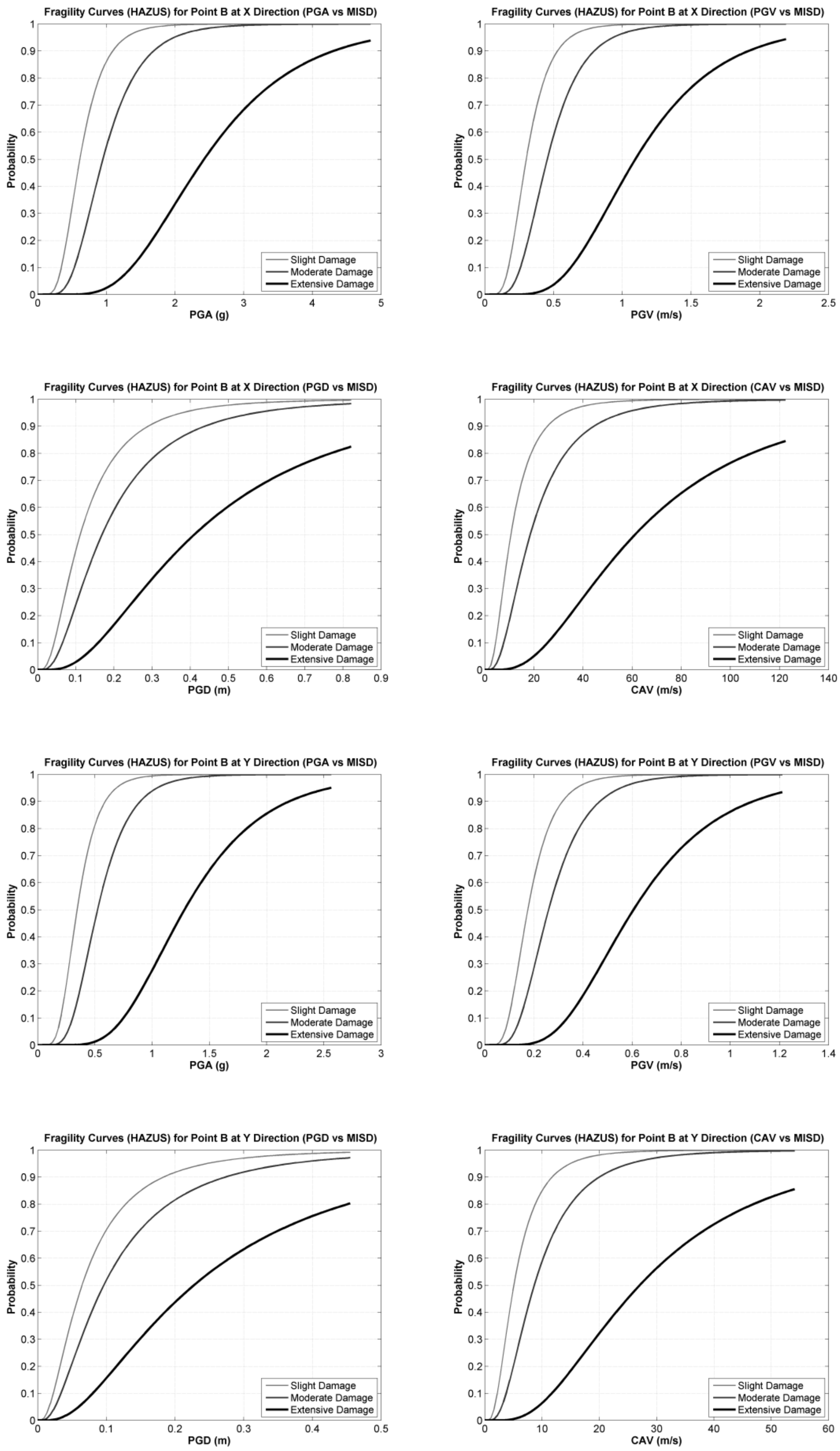

Figure B.9 Fragility Curves for Point B for various seismic motion indicators according to HAZUS damage states

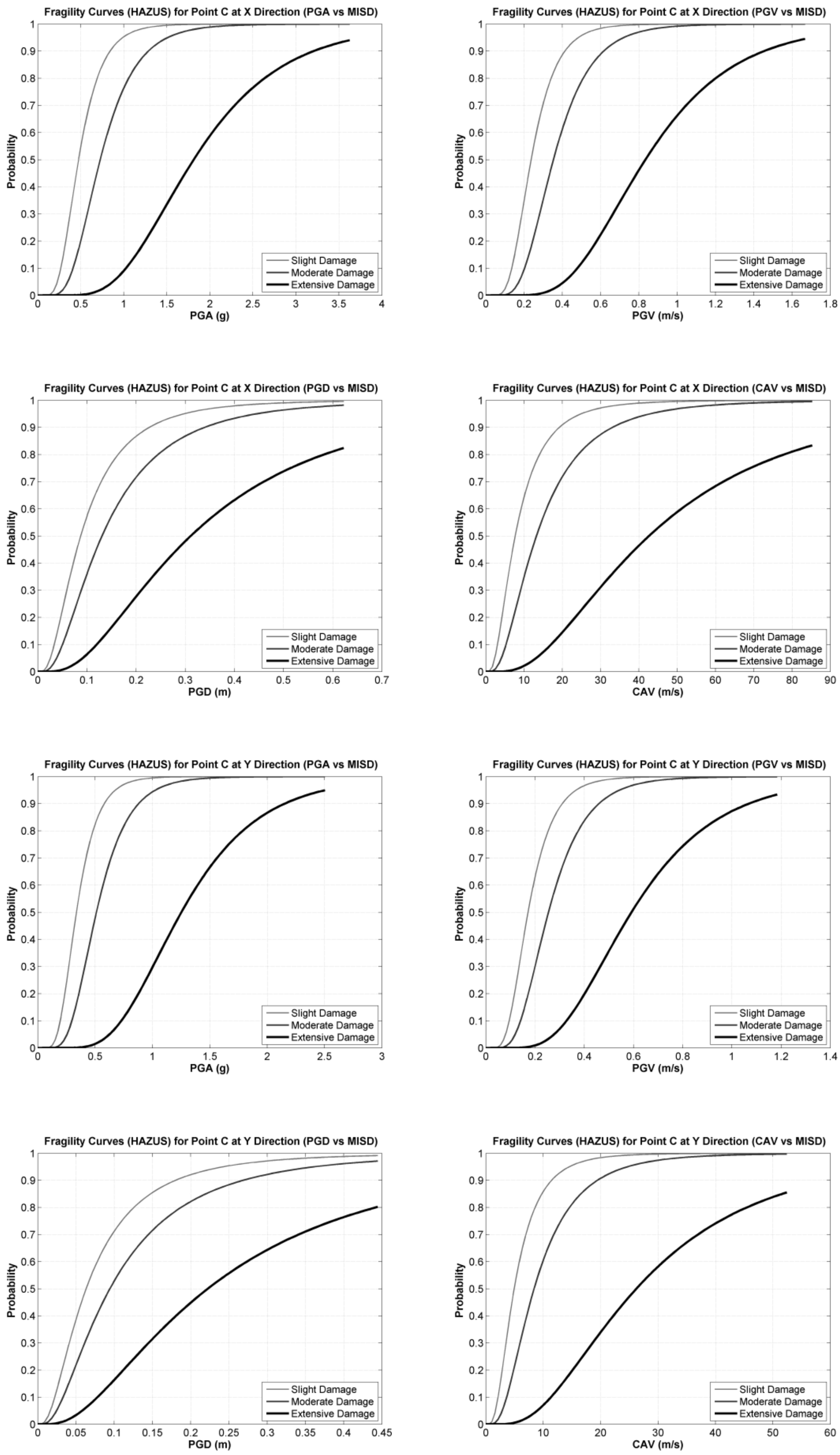

Figure B.10 Fragility Curves for Point C for various seismic motion indicators according to HAZUS damage states

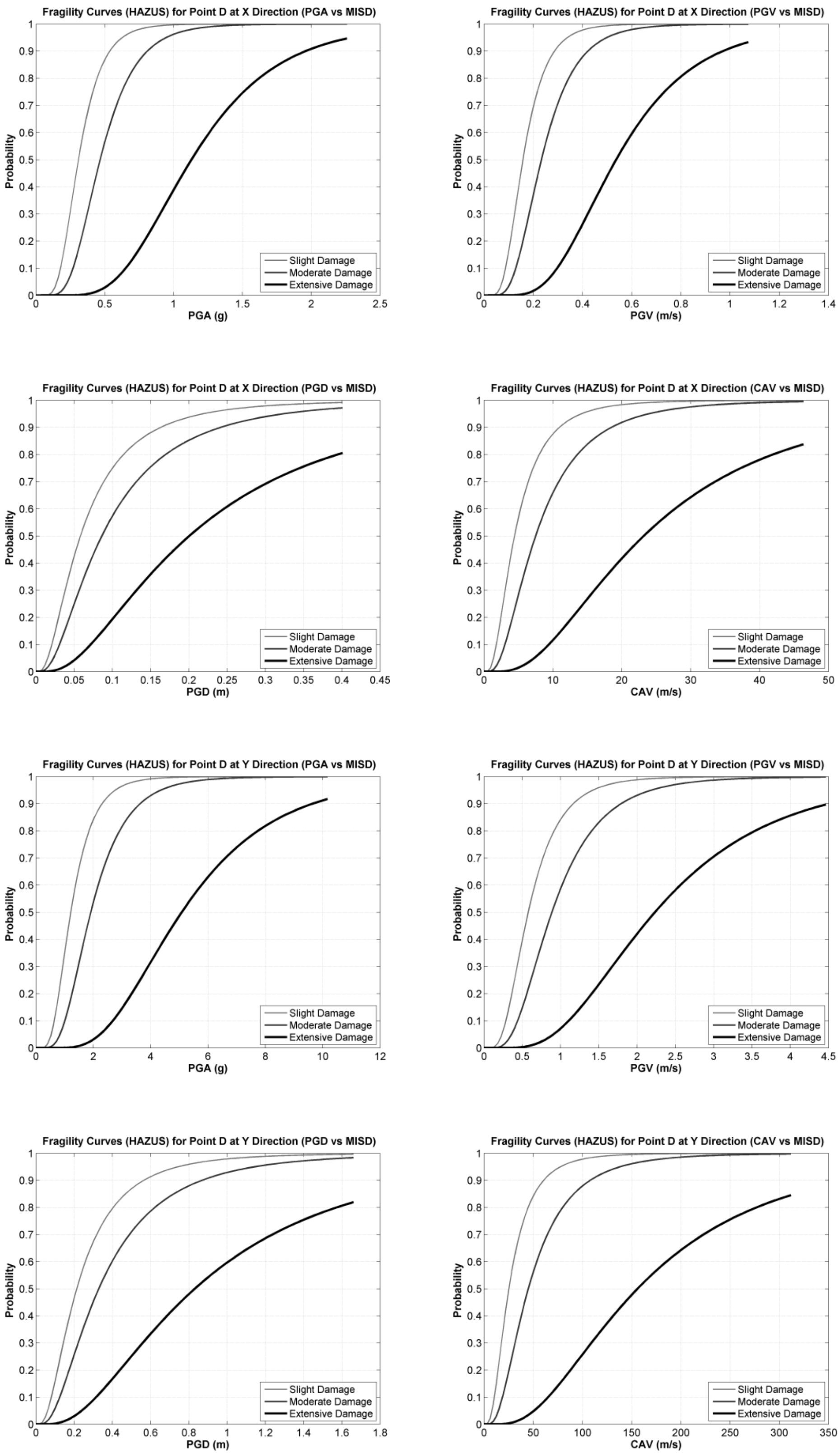

Figure B.11 Fragility Curves for Point D for various seismic motion indicators according to HAZUS damage states

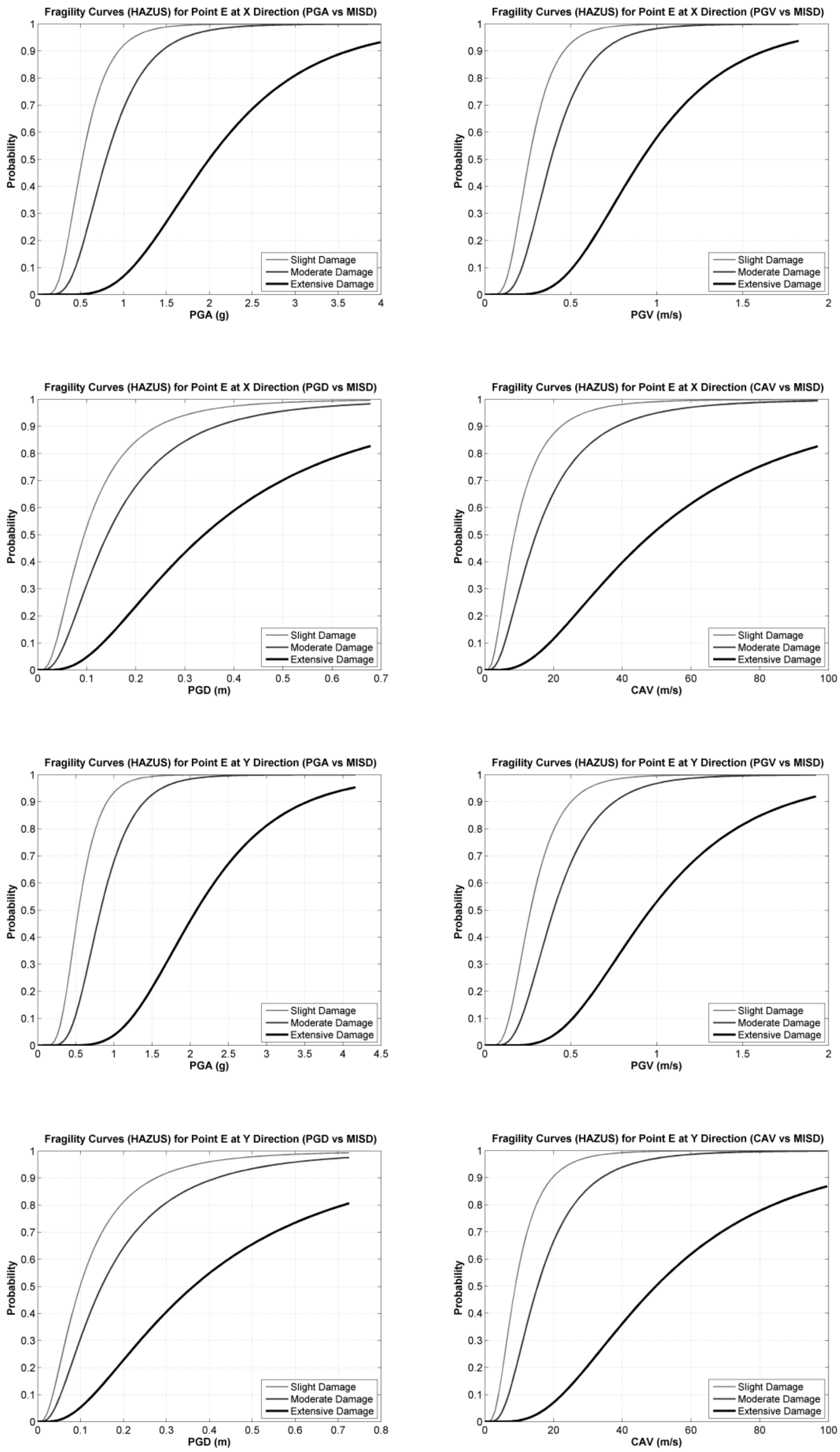

Figure B.12 Fragility Curves for Point E for various seismic motion indicators according to HAZUS damage states

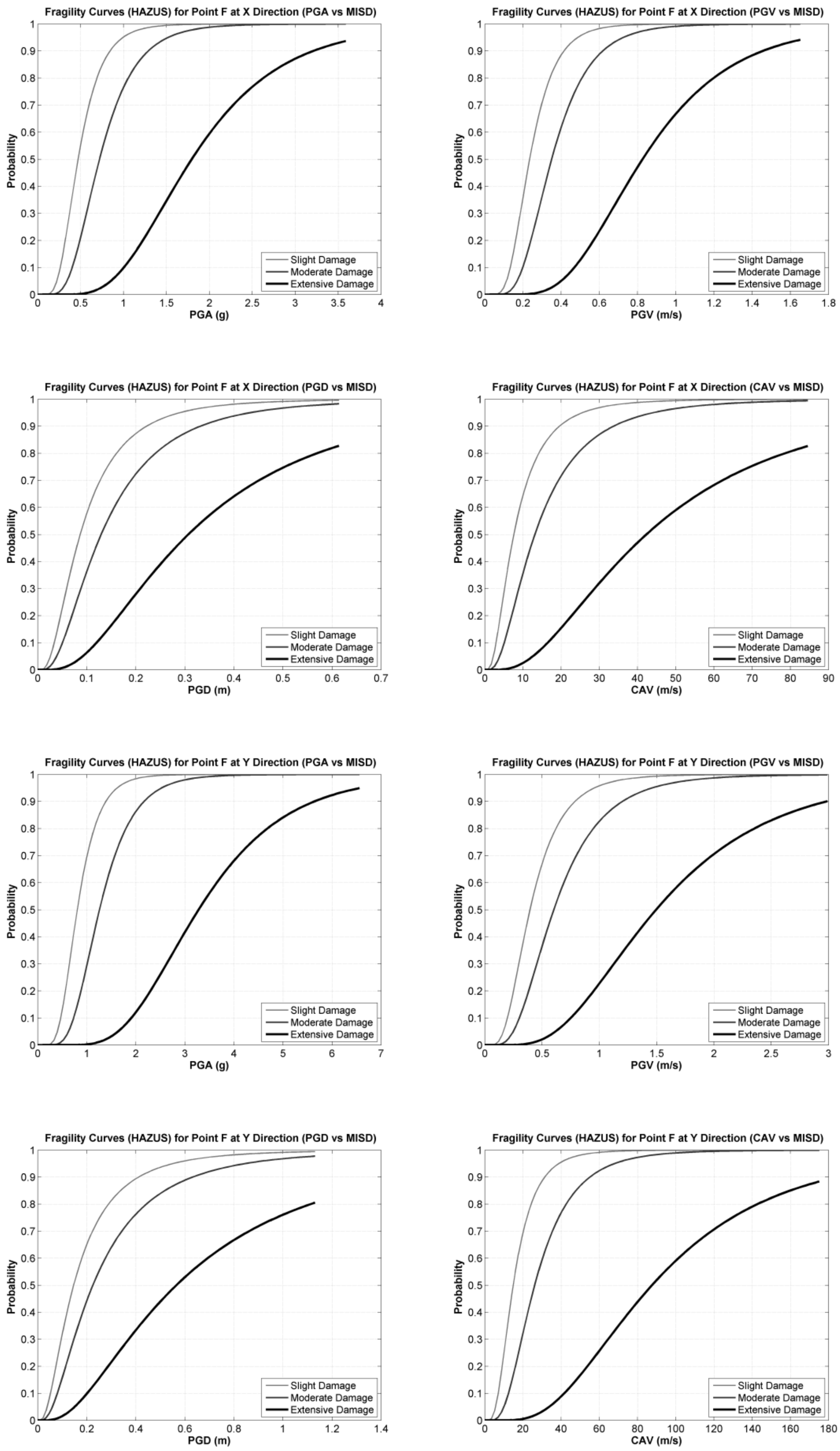

Figure B.13 Fragility Curves for Point F for various seismic motion indicators according to HAZUS damage states

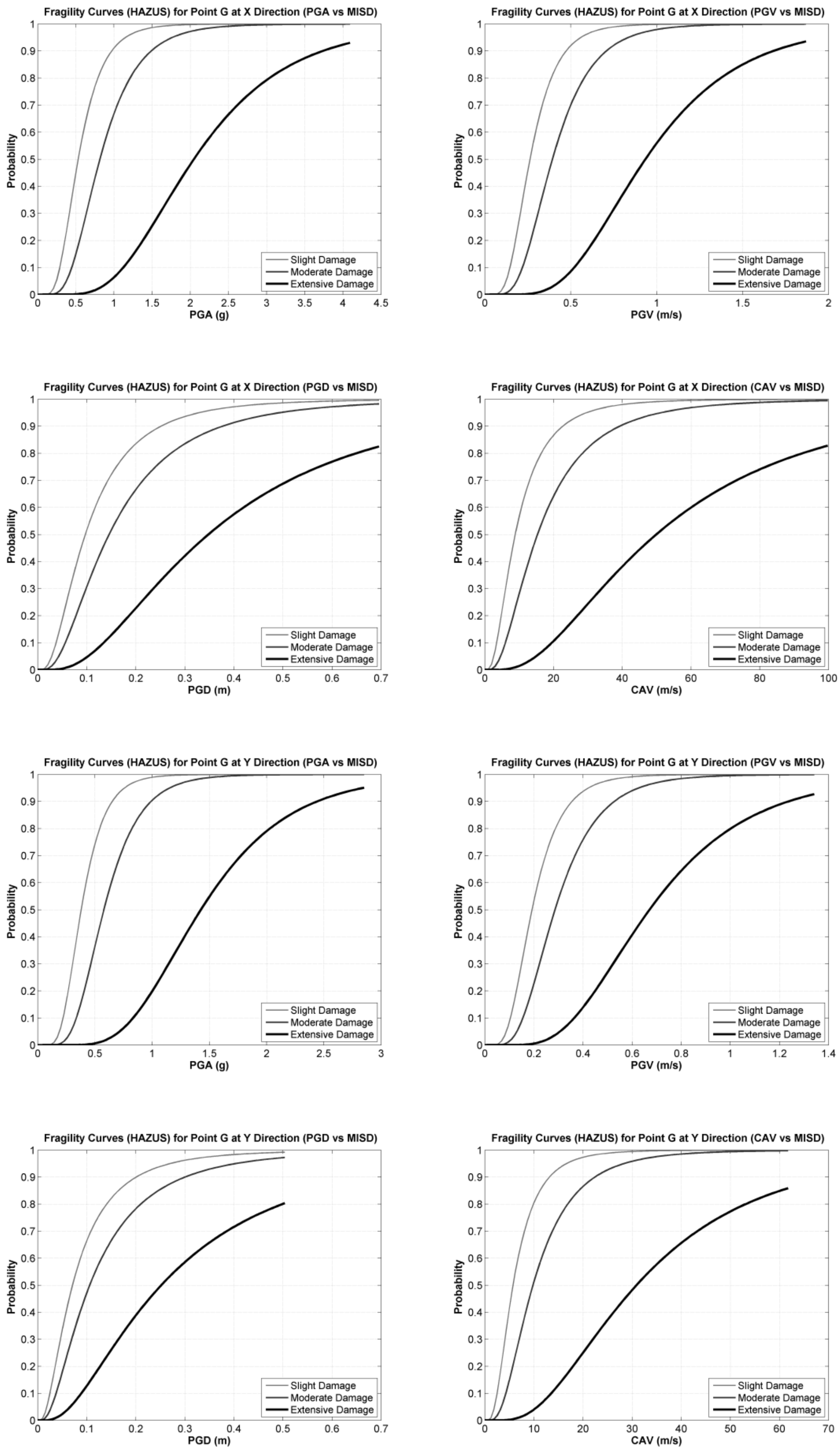

Figure B.14 Fragility Curves for Point G for various seismic motion indicators according to HAZUS damage states

APPENDIX C

Synthetic Accelerograms Used in Fragility Analysis

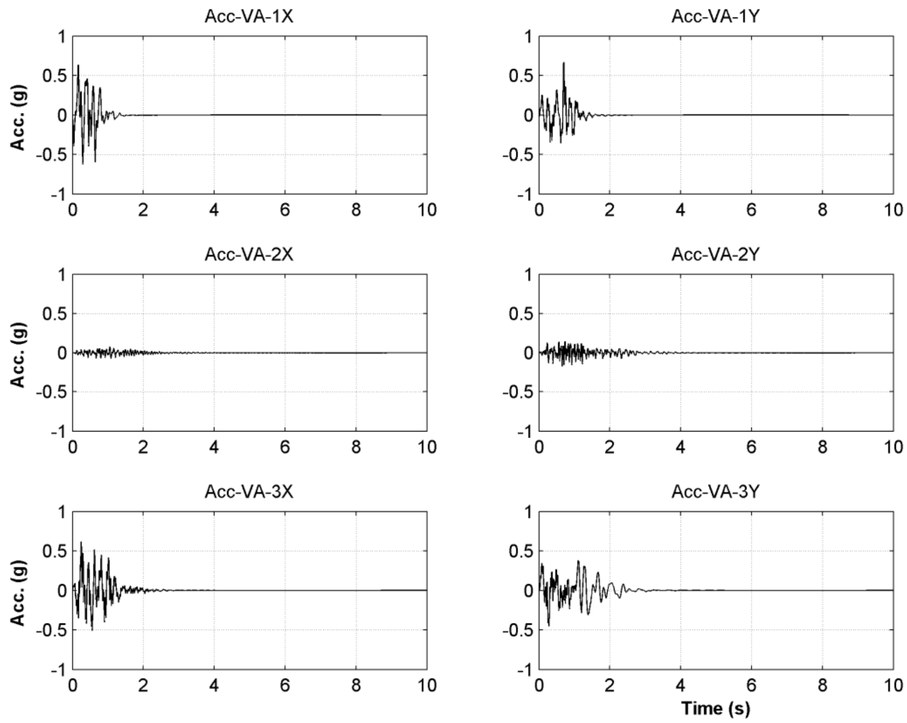

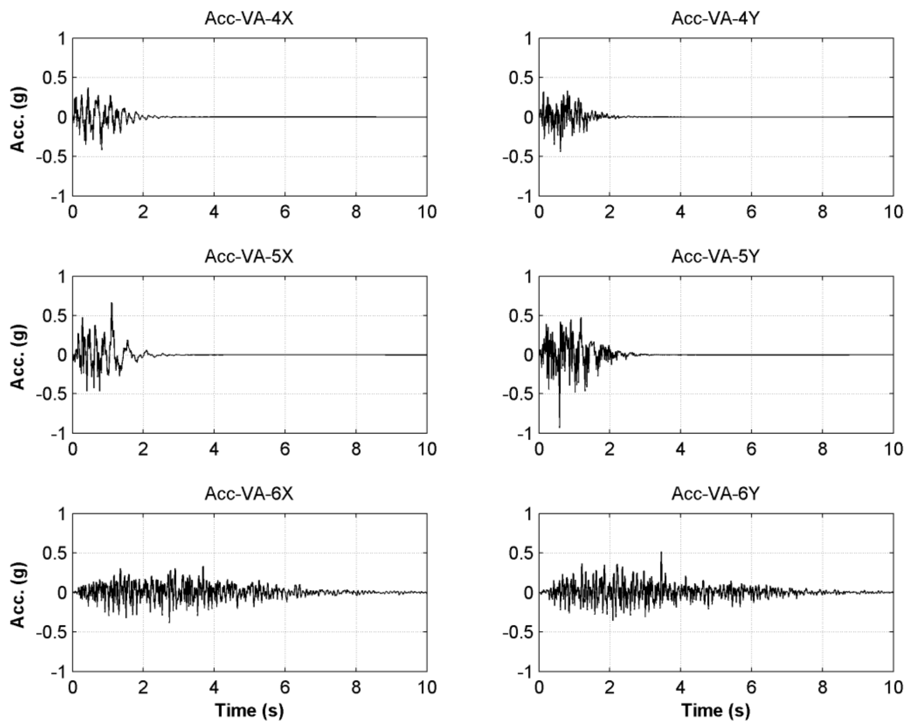

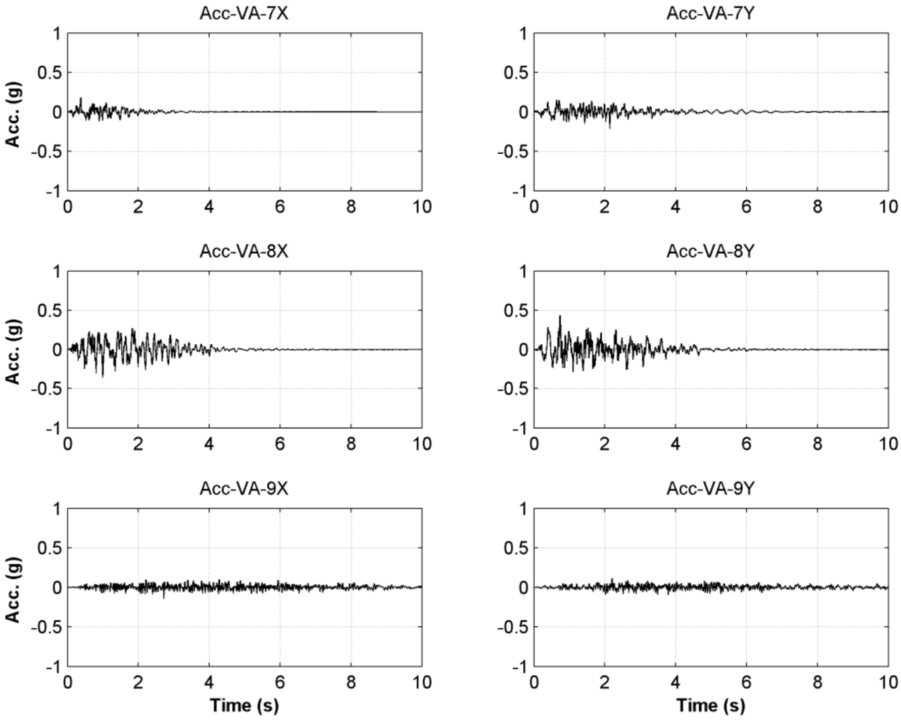
Acc-VA-7X
Acc-VA-7Y
Acc-VA-8X
Acc-VA-8Y
Acc-VA-9X
Acc-VA-9Y
Acc. (g)
Time (s)

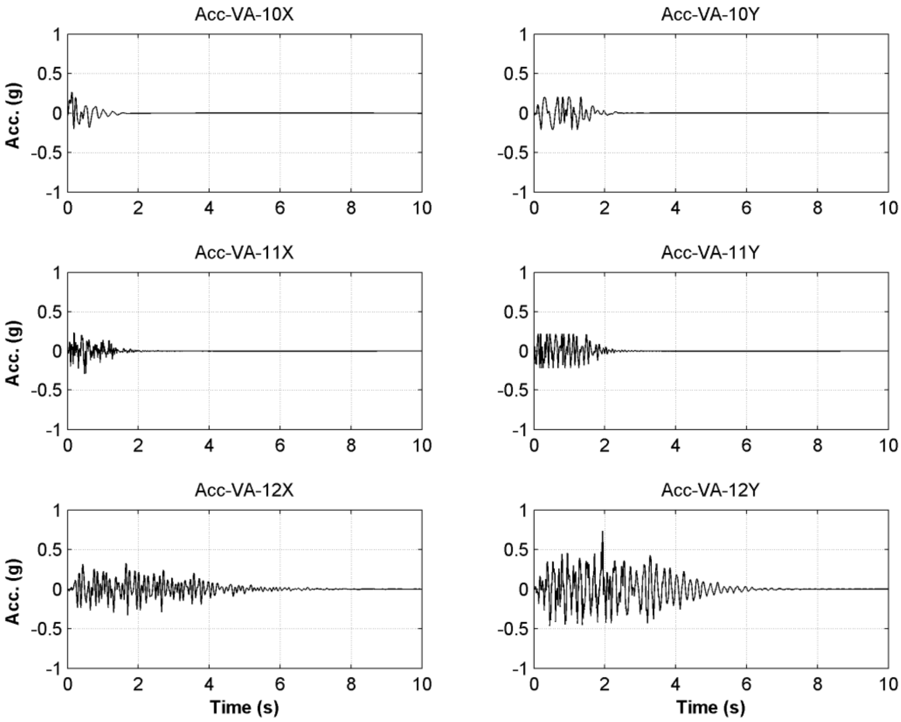
Acc-VA-10X
Acc-VA-10Y
Acc-VA-11X
Acc-VA-11Y
Acc-VA-12X
Acc-VA-12Y
Acc. (g)
Time (s)

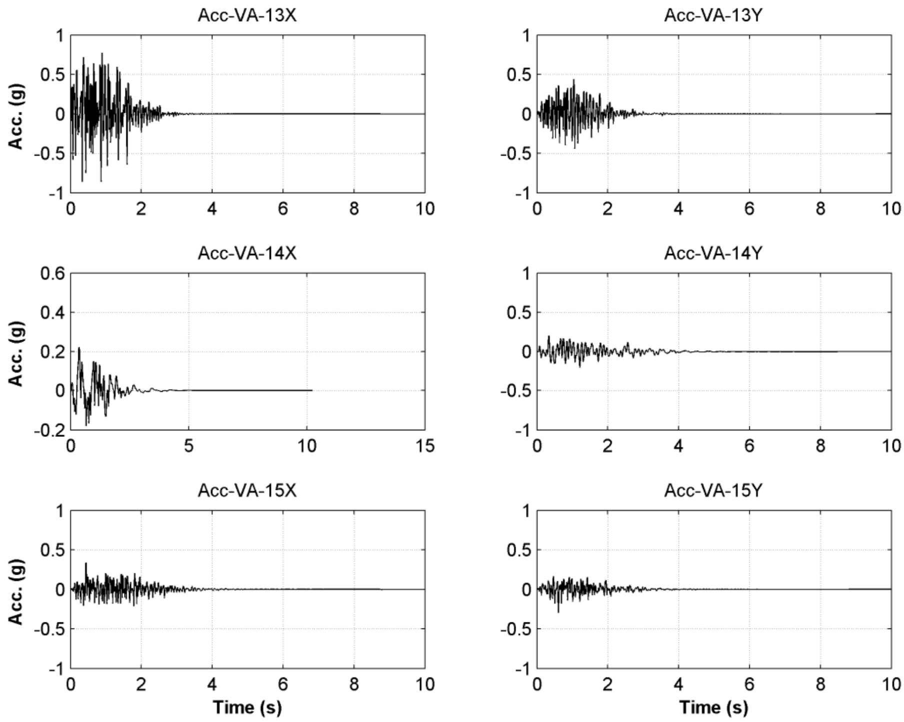
Acc-VA-13X
Acc-VA-13Y
Acc-VA-14X
Acc-VA-14Y
Acc-VA-15X
Acc-VA-15Y
Acc. (g)
Time (s)

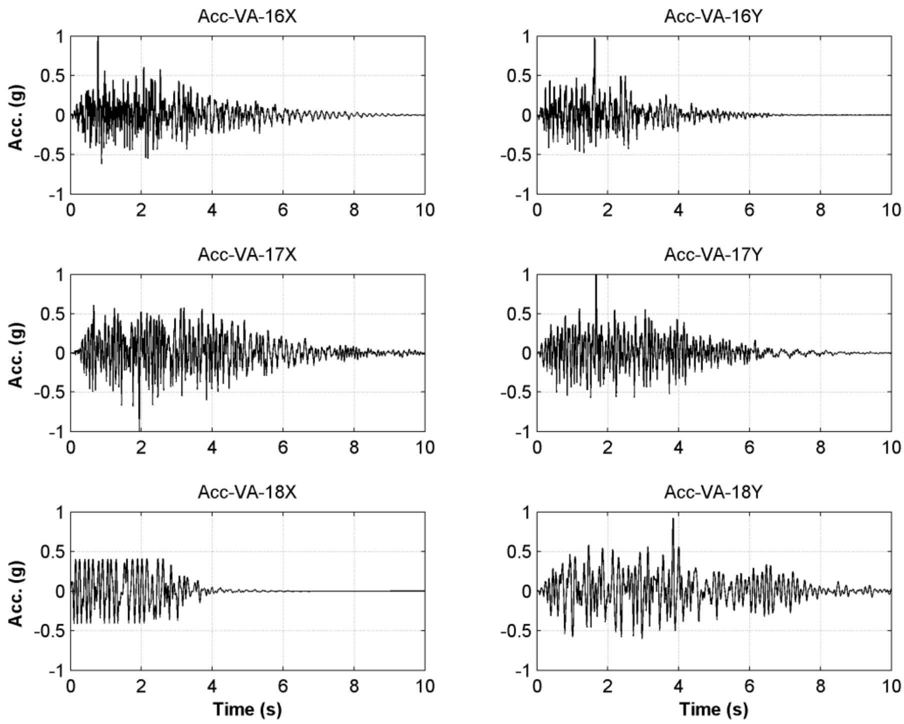
Acc-VA-16X
Acc-VA-16Y
Acc-VA-17X
Acc-VA-17Y
Acc-VA-18X
Acc-VA-18Y
Acc. (g)
Time (s)

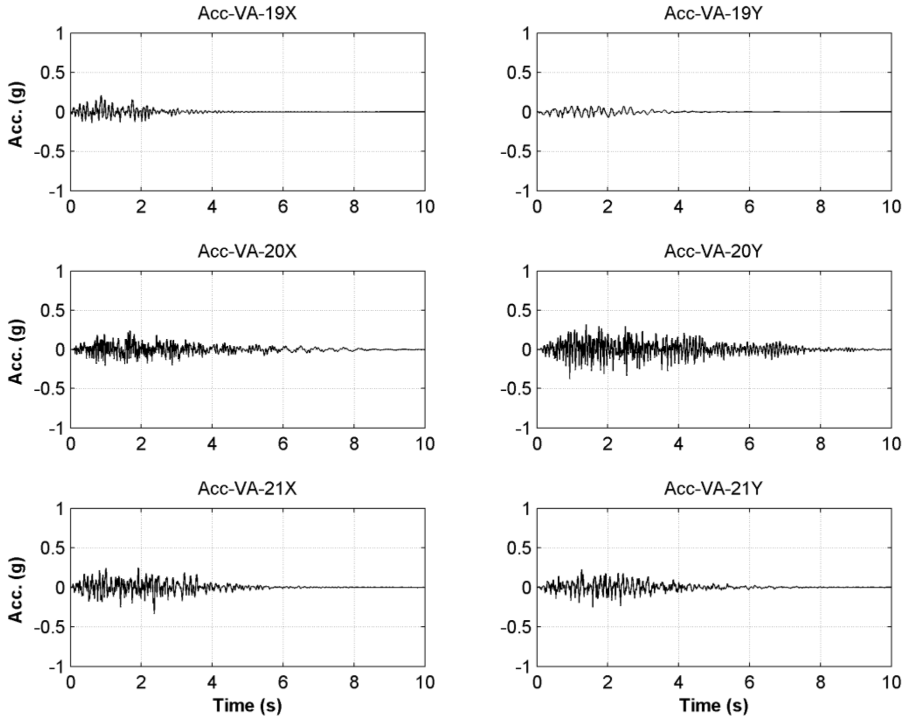
Acc-VA-19X
Acc-VA-19Y
Acc-VA-20X
Acc-VA-20Y
Acc-VA-21X
Acc-VA-21Y
Acc. (g)
Time (s)

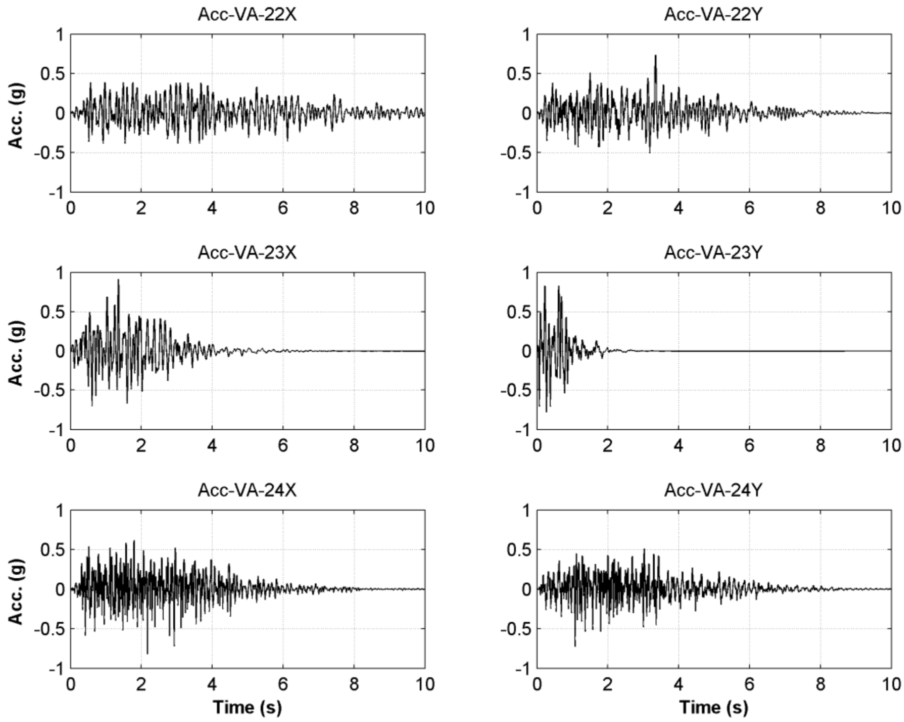
Acc-VA-22X
Acc-VA-22Y
Acc-VA-23X
Acc-VA-23Y
Acc-VA-24X
Acc-VA-24Y
Acc. (g)
Time (s)

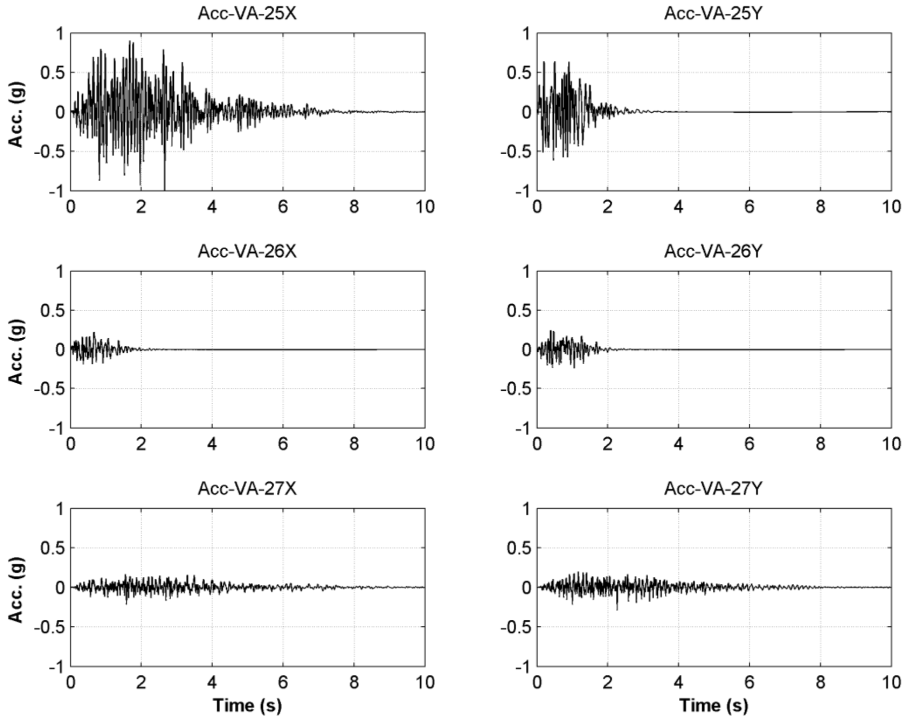
Acc-VA-25X
Acc-VA-25Y
Acc-VA-26X
Acc-VA-26Y
Acc-VA-27X
Acc-VA-27Y
Acc. (g)
Time (s)

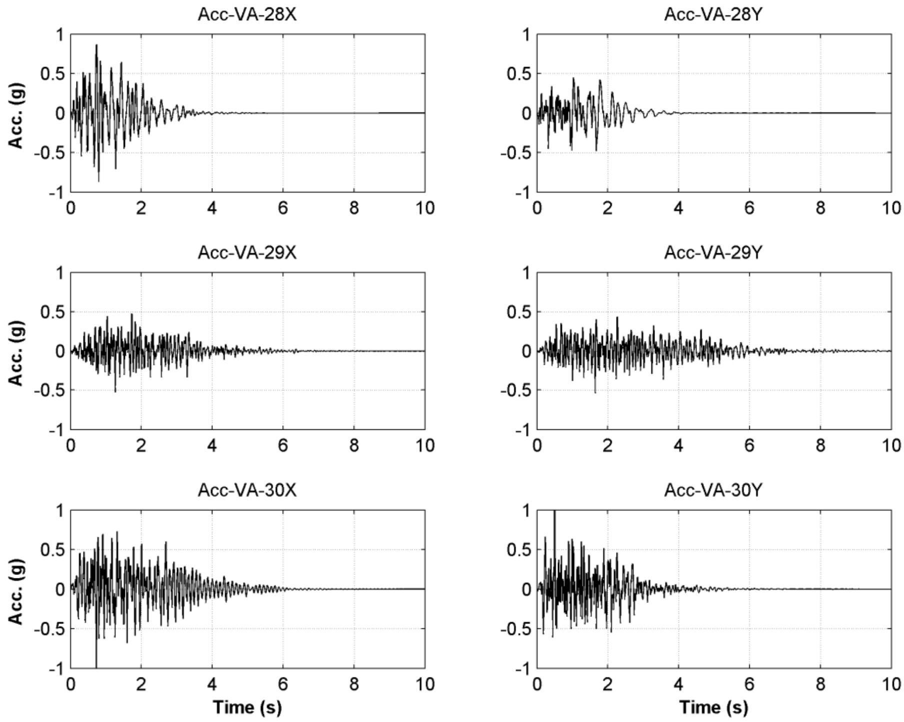
Acc-VA-28X
Acc-VA-28Y
Acc-VA-29X
Acc-VA-29Y
Acc-VA-30X
Acc-VA-30Y
Acc. (g)
Time (s)